

AD-A168 391

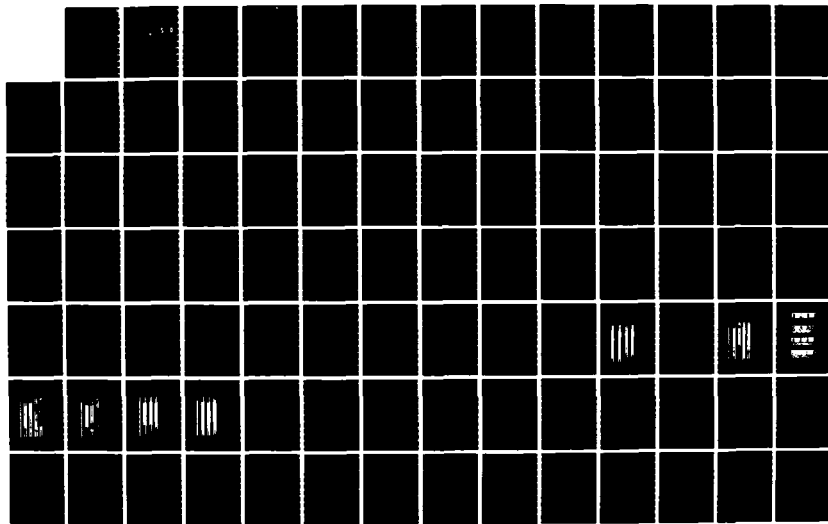
FILM CONDENSATION OF STEAM ON EXTERNALLY ENHANCED
HORIZONTAL TUBES(U) NAVAL POSTGRADUATE SCHOOL MONTEREY
CA E S MITROU MAR 86 NPS-69-86-001 NSF-NEA82-03567

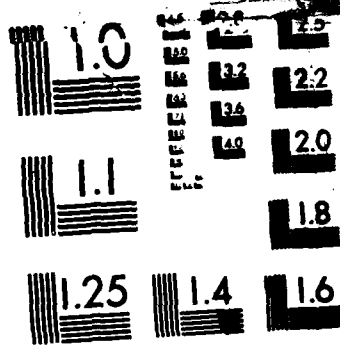
1/2

UNCLASSIFIED

F/G 20/13

NL





MICROCOPY RESOLUTION TEST CHART
NATIONAL BUREAU OF STANDARDS-1963-A

2

AD-A168 391

NPS-69-86-001

NAVAL POSTGRADUATE SCHOOL

Monterey, California



DTIC
ELECTE
JUN 10 1986
S D

THESIS REPORT

FILM CONDENSATION OF STEAM ON
EXTERNALLY ENHANCED HORIZONTAL TUBES

by

Evangelos S. Mitrou

March 1986

Thesis Advisor:
Co-Advisor:

P. J. Marto
A. S. Wanniarachchi

Approved for public release; distribution unlimited

Prepared for:
National Science Foundation
Division of Engineering
Washington, DC 20550

86 6 0 007

DTIC FILE COPY

NAVAL POSTGRADUATE SCHOOL
Monterey, California

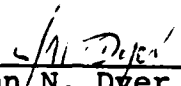
RADM Robert H. Shumaker
Superintendent

David A. Schradly
Provost

This thesis prepared in conjunction with research supported in part by National Science Foundation, Division of Engineering, Washington, DC, under MEA82-03567.

Reproduction of all or part of this report is authorized.

Released as a
Technical Report by:



John N. Dyer
Dean of Science
and Engineering

A168391

REPORT DOCUMENTATION PAGE

1a REPORT SECURITY CLASSIFICATION UNCLASSIFIED			1b. RESTRICTIVE MARKINGS		
2a SECURITY CLASSIFICATION AUTHORITY			3 DISTRIBUTION/AVAILABILITY OF REPORT Approved for public release; distribution is unlimited.		
2b DECLASSIFICATION/DOWNGRADING SCHEDULE					
4 PERFORMING ORGANIZATION REPORT NUMBER(S) NPS69-86-001			5 MONITORING ORGANIZATION REPORT NUMBER(S)		
6a. NAME OF PERFORMING ORGANIZATION Naval Postgraduate School		6b OFFICE SYMBOL (if applicable) Code 69	7a. NAME OF MONITORING ORGANIZATION Naval Postgraduate School		
6c ADDRESS (City, State, and ZIP Code) Monterey, California 93943-5000			7b. ADDRESS (City, State, and ZIP Code) Monterey, California 93943-5000		
8a NAME OF FUNDING/SPONSORING ORGANIZATION National Science Foundation		8b OFFICE SYMBOL (if applicable)	9 PROCUREMENT INSTRUMENT IDENTIFICATION NUMBER MEA82-03567		
8c ADDRESS (City, State, and ZIP Code) Washington, DC 20550			10 SOURCE OF FUNDING NUMBERS		
			PROGRAM ELEMENT NO	PROJECT NO	TASK NO
					WORK UNIT ACCESSION NO.
11 TITLE (Include Security Classification) FILM CONDENSATION OF STEAM ON EXTERNALLY ENHANCED HORIZONTAL TUBES					
12 PERSONAL AUTHOR(S) Mitrou Evangelos S.					
13a TYPE OF REPORT Engineer's Thesis		13b TIME COVERED FROM 4-1-1985 TO 2-30-86		14 DATE OF REPORT (Year, Month, Day) 1986 March	
15 PAGE COUNT 190					
16 SUPPLEMENTARY NOTATION					
17 COSATI CODES			18 SUBJECT TERMS (Continue on reverse if necessary and identify by block number)		
FIELD	GROUP	SUB-GROUP	Steam, Condensation, Filmwise, Horizontal Tube, Fins,		
			Wire-Wrapped, Heat-Transfer Coefficient, Enhancement.		
19 ABSTRACT (Continue on reverse if necessary and identify by block number)					
<p>Heat-transfer measurements were made for filmwise condensation of steam on externally enhanced horizontal tubes under vacuum and at atmospheric pressure. Data were obtained for copper tubes with circular fins of rectangular, triangular, trapezoidal, and parabolic cross sections for spiral fins of triangular cross section, for commercially available finned tubes and for wire-wrapped tubes. Four spirally finned tubes from each of Cu, Cu-Ni, Al and stainless steel and two tubes with fins of rectangular cross section from each of Cu-Ni and Al were manufactured and tested to investigate the effect of thermal conductivity.</p> <p>Among spirally finned tubes, the optimum fin pitch was found to be 1.6 mm. The tubes with a parabolic fin shape showed the best performance with steam-side enhancements of 4.1 and 6.2 under vacuum and at atmospheric pressure.</p>					
20 DISTRIBUTION/AVAILABILITY OF ABSTRACT <input checked="" type="checkbox"/> UNCLASSIFIED/UNLIMITED <input type="checkbox"/> SAME AS RPT <input type="checkbox"/> DTIC USERS			21 ABSTRACT SECURITY CLASSIFICATION Unclassified		
22a NAME OF RESPONSIBLE INDIVIDUAL P. J. Marto			22b TELEPHONE (Include Area Code) (408) 646-2586		22c OFFICE SYMBOL Code 69

respectively. Enhancement ratios as high as 3.5 and 2.1 were obtained under vacuum and at atmospheric pressure, respectively, for the commercially available finned tubes. The heat-transfer performance decreased with decreasing tube metal thermal conductivity.

For the wire-wrapped tubes, an optimum pitch to wire diameter ratio of about 5.1 was found, with steam-side enhancements of about 1.9 and 2.2 under vacuum and at atmospheric pressure, respectively. A recent theoretical analysis of laminar film of low-surface-tension fluids on wire-wrapped tubes was modified to include the condensate retention of the tube due to the high surface tension of water. Agreement between this modified analysis and the experimental data was favorable. K. S. G. 1967

Approved for public release; distribution is unlimited.

Film Condensation of Steam on
Externally Enhanced Horizontal Tubes

by

Evangelos S. Mitrou
Lieutenant, Hellenic Navy
B.S.M.E., Hellenic Naval Academy, 1976

Submitted in partial fulfillment of the
requirements for the degrees of

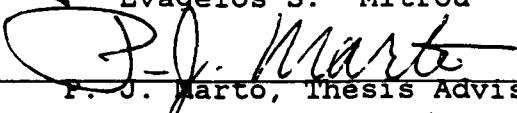
MASTER OF SCIENCE IN MECHANICAL ENGINEERING
and
MECHANICAL ENGINEER
from the

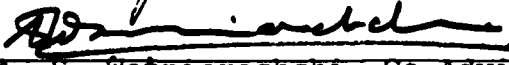
NAVAL POSTGRADUATE SCHOOL
March 1986

Author:



Evangelos S. Mitrou

Approved by:


P. J. Marto, Thesis Advisor


A. S. Wanniarachchi, Co-Advisor


Paul J. Marto, Chairman,
Department of Mechanical Engineering


John N. Dyer,
Dean of Science and Engineering

ABSTRACT

Heat-transfer measurements were made for filmwise condensation of steam on externally enhanced horizontal tubes under vacuum and at atmospheric pressure. Data were obtained for copper tubes with circular fins of rectangular, triangular, trapezoidal, and parabolic cross sections, for spiral fins of triangular cross section, for commercially available finned tubes and for wire-wrapped tubes. Four spirally finned tubes from each of Cu, Cu-Ni, Al, and stainless steel and two tubes with fins of rectangular cross section from each of Cu-Ni and Al were manufactured and tested to investigate the effect of thermal conductivity.

Among spirally finned tubes, the optimum fin pitch was found to be 1.6 mm. The tubes with a parabolic fin shape showed the best performance with steam-side enhancements of 4.1 and 6.2 under vacuum and at atmospheric pressure, respectively. Enhancement ratios as high as 3.5 and 2.1 were obtained under vacuum and at atmospheric pressure, respectively, for the commercially available finned tubes. The heat-transfer performance decreased with decreasing tube metal thermal conductivity.

For the wire-wrapped tubes, an optimum pitch to wire diameter ratio of about 5.1 was found, with steam-side enhancements of about 1.9 and 2.2 under vacuum and at atmospheric pressure, respectively. A recent theoretical analysis of laminar film of low-surface-tension fluids on wire-wrapped tubes was modified to include the condensate retention of the tube due to the high surface tension of water. Agreement between this modified analysis and the experimental data was favorable.

TABLE OF CONTENTS

I.	INTRODUCTION	13
A.	BACKGROUND	13
B.	OBJECTIVES	16
II.	PREVIOUS INVESTIGATIONS OF FILM CONDENSATION ON EXTERNALLY ENHANCED HORIZONTAL TUBES	18
A.	GENERAL OBSERVATIONS	18
B.	CONDENSATE RETENTION	22
C.	THEORETICAL MODELS	28
D.	FILMWISE CONDENSATION ON WIRE-WRAPPED TUBES	47
III.	DESCRIPTION OF TEST APPARATUS	52
A.	TEST APPARATUS	52
B.	INSTRUMENTATION	53
C.	VACUUM INTEGRITY	55
D.	DATA ACQUISITION SYSTEM	57
E.	TUBES TESTED	57
IV.	SYSTEM OPERATION AND DATA REDUCTION	71
A.	SYSTEM OPERATION	71
B.	DATA REDUCTION	73
1.	"Direct" Method	74
2.	"Modified Wilson Plot" Method	75
V.	RESULTS AND DISCUSSION	79
A.	INTRODUCTION	79
B.	WATER-SIDE HEAT-TRANSFER COEFFICIENTS	82
C.	REPEATABILITY OF DATA	92
D.	EFFECT OF FIN PITCH ON HEAT TRANSFER PERFORMANCE OF SPIRAL TUBES WITH TRIANGULAR-SHAPED FINs	94
E.	EFFECT OF FIN SHAPE ON HEAT-TRANSFER PERFORMANCE	102



Proprietary Codes	
Dist	Avail and/or Special
A-1	

F.	EFFECT OF FIN THERMAL CONDUCTIVITY ON PERFORMANCE	108
G.	PERFORMANCE OF WIRE WRAPPED TUBES	116
1.	Condensate Retention Angle for Wire-Wrapped Tubes	116
2.	Experimental Data of Wire-Wrapped Tubes	120
3.	Modifications to Fujii et al. Model	122
H.	HEAT-TRANSFER COEFFICIENT FOR COMMERCIAL TUBES	133
VI.	CONCLUSIONS AND RECOMMENDATIONS	139
A.	CONCLUSIONS	139
B.	RECOMMENDATIONS	140
APPENDIX A:	DERIVATION OF THE HEAT-TRANSFER COEFFICIENT OF FLOODED REGION FOR WIRE-WRAPPED TUBES	141
APPENDIX B:	LISTING OF RAW DATA	143
APPENDIX C:	UNCERTAINTY ANALYSIS	174
LIST OF REFERENCES	183
INITIAL DISTRIBUTION LIST	187

LIST OF TABLES

I	GEOMETRY OF FINNED TUBES TESTED	61
II	GEOMETRY OF WIRE-WRAPPED TUBES TESTED	62
III	SUMMARY OF FINNED TUBES TESTED AND THEIR HEAT-TRANSFER PERFORMANCE	80
IV	SUMMARY OF WIRE-WRAPPED TUBES TESTED AND THEIR HEAT-TRANSFER PERFORMANCE	81
V	CONSTANTS OF EQUATION (5.1) FOR FINNED TUBES TESTED	94
VI	CONSTANTS OF EQUATION (5.1) FOR WIRE-WRAPPED TUBES TESTED	95
VII	MEASURED RETENTION ANGLES (Ψ)	119
VIII	RAW DATA FOR TUBE WITH RECTANGULAR FIN PROFILE OF $S = 1.5$ MM, $T = 1.0$ MM AND $E = 1.0$ MM	144
IX	RAW DATA FOR TUBE WITH RECTANGULAR FIN PROFILE OF $S = 1.5$ MM, $T = 0.5$ MM AND $E = 1.0$ MM	145
X	RAW DATA FOR TUBE WITH PARABOLIC FIN PROFILE OF $S = 1.5$ MM, $T_B = 0.5$ MM AND $E = 1.0$ MM	146
XI	RAW DATA FOR SPIRAL TUBES WITH FINS OF $P = 2.1$ MM AND $E = 1.0$ MM	147
XII	RAW DATA FOR SPIRAL TUBES WITH FINS OF $P = 2.5$ MM AND $E = 1.0$ MM	148
XIII	RAW DATA FOR SPIRAL TUBES WITH FINS OF $P = 1.6$ MM AND $E = 1.0$ MM	149
XIV	RAW DATA FOR SPIRAL TUBES WITH FINS OF $P = 1.05$ MM AND $E = 1.0$ MM	150
XV	RAW DATA FOR COMMERCIALY AVAILABLE FINNED TUBES WITH FINS OF $S = 0.5$ MM, $T_B = 0.3$ MM AND $E = 1.0$ MM	151
XVI	RAW DATA FOR HPTI SMOOTH TUBE	152
XVII	RAW DATA FOR COMMERCIALY AVAILABLE FINNED TUBES WITH FINS OF $S = 0.6$ MM, $T_B = 0.3$ MM AND $E = 1.0$ MM	153
XVIII	RAW DATA FOR TUBE WITH TRIANGULAR FIN PROFILE OF $S = 1.5$ MM, $T_B = 0.5$ MM AND $E = 1.0$ MM	154
XIX	RAW DATA FOR TUBE WITH TRAPEZOIDAL FIN PROFILE OF $S = 1.5$ MM, $T_B = 0.5$ MM AND $E = 1.0$ MM	155

XX	RAW DATA FOR TUBE WITH PARABOLIC FIN PROFILE OF $S = 1.5$ MM, $T_B = 1.0$ MM AND $E = 1.0$ MM	156
XXI	RAW DATA FOR TUBE WITH TRAPEZOIDAL FIN PROFILE OF $S = 1.5$ MM, $T_B = 1.0$ MM AND $E = 1.0$ MM	157
XXII	RAW DATA FOR TUBE WITH TRIANGULAR FIN PROFILE OF $S = 1.5$ MM, $T_B = 1.0$ MM AND $E = 1.0$ MM	158
XXIII	RAW DATA FOR SPIRAL COPPER TUBE WITH TRIANGULAR FIN PROFILE OF $P = 2.1$ MM, $E = 1.0$ MM AND $DO = 13.7$ MM	159
XXIV	RAW DATA FOR SPIRAL COPPER-NICKEL TUBE WITH TRIANGULAR FIN PROFILE OF $P = 2.1$ MM, $E = 1.0$ MM AND $DO = 13.7$ MM	160
XXV	RAW DATA FOR SPIRAL STAINLESS STEEL TUBE WITH TRIANGULAR FIN PROFILE OF $P = 2.1$ MM, $E = 1.0$ MM AND $DO = 14.5$ MM	161
XXVI	RAW DATA FOR SPIRAL ALUMINUM TUBE WITH TRIANGULAR FIN PROFILE OF $P = 2.1$ MM, $E = 1.0$ MM AND $DO = 13.7$ MM	162
XXVII	RAW DATA FOR COPPER-NICKEL TUBE WITH RECTANGULAR FIN PROFILE OF $S = 1.5$ MM, $T = 1.0$ MM, $E = 1.0$ MM	163
XXVIII	RAW DATA FOR ALUMINUM TUBE WITH RECTANGULAR FIN PROFILE OF $S = 1.5$ MM, $T = 1.0$ MM, $E = 1.0$ MM AND $DO = 13.7$ MM	164
XXIX	RAW DATA FOR WIRE-WRAPPED TUBE WITH $D_W = 1.6$ MM AND $P = 2.5$ MM	165
XXX	RAW DATA FOR WIRE-WRAPPED TUBE WITH $D_W = 1.6$ MM AND $P = 3.6$ MM	166
XXXI	RAW DATA FOR WIRE-WRAPPED TUBE WITH $D_W = 1.6$ MM AND $P = 4.6$ MM	167
XXXII	RAW DATA FOR WIRE-WRAPPED TUBE WITH $D_W = 1.0$ MM AND $P = 2.0$ MM	168
XXXIII	RAW DATA FOR WIRE-WRAPPED TUBE WITH $D_W = 1.0$ MM AND $P = 2.8$ MM	169
XXXIV	RAW DATA FOR WIRE-WRAPPED TUBE WITH $D_W = 1.0$ MM AND $P = 3.9$ MM	170
XXXV	RAW DATA FOR WIRE-WRAPPED TUBE WITH $D_W = 0.5$ MM AND $P = 1.6$ MM	171
XXXVI	RAW DATA FOR WIRE-WRAPPED TUBE WITH $D_W = 0.5$ MM AND $P = 2.5$ MM	172
XXXVII	RAW DATA FOR WIRE-WRAPPED TUBE WITH $D_W = 0.5$ MM AND $P = 3.6$ MM	173

LIST OF FIGURES

2.1	Schematic of Condensate Profile on Unflooded Fin	19
2.2	Schematic of Condensate Retention on Finned Tubes	24
2.3	Adamek [24] Condensate Surface Profiles	39
2.4	Fin Geometry for the Webb et al. Model [31]	46
2.5	Condensate Film Profile on Wire-Wrapped Tubes	50
2.6	Comparison Between Experimental Data and Semi-Theoretical Model of Fujii et al. [32]	51
3.1	Schematic of Test Apparatus	54
3.2	Schematic of Test Section (Insert Removed)	56
3.3	Schematic of Vacuum System and Cooling Water Sump	58
3.4	Photographs of Tubes with Different Fin Shapes ($t_b = 1.0$ mm)	63
3.5	Tracing of the Fin Profile of Tube 54	64
3.6	Photographs of Tubes with Different Fin Shapes ($t_b = 0.5$ mm)	65
3.7	Cross-Sectional Photographs of Tubes with Different Fin Shapes $t_b = 0.5$ mm)	66
3.8	Photograph of Tubes with Spiral Triangular Fins ($e = 1.0$ mm)	67
3.9	Photograph of Wire-Wrapped Tubes ($D_w = 0.5$ mm)	68
3.10	Photograph of Wire-Wrapped Tubes ($D_w = 1.0$ mm)	69
3.11	Photograph of Wire-Wrapped Tubes ($D_w = 1.6$ mm)	70
5.1	Comparison of Finned-Tube Data with Data of Georgiadis [5] and Flook [6] (Vacuum Runs, Tube 6)	83
5.2	Comparison of Finned-Tube Data with Data of Georgiadis [5] (Atmospheric Runs, Tube 6)	84
5.3	Comparison of Finned-Tube Data with Data of Georgiadis [5] and Flook [6] (Vacuum Runs, Tube 17)	85
5.4	Comparison of Finned-Tube Data with Data of Georgiadis [5] and Flook [6] (Atmospheric Runs, Tube 17)	86

5.5	Comparison of Finned-Tube Data with Data of Flook [6] (Vacuum Runs, Tubes 27 and 28)	87
5.6	Comparison of Finned-Tube Data with Data of Flook [6] (Vacuum Runs, Tube 36)	88
5.7	Comparison of Finned-Tube Data with Data of Flook [6] (Atmospheric Runs, Tube 36)	89
5.8	Comparison of Finned-Tube Data with Data of Flook [6] (Vacuum Runs, Tube 38)	90
5.9	Comparison of Finned-Tube Data with Data of Flook [6] (Atmospheric Runs, Tube 38)	91
5.10	Variation of Heat-Transfer Coefficient with Heat Flux for the Set of Tubes with Spiral Triangular Fins (Vacuum Runs)	96
5.11	Variation of Heat-Transfer Coefficient with Heat Flux for the Set of Tubes with Spiral Triangular Fins (Atmospheric Runs)	97
5.12	Enhancement Ratio for Tubes with Spiral Triangular Fins ($e = 1.0$ mm)	98
5.13	Enhancement Ratio for Tubes with Spiral Triangular Fins ($e = 1.0$ mm)	99
5.14	Effect of Fin Shape on Heat-Transfer Coefficient for Vacuum Runs ($t_b = 0.5$ mm)	103
5.15	Effect of Fin Shape on Heat-Transfer Coefficient for Atmospheric Runs ($t_b = 0.5$ mm)	104
5.16	Effect of Fin Shape on Heat-Transfer Coefficient for Vacuum Runs ($t_b = 1.0$ mm)	105
5.17	Effect of Fin Shape on Heat-Transfer Coefficient for Atmospheric Runs ($t_b = 1.0$ mm)	106
5.18	Effect of Wall Thermal Conductivity on Heat-Transfer Coefficient for Tubes with Spiral Triangular Fins (Vacuum Runs, Tubes 57, 58, 59 and 60)	110
5.19	Effect of Wall Thermal Conductivity on Heat-Transfer Coefficient for Tubes with Spiral Triangular Fins (Atmospheric Runs, Tubes 57, 58, 59 and 60)	111
5.20	Effect of Wall Thermal Conductivity on Heat-Transfer Coefficient for Tubes with Rectangular Fin Shape (Vacuum Runs, Tubes 39, 61 and 62)	112
5.21	Effect of Wall Thermal Conductivity on Heat-Transfer Coefficient for Tubes with Rectangular Fin Shape (Atmospheric Runs, Tubes 39, 61 and 62)	113
5.22	Effect of Tube Metal Thermal Conductivity on Enhancement Ratio for Tubes with Spiral Triangular-Shaped Fins	114
5.23	Effect of Normalized Tube Metal Thermal Conductivity on Enhancement Ratio for Tubes with Spiral Triangular-Shaped Fins	115

5.24	Photograph Showing the Condensate Retention on Three Wire-Wrapped Tubes ($D_w = 0.5$ mm)	117
5.25	Comparison of Measured and Calculated Condensate Retention Angles for Wire-Wrapped Tubes	118
5.26	Effect of Wire Pitch on Heat-Transfer Coefficient for Wire-Wrapped Tubes with $D_w = 1.6$ mm (Vacuum Runs)	123
5.27	Effect of Wire Pitch on Heat-Transfer Coefficient for Wire-Wrapped Tubes with $D_w = 1.6$ mm (Atmospheric Runs)	124
5.28	Effect of Wire Pitch on Heat-Transfer Coefficient for Wire-Wrapped Tubes with $D_w = 1.0$ mm (Vacuum Runs)	125
5.29	Effect of Wire Pitch on Heat-Transfer Coefficient for Wire-Wrapped Tubes with $D_w = 1.0$ mm (Atmospheric Runs)	126
5.30	Effect of Wire Pitch on Heat-Transfer Coefficient for Wire-Wrapped Tubes with $D_w = 0.5$ mm (Vacuum Runs)	127
5.31	Effect of Wire Pitch on Heat-Transfer Coefficient for Wire-Wrapped Tubes with $D_w = 0.5$ mm (Atmospheric Runs)	128
5.32	Effect of p/D_w Ratio on Heat-Transfer Performance for Wire-Wrapped Tubes	129
5.33	Variation of Function $F_1(\phi, A)$ with ϕ and A	132
5.34	Measured and Calculated Values for the Slope of Function $F_1(\phi, A)$	135
5.35	Effect of p/D_w Ratio on Enhancement Ratio for Wire-Wrapped Tubes	136
5.36	Variation of Heat-Transfer Coefficient with Heat Flux for High Performance Tubes (Vacuum Runs)	137
5.37	Variation of Heat-Transfer Coefficient with Heat Flux for High Performance Tubes (Atmospheric Runs)	138
A.1	Condensate Film Profile for Fully Flooded Wire-Wrapped Tube	142

ACKNOWLEDGEMENTS

The author would like to thank his thesis advisor, Professor P. J. Marto for his support and guidance throughout this thesis effort.

The author would also like to thank Dr. A. S. Wanniarachchi for his patience, support, and guidance.

Special thanks to my wife Mary and daughters Despina and Spyridoula, for their patience during my studies at the Naval Postgraduate School.

The author would also like to thank Mr. Tom McCord and his machine shop crew for their support throughout this thesis effort.

I. INTRODUCTION

A. BACKGROUND

It is well known that the power required to operate a naval vessel at a given speed is proportional to its displacement. Therefore, a major effort is necessary to reduce the displacement in order to minimize the required power. One of the largest components of a naval vessel is the main condenser. In fact, present-day condensers are equipped with smooth tubes, and therefore are large in size and weight. Increasing the performance or the effectiveness of the condenser can reduce the material and the construction cost and of course the weight.

The effectiveness of the condenser is limited by the thermal resistances of the water side, the steam side and through the tube wall. Generally, the thermal resistances of the water side and steam side are the most dominant. Reducing any one of these thermal resistances will contribute to an improved overall heat-transfer coefficient. Therefore, for a given heat duty, this corresponds to a smaller and lighter condenser. Improved heat-transfer performance can be achieved by enhancement of the water side and/or the vapor side. Enhancement on the water side is possible with turbulence promoters, twisted-tape inserts, and deformation of the tube to produce a "roped" scheme, internal fins or ribs [1]. The main disadvantage of water-side enhancement is the requirement of increased power for pumping. Therefore, vapor-side enhancement may promise better economic advantage, while the best advantage may be achieved by enhancing both sides based on a comprehensive analysis. The enhancement of the vapor-side can be achieved by using low-integral fins, roped tubes or fluted tubes or by applying coatings to promote dropwise condensation.

While externally finned tubes have been used since the 1940s in order to enhance the vapor-side coefficient of tubes used in refrigeration systems, such tubes have not been used in steam condensers. The reason for this appears to be the common belief that externally finned tubes could not enhance steam condensation mainly owing to the large amount of condensate that floods between fins in the lower portion of the tube. Since the surface tension of water is four times greater than that of the refrigerants, a very significant proportion of the tube may trap water between fins, which could result in poor heat-transfer performance.

The theoretical treatment of the steam condensation problem on horizontal finned tubes is very difficult due to the large number of controlling parameters, such as gravitational and surface tension forces, fin spacing, height, thickness and shape leading to three-dimensional flow of condensate. Due to the complexity of the problem, any theoretical model requires simplifying assumptions which can lead to inadequate results. Therefore, a large pool of reliable data, systematically covering all of the relevant variables, is essential in order to test simplified theoretical models and/or to arrive at a satisfactory correlation.

This thesis effort is a continuation of research being conducted at the Naval Postgraduate School (NPS) under a grant from the National Science Foundation. The basic test apparatus has been constructed by Krohn [2]. Graber [3] provided the instrumentation, and took preliminary data as the system experienced problems with non-condensing gases and partial dropwise condensation on copper tubes. Poole [4] made further improvements on the apparatus especially for leak tightness. He operated the apparatus both under vacuum and at atmospheric pressure, and tested a total of six finned tubes, with different fin spacing, as well as a smooth tube. Unfortunately, Poole had problems owing to the

occurrence of partial dropwise condensation. Using this system, Georgiadis [5] was able to obtain complete filmwise condensation on 26 copper tubes. The repeatability of data obtained by Georgiadis proved the accuracy of the test apparatus and associated instrumentation which was basically the same as that used by Poole [4] with some minor modifications. Georgiadis tested a total of 23 finned tubes with rectangular-section fins and three smooth tubes. He systematically varied the fin spacing (0.5, 1.0, 1.5, 2.0, 4.0 and 9.0 mm), fin thickness (0.5, 0.75, 1.0 and 1.5 mm) and fin height (1.0 and 2.0 mm). Table I shows the combinations of fin dimensions used for these tubes. Based on both vacuum and atmospheric runs, Georgiadis reported an optimum fin spacing of 1.5 mm and an optimum fin thickness of 0.75 to 1.0 mm. Among the finned tubes with a fin height of 1.0 mm, the tube with a fin spacing of 1.5 mm and fin thickness of 1.0 mm provided the best heat-transfer performance. This tube resulted in a steam-side enhancement (i.e., the ratio of steam-side coefficient for the finned tube to the value for the smooth tube at the same heat flux) of about 4 and 5.7 for vacuum and atmospheric pressure, respectively. He found that the heat-transfer performance was most sensitive to the fin spacing, while the effect of fin thickness was relatively small. Further, he found that the performance increased with increasing fin height. However, he showed that the ratio E_o/A_r (i.e., the enhancement beyond the area enhancement) decreased with increasing fin height (for example, tube 6 with $e = 1.0$ mm gave E_o/A_r values of 2.13 and 3.01 for vacuum and atmospheric pressure, respectively, while tube 23 with $e = 2.0$ mm gave values of 1.69 and 2.25). It appears that the surface-tension induced thinning of the condensate film diminishes with increasing fin height.

Continuing with this investigation, Flook [6] tested 19 additional tubes (see Table I for details). These tubes

included two sets of four tubes with fin heights of 0.5 and 1.5 mm, respectively. In addition, he studied the effect of fin shape using machined fins of triangular, trapezoidal, and "parabolic" fin shapes, (these tubes had a fin height of 1.0 mm, a fin base thickness of 0.5 mm and a fin spacing of 1.5 mm at the fin root). Flook showed that the tube with parabolic fins (tube 38) outperformed the corresponding tube with rectangular-section fins (tube 17) by 10 and 15 percent under vacuum and at atmospheric pressure, respectively. As also pointed out by Flook, this tube did not have truly parabolic fins. Like previous researchers [7,8], Flook also pointed out that a fin shape, such as parabolic, that has a continuously decreasing curvature from fin tip to fin root provides considerable thinning of the condensate film, thus resulting in improved heat-transfer performance.

Despite considerable achievements made by Georgiadis and Flook, the very complicated nature of the problem being studied demands much more attention. This includes more testing to study the effect of fin shape, the effect of fin thermal conductivity, performance of commercially available tubes and the enhancement that can be achieved by wire-wrapping smooth tubes.

B. OBJECTIVES

The main objectives of this thesis are as follows:

Take data on a number of tubes to check the repeatability with previous data [5,6],

Take data on tubes with fins of different shapes (triangular, trapezoidal, parabolic, etc.),

Take data on commercially available tubes,

Take data on tubes with different thermal conductivity having rectangular, triangular, and spiral fin shapes, and

Take data on wire-wrapped tubes with different spacing and wire diameter.

Develop a theory to predict the data for wire-wrapped tubes.

II. PREVIOUS INVESTIGATIONS OF FILM CONDENSATION ON EXTERNALLY ENHANCED HORIZONTAL TUBES

A. GENERAL OBSERVATIONS

When vapor condenses on smooth horizontal tubes in a filmwise mode, the condensate flows down by gravity and a continuous film always exists around the tube. The latent heat released by the vapor will eventually be absorbed by the cooling liquid that flows through the tube.

The condensate film resists this heat flow because of the low conductivity of the liquid. The resistance increases as the film thickness increases. At the top of the tube, the condensate film thickness is small and thereby the resistance is low and it increases with increasing distance around the perimeter of the tube. Since the thermal resistance of the condensate limits the heat-transfer performance of the tube, to enhance heat transfer, it is necessary to reduce condensate film thickness. For horizontal tubes, thinning of the condensate may be achieved by using a finned, grooved or a fluted surface.

In 1984, Yau et al. [9] measured the enhancement provided by copper finned tubes over smooth tubes for filmwise condensation of steam. Similar experiments by Wanniarachchi et al. [10] also in 1984 confirmed that the observed enhancements were greater than could be explained by the increased surface area alone. This additional enhancement may be a result of the surface-tension forces which act to thin the condensate film. The effect of surface tension was first described by Gregorig [7] using a fluted surface. The surface tension induced a large pressure gradient along the fin surface. This induced pressure gradient can be explained by using Figure 2.1.

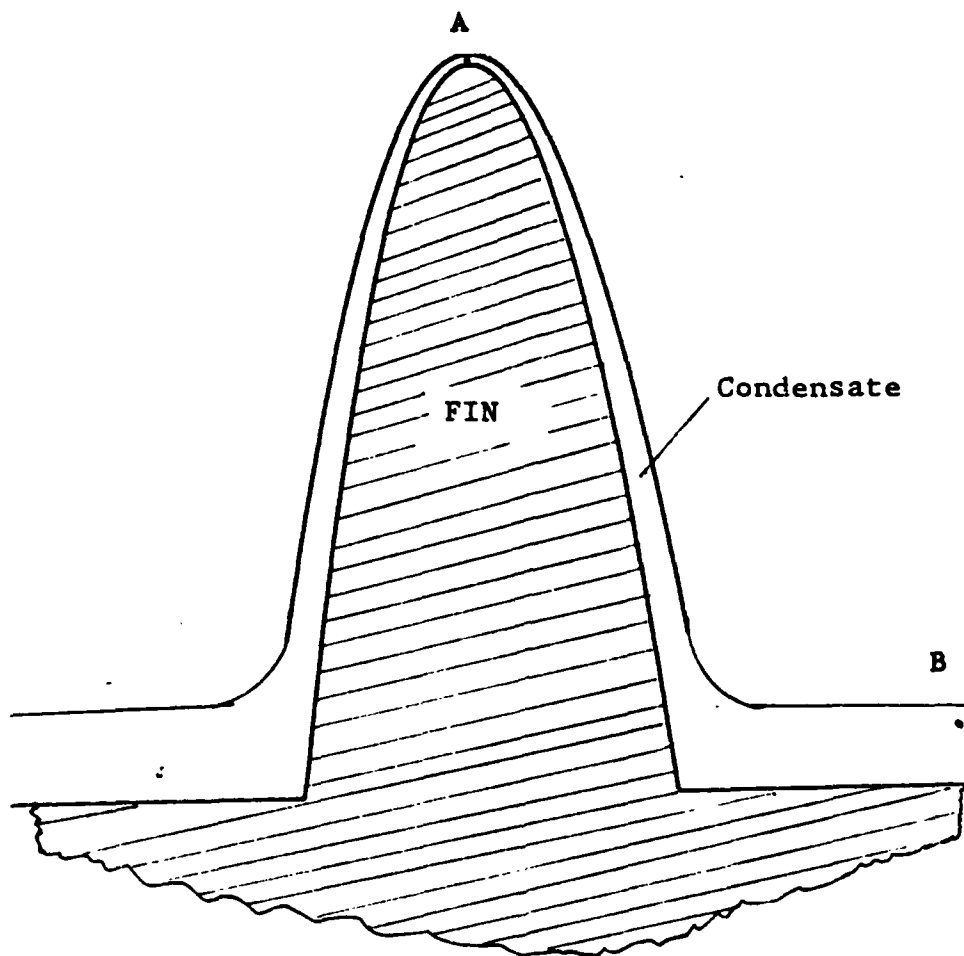


Figure 2.1 Schematic of Condensate Profile on Unflooded Fin.

The pressure gradient due to the effect of the surface tension between a liquid and vapor is inversely proportional to the radius of curvature of the condensate surface.

The pressure of the condensate at point A is higher than the vapor pressure because of the convex condensate surface at this point. The condensate surface at the valley is rather flat. This nearly infinite radius of curvature of the condensate surface results in no pressure difference

induced by the surface tension at this point. Therefore, the pressure at point B is almost the same as the vapor pressure. These pressures are given by:

$$P_A = P_v + \frac{\sigma}{r_A} \quad (2.1)$$

$$P_B \approx P_v \quad (2.2)$$

where

P_v = vapor pressure,

P_A, P_B = liquid pressure at points A, B, and

r_A, r_B = radius of curvature of the condensate film at points A, and B.

At point A, the radius of curvature is small, so the pressure at point A is higher than the pressure at point B (see equations (2.1) and (2.2)). Since, in reality, the radius of curvature changes along the condensate surface, between points A and B, the pressure within the condensate film varies along the height of the fin. The overall pressure difference between points A and B is given by equation (2.3).

$$\Delta P_{AB} = \frac{\sigma}{r_A} \quad (2.3)$$

where

ΔP_{AB} = pressure difference between points A and B.

Since the radius of curvature of the condensate film at point A is very small, we can see from equation (2.3) that there is a large pressure difference between points A and B. This pressure difference causes the condensate to flow from point A to point B, thinning the condensate layer. On the other hand, the flow of condensate between the fins depends on the ratio of surface tension forces to gravity forces since the former acts to retain the condensate between the fins while the latter acts to drain the condensate. As surface tension increases, the condensate tends to flood a larger area of the tube in which the condensate layer is thick and the thermal resistance increases, so a small heat transfer coefficient results. The flooded portion of the tube, as mentioned in section A, is defined by the retention angle, (ψ) (i.e., the angle from the bottom of the tube to the highest position of the tube where the interfin space is still full of condensate). The retention angle depends on the fin spacing, surface tension and gravity forces, and the fin shape. Therefore, on the one hand, using fins around a smooth tube increases the condensing area and thins the condensate film along the fin surface. However, these beneficial effects are offset by the flooding that occurs. Decreasing the retention angle increases the heat transfer performance. Therefore, any means reducing the retention angle is beneficial. As mentioned in section A, one way to decrease the retention angle is by attaching drainage strips at the lower part of the tube.

B. CONDENSATE RETENTION

In 1946, the first measurements of condensate retention were made by Katz et al. [11]. These measurements were made under static conditions (i.e., no condensation taking place) using water, aniline, acetone, and carbon tetrachloride on ten different tubes with fin densities from 276 to 984 fins/m, and fin heights from 1.2 to 5.7 mm. They measured the retention angle by visual observation and by weighing the amount of retained liquid. Theoretical treatment of the problem using the measurement of surface tension by a capillary tube and by the pendant drop method was made to develop a formula to predict condensate retention as a function of condensate properties and the dimensions of the tube. Their result for the condensate retention angle, ψ is given by equation (2.4):

$$\frac{\psi}{\sin \psi} = \frac{\sigma}{\rho_f} \left[\frac{(4D_f - 2D_o + 2s)}{\frac{\pi}{4} (D_f^2 - D_o^2)s} \frac{180}{980} \right] \quad (2.4)$$

where

σ = surface tension,

ρ_f = density of condensate,

g = acceleration of gravity,

D_f = fin Diameter,

D_o = outside diameter of tube, and

s = fin spacing.

It was shown that condensate retention depends mainly on the ratio of surface tension to liquid density and on the fin spacing.

In 1981, Rudy and Webb [12] measured condensate retention angles on three integral-fin tubes with three fin densities (748, 1024, 1378 fins/m). They used three different fluids (water, R-11, and n-pentane) under both static and dynamic conditions. Their results showed that the retention angle increases with increasing surface tension to density ratio of the fluid. They also showed that the difference between static and dynamic retention angles was very small. For water, they reported that a significant portion of the tube surface was flooded.

In 1982, Rifert [13] reported equation (2.5) for the retention angle using a model of the capillary rise height of the fluid along a vertical plate.

$$\psi = \cos^{-1} \left[1 - \frac{2 \sigma (P - P_f)}{\rho_f g D_o A_p} \right] \quad (2.5)$$

where

P = wetted perimeter,

P_f = fin pitch, and

A_p = Profile area of the fin.

Later, in 1983, Rudy and Webb [14] developed an analytical model to predict condensate retention. They used two finned sections, one in tubular form and the other by splitting the tubular section and unrolling it into a vertical plate. They found that the vertical rise height of the condensate was the same for these two cases. Based on this observation, they modelled condensate retention on a flat plate to express the same on the finned tube. They made a simple force balance on the free body of condensate and

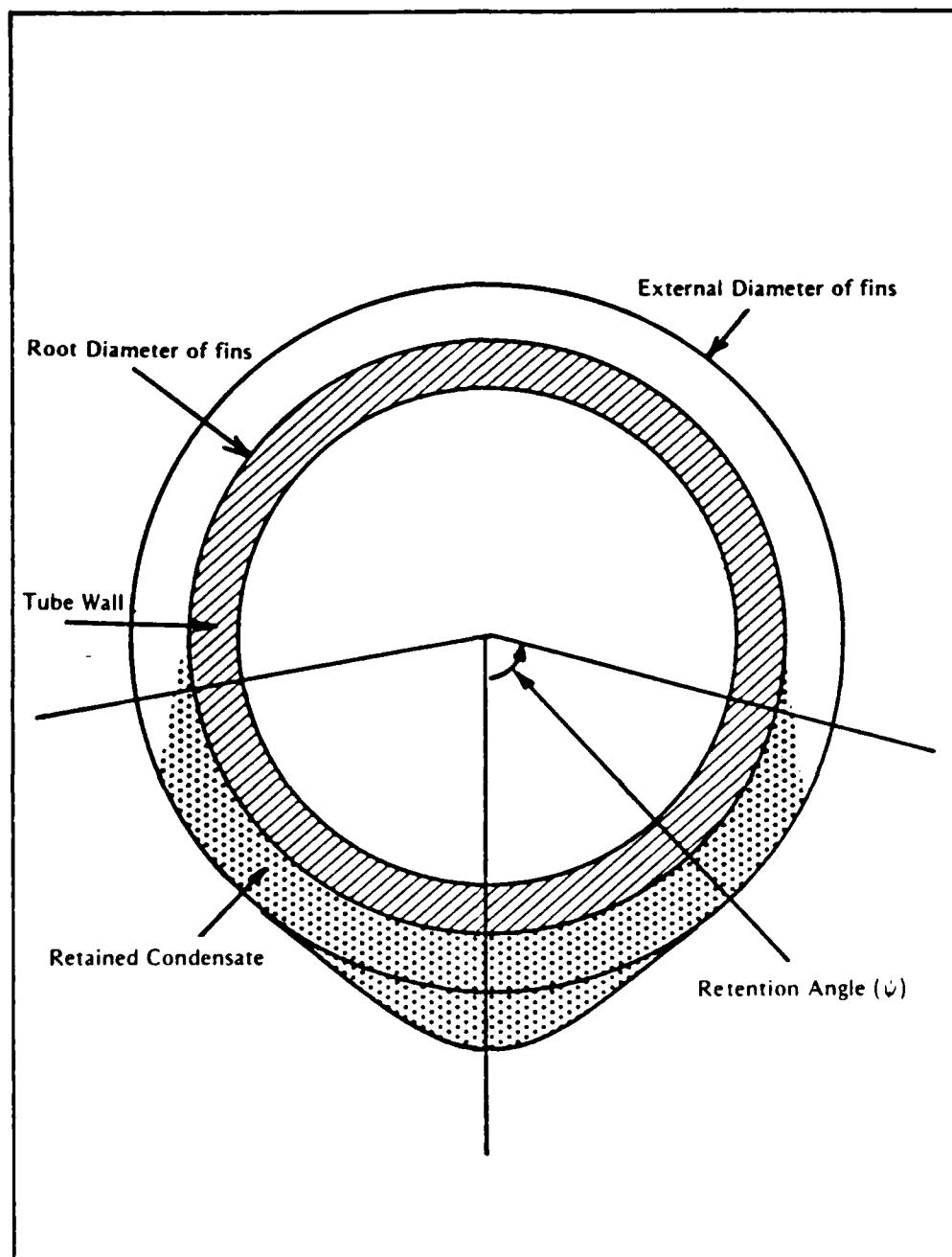


Figure 2.2 Schematic of Condensate Retention on Finned Tubes.

developed an expression for the condensate retention angle as given by equation (2.6):

$$\psi = \cos^{-1} \left[1 - \frac{2 \sigma (2 e - t)}{\rho_f g e s D_o} \right] \quad (2.6)$$

where

e = fin height.

Both their analytical and test results showed that the retention angle increases with increasing surface tension-to-density ratio. Experimental results involving the use of water, R-11, R-12, ammonia, and n-pentane were predicted to within 10 percent.

Owen et al. [15] also recognized the necessity of including the effects of condensate retention in the heat-transfer models. The main simplifying assumption for their model was that the condensate retention angle was independent of condensation rate, so there is no difference between a static test and dynamic condensation. Therefore, they considered only a static analysis. A simple force balance between surface tension and gravitational forces resulted in an equation for the condensate retention angle as shown below:

$$\psi = \cos^{-1} \left[1 - \frac{4 \sigma}{\rho_f g s D_f} \right] \quad (2.7)$$

This equation is the same as equation (2.6), except that equation (2.7) is independent of fin thickness (t). A good agreement between this equation and the available data were reported by Rudy and Webb [12].

In 1983, Honda et al. [16] performed experiments on finned tubes with and without porous drainage plates using R-113 and methanol as working fluids. They revealed from a photographic study that the static and dynamic profiles of the retained condensate were almost the same, and, by attaching a porous drainage plate, they demonstrated a significant reduction in the retention angle. Considering a force balance between gravity and the surface tension force acting on the condensate, they made a theoretical analysis to predict condensate retention, leading to equation (2.8):

$$\psi = \cos^{-1} \left[1 - \frac{4 \sigma \cos \theta}{\rho_f g s n_f} \right] \quad (2.8)$$

where

θ = fin tip half-angle.

They reported very good agreement between their theory, their own data and other available experimental data [11,12].

Yau et al. [9] measured the condensate retention angle using water, ethylene glycol, and R-113 for finned tubes with and without drainage strips. They used an apparatus to simulate condensation on finned tubes. From their results, it appears that a drainage strip attached edgewise to the bottom of a tube has a significant effect on removing the condensate, so liquid retention is significantly reduced. They modified equation (2.8) in order to fit their experimental data, and developed the empirical relation given by equation (2.9):

$$\psi = \cos^{-1} \left[1 - \frac{1.66 \sigma \cos \theta}{\rho_f g s n_f} \right] \quad (2.9)$$

where

θ = fin tip half angle.

Continuing with their investigation on condensate retention, Rudy and Webb [17], in 1985, modified their previous model [14] for predicting condensate retention on horizontal tubes with fins of arbitrary shape. Experiments were made on four finned tubes with fin densities from 748 to 1378 fins/m and one spine tube with a fin density of 1378 fins/m. The fluids tested were R-11, n-pentane, and water. In addition, they tested a Thermoexcel-C tube with fin density of 1417 fins/m and R-11 as the working fluid. As in the previous models, this model is based on the equal capillary rise height for a tubular section and another section that was made by splitting a tube section and unrolling it into a vertical flat surface. Equation (2.10) is recommended to predict the condensate retention angle :

$$\psi = \cos^{-1} \left[1 - \frac{2 \sigma (P_L - t_b)}{D_o \rho_f g [(t_b + s) e - A_p]} \right] \quad (2.10)$$

where

P_L = wetted perimeter of fin cross section,

t_b = fin base thickness, and

A_p = profile area of fin over fin cross section.

From equation (2.10), the retention angle increases for an increase of surface tension to density ratio of the liquid, fin density or for an decrease of tube diameter.

For the case of a horizontal tube with rectangularly-shaped fins, equation (2.10) reduces to equation (2.7). The experimental deviation from the predictive value of equation (2.10) was ± 10 percent.

C. THEORETICAL MODELS

In 1948, Beatty and Katz [18] performed experiments with propane, n-butane, n-pentane, sulfur-dioxide, methyl chloride, and Freon-12 condensing on single finned tubes with fin densities from 422 to 630 fins/m to obtain the vapor-side heat-transfer coefficient. They used the Nusselt equations for condensation on a horizontal tube and on a vertical surface, and considered the finned tube to be a combination of two parts, a horizontal plain tube and vertical fins. Thus, they expressed the average heat-transfer coefficient by a Nusselt-type equation based on an equivalent diameter. They modified the customary leading constant (0.728) found in the Nusselt equation to fit their experimental data and their correlation is given below:

$$\bar{h}_{BK} = 0.689 \left[\frac{k_f^3 \rho_f (\rho_f - \rho_v) g h_{fg}}{\mu_f \Delta T} \right]^{1/4} \left[\frac{1}{D_e} \right]^{1/4} \quad (2.11)$$

$$\left[\frac{1}{D_e} \right]^{1/4} = \frac{A_r}{A_{eff}} \left[\frac{1}{D_o} \right]^{1/4} + 1.3 \frac{\eta A_f}{A_{eff}} \left[\frac{1}{x} \right]^{1/4} \quad (2.12)$$

where

$$A_r = \pi D_o L \quad (2.13)$$

$$A_f = \frac{\pi}{2} (D_f^2 - D_o^2) N L \quad (2.14)$$

$$A_{eff} = A_r + n A_f \quad (2.15)$$

$$x = \frac{\pi (D_f^2 - D_o^2)}{4 D_f} \quad (2.16)$$

where

A_{eff} = effective area of finned tube,

A_f = total surface area of finned tube,

A_r = surface area of smooth tube,

D_e = equivalent tube diameter,

h_{BK} = average vapor-side heat-transfer coefficient,

h_{fg} = specific enthalpy of vaporization,

k_f = thermal conductivity of condensate,

n = fin efficiency,

ΔT = vapor-side temperature drop,

μ_f = viscosity of condensate, and

ρ_v = density of vapor.

The empirically determined leading constant (0.689) in equation (2.11) is only 5 percent less than the theoretically derived constant (0.728) using Nusselt theory. But the average heat-transfer coefficient is greater than that predicted by Nusselt theory for a smooth tube since the equivalent diameter is smaller than the outside diameter of

the tube. They claimed a maximum error of + 7.2 percent and - 10.8 percent for the fluids they tested. However, they did not take into account surface-tension effects for thinning the condensate along the fin height. They also neglected condensate retention and assumed gravity to be entirely responsible for the flow of condensate. Over the decades following their work, many researchers have found this model to be quite adequate for low-surface-tension fluids and for tubes with moderate fin densities (i.e., for condensing fluid-fin density combinations to yield low retention angles). However, as the fin density or the surface tension increases, the model tends to overpredict the heat-transfer coefficient [12].

Some years later in 1971, analytical and experimental studies of condensation on horizontal tubes with trapezoidally shaped fins were performed by Karkhu and Borovkov [19] for condensation assuming surface tension to create the dominant force. The analytical solutions were based on the following assumptions: 1) the thin condensate film represents a laminar boundary layer; 2) surface tension causes a pressure gradient along the fin side; 3) gravitational and inertial terms in the equation of motion of the film along the side of the fins were small compared to surface tension terms and were neglected; 4) the motion of condensate in the trough area is laminar; 5) condensate drains by gravity into the trough; 6) no condensation takes place on the flooded portion of the tube; and 7) the fin temperature is constant along the height of the fin. Using Nusselt's basic assumptions and the differential equation of condensate motion (assuming radial flow of condensate feeding into the interfin space) with appropriate boundary conditions, they were able to obtain the thickness of the condensate film in the interfin spacing (equation (2.17)). In order to calculate the temperature distribution along the fin height, they

assumed one-dimensional heat conduction. Using numerical methods to solve the resulting differential equations, they found expressions for the heat-transfer coefficient:

$$Z_b = 1.6 H^{0.2} (1 - 0.35 H^{-0.3} m) \quad (2.17)$$

$$\bar{h} = \frac{G h_{fg}}{F_S \Delta T} \quad (2.18)$$

where

$$F_S = \frac{s}{2} + b + \frac{e}{\cos \theta} - \frac{\pi D_o}{2} \quad (2.19)$$

$$\overline{\Delta T} = 0.38 + 0.62 n^{+1} - 0.012 n \quad (2.20)$$

$$n = 1.4 \frac{[\rho_f h_{fg} \sigma]^{1/4} k_f^{3/4} e^{3/2}}{[\mu_f b \Delta T]^{1/4} k [1 + \tan \theta] [2 b + e \sin \theta]} \quad (2.21)$$

where

$$H = 2.86 \frac{\sigma^{1/4} (\mu_f k_f T_s)^{3/4} R_o}{\sin^3 \theta (1 + \tan \theta)^{1/4} \cos^{1/4} \theta \rho_f^{7/4} e^{7/2} h_{fg}^{3/4}} \quad (2.22)$$

$$We = \frac{\sigma \cos \theta}{b (1 + \tan \theta) e \rho_f} \quad (2.23)$$

where

b = half of fin tip width,

e = fin height,

- F_s = effective condensate surface,
- G = condensate flow rate,
- h = heat-transfer coefficient,
- Z = dimensionless depth of condensate between fins,
- Z_b = dimensionless depth of condensate at fin base, and
- θ = fin semivertex angle.

Experiments were performed with four different finned tubes to condense both steam and R-113 with slowly moving vapor and when the Weber number (equation (2.23)) is greater than 10. Using the measured temperature at the fin root, they found equation (2.21) for the dimensionless depth of the condensate at the fin base within ± 2 percent of the experimental data. Also, they solved the heat conduction equation over the fin to find the temperature distribution over the fin height (equation (2.19)). They found the vapor-side coefficients to be 50 to 100 percent greater than that for a smooth tube. Further, they reported that their predictions agreed to within ± 5 percent with their experimental data.

In 1973, Edwards et al. [20] reported an analytical model for condensation on circumferential grooves on horizontal tubes that included the surface tension effect, gravity, viscous, capillary pressure, and condensate acceleration during the flow around the tube. This model is based on the following assumptions: 1) the condensate pressure is uniform over any cross section; 2) the radius of curvature of the meniscus in the flow region at the trough is constant; 3) the heat transfer and vapor friction on the meniscus are negligible; 4) the draining condensate from the fin side has zero velocity; 5) the grooves have small

height compared to the tube radius; and 6) the film has a contact angle to the fin tip.

Using conservation of mass, with the overall heat-transfer coefficient as a function of local pressure difference and making a simple force-momentum balance over an element of condensate film, they found a relationship for the local heat-transfer coefficient as given by equation (2.24):

$$h = \frac{2}{w} \left[\frac{k_f k_m \theta_g}{\theta_c + \theta_o} \right]^{1/2} \quad (2.24)$$

where

$$\theta_o = \frac{1}{2} \left[z \left(\ln \frac{1}{z} + 0.11593 \right)^2 \cot \theta_g \right] \quad (2.25)$$

$$z = 2 \left[\frac{2 k_f \tan \theta_g}{\theta_g k_m} \right]^{1/2} \quad (2.26)$$

where

k_f = liquid thermal conductivity,

k_m = fin thermal conductivity,

w = groove width,

θ_c = contact angle, and

θ_g = groove half angle.

They assumed no heat transfer through the flooded portion of the tube. Further, they assumed only circumferential flow of condensate, thus neglecting any flow along the fin surface in the radial direction. While this assumption could result in poor predictions, they did not provide a comparison of their theory with any experimental data.

In 1977, Zozulya et al. [21] modified their previous model [19] to find expressions for the rate of heat transfer. Using the differential equation of condensate motion at the trough, and the average temperature difference determined by numerical methods, they arrived at equation (2.27) which gives the dimensionless height of the condensate at the interfin spacing:

$$Z = 1.8 F_i^{0.32} \quad (2.27)$$

$$F_i = \frac{2 \sigma^{1/2} (k_f \mu_f \Delta T)^{3/4} \cos^{5/4} \phi D_o}{t_b t_f h_{fg}^{3/4} e^{5/2} (\rho_f g)^{1/4} (1 + \tan \phi)^{1/4}} \quad (2.28)$$

b = thickness at top of fin,

t_b = thickness at fin base, and

z = dimensionless condensate film thickness

in the interfin spacing.

They compared the results of equation (2.27) and available data of refrigerants (R-11, R-12, and R-21) for condensation on finned tubes manufactured of copper, brass, and steel with rectangular and trapezoidal fin-shapes. Also, they compared experimental data for condensation of R-113 and steam on different finned tubes. Discrepancies within ± 15 percent were reported.

In 1979, Webb [22] reported a procedure for the design and optimization of a fin surface for heat-transfer performance. Equations (2.31), (2.32) and (2.33) were recommended to calculate the optimum profile given by equation (2.29) in order to maximize the heat-transfer coefficient given by equation (2.30):

$$S_{opt} = \left(\frac{1}{5\beta} + \frac{F_1}{h_w} \right)^{4/3} \quad (2.29)$$

$$h_w = 1.055 F_1 (F_1 F_2)^{-0.2} \quad (2.30)$$

$$F_1 = K (B \theta_m)^{1/4} \quad (2.31)$$

$$F_2 = \frac{25 \sigma}{\pi g} \frac{2 L \Delta T}{\rho_f} \quad (2.32)$$

$$B = \frac{h_{fg} \rho_f g \sigma}{\mu_f k_f \Delta T} \quad (2.33)$$

where

h_w = heat-transfer coefficient,

p = projected area of convex surface,

S = value of s at $\theta = \theta_m$,

θ = angular coordinate measured,

from the crest of convex surface, and

$\beta = p/2S$.

According to the author, this model underpredicts the heat-transfer coefficient. The calculated augmentation ratio based on the projected surface area h_p/h_{Nu} ranged from 3.4 to 3.8 for tubes with length from 4 ft to 40 ft while his experiment showed values in the range from 4 to 8.

In 1980, Rifert [23] studied condensation of stationary vapor on horizontal finned tubes enhanced by the effect of surface-tension forces that tend to pull the condensate to the fin root. In his analysis, he divided the tube into two

zones: a) the unflooded zone where the condensate film is thin, and b) the flooded zone where the condensate film is thick. He solved the two-dimensional heat-conduction problem for the wall by numerical methods for each zone and then determined the mean heat flux. In cases where condensate is retained in more than half of the tube perimeter, Rifert pointed out that a three-dimensional form of the heat-conduction equation must be used. Solutions to these equations by numerical methods revealed that, in most cases, the fin temperature is very nonuniform and it depends on the properties of the wall and the vapor and the heat flux. He stated that for the highly non-isothermal fin surface, the use of an average temperature drop from vapor to the outer wall temperature (ΔT) yields computed heat flux values that are very sensitive to ΔT . Since this is unacceptable, he recommended the use of the average heat flux for the computation.

In 1981, Adamek [24] presented a method for the design of an optimum surface for condensing heat-transfer performance. Similar to other researchers [7,8,22], Adamek recognized the importance of surface tension on the heat-transfer performance of finned surfaces. Since the dominant force on the crest is the surface tension, he neglected gravitational forces in this region. He derived equations for the condensate film thickness (equation (2.34)) and the wall surface profile by defining the curvature as a function of the distance along the surface (equation (2.35)). Using equation (2.36) for the curvature of the profiles of the wave crest, and the necessity that the pressure within the condensate must decrease from wave crest to the trough, he defined a family of condensate surface profiles, whose curvatures are given by equation (2.38). A number of ξ values and their corresponding condensate surface profiles are shown in Figure 2.3. He found equations (2.37), (2.39),

and (2.40) for the film thickness, the average heat-transfer coefficient and condensate flowrate, respectively. The parameter ξ in equation (2.37) characterizes the aspect ratio of the fin cross section (ratio of the height to the thickness). As the aspect ratio increases, the parameter ξ decreases. As shown by Adamek, $\xi = -0.5$ represents the optimum surface for maximum values of the condensate flowrate and the average heat-transfer coefficient.

$$\delta(s) = \left[(\kappa)^{-1/3} \left(4 \int_0^{\delta} C(\kappa)^{1/3} ds + C_0 \right) \right]^{1/4} \quad (2.34)$$

$$W(s) = f(s) - \delta(s) \eta_f(s) \quad (2.35)$$

$$\kappa(s) = \alpha s^{\xi} - \kappa_0 \quad -1 < \xi < 0 \quad (2.36)$$

$$\delta(s) = 12 \left[\frac{k_f \mu_f \Delta T}{\sigma h_{fg}} \frac{1}{O_m} \frac{S_m^{\xi+1} s^{2-\xi}}{(\xi+1)(\xi+2)} \right]^{1/4} \quad (2.37)$$

$$\frac{1}{r} = \frac{\theta_m}{S_m} \frac{(\xi+1)}{\xi} \left[1 - \left(\frac{s}{S_m} \right)^{\xi} \right] \quad (2.38)$$

$$\bar{h} = 2.149 \frac{k_f}{S_m} \left[\frac{\sigma h_{fg} O_m S_m \rho_f (\xi+1)}{\mu_f k_f \Delta T (\xi+2)^3} \right]^{1/4} \quad (2.39)$$

where

$W(s)$ = wall profile,

$f(s)$ = film profile,

$\kappa(s)$ = local curvature of the condensate surface,

s = length of path in liquid film,

S_m = length of convex surface over which
the condensate flow,

δ = film thickness,

θ = rotation angle of normal to fin surface,

Θ_m = angle from origin to S_m ,

ξ = ratio of slenderness, and

r = radius of curvature.

In 1981, Shklover et al. [25] treated film condensation for finned tubes to investigate the effect of metal thermal conductivity on the heat-transfer performance. Stationary steam was used as the condensing fluid. They showed that as the thermal conductivity decreases, the temperature difference through the film decreases and the temperature difference through the wall increases. For this reason, the finned tubes made of stainless steel or german silver have the same heat-transfer performance as the smooth tube, while brass and copper finned tubes outperformed the smooth tubes.

Rudy and Webb [12] proposed a possible improvement to the Beatty and Katz [18] model by taking into consideration condensate retention. They applied equation (2.11) only for

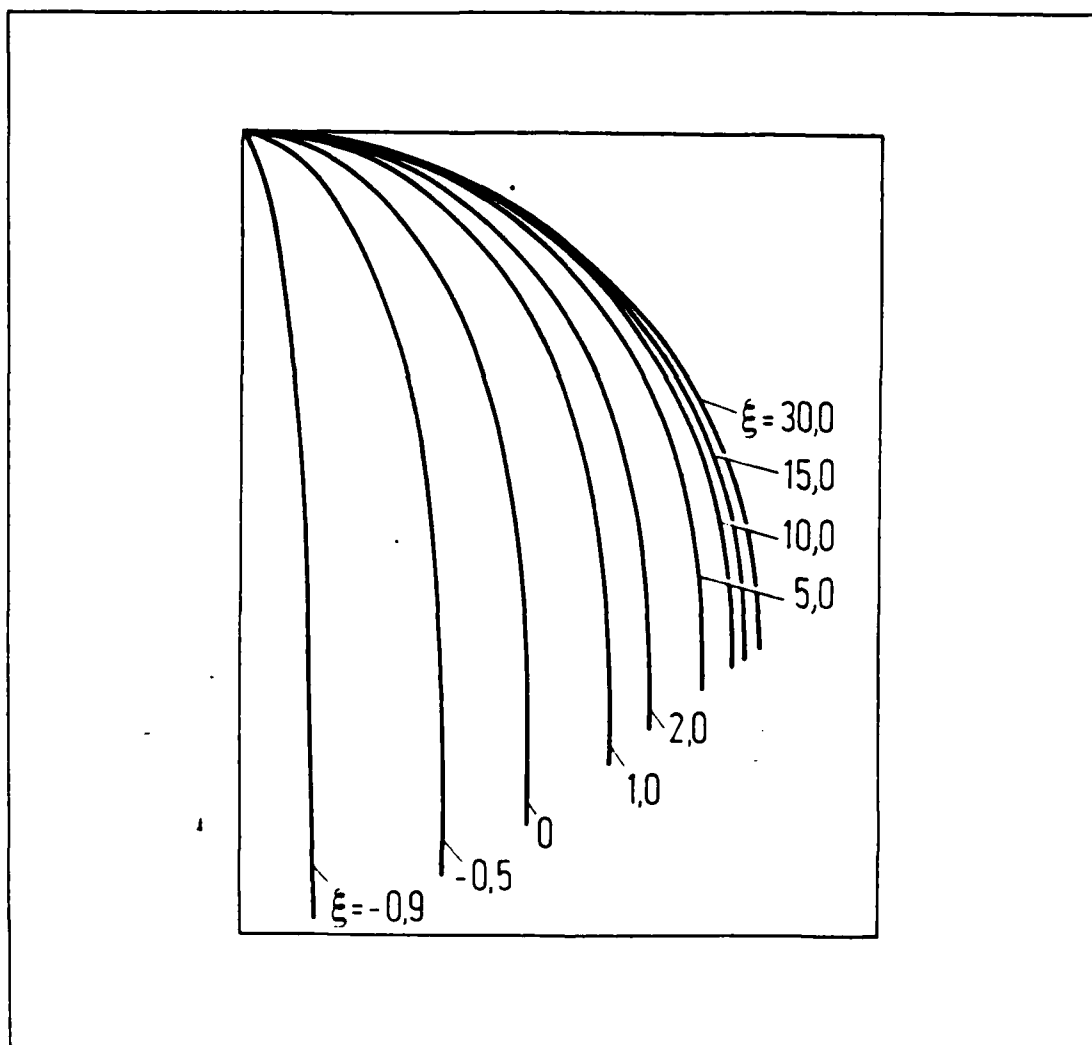


Figure 2.3 Adamek [24] Condensate Surface Profiles.

the unflooded part of the tube and recommended equation (2.41) for the average heat-transfer coefficient.

$$\bar{h} = h_{BK} \left[\frac{\pi - \psi}{\pi} \right] \quad (2.41)$$

where h_{BK} is computed using equation (2.11). But, since this is a gravity-based model and it neglects any heat transfer through the flooded portion of the tube, it underpredicts the average heat-transfer coefficient of condensing R-11 by 10 to 30 percent. They recognized that the surface tension effect must be taken into account.

In 1982, Webb et al. [26] developed a new model which included surface tension effects. They modified the original Nusselt equation for a vertical plate so that surface tension causes the condensate to drain from the fin tip to the base and gravity causes the condensate to flow in the channel between the fins. Assuming surface tension as the dominant force along the fin side, they proposed equation (2.42) for the fin side coefficient h_{fin} and the average heat-transfer coefficient for the entire tube is given by equation (2.43):

$$h_{fin} = 0.943 \left[\frac{k_f^3 \rho_f h_{fg}}{\mu_f \Delta T} \right]^{1/4} \left[\frac{2\sigma}{e^2} \left(\frac{1}{s} + \frac{1}{t} \right) \right]^{1/4} \quad (2.42)$$

where h_b was computed using the Nusselt [27] equation, and

$$h = \frac{A_r}{A_p} h_b + n_f \frac{A_f}{A_p} h_{fin} \quad (2.43)$$

This model predicted the heat-transfer coefficient within ± 10 percent for R-12.

Using equation (2.7) for the condensate retention angle they developed earlier, Owen et al. [15] modified the Beatty and Katz model to include the retention angle. They divided the tube into two parts: the unflooded portion, and the flooded portion with the condensation occurring on both the retained condensate and the fin tips. The equations necessary for this model are listed below:

$$\bar{h} = \frac{(\pi - \psi)}{\pi} h_u + \frac{\psi}{\pi} h_f \frac{A_t}{A_s} \quad (2.44)$$

where h_u was computed using equation (2.11) with a leading coefficient of 0.725 instead of the value of 0.689, and

$$h_f = \left(\frac{1}{h_{eff}} + \frac{1}{h_c} \right)^{-1} \quad (2.45)$$

where h_c was computed using Nusselt [27] equation, and

$$h_{eff} = \frac{k_{eff}}{e} \quad (2.46)$$

$$k_{eff} = (1 - sN) k_{fin} + sNk_f \quad (2.47)$$

where

h_u = heat-transfer coefficient for the unflooded portion of the tube,

h_c = heat-transfer coefficient for a plain tube,

h_f = heat-transfer coefficient for the flooded portion of the tube,

h_{eff} = heat-transfer coefficient of the combined fin and retained condensate,

k_{eff} = effective thermal conductivity,

k_{fin} = fin thermal conductivity,

N = number of fins per meter, and

ψ = retention angle.

s = fin spacing

Owen et al. showed their model to predict the data for R-11, R-22, methyl chloride, n-pentane, sulfur dioxide, propane, and n-butane to within ± 30 percent. However, as shown by Honda and Nozu [16], this model overpredicted the steam data by up to a factor of 2.

In 1983, Rudy and Webb [29] developed a model based on surface-tension-induced linear pressure gradient along the fin height, thus assuming radial flow of the condensate feeding into the interfin space. Further, they assumed gravity-drained flow of condensate in the space between fins. The Nusselt equation for horizontal tubes was used for the tube area between fins, while the fin surface was treated by replacing the body-force term (i.e., " ρg ") in the Nusselt equation by an equivalent expression based on surface-tension-induced pressure gradient as developed by Webb et al. [26] and Rudy [28] earlier. Once again, they assumed no heat transfer through the flooded portions and the resulting expression is given by equation (2.48):

$$\bar{h} = \left\{ 0.725 \frac{\pi D_o L}{A_{bt}} \left[\frac{k_f^3 \rho_f^2 h_{fg} g}{D_o \mu_f \Delta T} \right]^{1/4} + 0.943 n \frac{A_{ft}}{A_{bt}} \left[\frac{k_f^3 \rho_f h_{fg} \sigma (r_A + r_B)}{\mu_f e^2 r_A r_B \Delta T} \right]^{1/4} \right\} \left(\frac{\pi - \psi}{\pi} \right) \quad (2.48)$$

where

L = length of tube,

A_{bt} = surface area of tube between fins, and

A_{ft} = fin surface area.

This expression provided an accuracy of better than 10% for condensation of R-11 on short, finely-spaced fins, but the accuracy dropped sharply with fins of increasing height and for larger fin spacing. This was, according to the authors, due to the assumed linear pressure gradient on the fin surface as this model is not valid when gravity forces become dominant (i.e., as e increases). Therefore, equation (2.48) is valid for fin densities from 1200 to 1400 fins/m, and fin heights of less than 1 mm.

Continuing their research on film condensation, Honda et al. [16] did experiments on horizontal finned tubes by attaching a vertical drainage strip at the bottom of the tube to reduce condensate retention. Using R-113 and methanol as condensing fluids, they found vapor-side enhancement ratios (compared to the case without drainage strips) as high as 1.36 for R-113 and 2.08 for methanol.

In 1984, Honda and Nozu [30] developed an analytical model for film condensation on horizontal low integral-fin tubes. They divided the tube into flooded and unflooded regions. This model is based on the following assumptions: 1) the wall temperature is uniform; 2) the flow is laminar; 3) the condensate film thickness is small; 4) the dominant flow on the fin is in the radial direction. Based on these assumptions, expressions for Nusselt number representing the flooded and unflooded regions were found. The average Nusselt number is given by equation (2.49):

$$Nu_d = \frac{(Nu_{du} n_u (1 - \bar{T}_{wu}) \bar{\phi}_f + Nu_{df} n_f (1 - \bar{T}_{wf}) (1 - \bar{\phi}_f))}{(1 - \bar{T}_{wu}) \bar{\phi}_f + (1 - \bar{T}_{wf}) (1 - \bar{\phi}_f)} \quad (2.49)$$

where

$$n_u = \text{Fin Efficiency,}$$

n_f = fin efficiency for the flooded region,
 Nu_d = average Nusselt number,
 Nu_{du} = average Nusselt number for the unflooded region,
 Nu_{df} = average Nusselt number for the flooded region,
 ϕ = angular coordinate,
 T_{wu} = dimensionless temperature for the unflooded region, and
 T_{wf} = dimensionless temperature for the flooded region.

Comparison of the results of this model with the available experimental data showed agreement to within ± 20 percent for 11 fluids and 22 finned tubes. However, their model overpredicted steam data by up to 40 percent.

In 1985, Rudy and Webb [31] modified their previous models taking into account surface-tension effects on film drainage and condensate retention. They treated the condensation problem considering two major regions: unflooded and flooded regions. They further divided the unflooded region into finned area and the interfin area. They computed the average heat-transfer coefficient for the entire tube as given by equation (2.29).

$$h_{RW} = h_{no} = \left[h_r \frac{A_r}{A} + n h_{fin} \frac{A_f}{A} \right] \left[\frac{\pi - \psi}{\pi} \right] + h_f \frac{\psi}{\pi} \quad (2.50)$$

In order to compute the heat-transfer coefficient for the finned area (h_{fin}), they used an expression developed by Adamek (equation 2.39)). One of the profiles they used for

the trapezoidal-shaped fin is shown in Figure 2.4. They used equation (2.38) with $\theta_m = 85$ degrees and for each fin geometry an iterative procedure to establish the ξ value for each profile to correct the fin thickness at the fin base given by equation (2.51).

$$t = t_b - t_t + 2 \delta(S_m) \quad (2.51)$$

Further, since they assumed that the length of the convex surface is from fin tip to fin base, they corrected for the film thickness equation (2.52) resulting from the additional condensation at the fin tip:

$$S_m = S_m + t/2 - \delta_r \quad (2.52)$$

where

$$\delta_r = \frac{k_f}{h_r} \quad (2.53)$$

where h_r is the heat-transfer coefficient for the interfin area in the flooded region. In order to calculate the interfin area (h_r), they used the Nusselt equation with an iteration to account for the additional condensate drainage from the fins. Finally, to compute the heat-transfer coefficient in the flooded region they used the following equations:

$$\beta = q_{b2} / q_{b1} \quad (2.54)$$

$$q_{b1} = k \frac{\Delta T}{e} = h_f \Delta T \quad (2.55)$$

$$h_f = \beta \frac{k_f}{e} \quad (2.56)$$

where q_{b1} is the heat flux if the fin thickness were zero. Using a numerical technique, they computed q_{b2} based on two-dimensional conduction through the fins and the condensate film.

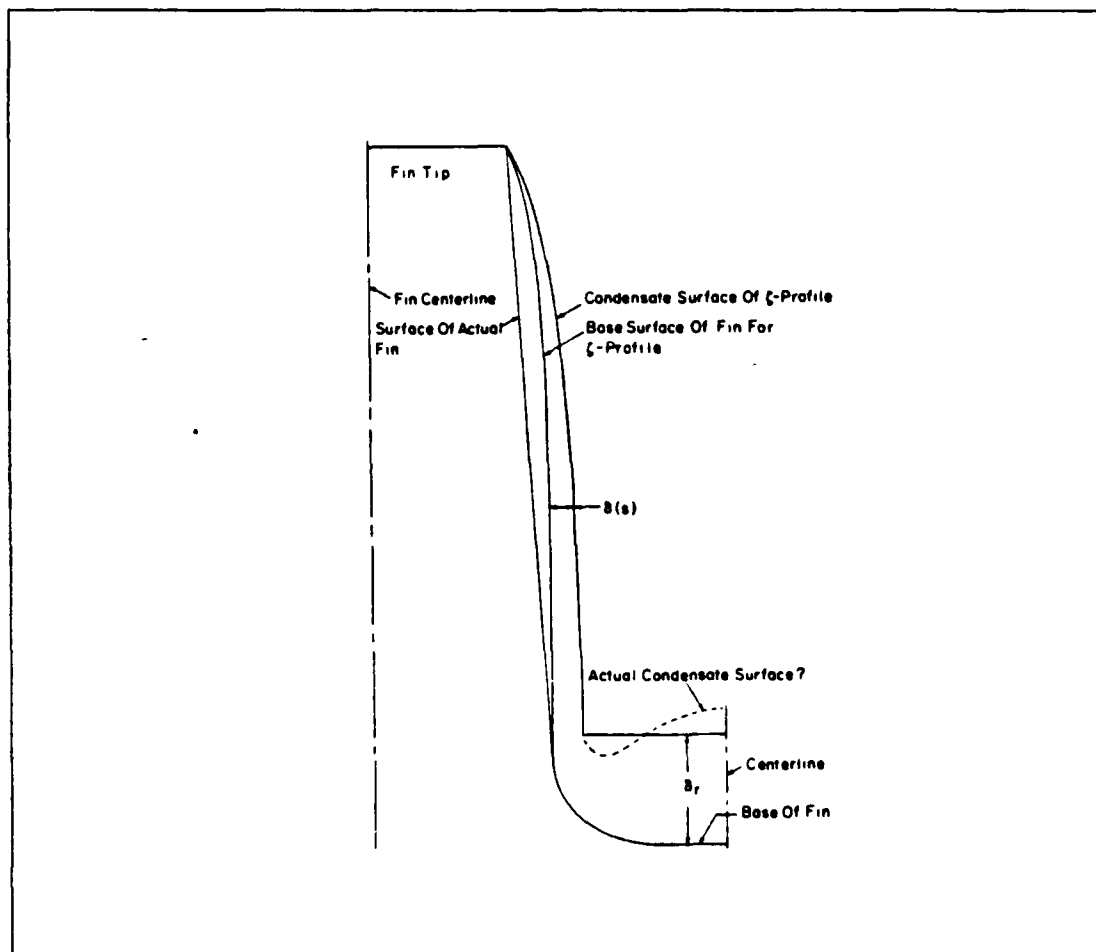


Figure 2.4 Fin Geometry for the Webb et al. Model [31].

D. FILMWISE CONDENSATION ON WIRE-WRAPPED TUBES

Similar to fin tubes, surface-tension effects can be beneficial for filmwise condensation on wire-wrapped tubes. However, the surface-tension effect on wire-wrapped tubes is different than that on finned tubes mainly because of the very little heat transfer through the wires compared to fins that would transfer the majority of the heat.

As can be seen from Figure 2.5, the condensate surface in the space between wires on the wire-wrapped tube is rather flat and the pressure difference between the condensate and the surrounding vapor is zero. However, due to the existence of a concave condensate surface at the point of contact between the wire and the condensate surface, a reasonable pressure difference within the condensate will exist from the inter-wire space to the immediate vicinity of the wire. In fact, the pressure at point A is the smallest, thus resulting in a condensate flow toward the wire, at which point the condensate would rapidly flow around the tube and eventually leave the tube at the lowest point. This axial flow of condensate toward the wires generally results in a smaller film thickness than on a plain tube. On the other hand, the film is generally quite thick in the region between the wire and the tube, resulting in negligible heat transfer through this region. As can be seen from Figure 2.5, the radius of curvature of the condensate surface near the wire strictly depends on the wire diameter. Further, the extent of thinning of the condensate film depends on the wire spacing. Based on the above-mentioned observations, an optimum combination of wire diameter and pitch must exist to yield the best heat-transfer performance.

In 1985, analytical and experimental studies of condensation on horizontal wire-wrapped tubes were performed by Fujii et al. [32]. Their model is based on the following

assumptions: 1) the liquid film is very thin compared to the diameter of the tube; 2) the condensate film flow is laminar; 3) the inertia forces in the momentum equation of the condensate are negligible; 4) the shear stress at the vapor-liquid interface is negligible; 5) the properties of the condensate are constant; and 6) the temperature of the cooling surface is uniform. They also assumed that heat transfer occurred only through the thin film between wires and they neglected any heat transfer through the wires. They developed semi-theoretical equations to predict a heat-transfer coefficient enhancement ratio as shown below:

$$\frac{Nu_w}{Nu_s} = \frac{s}{(s + D_w)} \frac{F_2(A)}{F_2(0)} \quad (2.57)$$

where

$$F_2(A) = \frac{1}{\pi} \int_0^\pi F_1(\phi, A) d\phi \quad (2.58)$$

and

$$F_1(\phi, A) = \frac{(\tan(\phi/2))^{A/3} (\sin \phi)^{1/3}}{\left[\int_0^\phi (\tan(\phi/2))^{4A/3} (\sin \phi)^{1/3} d\phi \right]^{1/4}} \quad (2.59)$$

where

$$A = \frac{4 \sigma D_o}{\rho_f g s^2 r_s} \quad (2.60)$$

$$r_s = C \left[\frac{2 \sigma}{\rho_f g} \right]^{3/2} D_w^{-2} \quad (2.61)$$

They noticed that for $A > 15$

$$F_1(\phi, A) = F_1(0, A) = \left(\frac{4(1+A)}{3} \right)^{1/4} \quad (2.62)$$

Therefore, in this situation with $A > 15$,

$$F_2(A) = \left[\frac{4(1+A)}{3} \right]^{1/4} \quad (2.63)$$

$$F_2(0) = \left(\frac{4}{3} \right)^{1/4} \quad (2.64)$$

and equation (2.57) simplifies to¹ :

$$\frac{Nu_w}{Nu_s} = \frac{s}{(s + D_w)} \left[\frac{4(1+A)}{3} \right]^{1/4} \quad (2.65)$$

They selected a value of 0.03 for the coefficient C in equation (2.61) in order to fit their experimental data. Experiments were performed with three wire-wrapped tubes to condense ethanol and R-11 vapor. Enhancement ratios of 3.7 and 3.3 for R-11 and ethanol, respectively, were reported (see Figure 2.6). The maximum enhancement ratio occurred at a p/D_w value of 2.

¹In the original Fujii et al. paper equation (2.65) contained an error by retaining the term $(4/3)^{1/4}$.

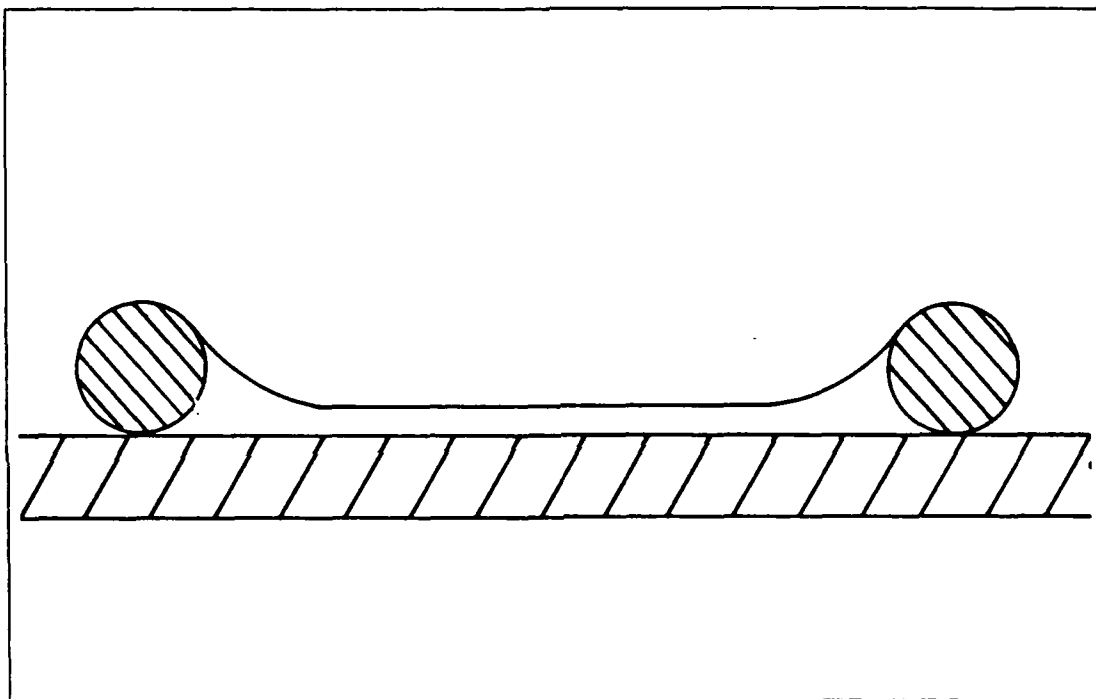


Figure 2.5 Condensate Film Profile on Wire-Wrapped Tubes.

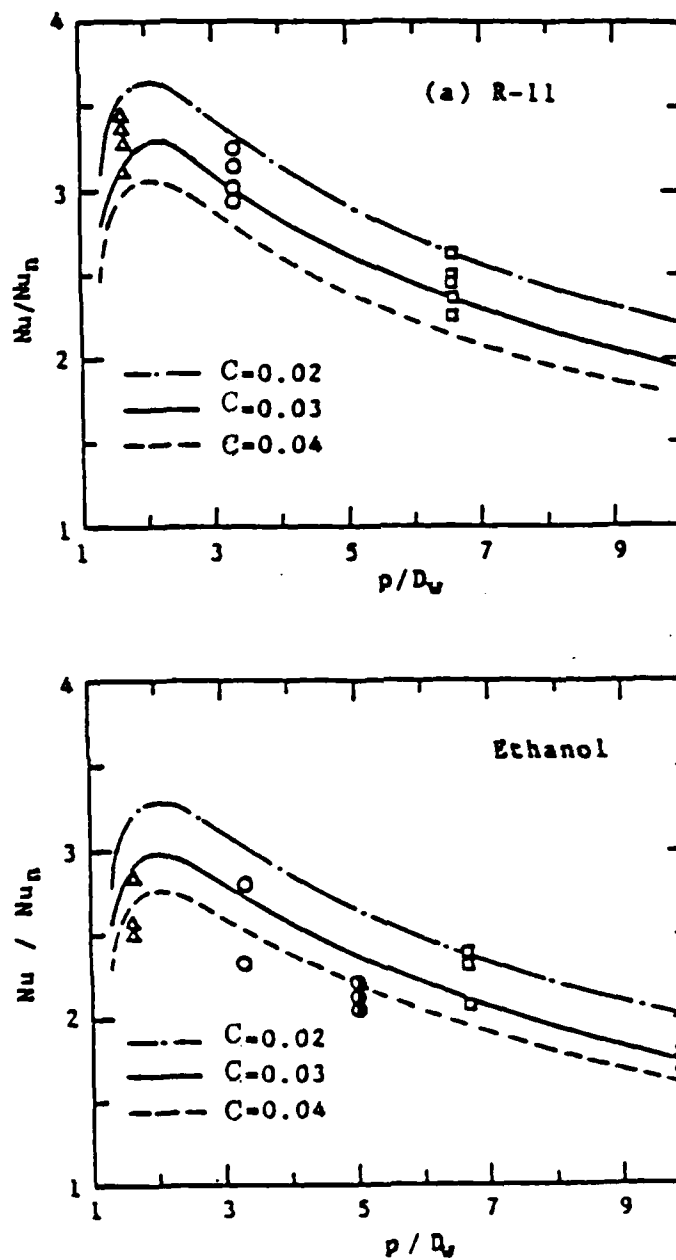


Figure 2.6 Comparison Between Experimental Data and Semi-Theoretical Model of Fujii et al. [32].

III. DESCRIPTION OF TEST APPARATUS

A. TEST APPARATUS

The test apparatus used for this investigation was essentially the same as used by Georgiadis and Flook [5,6]. A schematic of this apparatus is shown in Figure 3.1. Steam was generated using distilled water in a 304.8 mm (12 in.) Pyrex glass section which was fitted with ten 4000-Watt, 440-Volt Watlow immersion heaters. The steam from the boiler flowed upward and passed through a 304.8 mm (12 in.) to 152.4 mm (6 in.) reducing section to a 2.44 m (8 ft.) long section of Pyrex glass piping. The steam flowed through a 180-degree bend and entered a 1.52-m-long section before finally entering the stainless-steel test section, which is shown in Figure 3.2. The test tube was mounted horizontally in the test section. A portion of the steam condensed on the test tube, while the excess steam travelled downward and condensed in the auxiliary condenser. The condensate drained back to the boiler by gravity, completing the closed-loop operation of the system.

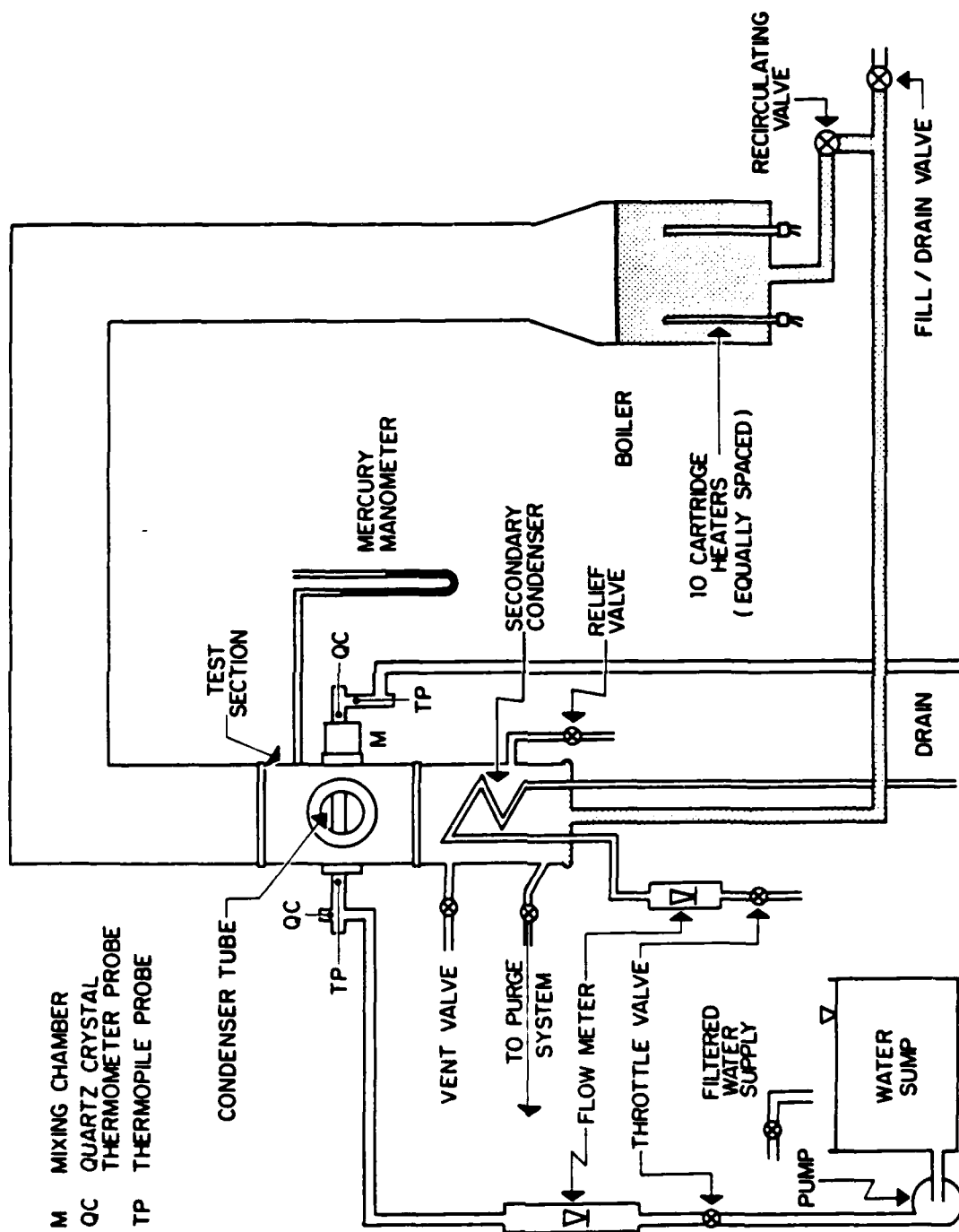
The exit side of the test tube was provided with a mixing chamber for accurate measurement of the outlet temperature of the coolant. A view port was provided in the test section to allow visual observation of the condensation mode to ensure complete filmwise condensation during data collection. The auxiliary condenser consisted of two 9.5 mm (3/8 in.) diameter water-cooled copper tubes helically coiled to a height of 457 mm (18 in.). The auxiliary condenser was cooled by a continuous supply of tap water through a flow meter. A throttle valve was provided to control the flow rate through the auxiliary condenser, thus keeping the system at the desired internal pressure. For example, when the flowrate through the test tube was

decreased, the flowrate through the auxiliary condenser had to be increased. Filtered tap water was collected in a large sump with a capacity of about 0.4 cubic meters (Figure 3.3), and was used to cool the test tube. Two centrifugal pumps connected in series took the water from the sump and passed it through a flow meter into the test tube. A valve on the discharge side of the second pump, and before the flow meter, allowed the velocity of water flowing through the test tube to be varied from 0 to 4.4 m/s (14.4 ft/sec).

A vacuum pump was operated continuously during the operation of the apparatus to remove non-condensing gases from the test section. The system used to remove non-condensing gases is shown in Figure 3.3. It was unavoidable that the vacuum pump mainly drew steam with trace amounts of air (non-condensing gases). To minimize the contamination of the pump by the steam, another condenser was provided to condense as much steam as possible. This condenser was cooled with the filtered tap water before it entered the large sump. The condensate from this steam collected in a Plexiglas cylinder to be drained later.

B. INSTRUMENTATION

The electrical power input to the boiler immersion heaters was controlled by a panel-mounted potentiometer. In order to compute the input power to the boiler, a root-mean converter with an input voltage of 440 VAC generated a signal which was fed to the data acquisition system. A more-detailed description of the boiler power supply is provided by Poole [4]. The temperatures of the steam, condensate and the ambient surroundings were measured using calibrated copper-constantan thermocouples made of 0.25-mm-diameter wires. Two of them were used for the steam temperature, one for the condensate return and one for the ambient temperature. These thermocouples had an accuracy within ± 0.1 K. when compared against a platinum-resistance



M MIXING CHAMBER
 QC QUARTZ CRYSTAL
 THERMOMETER PROBE
 TP THERMOPILE PROBE

Figure 3.1 Schematic of Test Apparatus.

thermometer. Since the temperature rise of the coolant through the test tube is the most critical measurement, considerable attention was paid to obtaining the highest possible accuracy. For this purpose two independent temperature measurement techniques were used: a Hewlett-Packard (HP) 2804A quartz thermometer with two probes having an accuracy of ± 0.02 K, along with a 10-junction, series-connected copper-constantan thermopile with a resolution of 0.03 K.

For most of the data collected, the quartz thermometer and the thermopile agreed to within ± 0.03 K and when the difference was more than ± 0.05 K, the data set was disregarded and a repeat set was made. The cooling water flow rate was measured using a calibrated rotameter and the value was fed manually to the computer. Another rotameter was provided to measure the cooling water flow rate through the auxiliary condenser.

A pressure tap located about 50 mm above the test tube was connected to a U-tube, mercury-in-glass manometer graduated in millimeters to measure the absolute pressure of the system. At the beginning and at the end of each test run, an accurate pressure reading was made and entered into the computer. The measured system pressure and the saturation pressure corresponding to the measured steam temperature were used to compute the concentration of any air that might have been present. For this purpose, a Gibbs-Dalton-type relationship was used. The computed non-condensing gas concentration was found to be within - 1.5 to 0 percent. Such a value revealed that major air leaks did not take place following the last vacuum test on the apparatus.

C. VACUUM INTEGRITY

Vacuum tightness for any condensation system, especially at low pressures similar to marine-vehicle condensers which operate at an absolute pressure of 2 inHg, is very important.

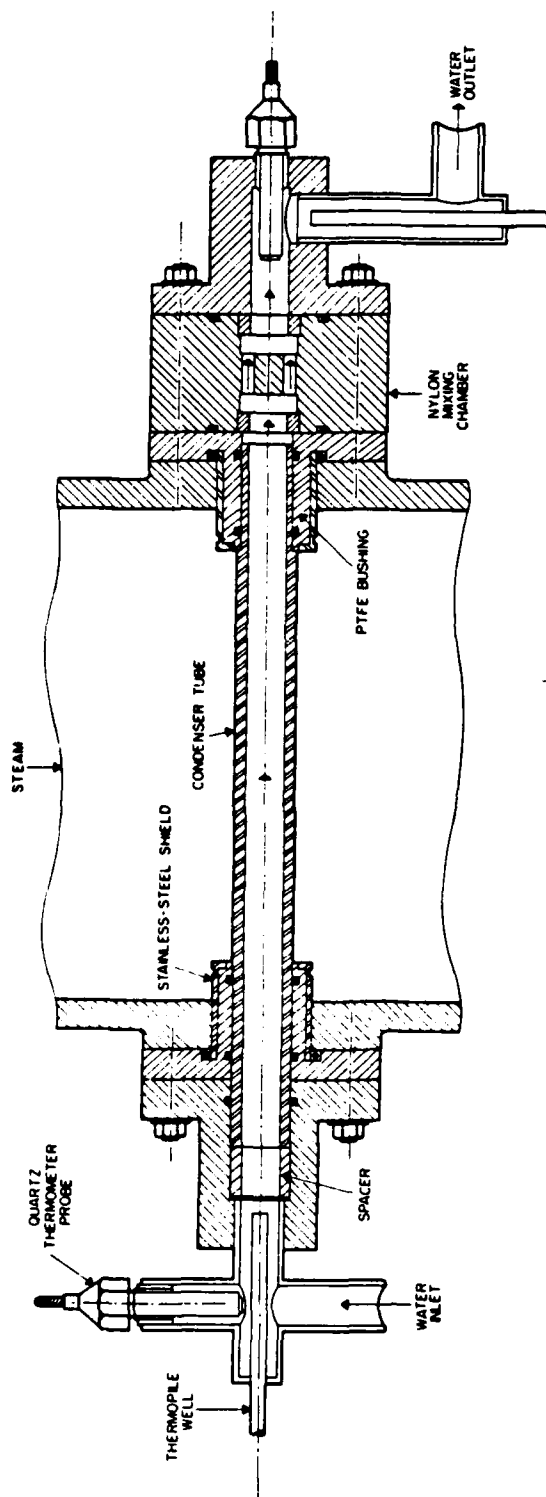


Figure 3.2 Schematic of Test Section (Insert Removed).

The reason for this is because any small amount of air or other non-condensing gas present with the condensing vapor tends to accumulate at the liquid-vapor interface. When this phenomenon takes place, an added thermal resistance occurs at the interface, which will degrade the heat-transfer performance considerably. Therefore, in order to be able to collect consistent and reliable data, extreme care was taken to ensure a leak-tight apparatus. In fact, during the early stages of this investigation, a major leak was found through the screws at the test section. After this was fixed, a vacuum test was carried out routinely about once a month. A leak rate that corresponds to a pressure rise of about 2 mmHg in 24 hours nearly at the operating pressure was found. Also, since the vacuum pump was operated continuously during the experiment, any accumulation of non-condensing gases within the apparatus was effectively eliminated.

D. DATA ACQUISITION SYSTEM

An HP-9826A computer was used to control an HP 3497A Data Acquisition System to monitor the system temperatures and boiler input power (using the converter signal). Raw data were processed immediately and stored on diskette for reprocessing at a later time. After all the runs were collected, the data were reprocessed using a new Sieder-Tate Coefficient found by the modified Wilson method.

E. TUBES TESTED

For this thesis effort, a total of twenty six tubes were manufactured. Table I lists all the finned tubes tested and their dimensions, including two tubes tested also by Georgiadis [5] and Flook [6] and four tubes tested by Flook. Twenty one of them were made from copper, two from copper-nickel, two from aluminum and one from stainless steel. Each tube had a 133.4 mm length exposed to steam. Tubes 45,

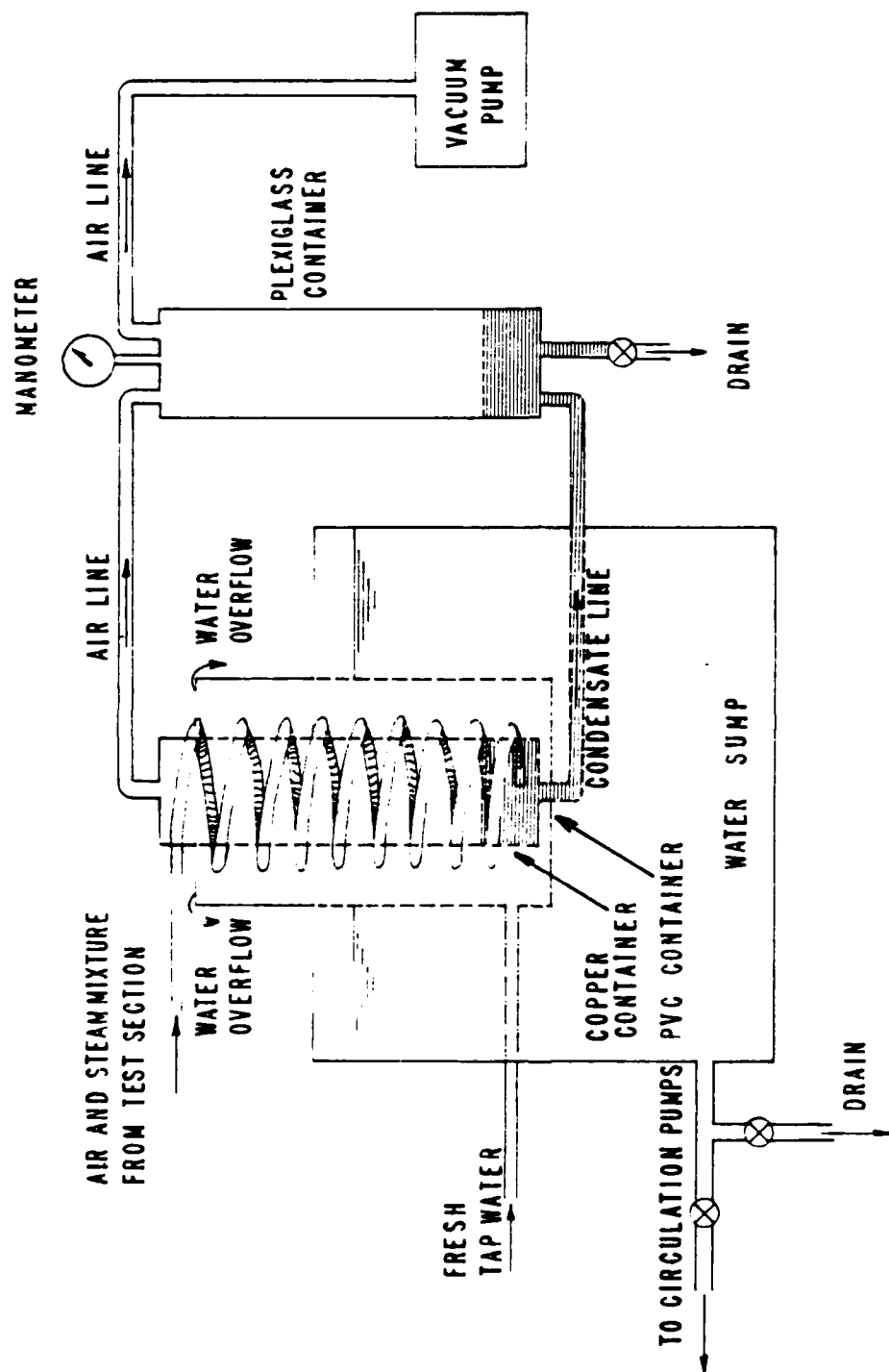


Figure 3.3 Schematic of Vacuum System and Cooling Water Sump.

46, 47, 52 thru 56 were finned tubes with bore diameter of 12.7 mm and fin root diameter of a 19.05 mm. Tubes 49, 51, and 57 thru 62 were finned tubes with fin root diameter of 13.7 mm. Table II lists all the wire-wrapped tubes tested and their dimension. Tubes 63 thru 71 had smooth exteriors with a bore diameter of 12.7 mm and an outside diameter of a 19.05 mm. Tube 36 and tubes 45 through 47 consisted of a family of spiral tubes, with triangular-shaped fins. Figure 3.8 shows a photograph of these four tubes which had a fin height of 1.0 mm and pitch of 1.06, 1.6, 2.1, and 2.5 mm (tubes 36, 45, 46, and 47).

Two commercially available tubes, manufactured by High Performance Tubes, Inc., were tested to investigate their heat-transfer performance compared to the other machined finned tubes. They were finned tubes (tubes 49 and 51) with fin height of a 0.75 mm and fin density of 1102 and 1181 fins/m, respectively. A smooth tube (tube 50) was also prepared by machining off the fins so that the effect of fins can be determined. These three tubes had the same outside root diameter (17.5 mm). In addition to these tubes, to study the effect of fin shape on the heat-transfer performance, four finned tubes were manufactured to complete two sets of tubes with different fin profiles. The first set consists of the tubes 06, 54, 55, and 56 with rectangular, parabolic, trapezoidal, and triangular fin-shapes, respectively, with a fin-base thickness of 1.0 mm. The other set consists of the tubes 17, 38, 53, and 52 with rectangular, parabolic, trapezoidal, and triangular fin-shapes, respectively, with a fin-base thickness of 0.5 mm. Each tube in these two sets has the same fin height of 1.0 mm and fin base spacing of 1.5 mm. Figure 3.4 shows a photograph of tubes 06, 54, 55, 56, while Figure 3.5 shows schematic cross-sectional of the "parabolic" fin. Figures 3.6 and 3.7 show a photograph and cross-sectional views of

tubes 17, 38, 52, and 53, respectively. As can be seen from Figure 3.5 and 3.7 these tubes do not have the exact shapes as stated above. For example, careful examination of the schematic cross-sectional of the parabolic tube (tube 54) showed that the fin-shape is almost straight near the fin base and circular at the fin tip, while the parabolic fin in Figure 3.7 shows that it had almost straight sides near the fin base with a sharp leading edge. Also, as seen in the same figure, a distinction between triangular and trapezoidal fins is not possible. The reason for this is that the very thin fins lead to nearly the same fin thickness at their tips, because of the difficulties associated with the machining process.

In order to test the effect of fin-metal thermal conductivity on the heat-transfer performance, four spiral tubes with triangular fin profile were manufactured: one each from copper, copper-nickel, stainless steel and aluminum (tubes 57, 58, 59 and 60, respectively). In addition, two tubes with rectangular fin profiles from copper-nickel and aluminum were manufactured (Tubes 61 and 62, respectively). Due to the low thermal conductivity of these tubes, a smaller outside diameter (13.5 mm) was selected to minimize the tube metal resistance (note that these tubes have the same nominal inside diameter as the other tubes). The spiral tubes had a fin base thickness of 2.1 mm, while the rectangular fins had a fin thickness of 1.0 mm and a fin spacing of 1.5 mm. Figure 3.8 shows a photograph of these tubes.

Finally, nine smooth copper tubes were manufactured, and each was wrapped with a titanium wire (0.5, 1.0 or 1.6 mm diameter) at a nominal wire spacing of 1.0, 2.0 or 3.0 mm. Photographs of these wire-wrapped tubes are shown in Figures 3.9, 3.10, and 3.11.

TABLE I
GEOMETRY OF FINNED TUBES TESTED

Tube No.	Fin Type	Inter-fin Spacing (mm)	Fin Base Thickness (mm)	Fin Height (mm)	Fin Root Diameter (mm)	Tube Inside Diameter (mm)	Tube Material
06	Rectangular	1.50	1.00	1.00	19.05	12.7	Copper
17	Rectangular	1.50	0.50	1.00	19.05	12.7	Copper
27	Rectangular	1.50	1.00	0.50	19.05	12.7	Copper
28	Rectangular	2.00	1.00	0.50	19.05	12.7	Copper
36	Spiral	0.00	2.10	1.00	19.05	12.7	Copper
38	Parabolic	1.50	0.50	1.00	19.05	12.7	Copper
45	Spiral	0.00	2.50	1.00	19.05	12.7	Copper
46	Spiral	0.00	1.60	1.00	19.05	12.7	Copper
47	Spiral	0.00	1.06	1.00	19.05	12.7	Copper
49	High Performance	0.51	0.34	1.00	17.50	15.6	Copper
50	Smooth	-----	-----	-----	17.50	15.6	Copper
51	High Performance	0.59	0.32	1.00	17.50	15.6	Copper
52	Triangular	1.50	0.50	1.00	19.05	12.7	Copper
53	Trapezoidal	1.50	0.50	1.00	19.05	12.7	Copper
54	Parabolic	1.50	1.00	1.00	19.05	12.7	Copper
55	Trapezoidal	1.50	1.00	1.00	19.05	12.7	Copper
56	Triangular	1.50	1.00	1.00	19.05	12.7	Copper
57	Spiral	0.00	2.10	1.00	13.70	12.7	Copper
58	Spiral	0.00	2.10	1.00	13.70	12.7	Copper-Nickel
59	Spiral	0.00	2.10	1.00	14.50	12.5	Stainless Steel
60	Spiral	0.00	2.10	1.00	13.70	12.7	Aluminum
61	Rectangular	1.50	1.00	1.00	13.70	12.7	Copper-Nickel
62	Rectangular	1.50	1.00	1.00	13.70	12.7	Aluminum

TABLE II
GEOMETRY OF WIRE-WRAPPED TUBES TESTED

Tube No.	Tube Type	Wire Diameter (mm)	Wire Spacing (mm)	Wire Pitch (mm)	Fin Root Diameter (mm)	Tube Inside Diameter (mm)	Tube Material
63	Smooth	1.60	0.94	2.54	19.05	12.7	Copper
64	Smooth	1.60	2.03	3.63	19.05	12.7	Copper
65	Smooth	1.60	3.02	4.62	19.05	12.7	Copper
66	Smooth	1.00	0.95	1.95	19.05	12.7	Copper
67	Smooth	1.00	1.82	2.82	19.05	12.7	Copper
68	Smooth	1.00	2.91	3.91	19.05	12.7	Copper
69	Smooth	0.50	1.10	1.60	19.05	12.7	Copper
70	Smooth	0.50	2.04	2.54	19.05	12.7	Copper
71	Smooth	0.50	3.13	3.63	19.05	12.7	Copper

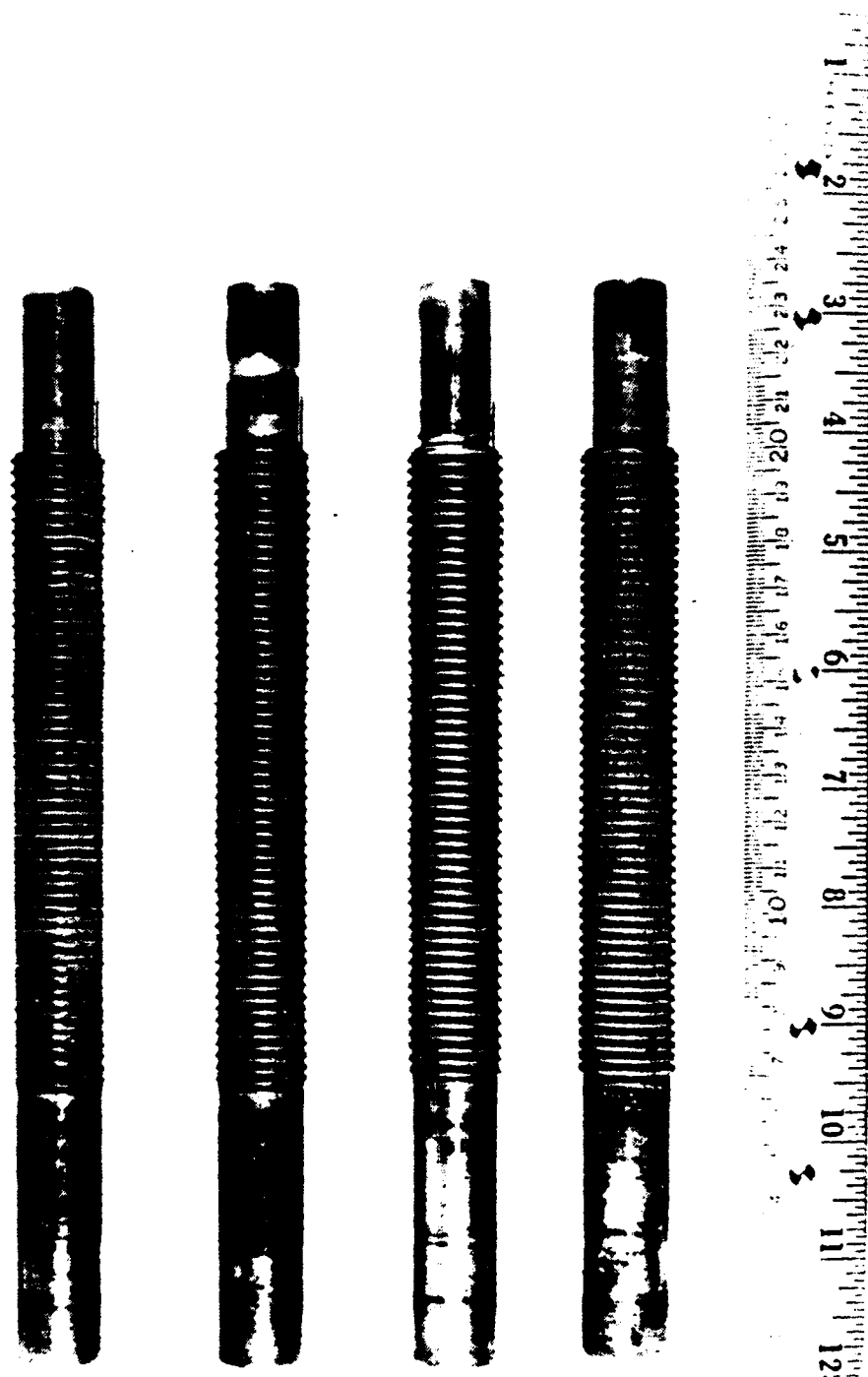


Figure 3.4 Photographs of Tubes with Different Fin
Shapes ($t_b = 1.0$ mm).

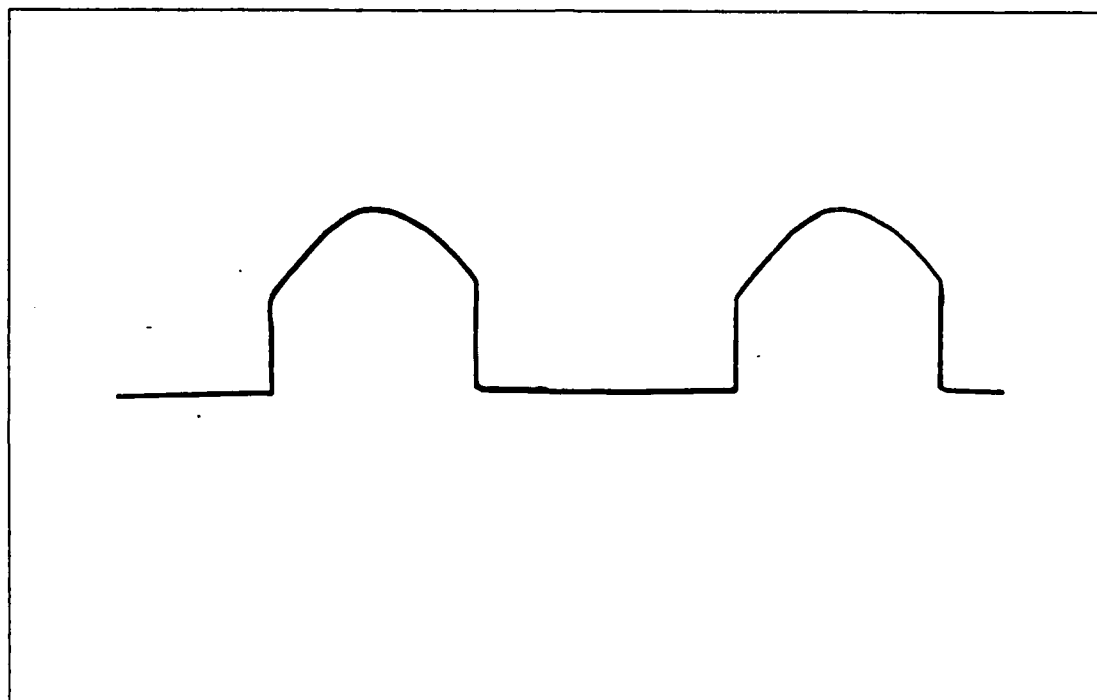


Figure 3.5 Tracing of the Fin Profile of Tube 54.

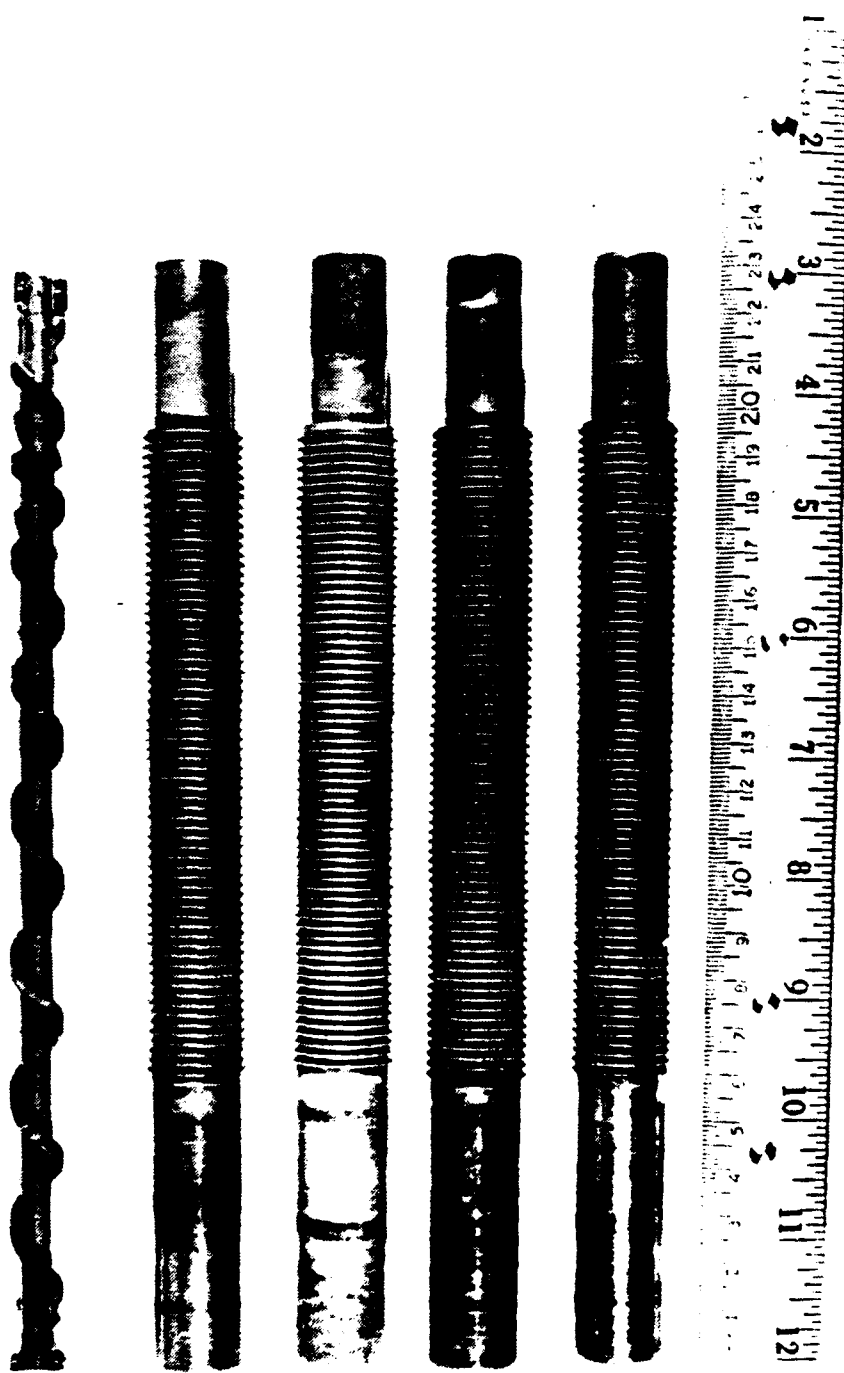
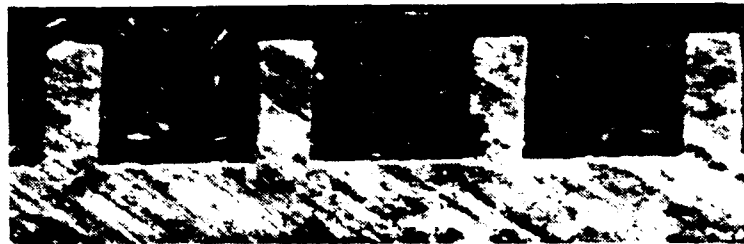


Figure 3.6 Photographs of Tubes with
Different Fin Shapes ($t_b = 0.5$ mm).



(a) Rectangular (Tube 17)



(b) Parabolic (Tube 38)



(c) Triangular (Tube 52)



(d) Trapezoidal (Tube 53)

Figure 3.7 Cross-Sectional Photographs of Tubes with
Different Fin Shapes $t_b = 0.5$ mm).

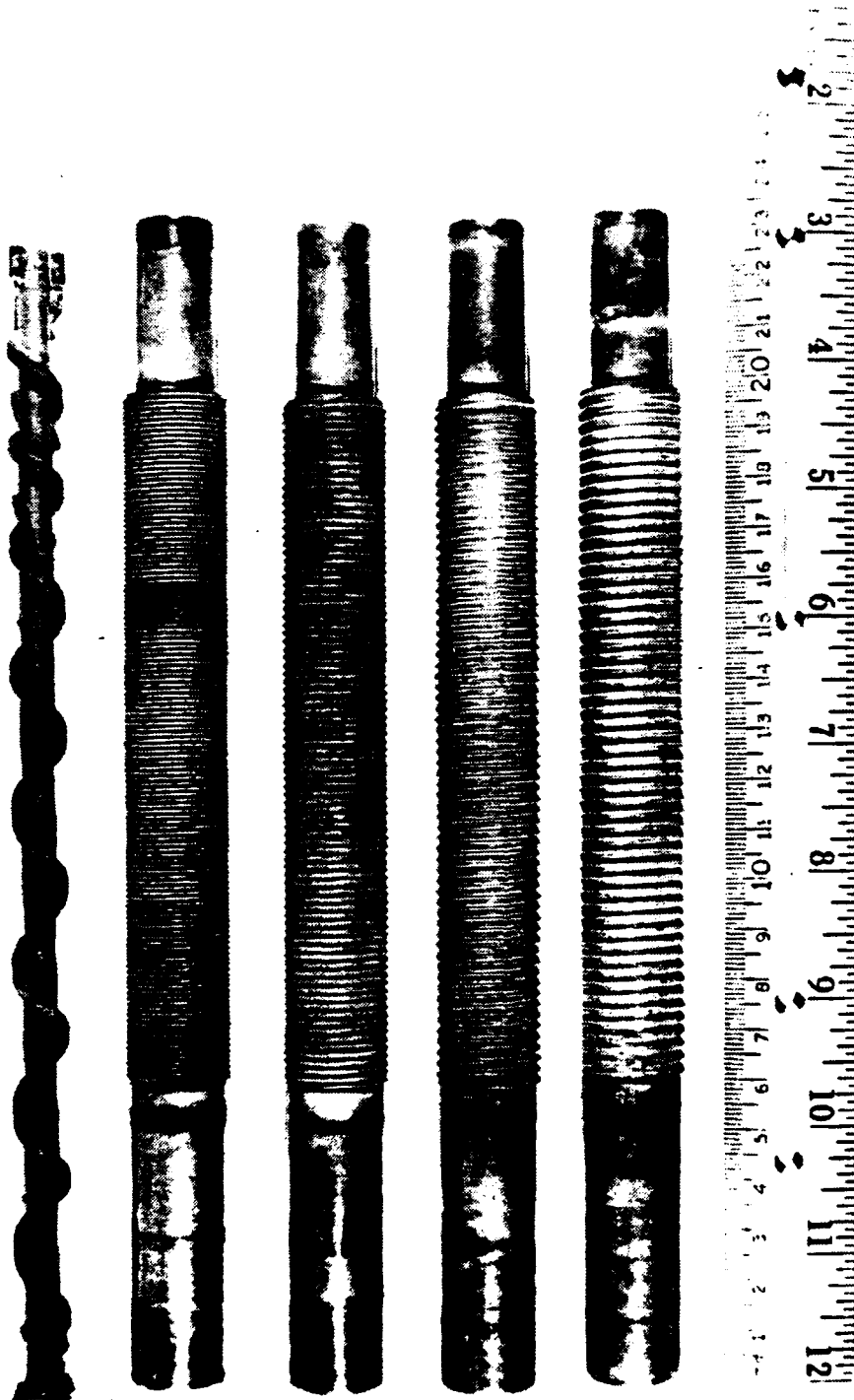


Figure 3.8 Photograph of Tubes with Spiral
Triangular Fins ($e = 1.0$ mm).

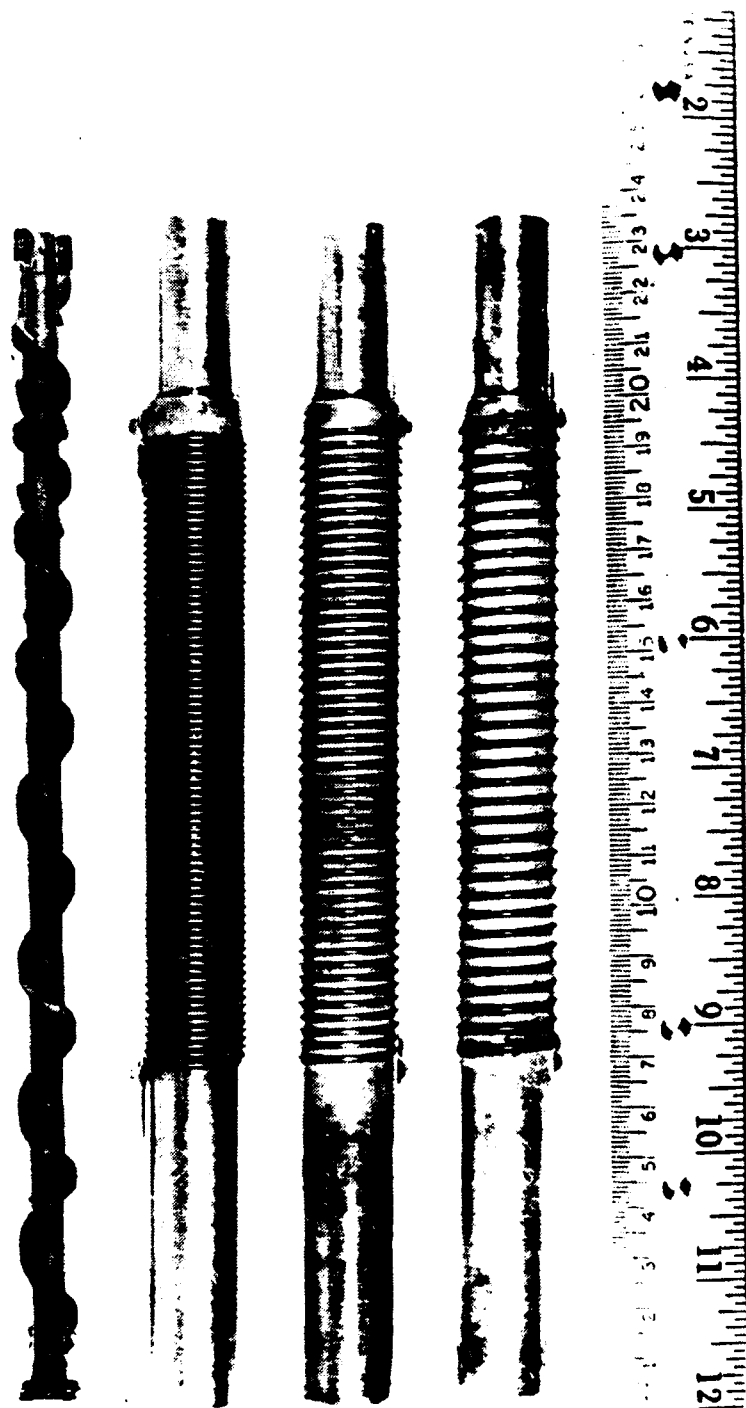


Figure 3.9 Photograph of Wire-Wrapped Tubes
($D_w = 0.5 \text{ mm}$).

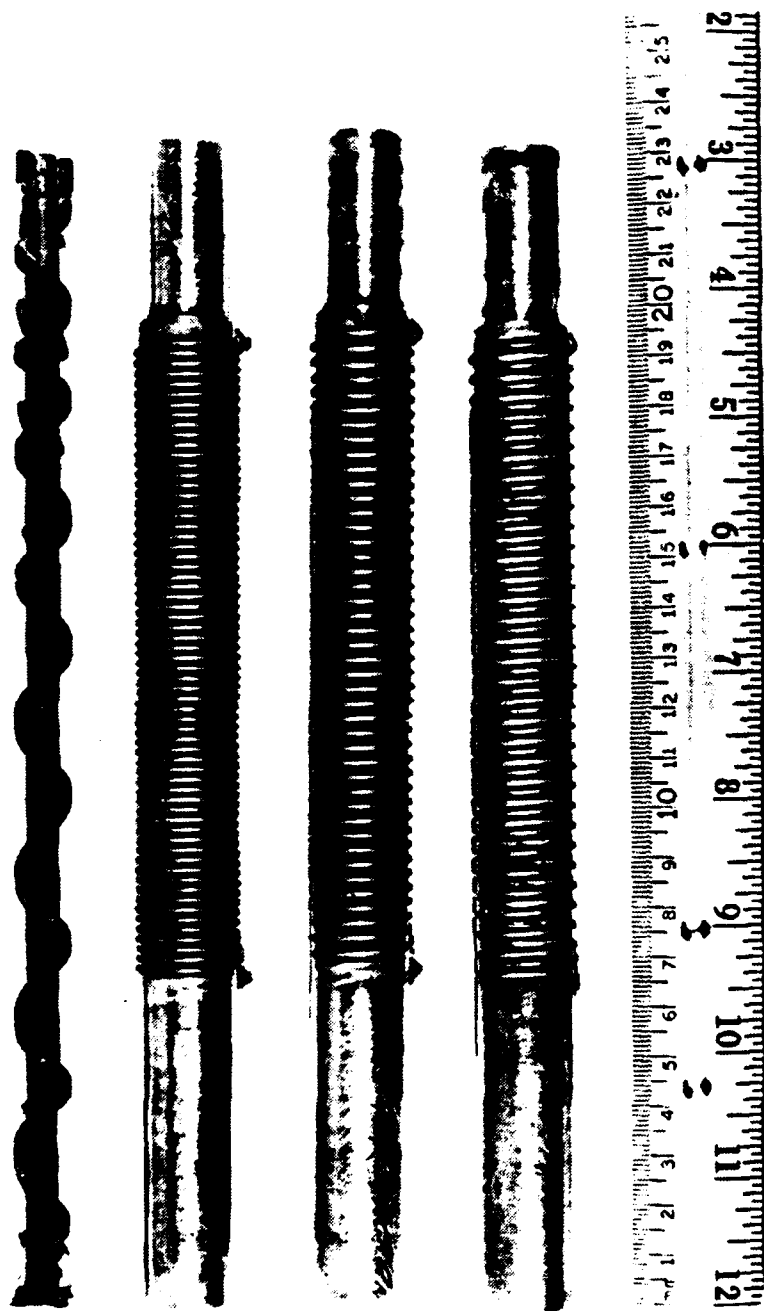


Figure 3.10 Photograph of Wire-Wrapped Tubes
($D_w = 1.0 \text{ mm}$).

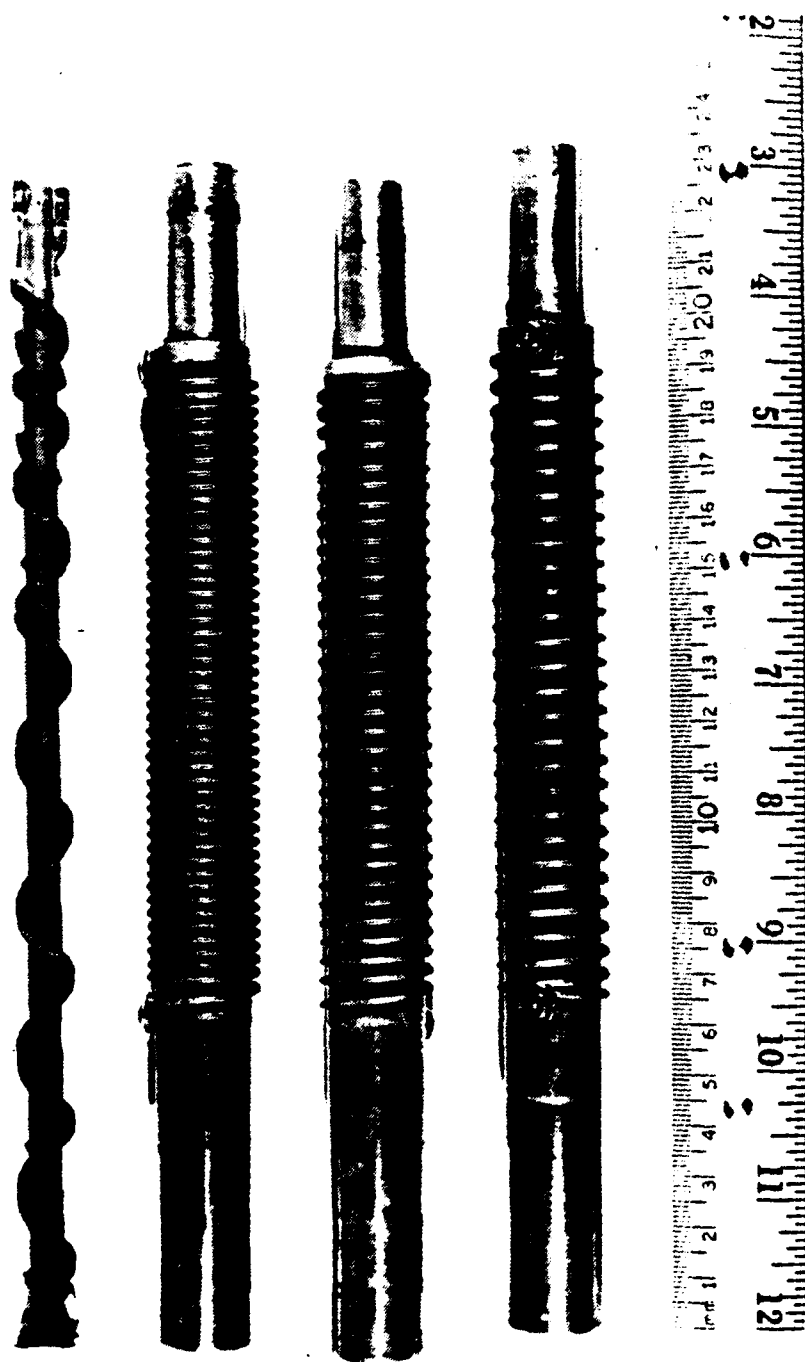


Figure 3.11 Photograph of Wire-Wrapped Tubes
($D_w = 1.6$ mm).

IV. SYSTEM OPERATION AND DATA REDUCTION

A. SYSTEM OPERATION

Since copper has poor wetting characteristics with water, steam will normally condense on copper under a partial dropwise condensation mode, which is more effective than the filmwise condensation mode. Since the purpose of this investigation was to take data with filmwise condensation and most of the tested tubes were made from copper, great care had to be taken to ensure that the filmwise condensation mode was in fact occurring. In order to ensure this, the tubes had to be treated according to the following procedure:

1. The tube was rinsed with tap water to remove any contaminants that are soluble in the water.
2. A mixture of equal parts of sodium-hydroxide and ethyl alcohol was prepared and heated to about 80°C, while frequently being stirred until it became watery.
3. A coating of this mixture was applied uniformly around the tube.
4. The tube was placed in a steam bath and was heated by the steam for about an hour.
5. A new coating was applied to the tube every 10 minutes.
6. The tube was then rinsed with distilled water and put immediately into the test section to avoid any contaminants depositing on the tube which may lead to the dropwise problem.

This process resulted in the formation of a thin layer of dark oxide that has high wetting characteristics. Since this layer was thin, its thermal resistance was negligible. This procedure was followed each time prior to the installation of a tube. However, when re-testing an already-darkened tube, it was heated in the steam only for 15 to 20 minutes.

Following the procedure described by Georgiadis [5], the test apparatus was brought to operating pressure and

temperature by adjusting the input power to the boiler heaters, the cooling water flow rate through the tube, and the cooling water flow rate to the auxiliary condenser. Steady-state conditions were assumed when the operating conditions were stabilized with a steam temperature variation of $\pm 2 \mu V$ and a temperature rise of the cooling water of $\pm 0.005 K$ and $\pm 0.01 K$ for atmospheric and vacuum, respectively. Once steady-state operating conditions were reached, the cooling water flow rate through the test tube was fed to the computer manually while the temperature rise of the cooling water through the test tube, vapor pressure and temperature were gathered automatically by the data acquisition system. For cooling water flow rates of 80 percent (4.44 m/s for 19 mm O.D. and 12.7 mm I.D. tubes, and 2.84 m/s for 17.5 mm O.D. with 15.6 mm I.D. tubes), 70, 62, 54, 45, 35, 26, and 20 percent, and again 80 percent, two sets of data were taken. These cooling water flow rates were selected to give approximately equally-spaced heat flux values. After each change of the cooling water flow rate through the tube, the system pressure experienced a slow drift; so an adjustment of the water flow rate through the auxiliary condenser was required to maintain the system pressure at the operating pressure. As mentioned in Chapter III, a view port was provided for visual observation to ensure filmwise condensation. Before each data collection, the appearance of the film was checked. If the film appeared to be patchy or there was an indication of dropwise condensation, the run was discontinued and the data were discarded. However, there were cases where the film appeared filmwise but the data collected at the end of the run (cooling water flow rate of 80 percent) were different from that collected at the beginning for the same flow rate. For example, the heat-transfer coefficient was as much as 10 percent greater for the last data point and the cooling

water temperature rise was also greater than that measured at the beginning. As discussed by Georgiadis [5], this increased heat-transfer coefficient appears to be a result of the tube undergoing partial dropwise condensation with exposure to the steam. Since this trend was observed even though no droplets were visible, it is possible that the dropwise condensation was taking place at a microscopic level, especially near fin edges with a very thin condensate film. This phenomenon was observed primarily for the runs which followed the first treatment for darkening, probably due to the contaminants of the machine shop and since not a good layer of the dark oxide was obtained. All data presented in this thesis displayed less than 3% disagreement in the steam-side heat-transfer coefficient between initial and final data sets.

B. DATA REDUCTION

Initially, the program used for data reduction was the same as that used by Flook [6] including property functions, calibration curves for the cooling water flowmeter and for all thermocouples as well as the temperature rise due to frictional heating within the mixing chamber. Since tubes 49, 50 and 51 had a different inside diameter than the tubes tested previously, and tubes 57 thru 62 were manufactured from metals with different thermal conductivity, the program was modified to include options for different tube diameter, thermal conductivity, fin shapes, and Sieder-Tate constant for the inside heat-transfer coefficient.

The separation of the individual thermal resistances (water-side, wall, and vapor-side) from the overall heat-transfer resistance is very important in order to obtain expressions for the vapor-side heat-transfer coefficient. The overall heat-transfer resistance is given by equation (4.1), while the inside heat-transfer coefficient is given by a Sieder-Tate type equation (equation (4.2)). The value

of the leading coefficient C_i must be known in order to calculate the inside heat-transfer coefficient from equation (4.2) and consequently the outside heat-transfer coefficient. In order to determine the value of C_i , two methods were considered: the "direct" method and the "modified Wilson plot" method.

$$\frac{1}{U_o A_o} = \frac{1}{h_i A_i} + \frac{1}{h_o A_o} + \frac{R_w}{A_o} \quad (4.1)$$

$$Nu = \frac{h_i D_i}{k} = C_i Re^{0.8} Pr^{1/3} \left[\frac{\mu_c}{\mu_w} \right]^{0.14} + B \quad (4.2)$$

1. "Direct" Method

This method is used to find the leading coefficient for the Sieder-Tate equation from an instrumented tube. As described by Georgiadis [5], a thick-wall smooth tube was manufactured with six thermocouples inserted into channels around the periphery of the tube. The average wall temperature was found by averaging the temperatures indicated by the six thermocouples. He showed that the wall temperature distribution followed a cosine curve given by equation (4.3) with a maximum drop of 18 K between the top and bottom of the tube.

$$\frac{\Delta T}{\Delta T} = 1 - \alpha \frac{\cos \theta}{\pi} \quad (4.3)$$

where a is found to be from 0.135 to 0.202 and from 0.115 to 0.179 under vacuum and at atmospheric pressure, respectively, in order to fit the temperature measurements. Using the average reading of all the thermocouples, Georgiadis [5] found values of 0.0635 and 26.4 for the leading Sieder-Tate coefficient and the constant B in equation (4.2), respectively, based on two runs each under vacuum and at atmospheric pressure. The value of C (0.0635) is greater than the well-known Sieder-Tate constant of 0.027 for the plain tubes, mainly owing to the coiled insert. The constant $B = 26.4$ is used for improved fitting of the experimental data.

2. "Modified Wilson Plot" Method

This method is a modification of the original Wilson plot method as modified by Briggs and Young [33] to accept data collected at various flow rates and temperatures. A Sieder-Tate equation was used for the inside heat-transfer coefficient, while a Nusselt type equation was used for the outside heat-transfer coefficient as given by equation (4.4):

$$h_o = \beta \left(\frac{k_f^3 \rho_f (\rho_f - \rho_v) h_{fg}}{\mu_f D_o q} \right)^{1/3} \quad (4.4)$$

Both constants in equations (4.2) and (4.4) had to be determined iteratively. Substituting equation (4.2) (with $B = 0.0$) and equation (4.4) in the equation for the overall heat transfer resistance given by equation (4.1), results in equation (4.5) below:

$$\left(\frac{1}{U_o} - R_w \right) \Gamma = \frac{D_o \Gamma}{C_1 k_f \Omega} + \frac{1}{\beta} \quad (4.5)$$

where

$$\Gamma = \left\{ \frac{k_f^3 \rho_f (\rho_f - \rho_v) h_{fg}}{\mu_f D_o q} \right\}^{1/3} \quad (4.6)$$

$$\Omega = \frac{k}{D_i} Re^{0.8} Pr^{1/3} \left(\frac{\mu_c}{\mu_w} \right)^{0.14} \quad (4.7)$$

Equation (4.5) is a linear equation of the form:

$$Y = mX + b \quad (4.8)$$

where

$$Y = \left(\frac{1}{U_o} - R_w \right) \Gamma \quad (4.9)$$

$$X = \frac{D_o \Gamma}{k_f \Omega} \quad (4.10)$$

$$m = \frac{1}{C_i} \quad (4.11)$$

$$b = \frac{1}{\beta} \quad (4.12)$$

To begin the iteration, reasonable values were assumed for C_i and β . With these values, the Y and X values

were calculated and a least-square technique was used to compute the slope and intercept values in equation (4.8). A new set of values for C_i and β was then computed according to equations (4.11) and (4.12). This procedure was repeated until the assumed and computed values for C_i and β agreed to within 0.1 percent. Based on the Nusselt theory, β should take a value of 0.655, which is true for the case of zero vapor shear. However, for the experimental conditions in this thesis, the vapor velocity was from 1 m/s (atmospheric runs) to 2 m/s (vacuum runs), thus resulting in β values as high as 0.75. To account for the vapor shear properly, a correlation developed by Fujii and Honda [34] was also considered as shown below:

$$\frac{Nu}{Re_{tp}^{0.5}} = 0.96 F^{1/5} \quad (4.13)$$

Using a Nusselt-type equation for the steam-side coefficient, Georgiadis [5] found the leading coefficient (for equation (4.2)) C_i to be 0.071, with the B value set equal to zero for a smooth tube. This C_i value resulted in an inside heat transfer coefficient up to 6 percent greater than that based on the direct method. Flook later used a Fujii-type [34] equation instead of the Nusselt-type equation for the steam-side coefficient. This resulted in a slightly higher value (up to 3 percent) for the leading coefficient C_i . The program used for the data collection allows an option for selecting either the Fujii-type or Nusselt-type equation for the steam-side coefficient.

Georgiadis [5] and Flook [6] thought that the "direct" method is more reliable, so the values of 0.0635 and 26.4 were used for the constants C_i and B,

respectively, for the data reduction for tubes with an inside diameter of 12.7 mm.

Later, Flook [6] used the "modified Wilson plot" method, with the Fujii-type equation for the steam-side coefficient to find the leading coefficient for the Sieder-tate equation for a copper tube and a stainless steel tube with thin (i.e., 0.5 mm thickness) tube walls since it was not possible to manufacture an instrumented tube for using the "direct" method to find the leading coefficient for the equation (4.1). For the copper and stainless steel tubes tube, values of $C_i = 0.0756$ and $C_i = 0.0688$ were obtained respectively. For this thesis effort, initially the values of $C_i = 0.0635$ and $B = 24.6$ were found with the "direct method" as said above, but finally the "Modified Wilson Plot" directly on the finned tubes was used. This was the same method as described above but for each tube a different Sieder-Tate coefficient was found and used for the data reduction.

V. RESULTS AND DISCUSSION

A. INTRODUCTION

During this thesis effort, a number of data runs were made using the procedures described in Chapter IV. Each tube was tested at least three times, both under vacuum and at atmospheric pressure on different days, to ensure repeatability of the data. Complete filmwise condensation conditions were maintained, and the non-condensing gas concentration was calculated at the beginning and at the end of each run for every tube to ensure there were no major leaks in the system. The computed mass concentration of non-condensing gases was kept between 0 and - 2.5 percent in order for the data run to be accepted. The mass concentration of the non-condensing gases was always a negative number because of the slight inaccuracies in the measurement of pressure and steam temperature. As discussed earlier in Chapter III, the test apparatus would allow only a negligible amount of non-condensing gases to be leaked into the apparatus. Since continuous venting was provided throughout all runs (see Chapter III), build up of non-condensing gases was not possible.

A summary of finned tubes tested by Georgiadis [5] and Flook [6] and those tested during this thesis effort, as well as the resulting enhancements are provided in Table III. Further, Table IV presents the wire-wrapped tubes tested and their heat-transfer performance.

TABLE III
SUMMARY OF FINNED TUBES TESTED AND THEIR
HEAT-TRANSFER PERFORMANCE

Tube No.	Tube Metal	Fin Type	$\tau(\phi)$ (mm)	$\tau(\phi)$ (mm)	ϕ (mm)	Do (mm)	Outside Area (ϕ) (mm ²)	Area Ratio Ar	$E_o(-)$ Vac	$E_o(Q)$ Atm	E_o/Ar Vac	E_o/Ar Atm	CL Vac	CL Atm
06 *	C	Rec	1.50	1.00	1.00	19.05	15000	1.88	3.54	5.18	1.88	2.75	0.066	0.063
17 *	C	Rec	1.50	0.50	1.00	19.05	16600	2.08	3.69	5.50	1.78	2.65	0.066	0.063
27 **	C	Rec	1.50	1.00	0.50	19.05	11400	1.43	2.54	-----	1.77	-----	0.068	-----
28 **	C	Rec	2.00	1.00	0.50	19.05	10900	1.36	2.79	-----	2.06	-----	0.068	-----
36 **	C	Spi	0.00	2.10	1.00	19.05	11600	1.45	3.72	5.31	2.56	3.65	0.068	0.064
38 **	C	Par	1.50	0.50	1.00	19.05	14800	1.97	4.09	6.21	2.07	3.15	0.066	0.064
45	C	Spi	0.00	2.50	1.00	19.05	10700	1.34	3.29	5.69	2.45	4.24	0.068	0.067
46	C	Spi	0.00	1.60	1.00	19.05	13500	1.69	3.94	6.08	2.33	3.60	0.066	0.064
47	C	Spi	0.00	1.06	1.00	19.05	18100	2.27	3.73	5.69	1.64	2.51	0.064	0.063
49	C	HPTI	0.51	0.34	1.00	17.50	24300	3.32	3.48	4.82	1.15	1.59	0.063	0.060
50	C	Smo	-----	-----	-----	17.50	7300	1.00	1.06	1.13	1.07	1.14	0.059	0.064
51	C	HPTI	0.59	0.32	1.00	17.50	22900	3.11	3.53	5.15	1.14	1.66	0.614	0.063
52	C	Tri	1.50	0.50	1.00	19.05	14600	1.84	3.73	5.48	2.04	2.99	0.065	0.063
53	C	Trap	1.50	0.50	1.00	19.05	15300	1.91	3.67	5.41	1.92	2.83	0.065	0.064
54	C	Par	1.50	1.00	1.00	19.05	12600	1.58	3.52	5.36	2.23	3.39	0.069	0.067
55	C	Trap	1.50	1.00	1.00	19.05	13100	1.64	3.98	5.00	2.43	3.06	0.068	0.068
56	C	Tri	1.50	1.00	1.00	19.05	12300	1.54	3.872	5.36	2.51	3.47	0.069	0.068
57	C	Spi	0.00	2.10	1.00	13.70	8500	1.48	3.504	4.44	2.38	3.01	0.065	0.062
58	C-Ni	Spi	0.00	2.10	1.00	13.70	8500	1.48	1.814	3.07	1.23	2.08	0.063	0.060
59	SS	Spi	0.00	2.10	1.00	14.50	8900	1.48	0.707	1.14	0.48	0.77	0.065	0.060
60	Al	Spi	0.00	2.10	1.00	13.70	8500	1.48	2.86	3.67	1.76	2.49	0.062	0.059
61	C-Ni	Rec	1.50	1.00	1.00	13.70	8500	1.92	1.63	2.99	0.85	1.56	0.059	0.057
62	Al	Rec	1.50	1.00	1.00	13.70	8500	1.92	2.29	3.92	1.20	1.67	0.058	0.056

Heat Flux = 7.565 W/m²
Heat Flux = 7.565 W/m²
Calculated Area
Measured at Fin Base
Tubes also tested by Georgiadis [5]
Tubes also tested by Floor [6]
C-Ni : Copper-Nickel
SS : Stainless Steel
Al : Aluminum

TABLE IV
SUMMARY OF WIRE-WRAPPED TUBES TESTED AND THEIR
HEAT-TRANSFER PERFORMANCE

Tube No.	Tube Metal	D _w (mm)	a (mm)	P (mm)	D _o (mm)	Outside Area (mm ²)	Area Ratio Ar	E _o (*) Vac	E _o (@) Atm	E _o /Ar Vac	E _o /Ar Atm	Vac	Cl Atm
63	C	1.6	0.94	2.54	19.05	7981	1.00	0.91	1.46	0.91	1.46	0.067	0.058
64	C	1.6	2.03	3.63	19.05	7981	1.00	1.30	1.89	1.30	1.89	0.065	0.059
65	C	1.6	3.02	4.62	19.05	7981	1.00	1.34	1.83	1.34	1.83	0.064	0.061
66	C	1.0	0.95	1.95	19.05	7981	1.00	0.98	1.52	0.98	1.520	0.063	0.061
67	C	1.0	1.82	2.82	19.05	7981	1.00	1.53	2.24	1.52	2.24	0.064	0.062
68	C	1.0	2.91	3.91	19.05	7981	1.00	1.59	2.22	1.58	2.22	0.065	0.066
69	C	0.5	1.10	1.60	19.05	7981	1.00	1.38	2.15	1.38	2.15	0.068	0.068
70	C	0.5	2.04	2.54	19.05	7981	1.00	1.84	2.61	1.84	2.61	0.066	0.065
71	C	0.5	3.13	3.63	19.05	7981	1.00	1.75	2.52	1.75	2.52	0.066	0.066

(*) : Heat Flux = 2.565 W/m²
 (@) : Heat Flux = 7.565 W/m²
 a : Area of Plain tube (i.e., with wires removed)
 C : Copper

B. WATER-SIDE HEAT-TRANSFER COEFFICIENTS

As mentioned in Chapter IV, Georgiadis [5] used two methods to find the Sieder-Tate coefficient: the "direct" method and the "modified Wilson plot" method. The "direct" method involved the measurement of the average tube wall temperature using six thermocouples embedded within the wall of a smooth tube. He took data with filmwise condensation occurring outside. He changed the water velocity from about 0.8 to 4.5 m/s and correlated the data resulting in a Sieder-Tate constant C_i of 0.064 (see equation (4.2)) with a B value of 26.4. Also, taking data on an uninstrumented smooth tube, and making a modified Wilson analysis, he found a Sieder-Tate constant of 0.071 with the B value set equal to zero. When the h_i values computed using the results of these two methods were compared, they agreed to within 6 percent.

During the present study, however, a third approach was tested. For this purpose, the modified Wilson analysis was carried out directly on finned-tube data, resulting in C_i values around 0.069 with the B value set equal to zero. The h_i values computed using this analysis in fact lie between the values computed by the two methods described earlier. For this reason, the third method was used throughout this investigation in computing the outside heat-transfer coefficient.

Since the water-side geometry for tubes 45 through 47, 49 through 51, 52 through 56, 57 through 62 and 63 through 71 was essentially the same, the values of C_i should be very nearly the same for all these tubes. However, circumferential temperature variations can influence the inside coefficient, and these variations will depend on the condensate retention angle. As discussed in Chapter II, the retention angle is strictly dependent on the fin spacing. Therefore, the experimentally found C_i values should vary from tube to tube.

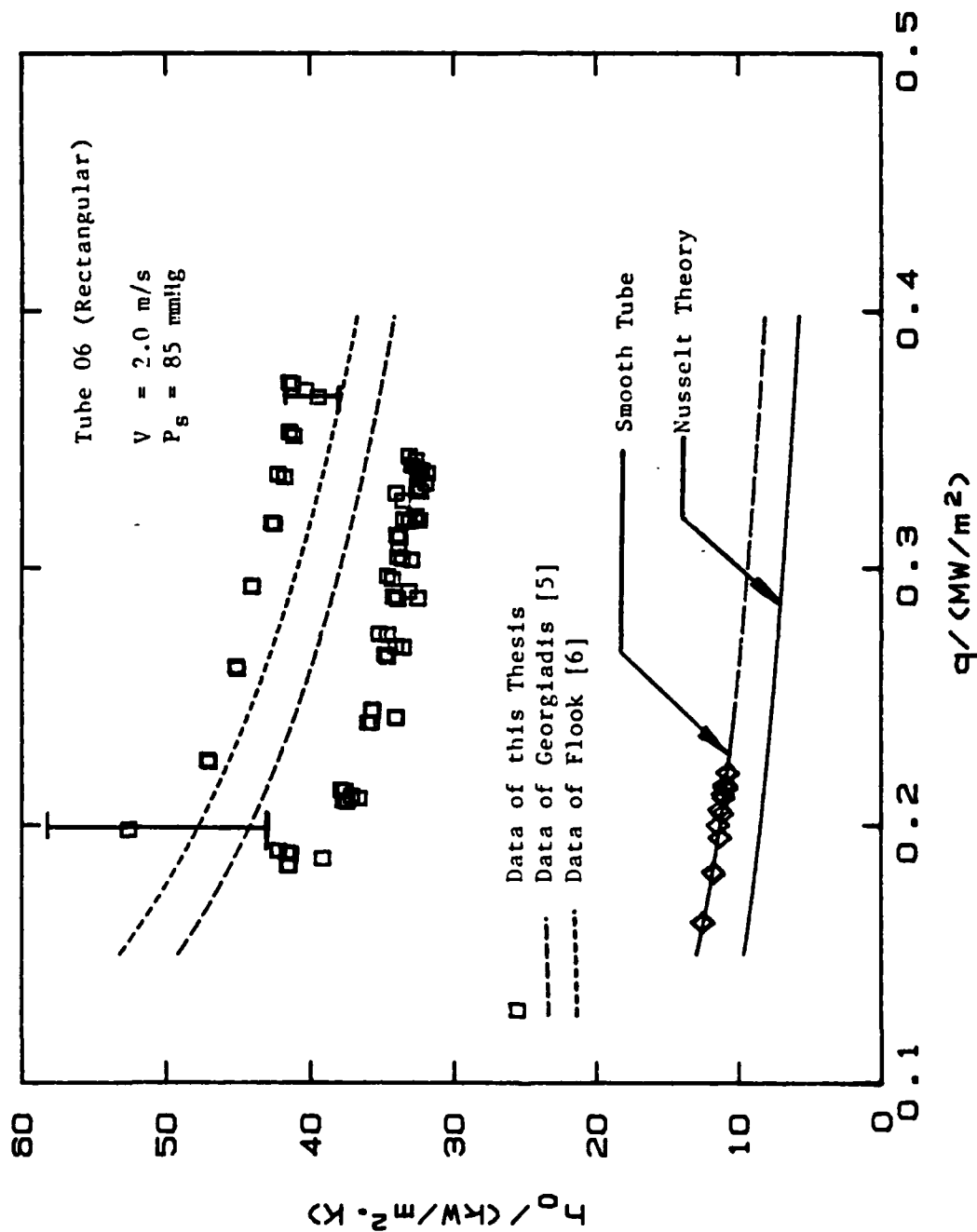


Figure 5.1 Comparison of Finned-Tube Data with Data of Georgiadis [5] and Flook [6] (Vacuum Runs, Tube 6).

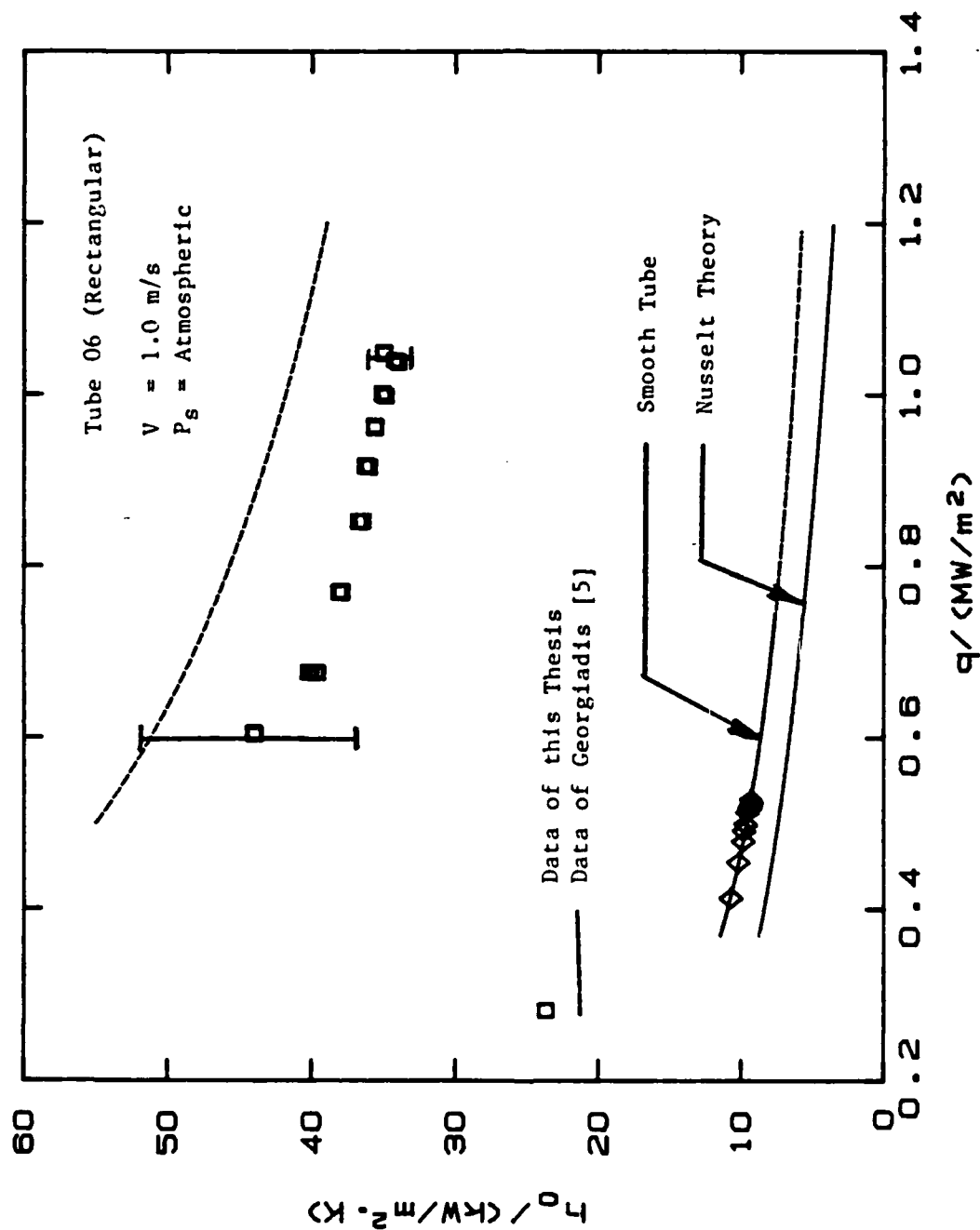


Figure 5.2 Comparison of Finned-Tube Data with Data of Georgiadis [5] (Atmospheric Runs, Tube 6).

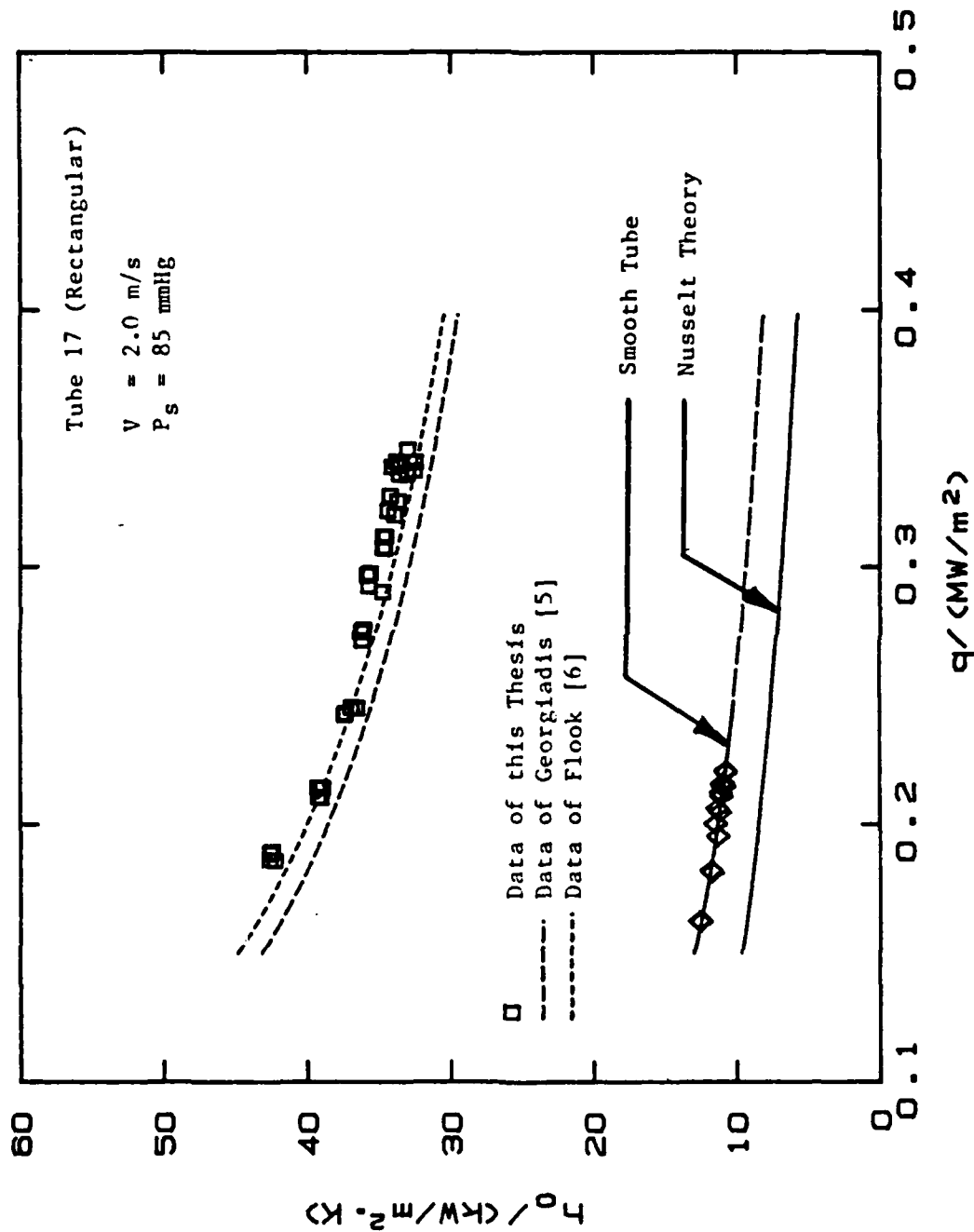


Figure 5.3 Comparison of Finned-Tube Data with Data of Georgiadis [5] and Flook [6] (Vacuum Runs, Tube 17).

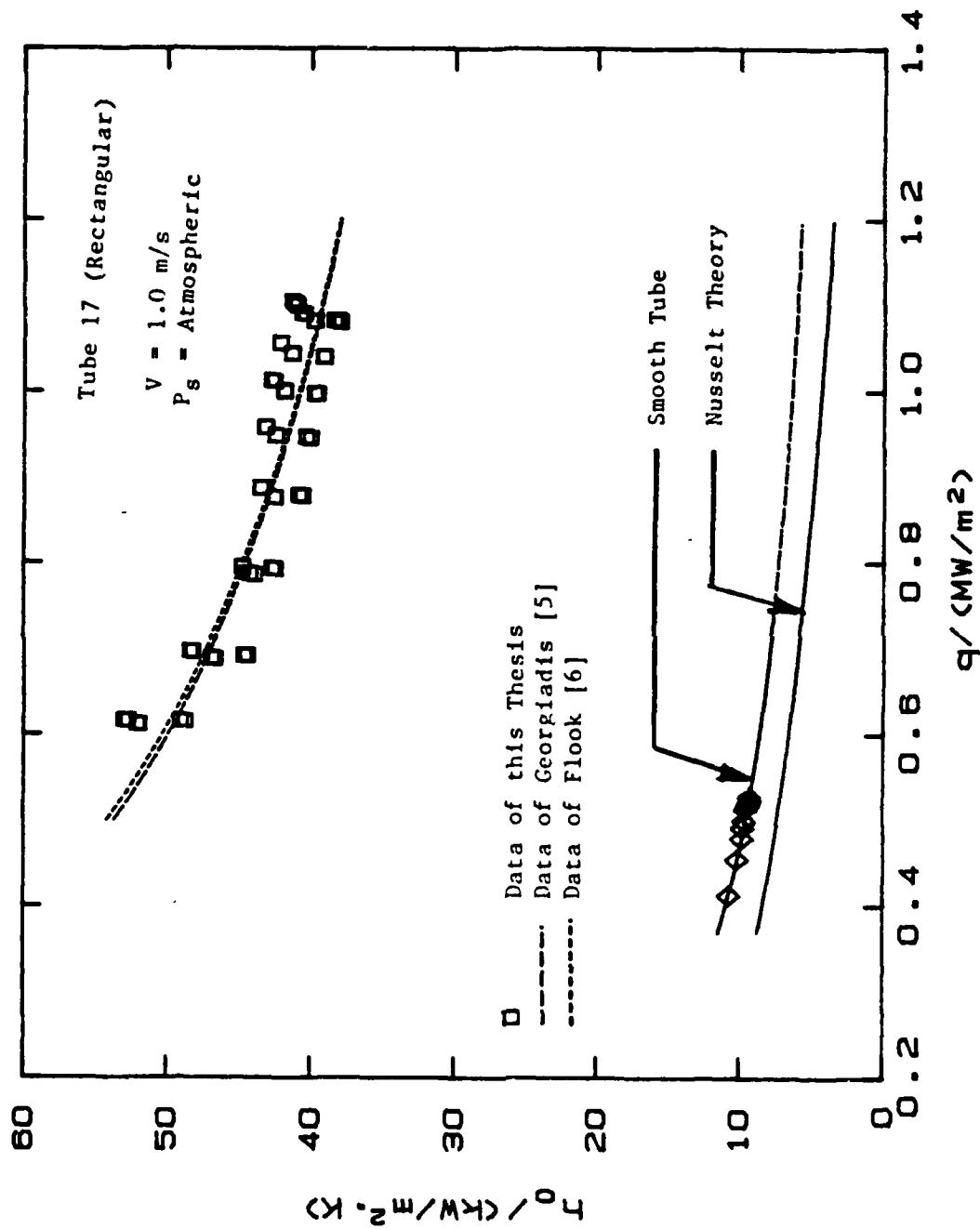


Figure 5.4 Comparison of Finned-Tube Data with Data of Georgiadis [5] and Flook [6] (Atmospheric Runs, Tube 17).

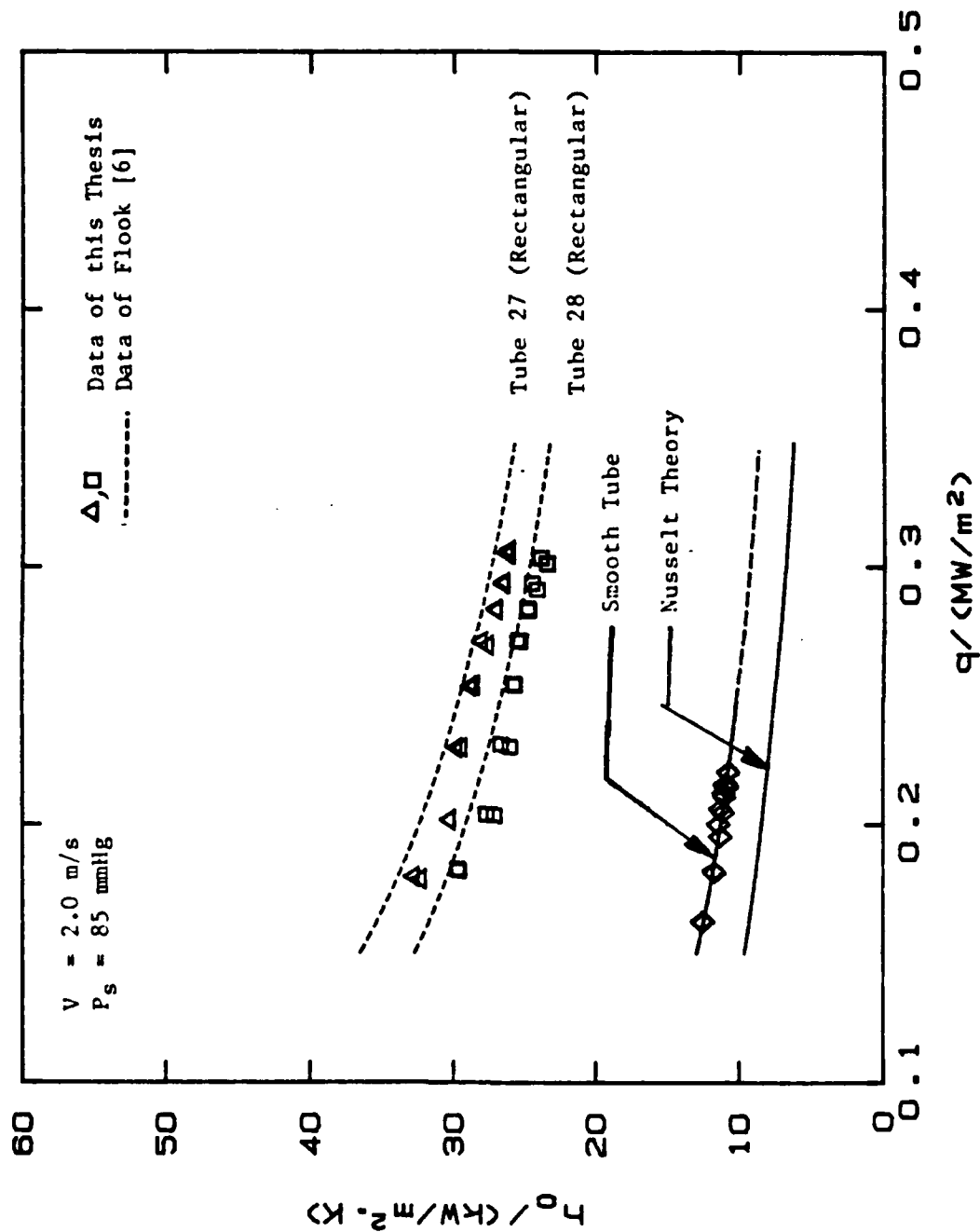


Figure 5.5 Comparison of Finned-Tube Data with Data of Flook [6] (Vacuum Runs, Tubes 27 and 28).

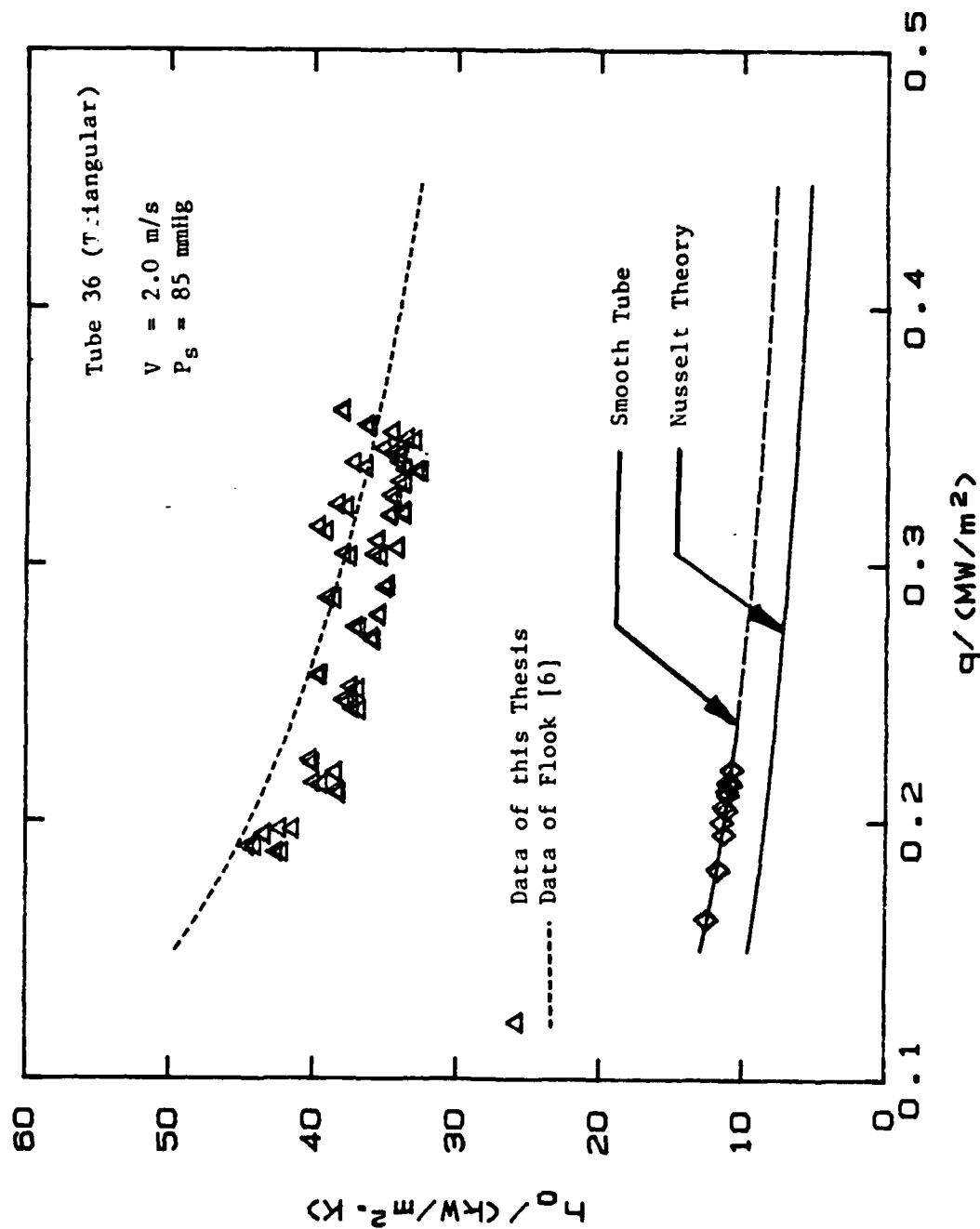


Figure 5.6 Comparison of Finned-Tube Data with Data of Flook [6] (Vacuum Runs, Tube 36).

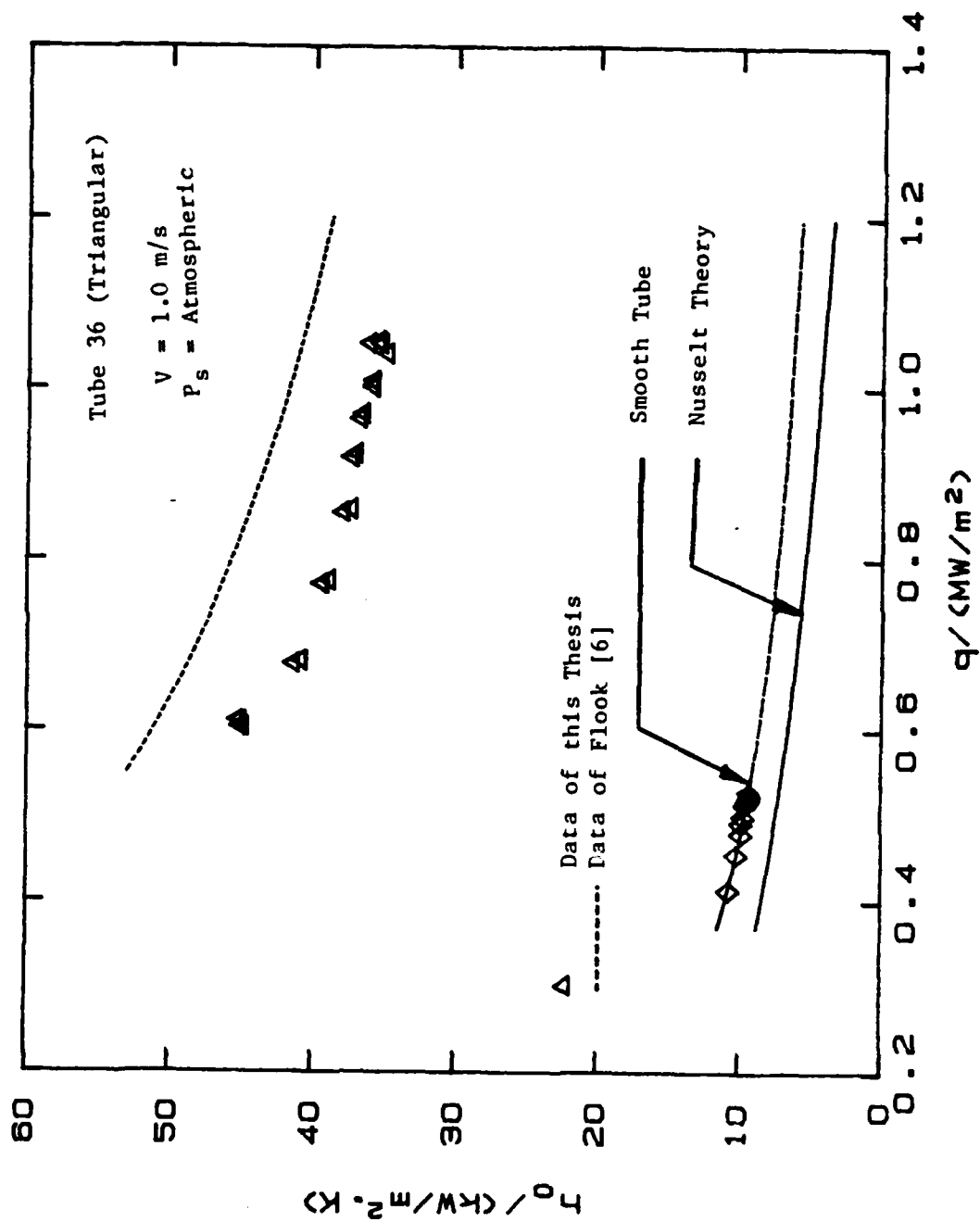


Figure 5.7 Comparison of Finned-Tube Data with Data of Flook [6] (Atmospheric Runs, Tube 36).

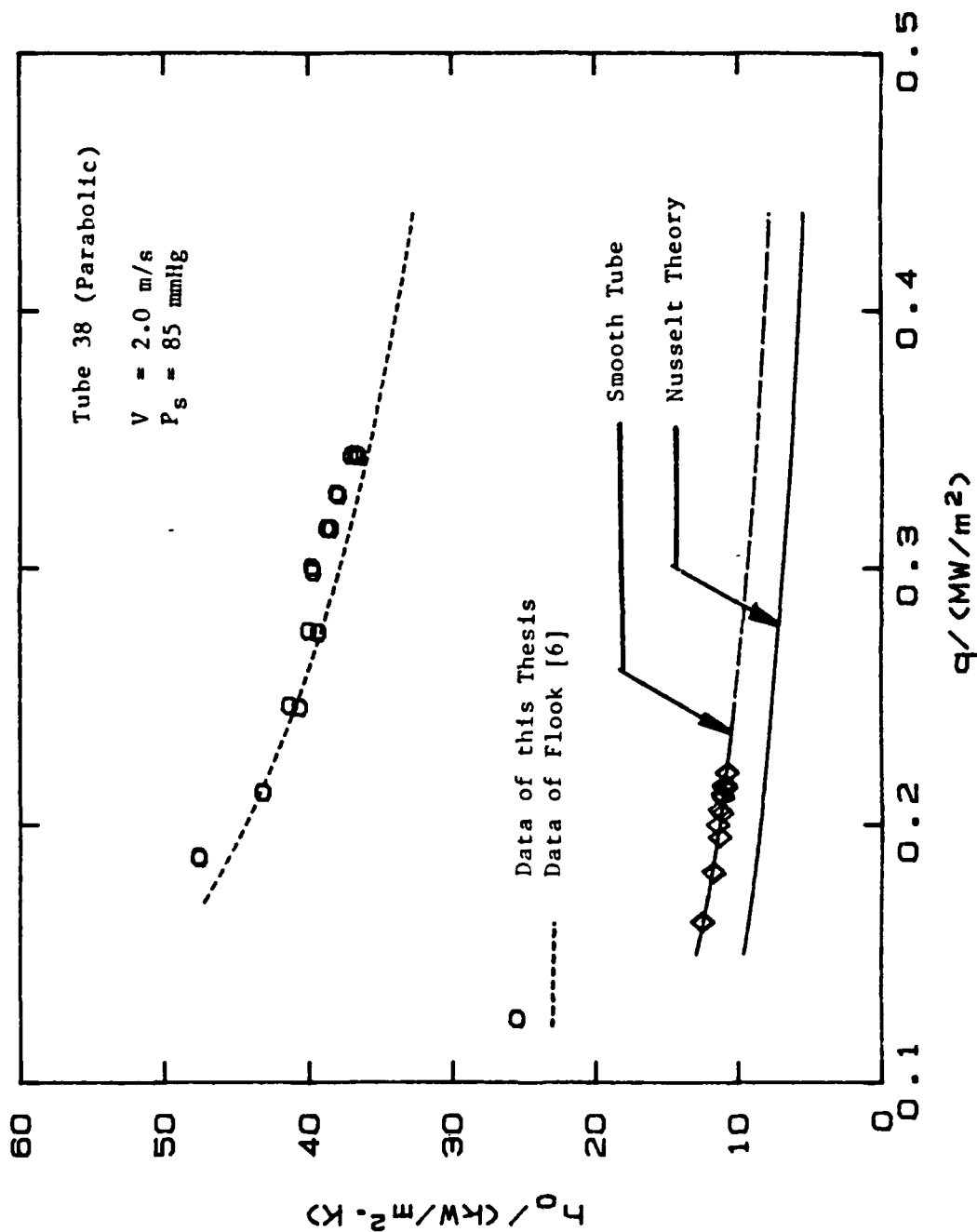


Figure 5.8 Comparison of Finned-Tube Data with Data of Flook [6] (Vacuum Runs, Tube 38).

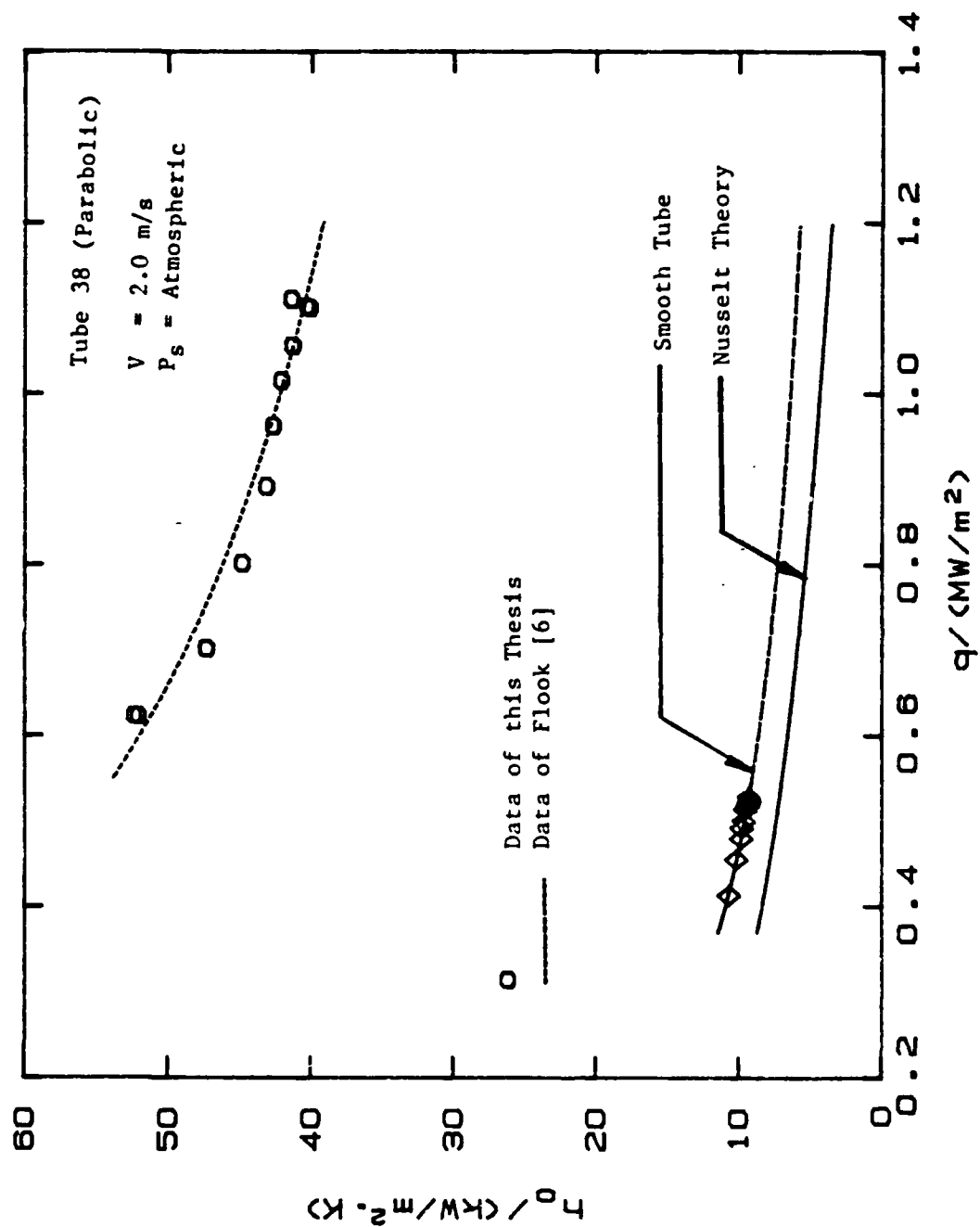


Figure 5.9 Comparison of Finned-Tube Data with Data of Flook [6] (Atmospheric Runs, Tube 38).

C. REPEATABILITY OF DATA

In order to insure the reliability of the data taken, all data runs were repeated, as Georgiadis [5] and Flook [6] did, at least three times on different days. The computed steam-side coefficients for similar conditions (i.e., same tube and about the same operating conditions) on different days agreed to within ± 5 percent for some tubes and ± 10 percent for others. Additionally, data runs were performed on six finned tubes (tubes 6, 17, 27, 28, 36, 38) under similar conditions to verify the repeatability with data taken by Flook [6]. Georgiadis [5] also had tested tubes 6 and 17. Georgiadis and Flook processed their data using the Sieder-Tate constant found by the "direct" method (see Section B of Chapter IV). Therefore, in order to perform a fair comparison, their data were reprocessed by the method used during this investigation (i.e., using the "modified Wilson plot" method directly on finned tube data). Figure 5.1 shows the experimental steam-side heat-transfer coefficients of Georgiadis [5] and Flook [6] and those obtained during this investigation for tube number 6 under vacuum. Figure 5.2 shows similar data for tube 6 under atmospheric pressure, whereas Figures 5.3 and 5.4 show similar data for tube 17. For comparison purposes, the smooth tube data were plotted as well as the data predicted by Nusselt theory. As can be seen from Figure 5.1, the data obtained during this work under vacuum conditions fall above and below the data of Georgiadis [5] and Flook [6] with a maximum variation of 20 percent. At atmospheric conditions, the data fall about 15-20 percent below those of Georgiadis [5]. The agreement with tube 17 is much better as can be seen from Figures 5.3 and 5.4. For tubes 27, 28, 36, and 38 (see Figures 5.5 through 5.9) the agreement is very good, with a deviation of only ± 5 percent except for tube number

36 at atmospheric pressure. In this case; the agreement was ± 26 percent. The disagreement, especially for tube 6, is probably due to a very small contamination on the outside tube surface area of the tube leading to partial dropwise condensation conditions during the runs made by Georgiadis and Flook. Typical uncertainty bands are also included at low and high heat flux to indicate the maximum possible uncertainty. However, the repeatability for most of the tubes shows that the experimental uncertainty is always less than that indicated by the uncertainty bands.

In these figures, the steam-side coefficient is plotted versus the heat flux, and as is always the case for condensation, the heat-transfer coefficient decreases as the heat flux increases. The curves shown in these figures (and subsequent figures) are the least-squares-fit curves according to the following equation:

$$q = a \overline{\Delta T}^b \quad (5.1)$$

where ΔT was computed using the following equation:

$$q = h_o \overline{\Delta T} \quad (5.2)$$

where q was measured experimentally and the steam-side coefficient was calculated by subtracting the inside and wall thermal resistances from the overall resistance as given by equation (5.3):

$$h_o = \frac{1}{\frac{1}{U_o} - R_w - \frac{A_o}{A_i} \frac{1}{h_i}} \quad (5.3)$$

where

$$R_w = \frac{D_o \ln(D_o/D_i)}{2 k_w} \quad (5.4)$$

In equation (5.1) the coefficient a and the exponent b are experimentally determined constants. The values of a and b both under vacuum and atmospheric conditions for all the finned tubes and for the wire-wrapped tubes tested are given in Tables V and VI, respectively.

TABLE V
CONSTANTS OF EQUATION (5.1) FOR FINNED TUBES TESTED

Tube				VACUUM RUNS		ATMOSPHERIC RUNS	
Tube No.	s (mm)	t (mm)	e (mm)	a	b	a	b
06	1.50	1.00	1.00	61190	0.72588	91685	0.71222
17	1.50	0.50	1.00	63210	0.72465	95079	0.71433
27	1.50	1.00	0.50	49315	0.71454	-----	----
28	2.00	1.00	0.50	52515	0.71739	-----	----
36	0.00	2.10	1.00	63847	0.72346	93246	0.71243
38	1.50	0.50	1.00	67881	0.72661	102870	0.71715
45	0.00	2.50	1.00	63459	0.72502	99843	0.70538
46	0.00	1.60	1.00	65976	0.72740	101200	0.71728
47	0.00	1.06	1.00	63456	0.72683	98200	0.71167
49	0.51	0.34	1.00	61325	0.72920	89327	0.71046
50	-----	-----	-----	28144	0.70192	43092	0.64361
51	0.59	0.32	1.00	61928	0.72950	93058	0.71267
52	1.50	0.50	1.00	63672	0.72542	95028	0.71388
53	1.50	0.50	1.00	62772	0.72613	94397	0.71270
54	1.50	1.00	1.00	61452	0.72125	94299	0.71061
55	1.50	1.00	1.00	66987	0.72326	90906	0.70660
56	1.50	1.00	1.00	65674	0.72303	94829	0.70866
57	0.00	2.10	1.00	65871	0.72540	94095	0.69296
58	0.00	2.10	1.00	42916	0.70566	73831	0.68875
59	0.00	2.10	1.00	24364	0.67314	38902	0.67594
60	1.50	1.00	1.00	57695	0.71805	82971	0.69082
61	1.50	1.00	1.00	40173	0.70228	72273	0.69034
62	1.50	1.00	1.00	50021	0.71093	85279	0.69645

D. EFFECT OF FIN PITCH ON HEAT TRANSFER PERFORMANCE OF SPIRAL TUBES WITH TRIANGULAR-SHAPED FINN

This section presents results showing the variations of the steam-side heat-transfer coefficient with heat flux having fin pitch as a parameter. Data were taken on four

AD-A168 391

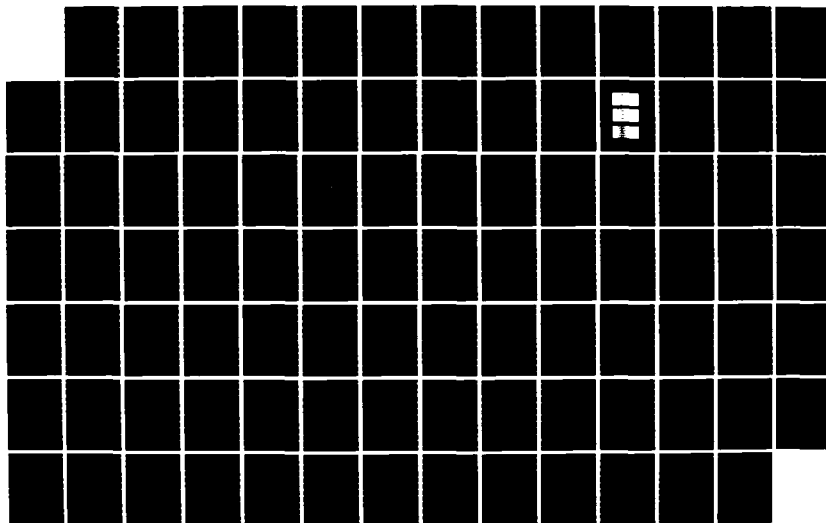
FILM CONDENSATION OF STEAM ON EXTERNALLY ENHANCED
HORIZONTAL TUBES(U) NAVAL POSTGRADUATE SCHOOL MONTEREY
CA E S NITROU MAR 86 NPS-69-86-001 NSF-HEA82-03567

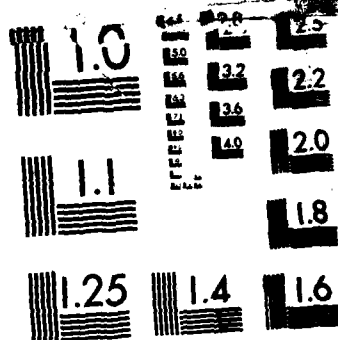
2/2

UNCLASSIFIED

F/G 20/13

NL





MICROCOPY RESOLUTION TEST CHART
NATIONAL BUREAU OF STANDARDS-1963-A

TABLE VI
CONSTANTS OF EQUATION (5.1)
FOR WIRE-WRAPPED TUBES TESTED

Tube				VACUUM RUNS		ATMOSPHERIC RUNS	
Tube No.	Dw (mm)	s (mm)	p (mm)	a	b	a	b
63	1.6	0.94	2.54	26207	0.68301	46280	0.65983
64	1.6	2.03	3.63	32515	0.69452	52572	0.67158
65	1.6	3.02	4.62	32815	0.69733	52403	0.66672
66	1.0	0.95	1.95	27097	0.68988	47762	0.65921
67	1.0	1.82	2.82	35403	0.70265	58145	0.67488
68	1.0	2.91	3.91	36521	0.70144	58421	0.67219
69	0.5	1.10	1.60	34291	0.69228	59000	0.66327
70	0.5	2.04	2.54	40254	0.70477	63569	0.67866
71	0.5	3.13	3.63	39179	0.70190	62272	0.67547

copper tubes with spiral triangular fins. These tubes have the same fin height of 1.0 mm and have fin pitches of 1.06, 1.6, 2.1, and 2.5 mm. Figures 5.10 and 5.11 present data for these tubes under vacuum and at atmospheric pressure, respectively. The smooth-tube data and a curve representing Nusselt theory also included for comparison. The best heat-transfer performance was obtained with the tube with a fin pitch of 1.6 mm.

As shown in Appendix C, the uncertainty in the calculation of the steam-side coefficient increases as the heat flux decreases. Therefore, the comparison of the finned tubes should be performed at a high heat flux, where the uncertainty is small. The comparison of finned tubes is made through the enhancement ratio, E_o . This ratio is defined as the steam-side heat-transfer coefficient of a

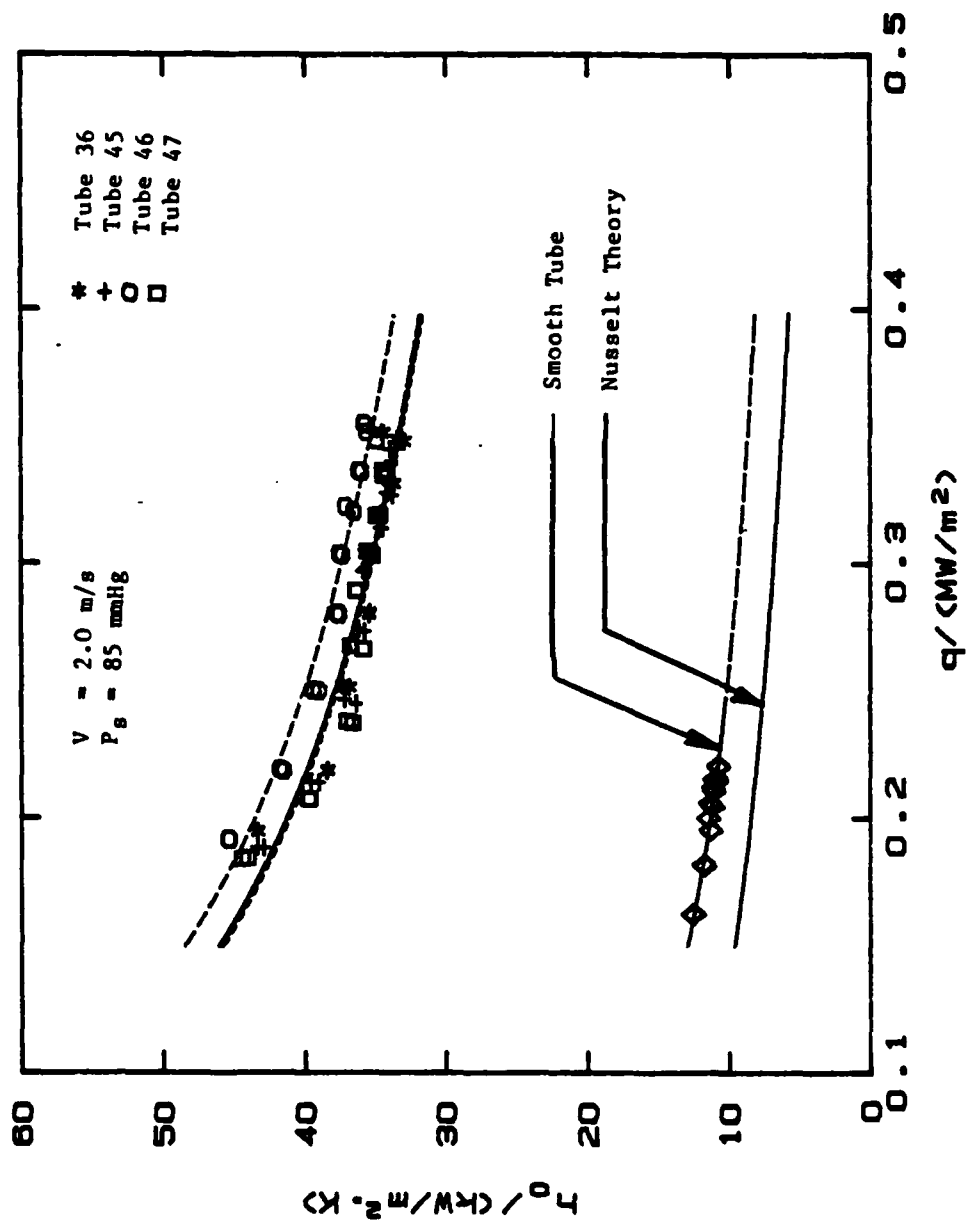


Figure 5.10 Variation of Heat-Transfer Coefficient
 with Heat Flux for the Set of Tubes
 with Spiral Triangular Fins (Vacuum Runs).

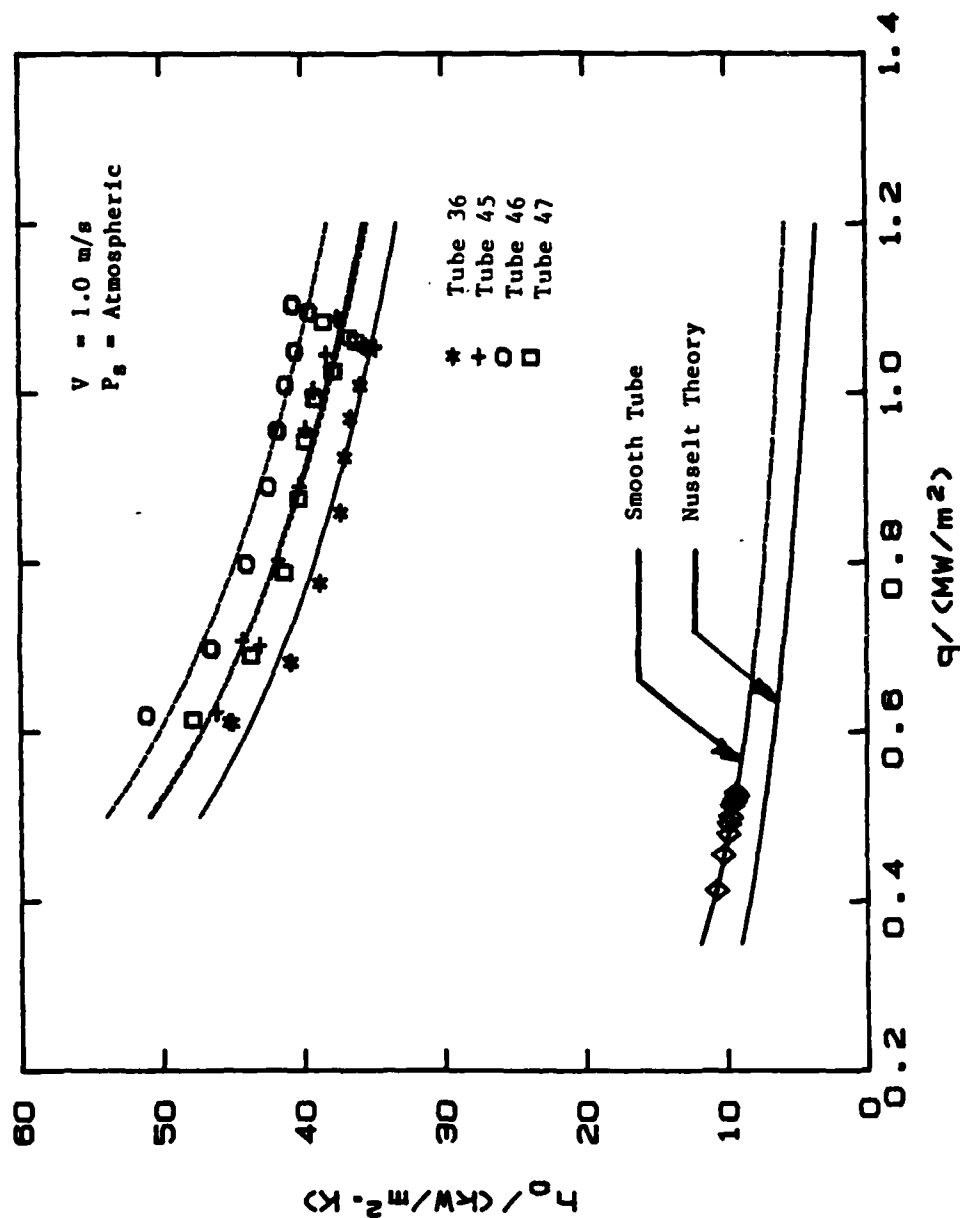


Figure 5.11 Variation of Heat-Transfer Coefficient with Heat Flux for the Set of Tubes with Spiral Triangular Fins (Atmospheric Runs).

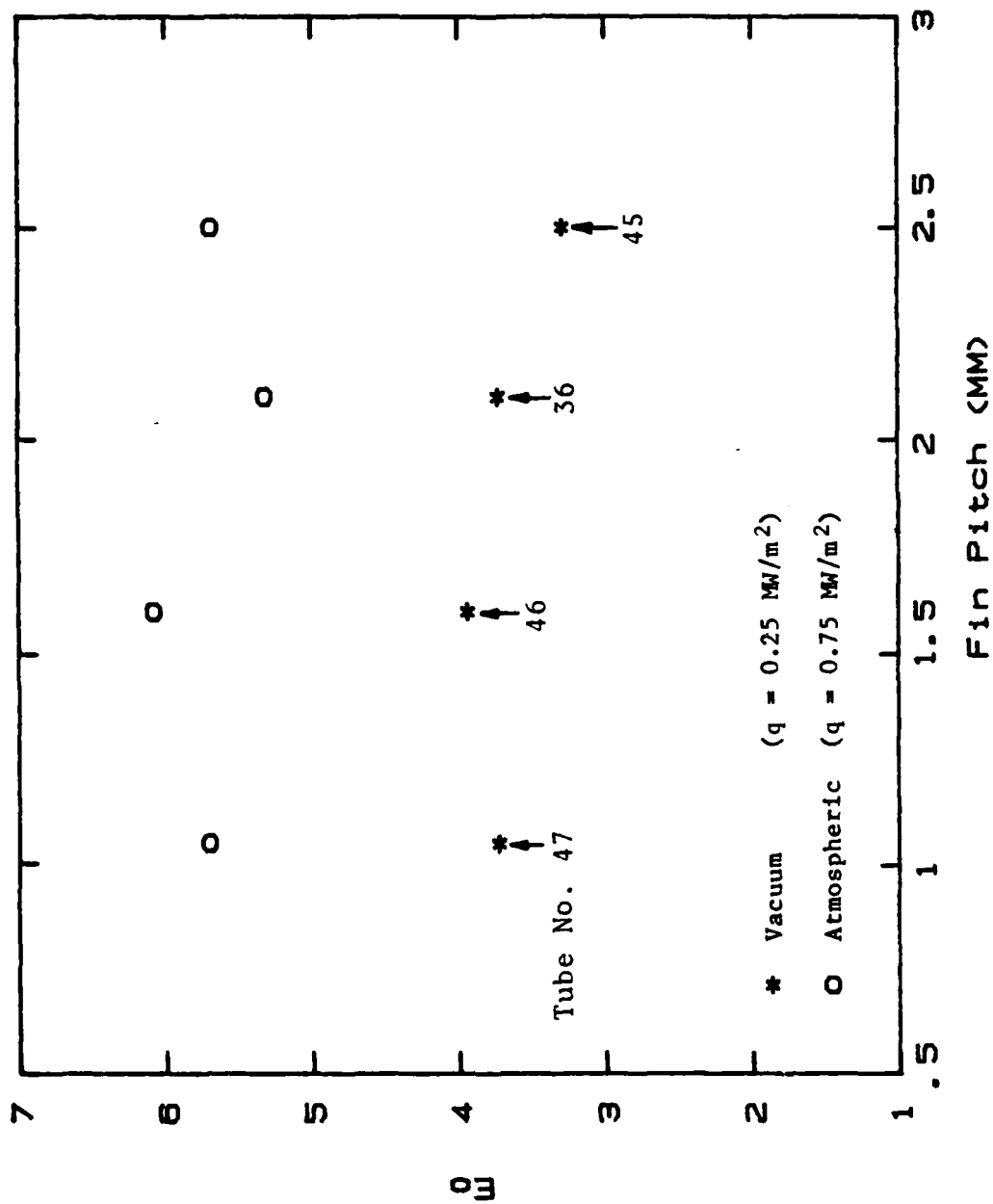


Figure 5.12 Enhancement Ratio for Tubes with Spiral Triangular Fins ($e = 1.0 \text{ mm}$).

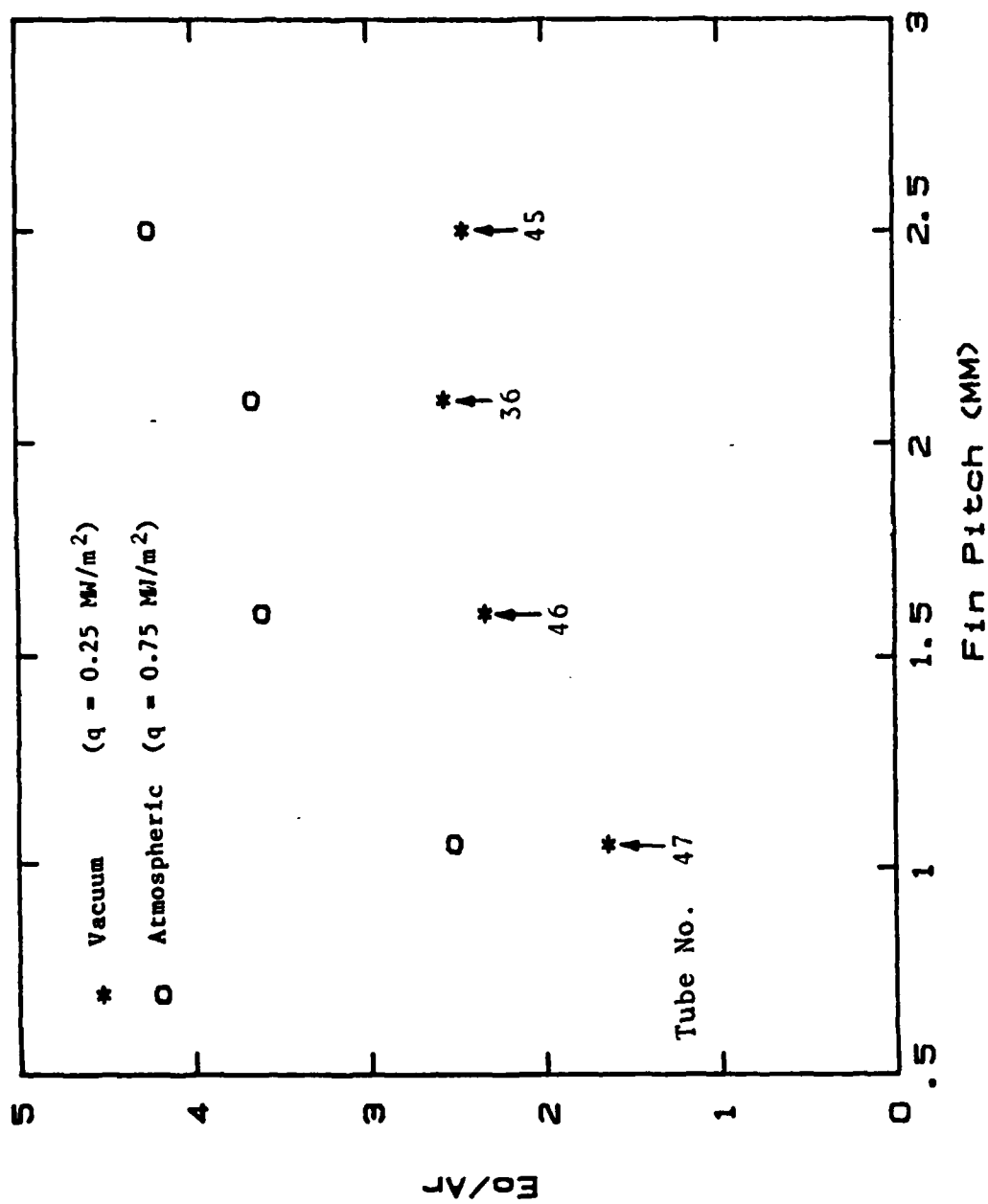


Figure 5.13 Enhancement Ratio for Tubes with Spiral Triangular Fins ($e = 1.0 \text{ mm}$).

finned tube to that of the smooth tube (same diameter as the finned tube root diameter) at the same heat flux. Heat flux values of 0.25 and 0.75 MW/m² were chosen for vacuum and at atmospheric conditions, respectively. For the spiral triangular fins, maximum enhancement ratios of about 3.9 and 6.1 under vacuum and at atmospheric pressure were found. The enhancement ratio at atmospheric pressure is always higher than that under vacuum conditions. At atmospheric pressure, a higher temperature exists, so the condensate has a smaller viscosity, which results in improved drainage from the fin valleys, and smaller surface tension which results in a smaller retention angle. As discussed in Chapter II, the flooded portion of the tube has another thermal resistance due to the thick layer of condensate. Reducing the flooded portion of the tube increases the heat-transfer performance.

Cross plots of the enhancement ratio versus fin pitch are shown in Figure 5.12, while Figure 5.13 shows a cross plot of the normalized ratio E_o/A_r (the ratio of the enhancement ratio to the area ratio). Generally, as the fin pitch increases, E_o/A_r increases. Table III shows that tube 47, with a fin pitch of 1.06 mm, has the largest area ratio, while tube 45 with fin pitch of 2.5 mm has the smallest area ratio, and tube 47 has a poorer performance than either tubes 45 or 46. The poor performance shown by tube 47 can be explained by the fact that, as the pitch decreases, the area of the tube increases, but at the same time the retention angle increases and more flooding occurs. This means that as the fin pitch increases, the interfin spacing was covered by a thick layer of condensate. The additional thermal resistance induced by this layer of condensate overpowers the benefit gained from increased surface area, so the heat-transfer performance is reduced.

As the pitch increases from 1.05 mm to 1.6 mm, the retention angle decreases more than the area decreases.

This results in a larger enhancement ratio for the tube with a pitch of 1.6 mm. Beyond this point, the area ratio decreases while the retention angle decreases slowly and results in a smaller heat transfer performance. In order to obtain a clearer understanding on the heat-transfer performance, the enhancement ratio was divided by the area ratio, and thus, the effect of the changing area was eliminated. As Figure 5.13 shows, the enhancement ratio depends on other factors in addition to the fin area, such as the surface tension effect. As discussed in Chapter II, the surface tension-induced pressure gradient from the fin tip to the fin root is responsible for thinning of the condensate film and thereby improving the heat-transfer performance in the unflooded portion of the tube. Also, the surface-tension forces cause condensate flooding, resulting in poorer performance in the flooded portion of the tube. Figure 5.13 shows that the normalized enhancement ratio is higher for the tube with fin pitches of 2.1 mm and 2.5 mm under vacuum and at atmospheric pressure, respectively. Therefore, the optimum fin pitch is between 2.1 and 2.5 mm based on normalized enhancement ratio, while the optimum fin pitch is 1.6 mm based on the enhancement ratio. As shown by Edwards et al. [20], as the pitch increases for the same fin height, the heat-transfer coefficient increases. However, as the fin pitch increases, the tube is easily flooded. Because the retention angle is greater under vacuum than that at atmospheric pressure, the tube with fin pitch of 2.5 mm has a smaller retention angle than that of the tube with fin pitch of 2.1 mm under vacuum, resulting in poorer heat-transfer performance. However, at atmospheric pressure, since the retention angle is less than under vacuum conditions, the tube with a fin pitch of 2.5 mm has a better heat-transfer performance than the tube with a fin pitch of 2.1 mm.

E. EFFECT OF FIN SHAPE ON HEAT-TRANSFER PERFORMANCE

In order to study the effect of fin shape, data were taken on two sets of copper tubes with fins of four different shapes. All the fins were manufactured with same fin spacing and fin height. The first set of tubes (17, 38, 52 and 53) had rectangular, parabolic, triangular and trapezoidal fin shapes, respectively, with a fin-base thickness of 0.5 mm, while the second set of tubes (6, 54, 55 and 56) had a fin-base thickness of 1.0 mm. Dimensions for these fins are given in Table III.

The performance of tubes 17, 38, 52, and 53 under vacuum conditions is shown in Figure 5.14, while Figure 5.15 depicts their performance at atmospheric pressure. For comparison purposes, data for a smooth tube are also shown. The tube with the "parabolic" fin profile (tube 38) showed the best heat-transfer performance, while the other three tubes performed about equally, under both pressure conditions. As shown in Table III, an enhancement ratio of 4.1 and 6.2 were obtained for the tube with "parabolic" fins under vacuum and at atmospheric pressure, respectively. Also, it can be seen that the area ratio of the tube with "parabolic" fins is less than that of the tube with rectangular fins and the tube with trapezoidal fins, and larger than that of the tube with triangular fins. Eliminating the effect of increased area, the ratio E_o/A_r is larger for the tube with "parabolic" fins under atmospheric and vacuum conditions.

The reason for the greater enhancement ratio is probably due to the continuous change of radius of curvature (increasing from the fin tip to the fin root) for the "parabolic" shaped fins. The condensate film has a convex shape at the fin tip and a concave shape at the fin root. The condensate film follows approximately the curvature of the wall surface at the fin tip. Because of the convex condensate surface at the fin tip and the concave condensate

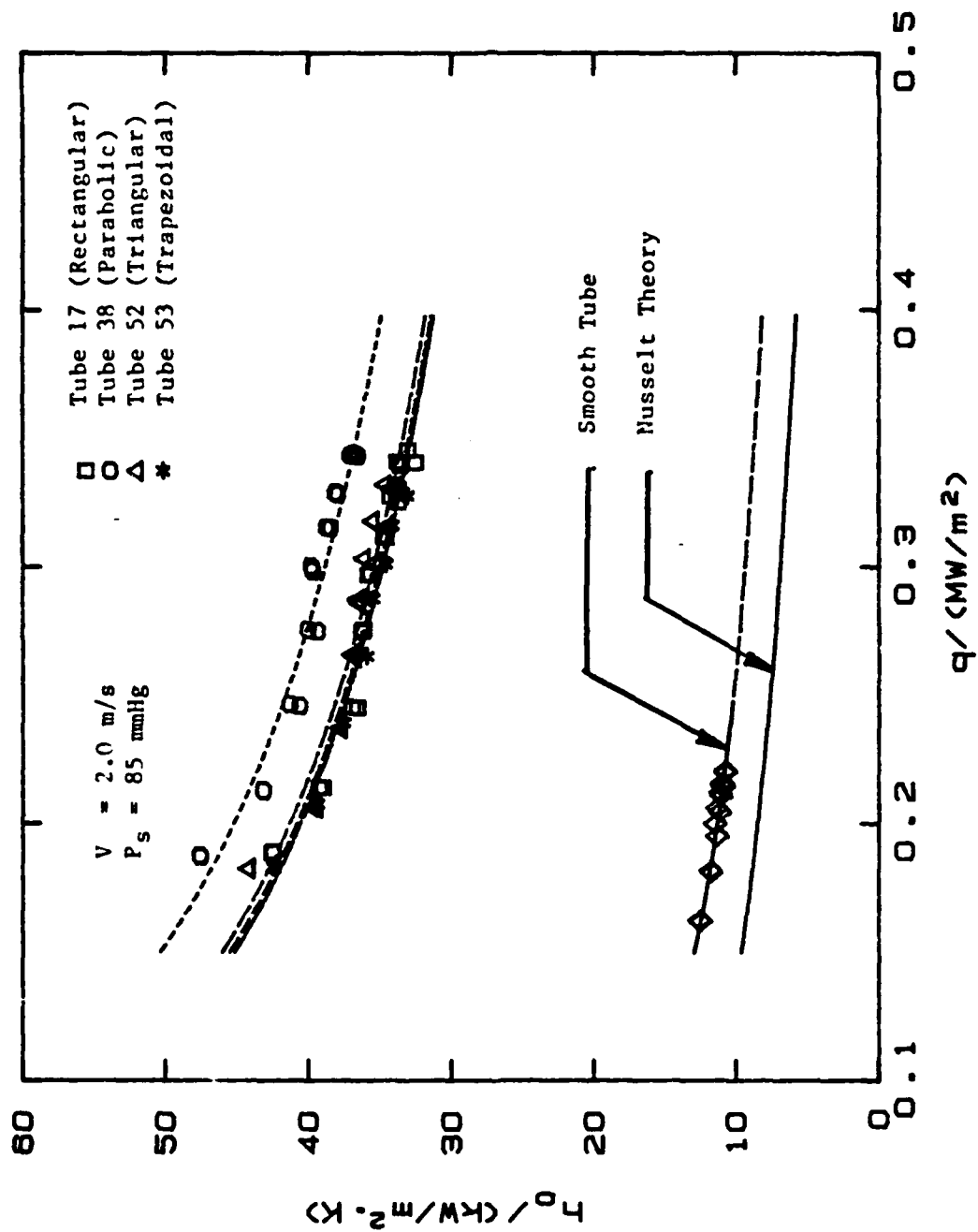


Figure 5.14 Effect of Fin Shape on Heat-Transfer Coefficient for Vacuum Runs ($t_b = 0.5 \text{ mm}$).

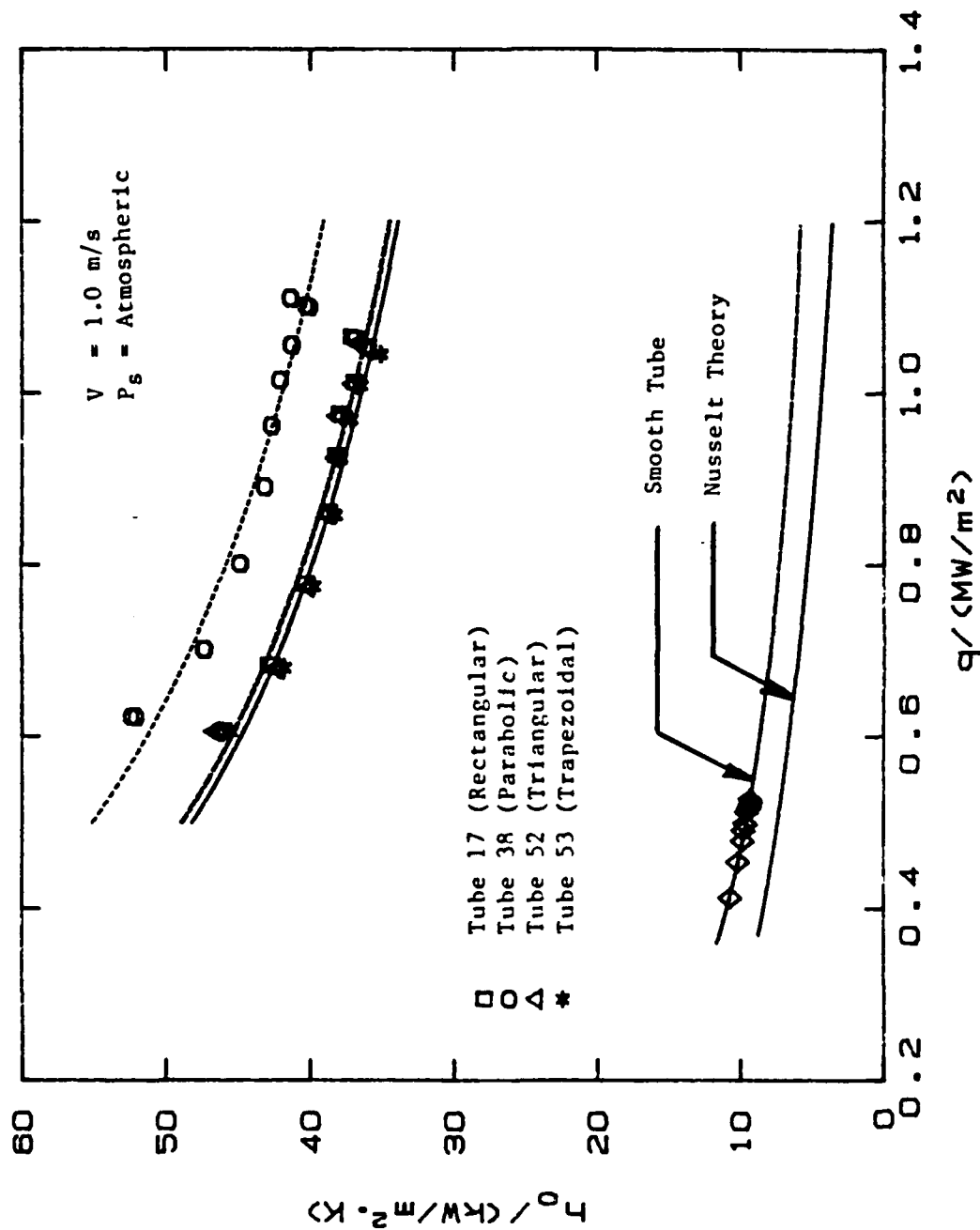


Figure 5.15 Effect of Fin Shape on Heat-Transfer Coefficient for Atmospheric Runs ($t_b = 0.5 \text{ mm}$).

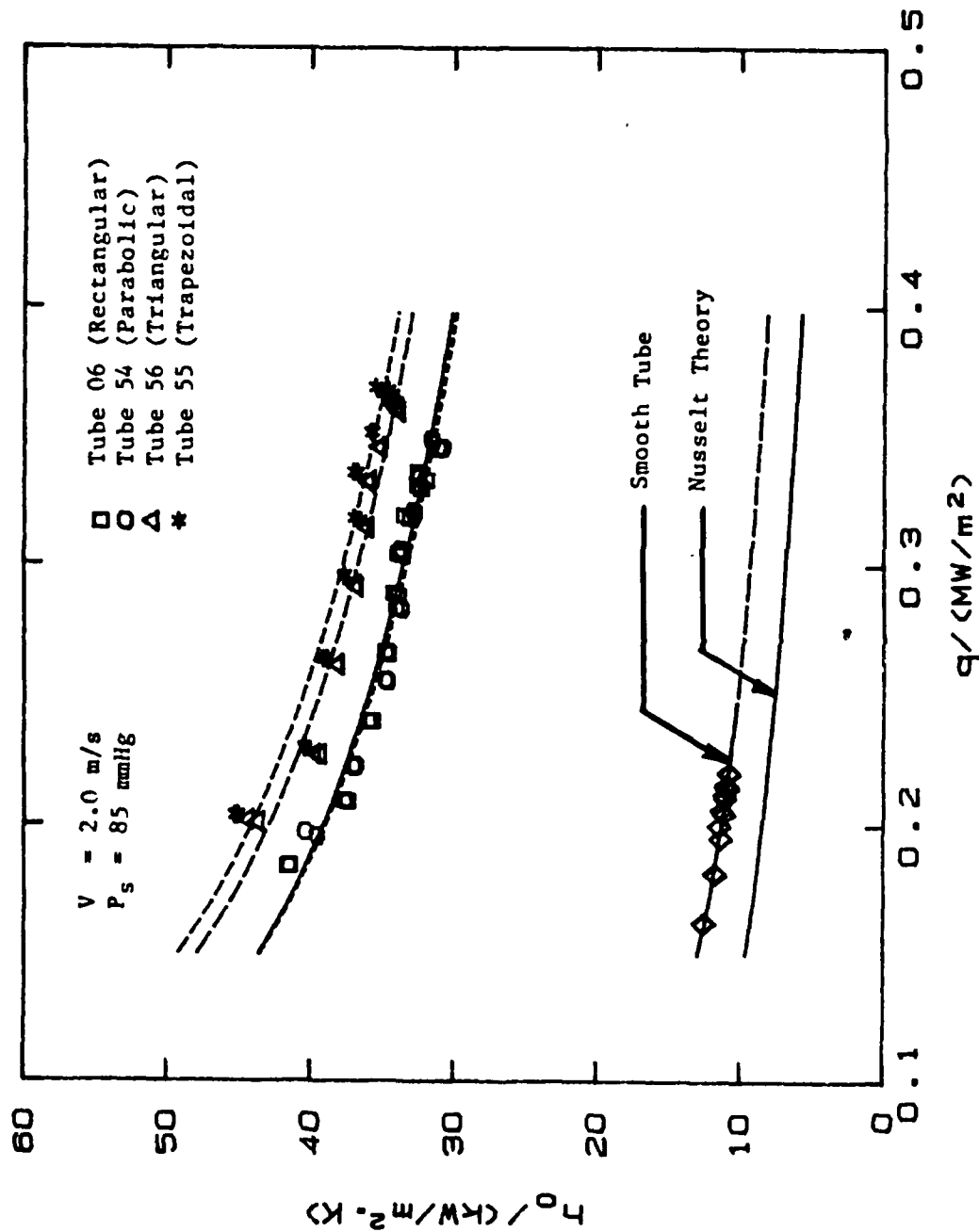


Figure 5.16 Effect of Fin Shape on Heat-Transfer Coefficient for Vacuum Runs ($t_b = 1.0 \text{ mm}$).

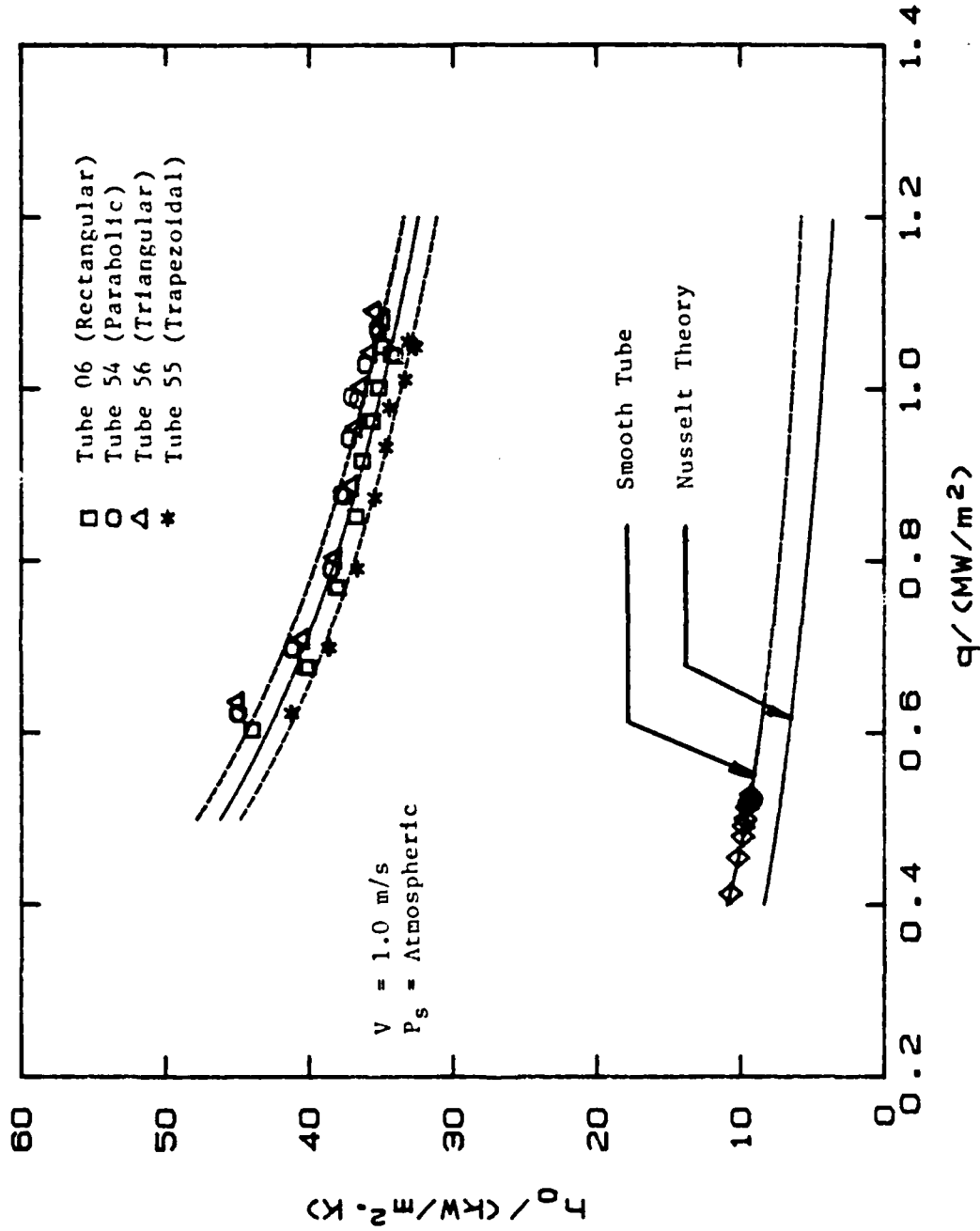


Figure 5.17 Effect of Fin Shape on Heat-Transfer Coefficient for Atmospheric Runs ($t_b = 1.0 \text{ mm}$).

surface near the fin root, the pressure within the condensate is larger at the fin tip and smaller at the fin root. Therefore, an appreciable pressure gradient exists from the fin tip to the fin root. The gradual increase of radius of curvature results in a gradual decrease in pressure within the condensate, which is very important for improved condensate flow, resulting in a thinner film and larger heat-transfer coefficient than if the fin sides were flat. Therefore, the parabolic fins should outperform all other three tubes, as shown in Figures 5.14 and 5.15.

Also, Adamek [24] and Mori et al. [8] have shown that the optimum fin shape is that which induces a continuous pressure gradient due to the surface tension effect or which has large curvature at the fin tip and continuously decreasing toward the fin root. Therefore a continuous decrease in the pressure gradient exists and this thins the condensate film continuously, resulting in better heat transfer performance. For the case of tube 38, there is a continuous decrease of the curvature, while this was not happening for the other three tubes of the first set although they had a sharp leading edge. Therefore tube 38 exhibits better heat-transfer performance than the other three tubes in its group.

Figures 5.16 and 5.17 show the performance of tubes 6, 54, 55 and 56 under vacuum and at atmospheric conditions, respectively. Again, the smooth tube data are included for comparison purposes. For this set of tubes, the best performance is obtained from tube 55 with the trapezoidal fins, while the tube with triangular fins performed second and the remaining two tubes performed about equally well under vacuum conditions. However, the parabolic and triangular shapes outperformed the other shapes for atmospheric conditions. The poorer performance of tube 54 under vacuum conditions was not expected. As Figure 3.7 shows, the fins

do not have the shapes as claimed above due to the difficulties encountered in machining. The unexplainable trends shown by the tube with "parabolic" fins (tube 54) was found to be the result of the actual fin shape that was very different from what was expected. At the conclusions of the data runs presented in this thesis, this tube was destroyed and a magnified photograph of the fin cross-section was taken. As can be seen from Figure 3.5, these fins do not have a profile with gradually decreasing curvature from the fin tip to root. Therefore, unlike in the previous set of tubes (17, 38, 52 and 53), the data taken on the second set of tubes are inconclusive. Since the condensation process on a finned tube is extremely complex, owing to the very large number of parameters, it may be unwise to draw conclusions from the above-mentioned results. Nevertheless, the data for the second set of tubes are presented in this thesis for completeness.

From Figure 3.7 it is clear that: 1) the "parabolic" fins of the tube 38 with fin base thickness of 0.5 mm had a straight fin side and a fin tip with a sharp leading edge, while careful examination of a cross-section of the "parabolic" fins of tube 54 shows a straight fin side with a near semicircle at the fin tip. Tube 38 had a small radius of curvature at the fin tip, while tube 54 had larger radius of curvature at the fin tip. These differences in geometry may have caused the observed data.

F. EFFECT OF FIN THERMAL CONDUCTIVITY ON PERFORMANCE

To investigate the effect of fin-metal thermal conductivity on the heat-transfer performance, four spirally finned tubes with triangular fins and two tubes with rectangular fins were manufactured. As shown in Table I, the four spiral tubes were made of copper, copper-nickel, stainless steel, and aluminum, respectively (tubes 57, 58, 59 and 60). The two tubes with rectangular fins were made of copper-nickel and aluminum (tubes 61 and 62). All tubes

had the same fin height of 1.0 mm. The tubes with a rectangular fin shape have the same fin dimensions as the "optimum" copper tube (tube 6) found by Georgiadis [5], while the spiral tubes had a fin pitch of 2.1 mm. The results for data runs taken under vacuum and at atmospheric pressure are shown in Figures 5.18 and 5.19, respectively, for the spiral tubes. For the tubes with rectangular fins, the variation of heat-transfer coefficient with heat flux is shown in Figures 5.20 and 5.21 under vacuum and at atmospheric conditions, respectively. Figure 5.18 shows that the copper tube exhibits the best heat-transfer performance, while the stainless steel shows the worst performance. The second best is the aluminum spiral tube followed by the copper-nickel tube. The same trend is also seen in Figure 5.19 at atmospheric pressure. Enhancement ratios as high as 3.5 and 4.4 under vacuum and atmospheric conditions, respectively, were found. Cross plots of enhancement ratio E_o and normalized enhancement ratio E_o/Ar versus the thermal conductivity are shown in Figures 5.22 and 5.23, respectively.

A similar trend exists for tubes with rectangular fin profiles as shown in Figures 5.20 and 5.21. For comparison, the data of Flook [6] for the copper tube with $D_o = 14.5$ mm and $D_i = 13.5$ mm with the same fin dimensions as the aluminum and copper-nickel tube (tube 39) are also included. Also in the same Figures the data of tube 6 are included.

The thermal conductivity of aluminum (167 W/m.K) is about half of copper (385 W/m.K), while copper nickel and stainless steel have much lower values (i.e., 45 W/m.K and 15 W/m.K, respectively). Since the thermal resistance through the fin increases (i.e., the fin efficiency decreases) with decreasing thermal conductivity, the copper tube must show the best heat-transfer performance, while the stainless steel tube must show the poorest performance. As

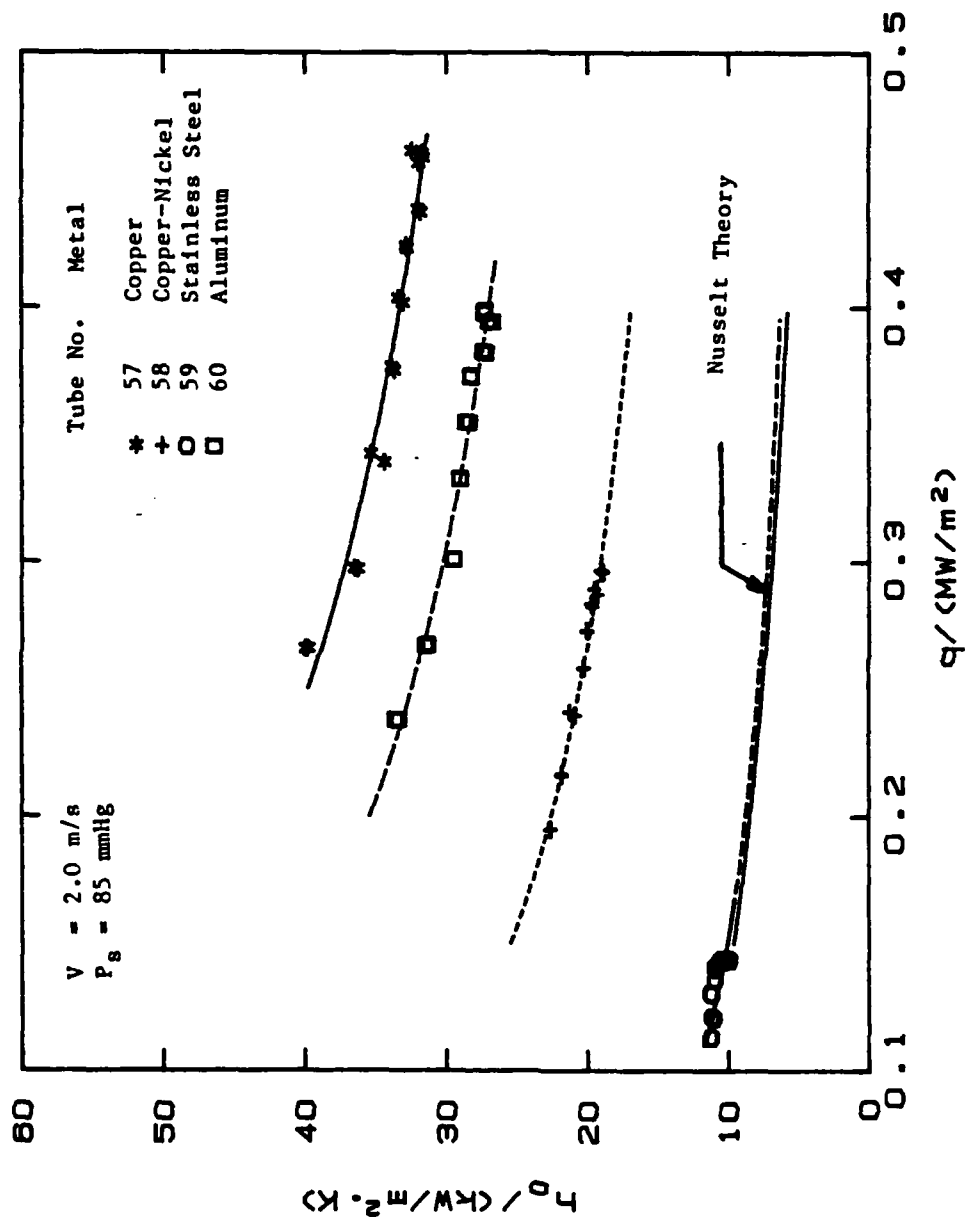


Figure 5.18 Effect of Wall Thermal Conductivity on Heat-Transfer Coefficient for Tubes with Spiral Triangular Fins (Vacuum Runs, Tubes 57, 58, 59 and 60).

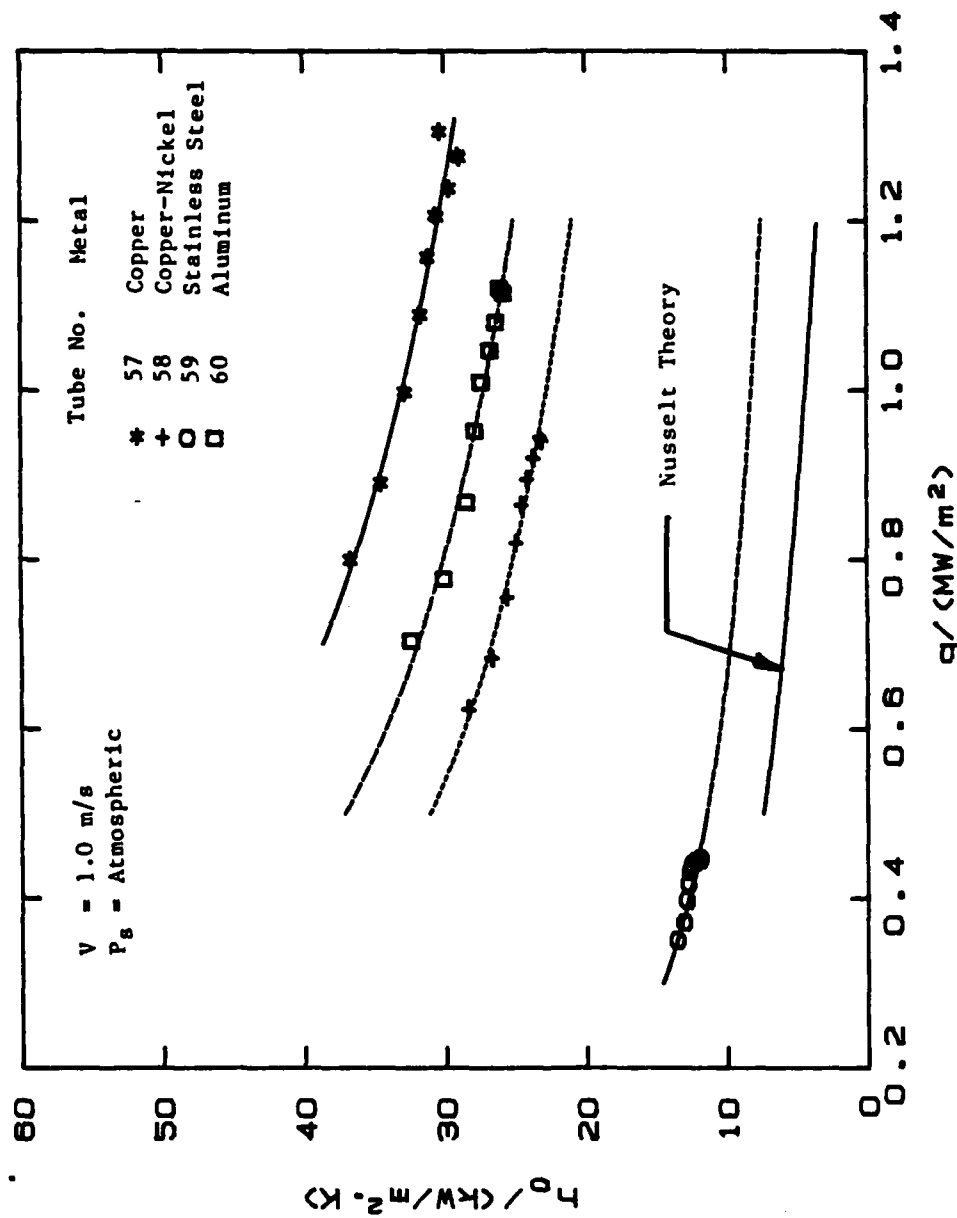


Figure 5.19 Effect of Wall Thermal Conductivity on Heat-Transfer Coefficient for Tubes with Spiral Triangular Fins (Atmospheric Runs, Tubes 57, 58, 59 and 60).

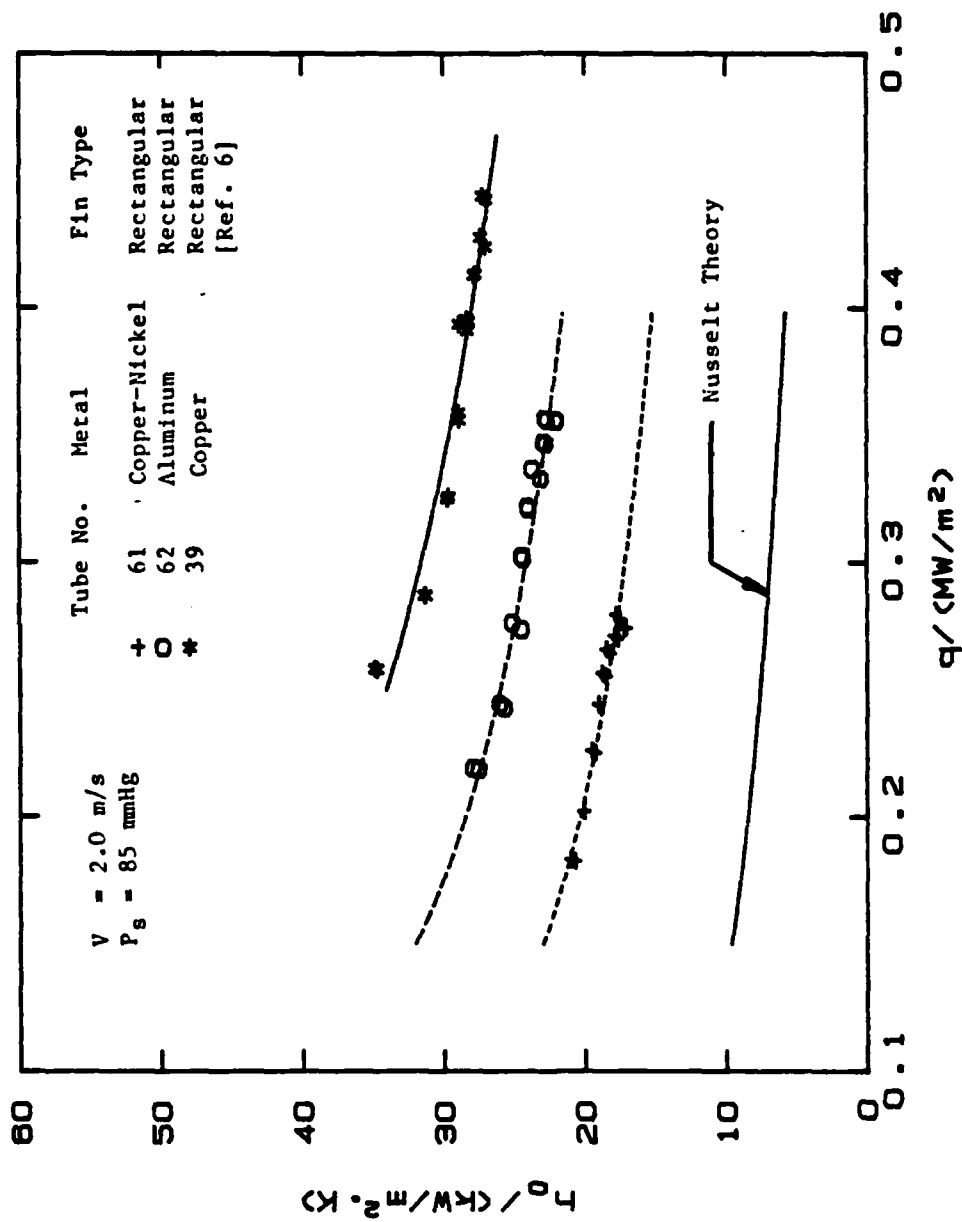


Figure 5.20 Effect of Wall Thermal Conductivity on Heat-Transfer Coefficient for Tubes with Rectangular Fin Shape (Vacuum Runs, Tubes 39, 61 and 62).

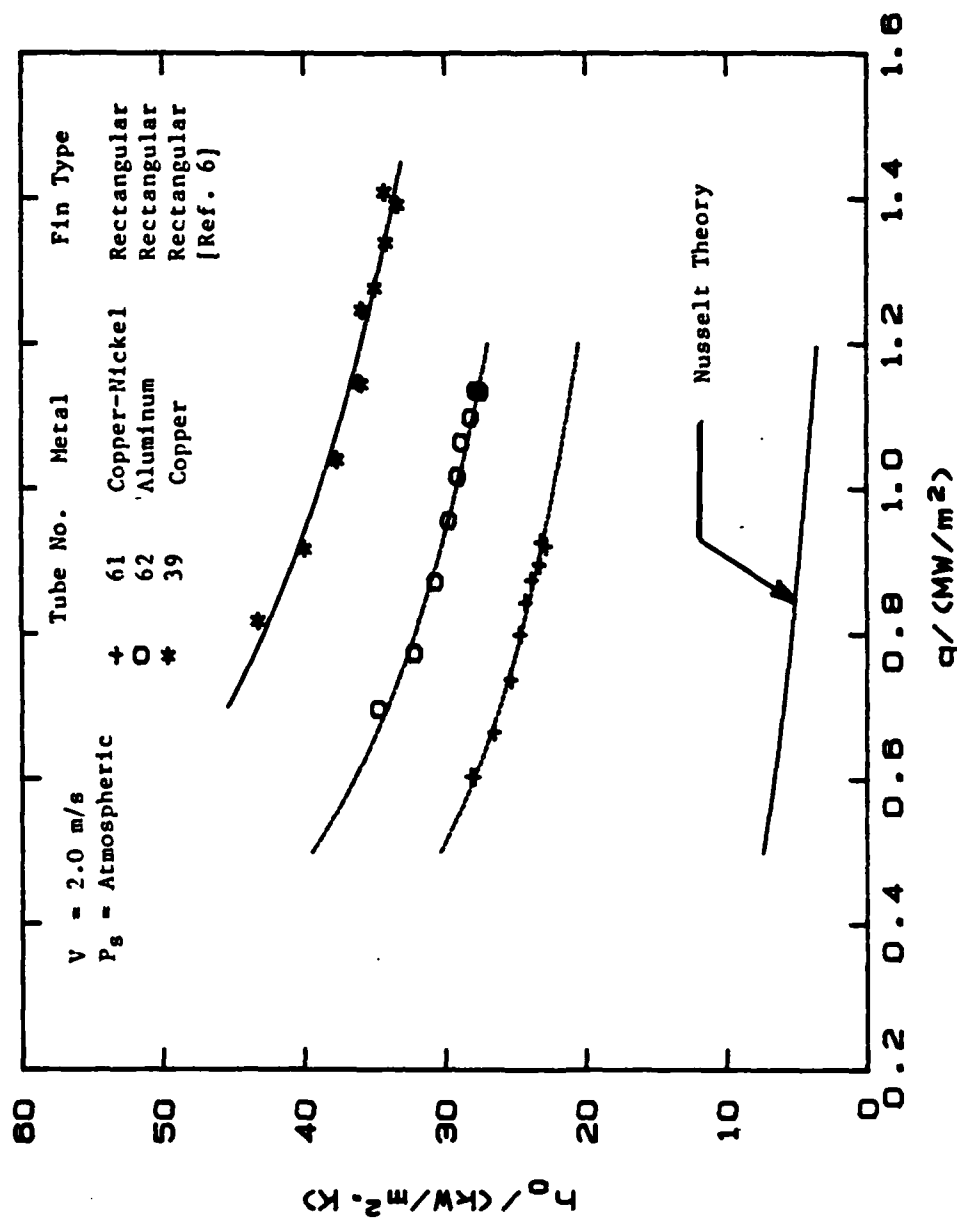


Figure 5.21 Effect of Wall Thermal Conductivity on Heat-Transfer Coefficient for Tubes with Rectangular Fin Shape (Atmospheric Runs, Tubes 39, 61 and 62).

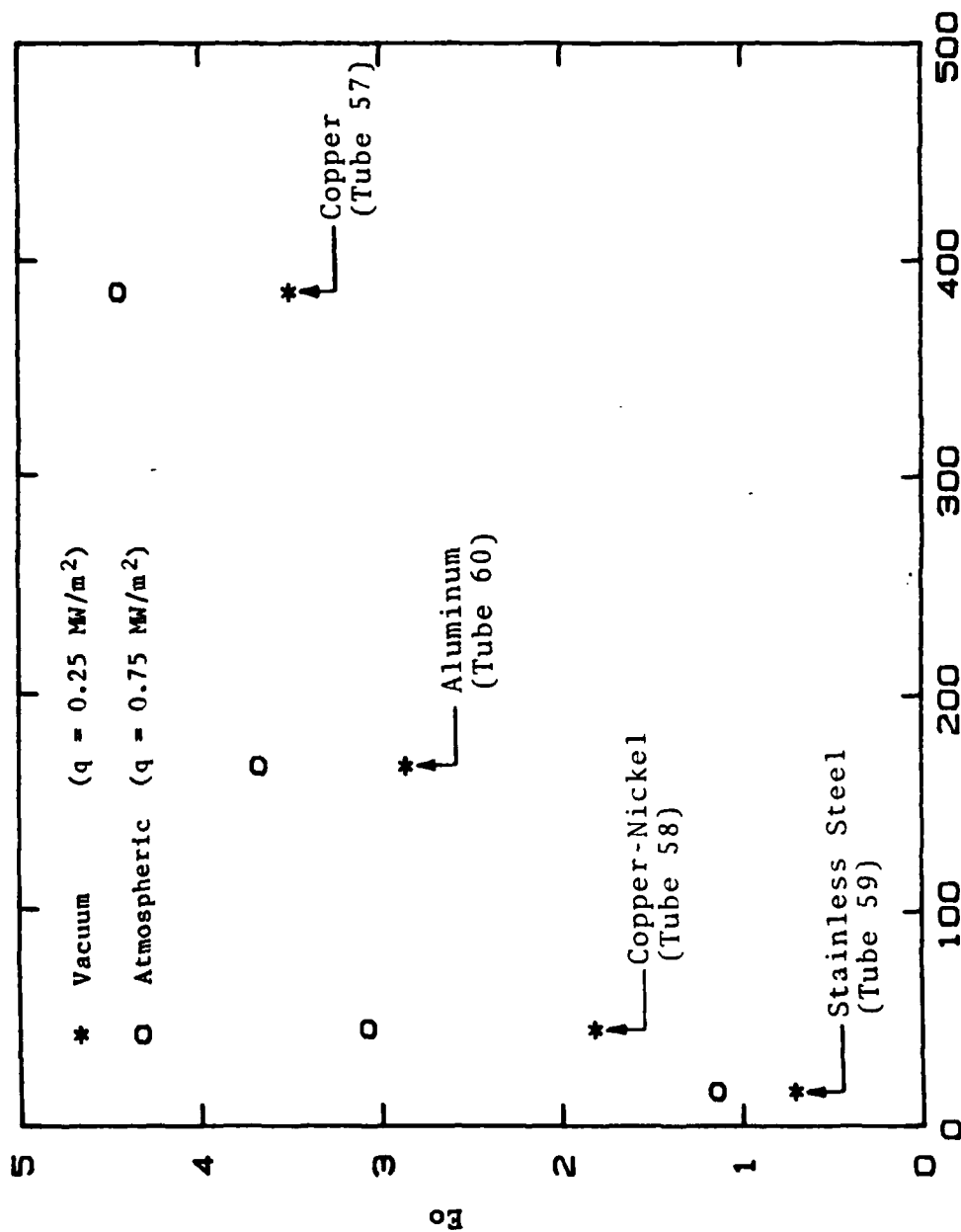


Figure 5.22 Effect of Tube Metal Thermal Conductivity on Enhancement Ratio for Tubes with Spiral Triangular-Shaped Fins.

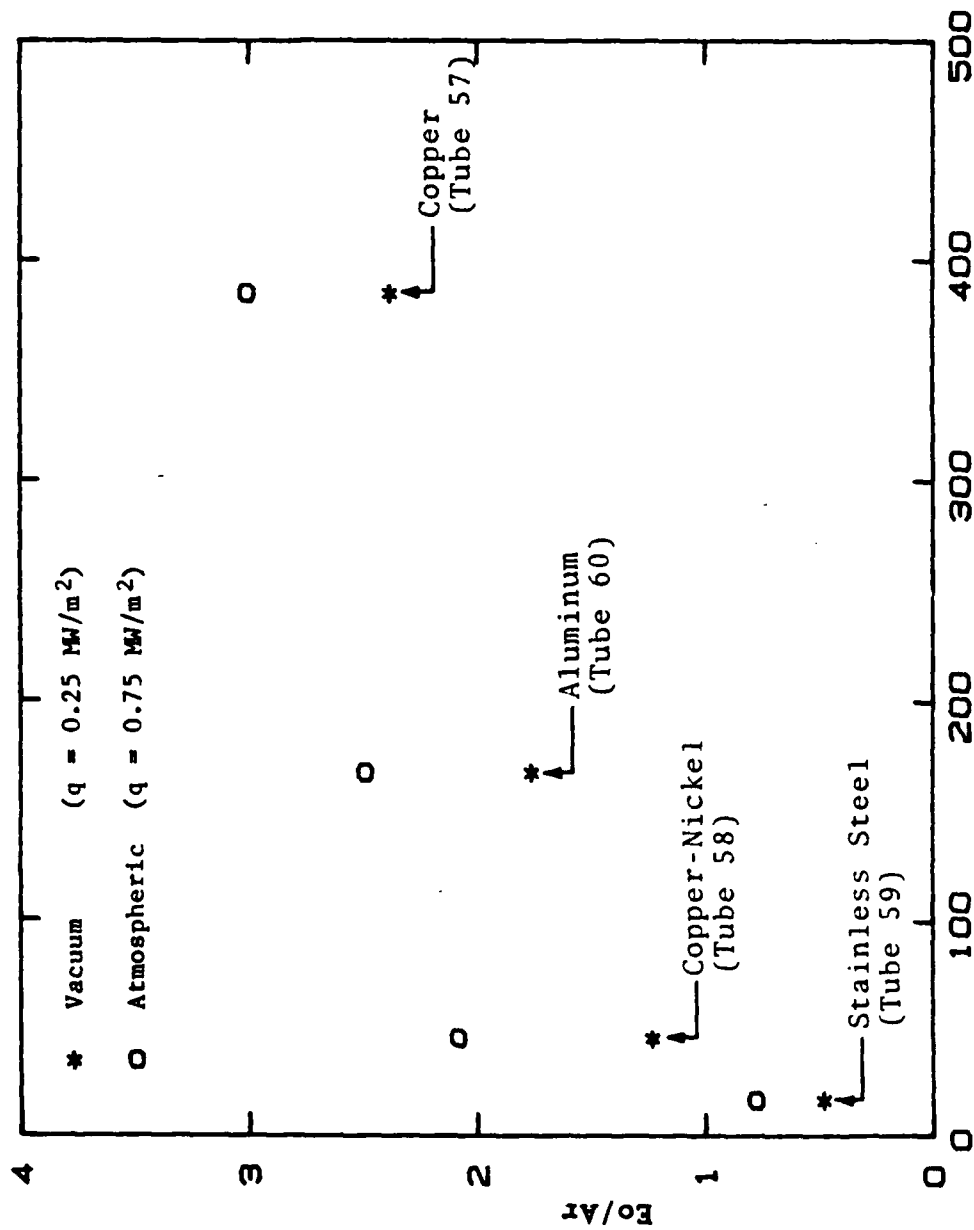


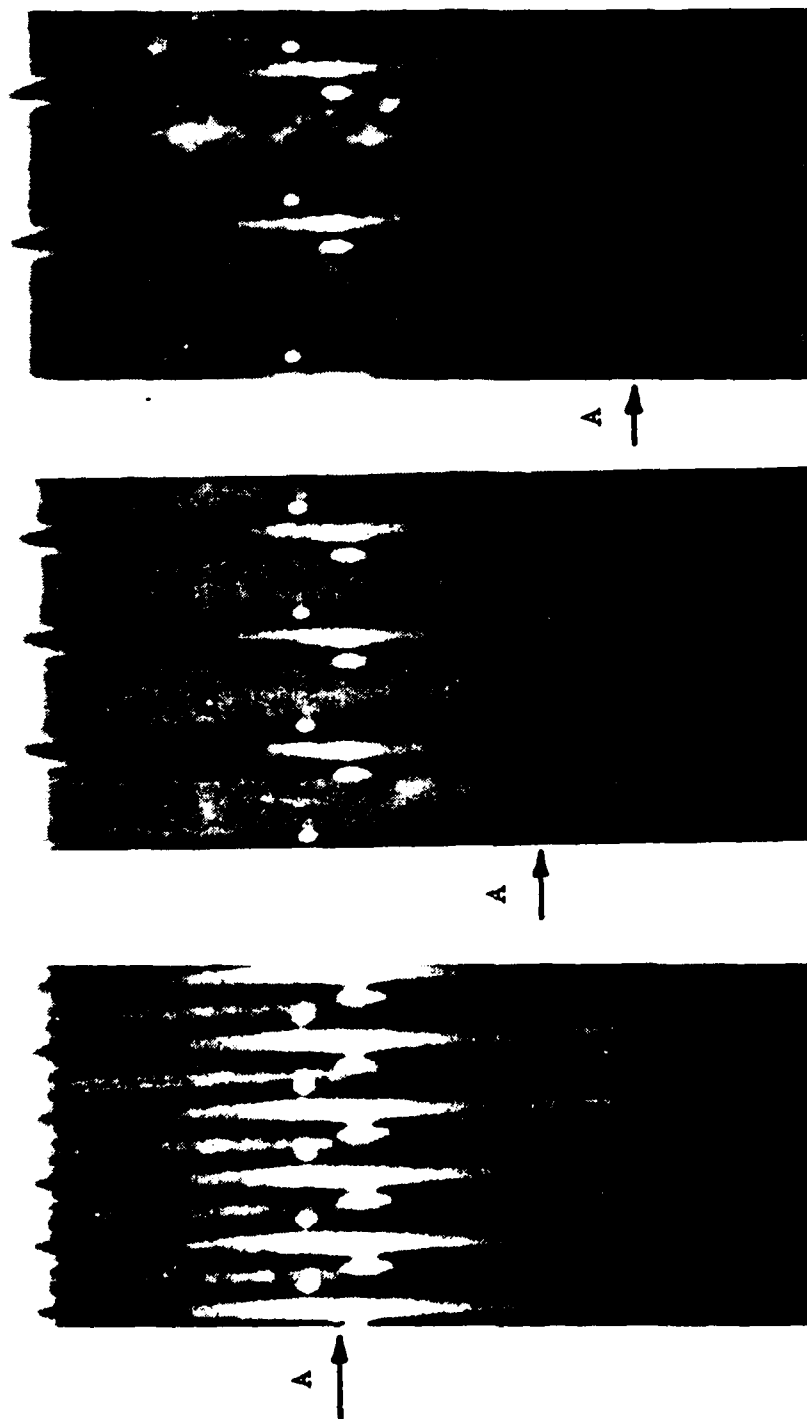
Figure 5.23 Effect of Normalized Tube Metal Thermal Conductivity on Enhancement Ratio for Tubes with Spiral Triangular-Shaped Fins.

can be seen from Figures 5.18 through 5.22, this trend is very clear.

G. PERFORMANCE OF WIRE WRAPPED TUBES

1. Condensate Retention Angle for Wire-Wrapped Tubes

Wire-wrapped tubes are somewhat similar to finned tubes with regard to their susceptibility to condensate retention. Since the portion of the tube with the retained condensate would result in a poor heat-transfer performance, it was necessary to study this phenomenon on these wire-wrapped tubes. For this purpose, it is possible to use the Webb et al. [17] model (as discussed in Chapter II), which was developed for a tube with fins of arbitrary shape (see equation (2.10)). However, they did not test this model for wire-wrapped tubes. Therefore, it was necessary to experimentally measure the condensate retention angle for these tubes, so that the Webb et al. model can be modified to predict it for wire-wrapped tubes. For this purpose, measurement of the condensate retention angles were made for the wire-wrapped tubes under static conditions. Photographs were taken; slides were made and accurate measurements were made on the screen. Figure 5.24 shows photographs of portions of tubes with a wire diameter of 0.5 mm and pitches of 1.6, 2.5 and 3.6 mm (tubes 69, 70 and 71), respectively. Careful examination of the photographs revealed that water was trapped all around the tube in a region very near of the wires. The film thickness was about the same along the distance from the top of the tube to the bottom, until some point where the meniscus of the water had a concave profile in the region where the tube starts to be fully flooded between two adjacent wires. In this case, the retention angle is defined as the angle from the bottom of the tube to point A (see Figure 5.24), where the surface tension forces balance the weight of the condensate. The retention angle was computed by equation (5.5) based on the height from the bottom of the tube to point A and the tube radius.



$p = 3.6 \text{ mm}$

$p = 2.5 \text{ mm}$

$p = 1.6 \text{ mm}$

Figure 5.24 Photograph Showing the Condensate Retention
on Three Wire-Wrapped Tubes ($D_w = 0.5 \text{ mm}$).

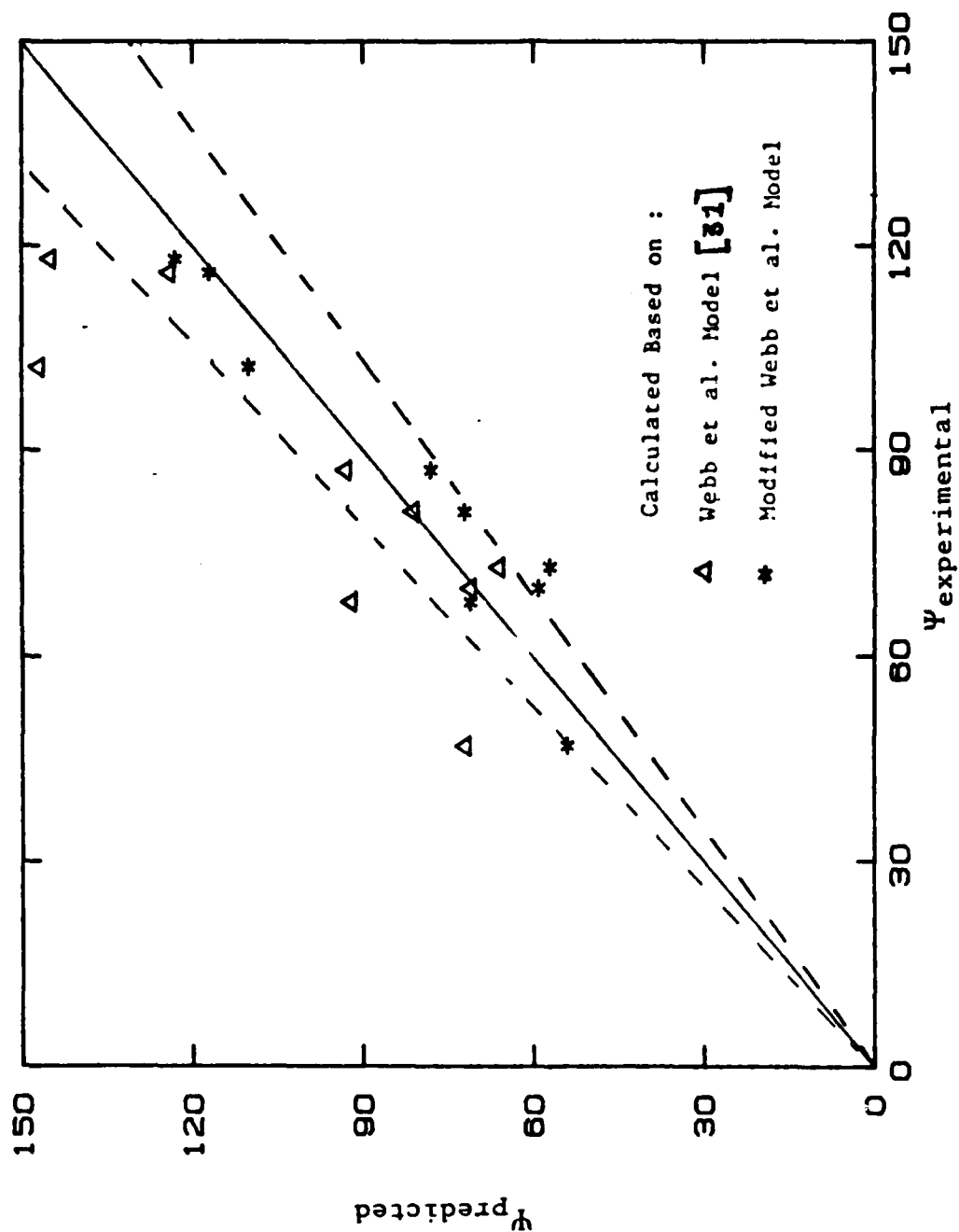


Figure 5.25 Comparison of Measured and Calculated Condensate Retention Angles for Wire-Wrapped Tubes.

TABLE VII
MEASURED RETENTION ANGLES (Ψ)

Tube #	D _w (mm)	P (mm)	Measured Degrees	Calculated Degrees
63	1.6	2.5	116	117
64	1.6	3.6	81	72
65	1.6	4.6	73	57
66	1.0	2.0	118	123
67	1.0	2.8	87	78
68	1.0	3.9	70	59
69	0.5	1.6	102	110
70	0.5	2.5	68	71
71	0.5	3.6	47	54

$$\psi = (1 - \frac{x}{R}) \quad (5.5)$$

Table VII lists the results for all nine tubes (tubes 63 through 70). Using the Webb et al. model [14], attempts were made to predict the measured retention angles, and comparison is shown in Figure 5.25 (see the "triangular" symbols--the "star" symbols will be discussed below). As can be seen, the Webb et al. model overpredicts the condensate retention angle for most of the tubes. Therefore, this model was modified for the present study (i.e., steam condensation on horizontal wire-wrapped tubes). The examination of equation (2.10), reveals that the condensate retention angle would decrease with increasing wire diameter while all other parameters are kept constant. However, the experimentally measured retention angles shown in Table VII show the opposite trend (i.e., ψ increases with increasing D_w). Therefore, it was necessary to modify the Webb et al. model as shown in equation (5.6).

$$\psi = \cos^{-1} \left[1 - \alpha \frac{2 \sigma (P_L - t_h)}{D_o \mu_f g [(\tau_h + s) e - A_p]} \left(\frac{D_w}{s} \right)^2 \right] \quad (5.6)$$

where α and β are empirical constants to fit the measured retention angle. In order to compute these α and β values, a numerical procedure was followed, by minimizing the sum of squares of the deviations of the computed and measured ψ values. This procedure resulted in α and β values of 0.85 and 0.18, respectively. The comparison between the values computed by equation (5.6) and the experimental values is shown in Figure 5.25. As can be seen, this equation agrees to within ± 15 percent with the experimental data.

2. Experimental Data of Wire-Wrapped Tubes

This section presents results showing the variation of the steam-side coefficient with heat flux for the wire-wrapped tubes tested. Three wire diameters (0.5, 1.0 and 1.6 mm) were used with three different pitches for each wire diameter. These are shown in Table IV; The tubes with a 1.6 mm wire diameter had pitches of 2.5, 3.6, and 4.6 mm; the tubes with 1.0 mm wire diameter had pitches of 2.0, 2.8, and 3.9 mm; and, the tubes with 0.5 mm wire diameter had pitches of 1.6, 2.5, and 3.6 mm. Figures 5.26 and 5.27 show the variation of heat-transfer coefficient with heat flux under vacuum and at atmospheric pressure, respectively, for the tubes wrapped with a 1.6-mm-diameter wire, while Figures 5.28 and 5.29 show the variation of the heat-transfer coefficient under vacuum and at atmospheric conditions, respectively, for the tubes wrapped with 1.0-mm-wire diameter. Figures 5.30 and 5.31, show similar results for the tubes wrapped with 0.5-mm-diameter wire under vacuum and at atmospheric pressure, respectively. Figures 5.26 to 5.31 show that the best performance was obtained for the tube with a wire diameter of 0.5 mm and a pitch of 2.5 mm, both under vacuum and at atmospheric pressure. The second best performance was given by the tube with a wire diameter of 0.5 mm

and a pitch of 3.6 mm under both pressure conditions. The third best performance was given by the tube with a wire diameter of 1.0 mm and a pitch of 2.8 mm under atmospheric pressure, and the tube with a wire diameter of 1.0 mm and a pitch of 3.9 mm, under vacuum pressure. The tubes with wire diameters of 1.6 mm and 1.0 mm with pitches of 2.5 and 2.0 mm, respectively, showed the worst performance among all the tubes tested.

As Figures 5.26 and 5.27 show, the performance of the tubes with a wire diameter of 1.6 mm and pitches of 3.6 and 4.6 mm interchanged as the pressure conditions were changed from vacuum to near-atmospheric. The same trend happened for the tube with wire diameter of 1.0 mm and pitches of 2.8, and 3.9 mm. This behavior can only be explained by the retention angle phenomenon. The tubes were wrapped in order to take advantage of the condensate thinning as a result of the varying surface-tension forces in the space between the wires. However, as mentioned in Chapter II, these surface-tension forces lead to a deleterious effect owing to condensate retention, especially when the fin spacing is small. If the extent of condensate retention is large, the enhancement gained over the unflooded portion of the tube (owing to condensate thinning) may be offset in poor performance in the flooded portion with retained condensate. As discussed in subsection 1 above, the retention angle is higher under vacuum conditions for tubes with a pitch of 3.6 than for tubes with a pitch of 4.6. This is true for tubes with pitches of 2.8 and 3.9 mm as well. However, under atmospheric pressure, the retention angle decreases resulting in less flooding, and better thermal performance. Figures 5.26 and 5.28 show that the tubes with wire diameters of 1.6 and 1.0 mm with pitches of 2.5, and 2.0 mm, respectively, had worse performance than the smooth tube under vacuum. Again these are the results

of the surface tension effects. For these tubes the retention angle was about 100 degrees, resulting in about half of the tube being effective for the heat transfer. The other half contributes a small amount to the heat transfer performance due to the thick layer of the condensate. The heat-transfer enhancement ratio is shown clearly in Figure 5.32, as a function of p/d_w . The optimum p/D_w appears to be near 5 to 6.

3. Modifications to Fujii et al. Model

As mentioned in Chapter II, Fujii et al. [32] developed a semi-theoretical expression to predict successfully their condensation data on wire-wrapped tubes, using ethanol and R-11 as the working fluids. As stated in Chapter II (Section E), the vapor-side enhancement could be easily computed using equation (2.65) provided $A > 15$. However, for most of the tubes tested during this investigation, the values of A were as low as 6. Thus, it was not possible to use equation (2.62) and equation (2.59) had to be used. When equation (2.59) is plotted as a function of A and ϕ , the result is shown in Figure (5.33). Notice that for $A > 18$, $F_1(\phi, A)$ is independent of ϕ . Also for $A > 18$ the functional dependence of F_1 on the angle ϕ can be approximated by a straight line:

$$F_1(\phi, A) = F_1(0, A) - m \phi \quad (5.7)$$

where m is the slope of the straight line. In equation (5.7), $F_1(0, A)$ for all values of A is given by equation (2.62).

Because of the flooding that occurs on the lower portion of the wire-wrapped tubes when steam is being

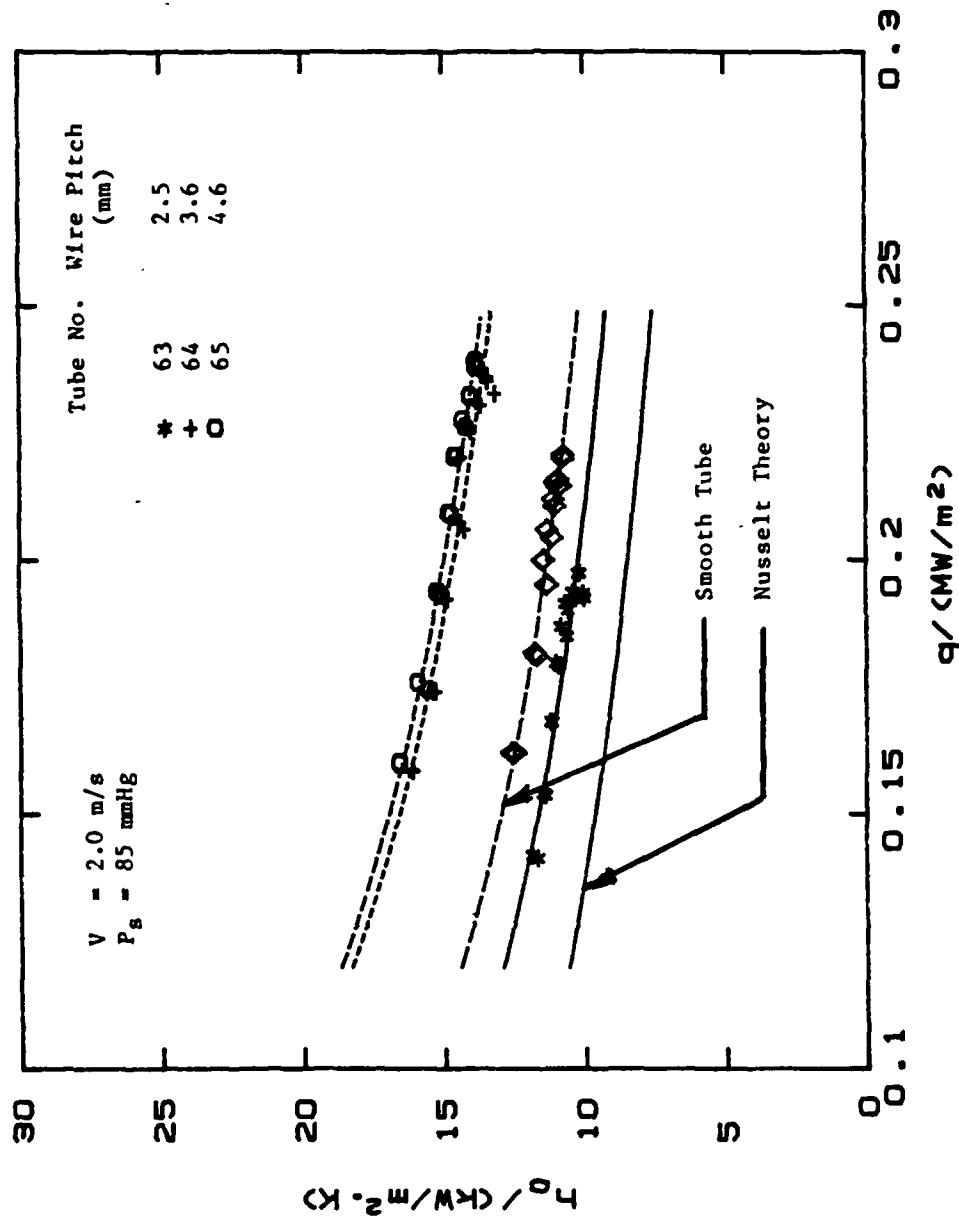


Figure 5.26 Effect of Wire Pitch on Heat-Transfer Coefficient for Wire-Wrapped Tubes with $D_w = 1.6 \text{ mm}$ (Vacuum Runs).

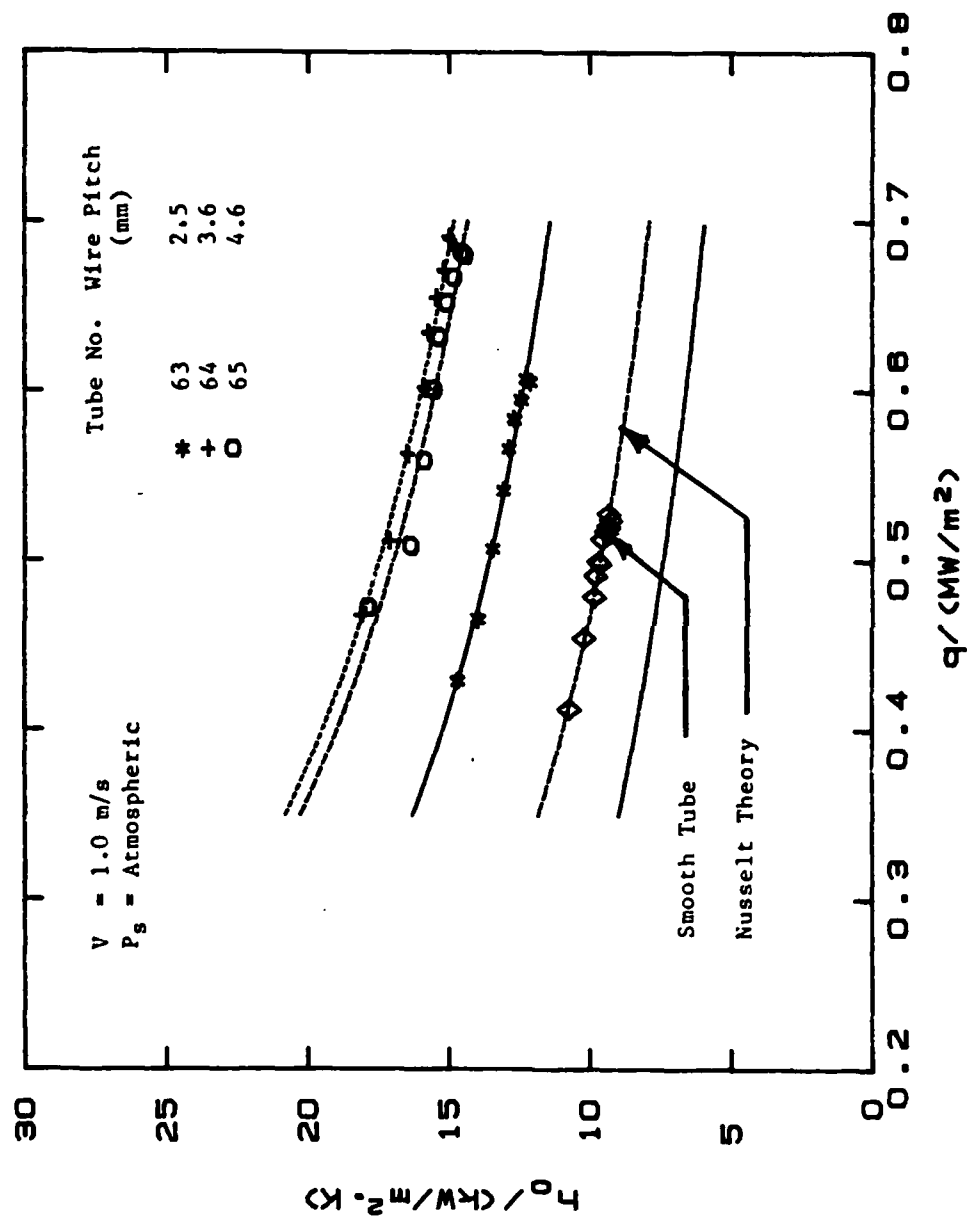


Figure 5.27 Effect of Wire Pitch on Heat-Transfer Coefficient for Wire-Wrapped Tubes with $D_w = 1.6 \text{ mm}$ (Atmospheric Runs).

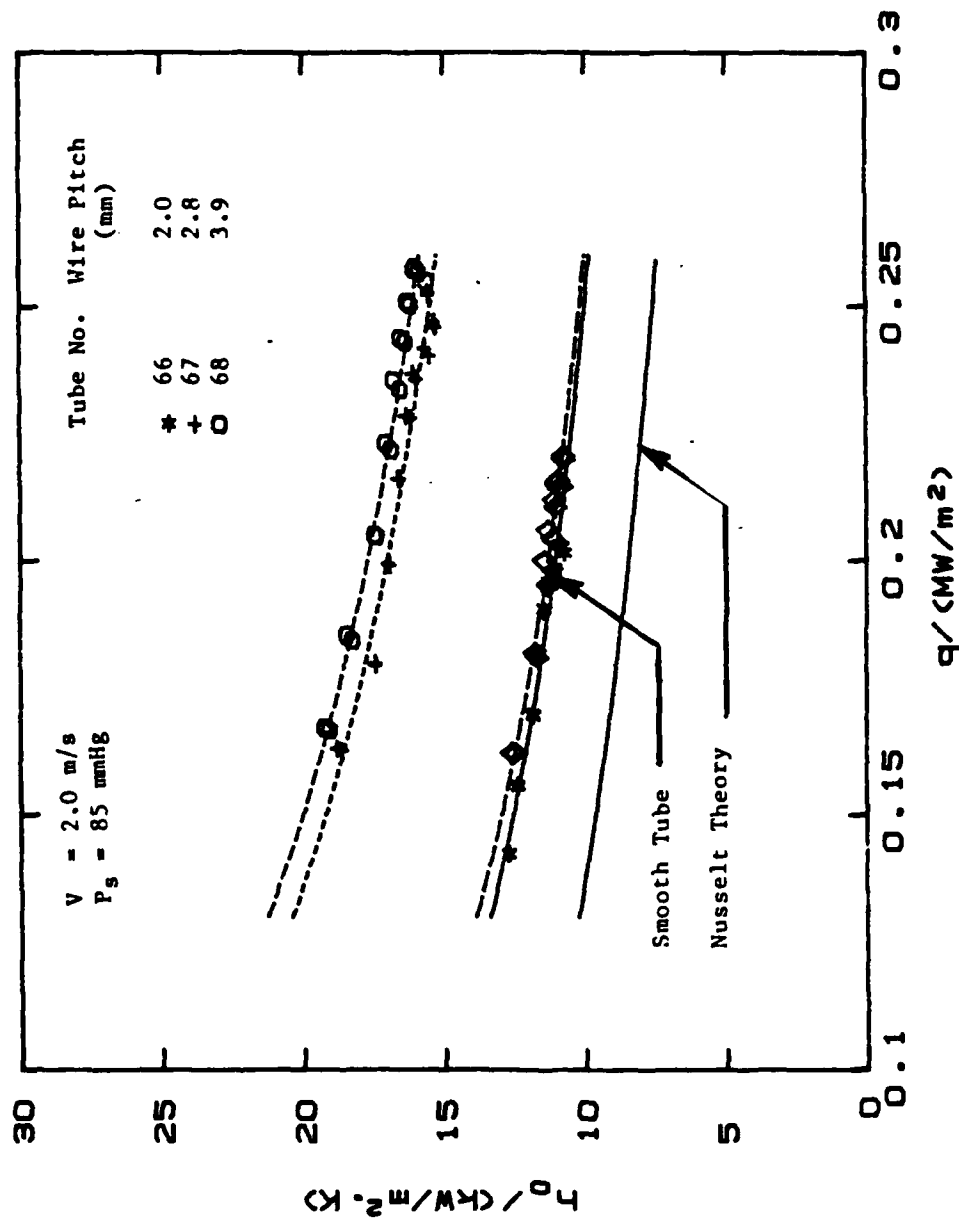


Figure 5.28 Effect of Wire Pitch on Heat-Transfer Coefficient for Wire-Wrapped Tubes with $D_w = 1.0 \text{ mm}$ (Vacuum Runs).

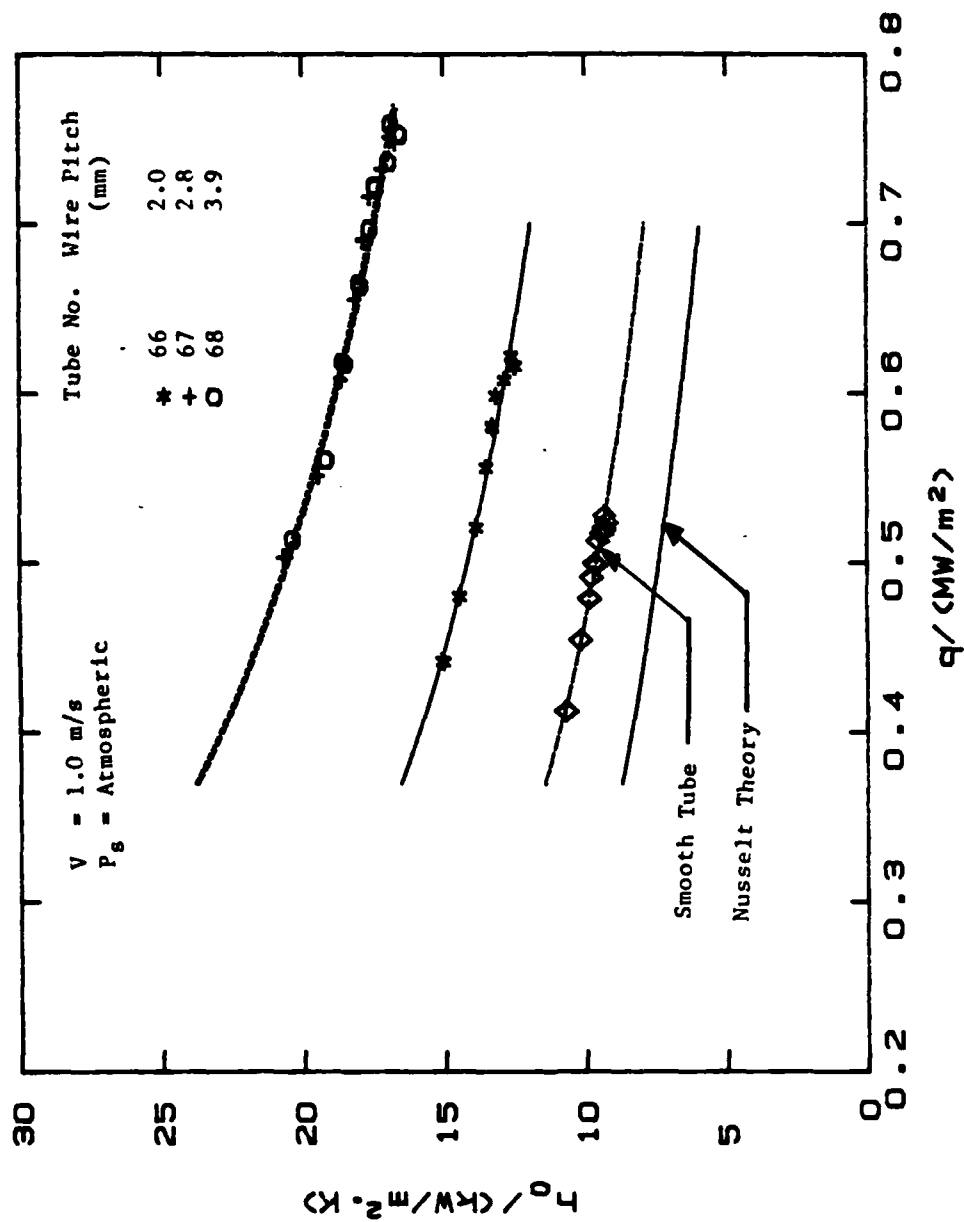


Figure 5.29 Effect of Wire Pitch on Heat-Transfer Coefficient for Wire-Wrapped Tubes with $D_w = 1.0 \text{ mm}$ (Atmospheric Runs).

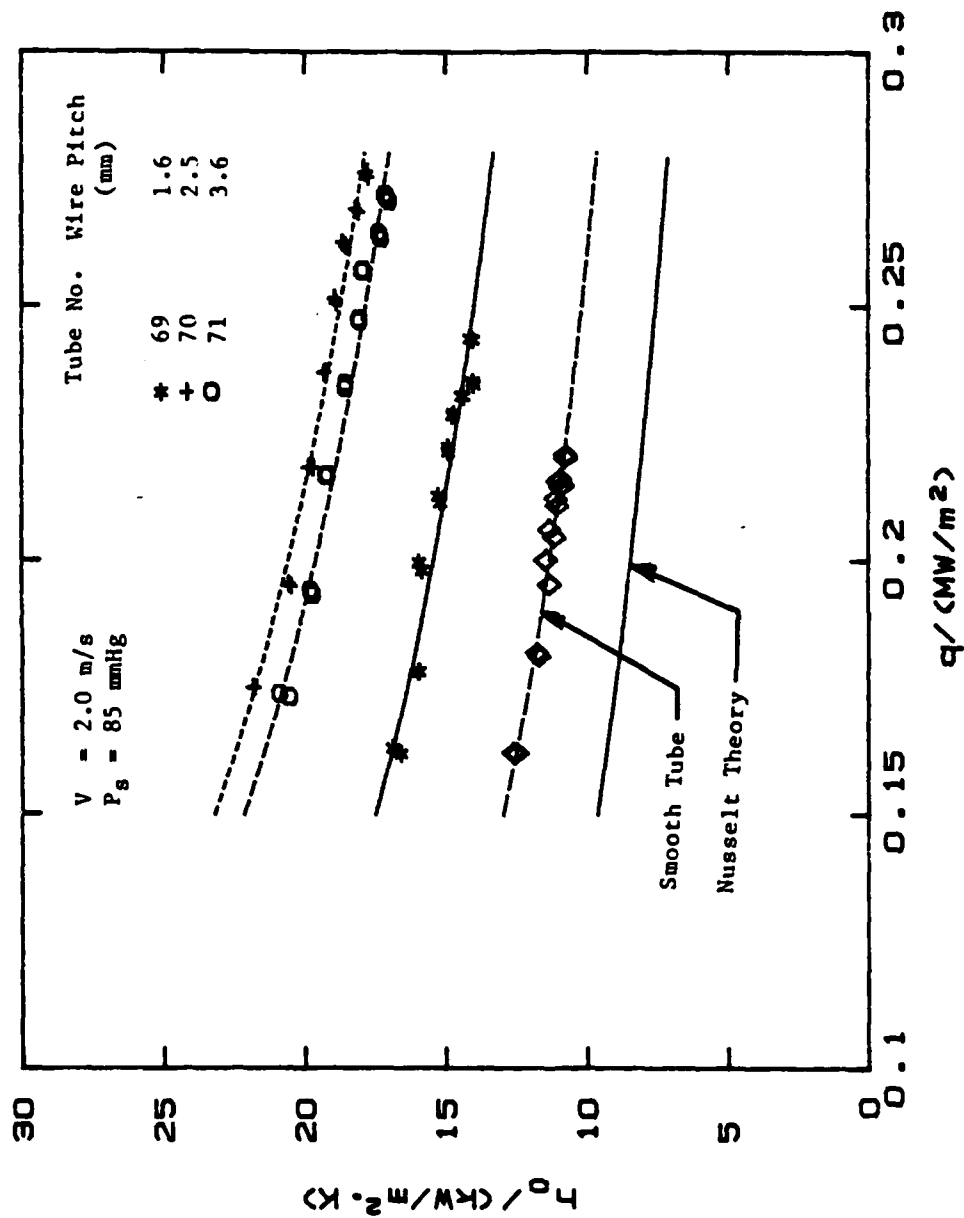


Figure 5.30 Effect of Wire Pitch on Heat-Transfer Coefficient for Wire-Wrapped Tubes with $D_w = 0.5 \text{ mm}$ (Vacuum Runs).

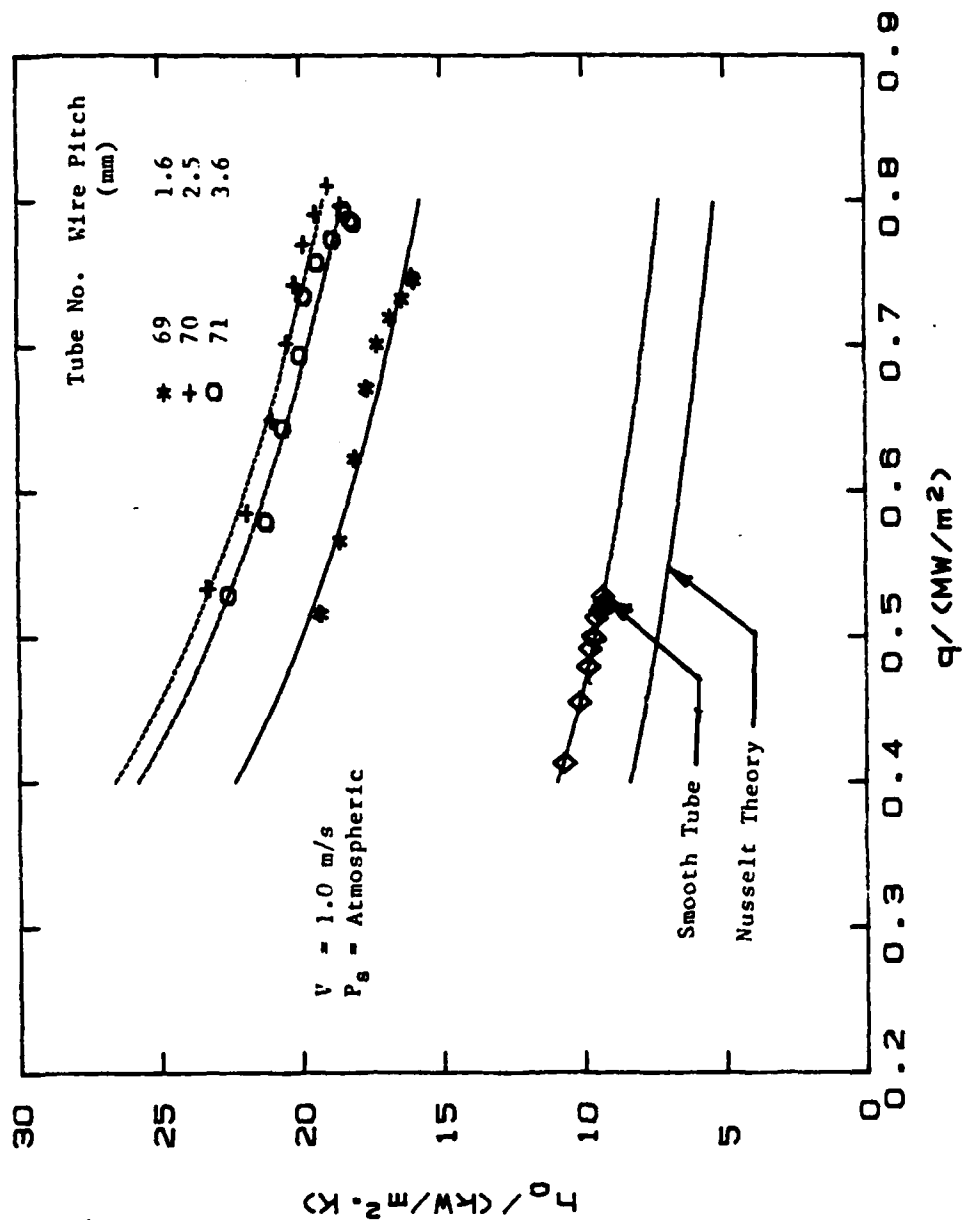


Figure 5.31 Effect of Wire Pitch on Heat-Transfer Coefficient for Wire-Wrapped Tubes with $D_w = 0.5 \text{ mm}$ (Atmospheric Runs).

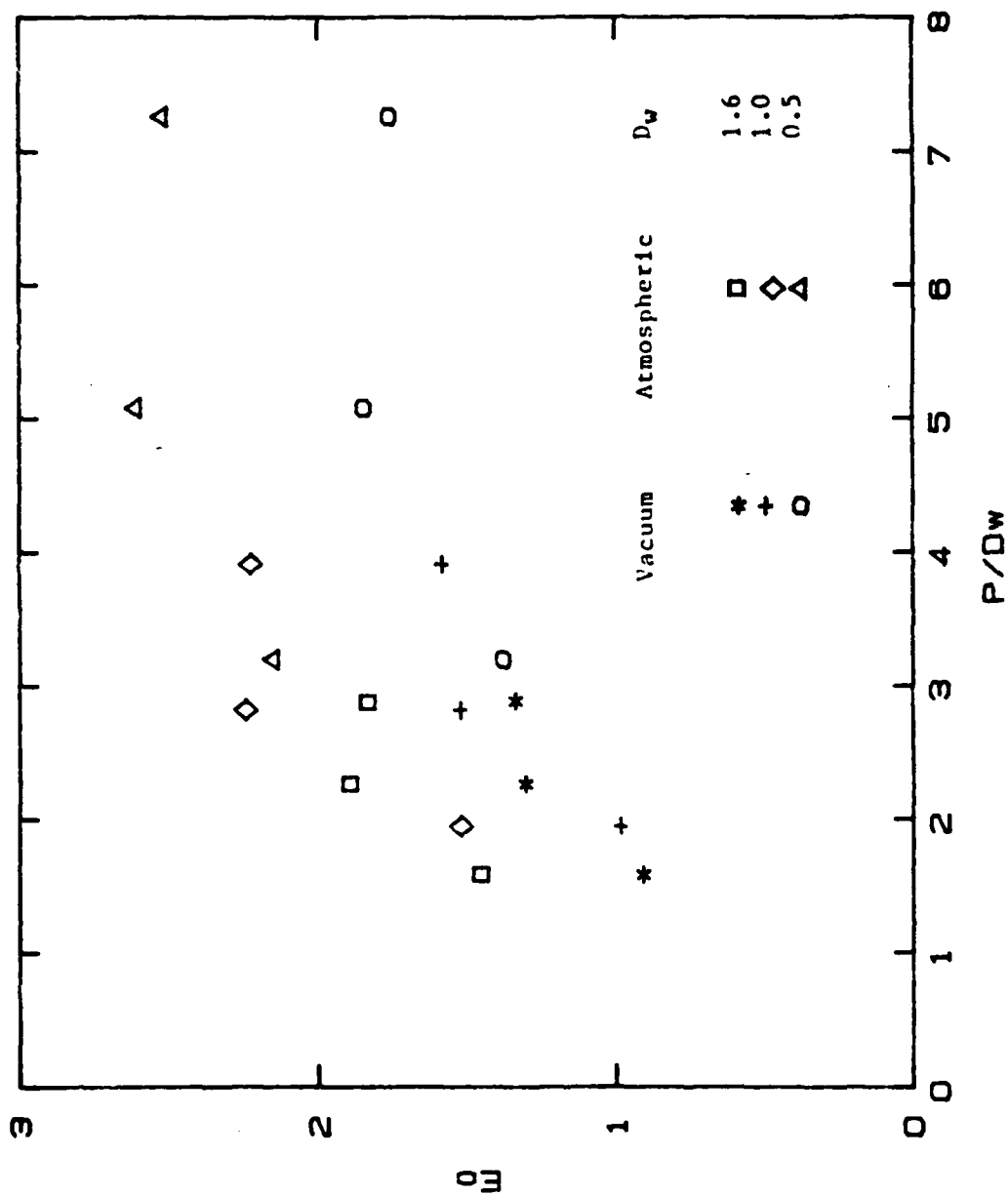


Figure 5.32 Effect of p/D_w Ratio on Heat-Transfer Performance for Wire-Wrapped Tubes.

condensed, in order to compute the heat-transfer performance of the unflooded portion of the tube, the function $F_1(\phi, A)$ must be integrated from $\phi = 0.0$ to $\phi = \pi - \psi$, as needed for equation (5.8):

$$F_2(\phi, A) = \frac{1}{\phi} \int_0^{\phi} F_1(\psi, A) d\psi \quad (5.8)$$

Notice that this equation is the same as equation (2.58) except that the integration is performed up to the angle ϕ (which is $\pi - \psi$). Fujii et al. neglected the retention-angle effect for their low-surface-tension fluids. As mentioned earlier, for $A > 15$, equation (5.7) is valid, but the slope m can depend on the value of A . In order to find the dependence, the slope was approximated for values of $A > 5$ and these slopes are plotted in Figure (5.34) as a function of A . Using a least square fit of the calculated data, the following functional form was derived:

$$m = a A^b, \quad A > 5 \quad (5.9)$$

where $a = 0.177$, and
 $b = -0.756$

Notice that the actual computation of m was performed only for $5 < A < 19$. The numerical integration of $F_1(\phi, A)$ for $A > 18$ was not possible owing to overflow limitations of the computer. Further, the integration of $F_1(\phi, A)$ for $A < 5$ was not performed since this was outside of the experimental conditions; the computed minimum A value was about 6. Figure 5.34 shows that the least-squares-fit curve has been extrapolated for $A > 18$. Even though such overextrapolations are not generally recommended, it appears reasonable

for this situation. The justification for this extapolation lies with the diminishing value of the slope m .

Substituting equation (5.7) into (5.8) yields:

$$F_2(\phi, A) = \frac{1}{\phi} [F_1(0, A) \phi - m \frac{\phi^2}{2}] \quad (5.10)$$

In order to modify the Fujii et al. model, three assumptions were made: 1) heat transfer through the wire is negligible compared to that through the interwire space for the unflooded portion of the tube; 2) heat transfer through the flooded portion is by one-dimensional conduction, and 3) in the flooded portion of the tube, heat transfer through the condensate between the wires is negligible compared to the heat flow across the wires. Based on assumption (1) above, the heat-transfer coefficient for the unflooded portion can be expressed as follows:

$$\frac{h_u}{h_s} = \frac{s}{(s + D_w)} \frac{F_2(0, A)}{F_2(0, 0)} \quad (5.11)$$

where $F_2(0, 0)$ is obtained numerically using equation (5.8). and where h_s is the heat-transfer coefficient for the smooth tube predicted by Nusselt theory [27]. Also, the heat-transfer coefficient across the wires in the flooded portion of the tube can be computed by equation (5.12) (derived in Appendix A):

$$h_f = \frac{1}{D_w} \int_0^{D_w} \frac{dx}{\frac{2y(x)}{k_f} + \frac{D_w - 2y(x)}{k_w}} \quad (5.12)$$

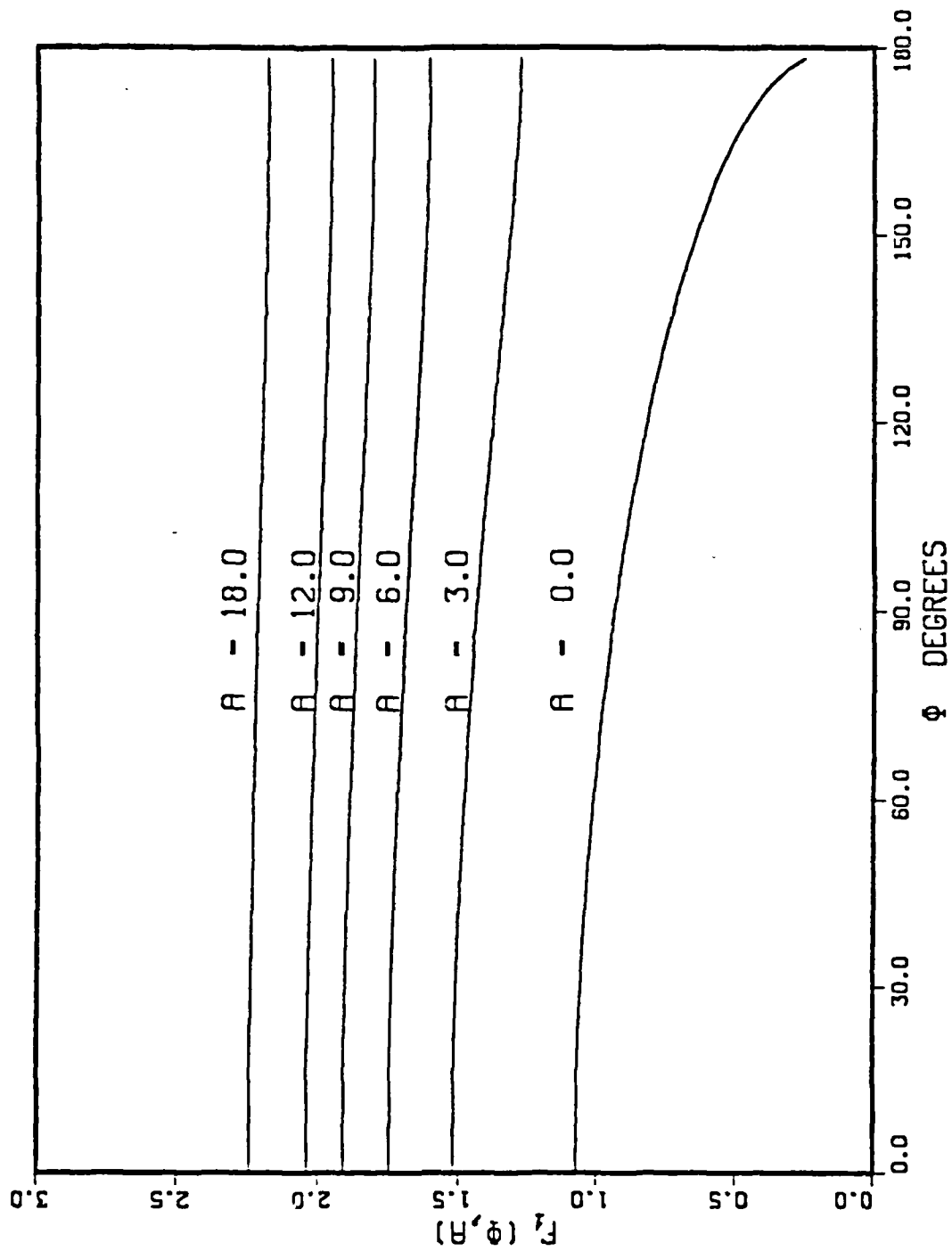


Figure 5.33 Variation of Function $F_1(\phi, A)$ with ϕ and A .

Now, combining equations (5.11) and equation (5.12), equation (5.13) can be obtained in order to express the average heat-transfer coefficient for the entire wire-wrapped tube.

$$\bar{h} = \bar{h}_u \left(1 - \frac{\psi}{\pi}\right) + \bar{h}_f \frac{\psi}{\pi} \cdot \frac{D_w}{(s+D_w)} \quad (5.13)$$

Then the enhancement ratio is given by equation (5.14):

$$E_o = \frac{h_u}{h_s} \left(1 - \frac{\psi}{\pi}\right) + \frac{h_f}{h_s} \frac{\psi}{\pi} \cdot \frac{D_w}{(s+D_w)} \quad (5.14)$$

In order to fit the experimental data, a value of 0.02 was selected for the constant C in equation (2.61). Figure 5.35 shows the experimental data and the values calculated from the modified Fujji et al. model. As can be seen from this figure, good agreement of the experimental data and the predicted values exists. However, a clear trend does not exist for the effect of wire diameter on the heat-transfer performance. The assumptions made during this study, and other possible mechanisms not taken into consideration owing to the complex nature of this problem, such as convective effects may be responsible for the observed comparison.

H. HEAT-TRANSFER COEFFICIENT FOR COMMERCIAL TUBES

As mentioned in Chapter IV, two commercially available finned tubes were tested. These tubes were manufactured by High Performance Tube, Inc., and had fin densities of 1.1 and 1.18 fins/mm (tubes 51 and 49). Figures 5.36 and 5.37 show the variation of the heat-transfer coefficient for these tubes with heat flux under vacuum and at atmospheric pressure, respectively. Data for a smooth tube (tube 50), are also shown. The best performance was given by the tube with fin density of 1.1 fins/mm under both pressure

conditions. Visual examination of the condensation process revealed that both finned tubes were fully flooded. This was also observed, under static conditions. Since these tubes had a high density of fins with small fin height, the surface tension effect is not important for the flow of the condensate along the fin side. However, the surface tension retained the condensate between the fins, so these tubes were fully flooded. Therefore, as Table III shows, although they have the largest area ratio, the heat-transfer performance is worse than most of the other copper finned tubes tested during this thesis effort. Nevertheless, even though these tubes were fully flooded, the normalized enhancement ratio (E_o/A_r) was greater than unity in both cases (especially for atmospheric pressure), indicating an enhancement greater than first due to an area increase.

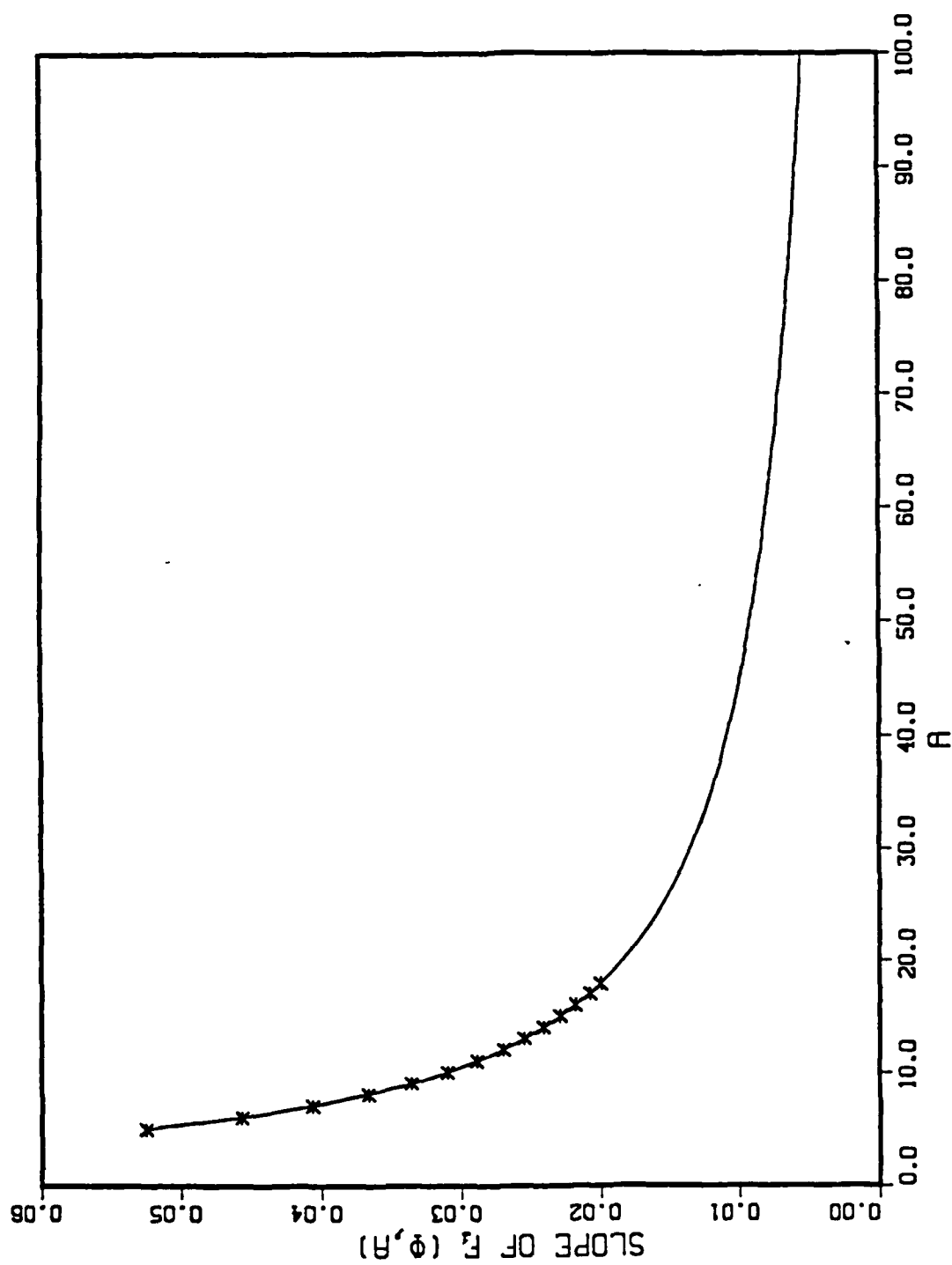


Figure 5.34 Measured and Calculated Values for
the Slope of Function $F_1(\phi, A)$.

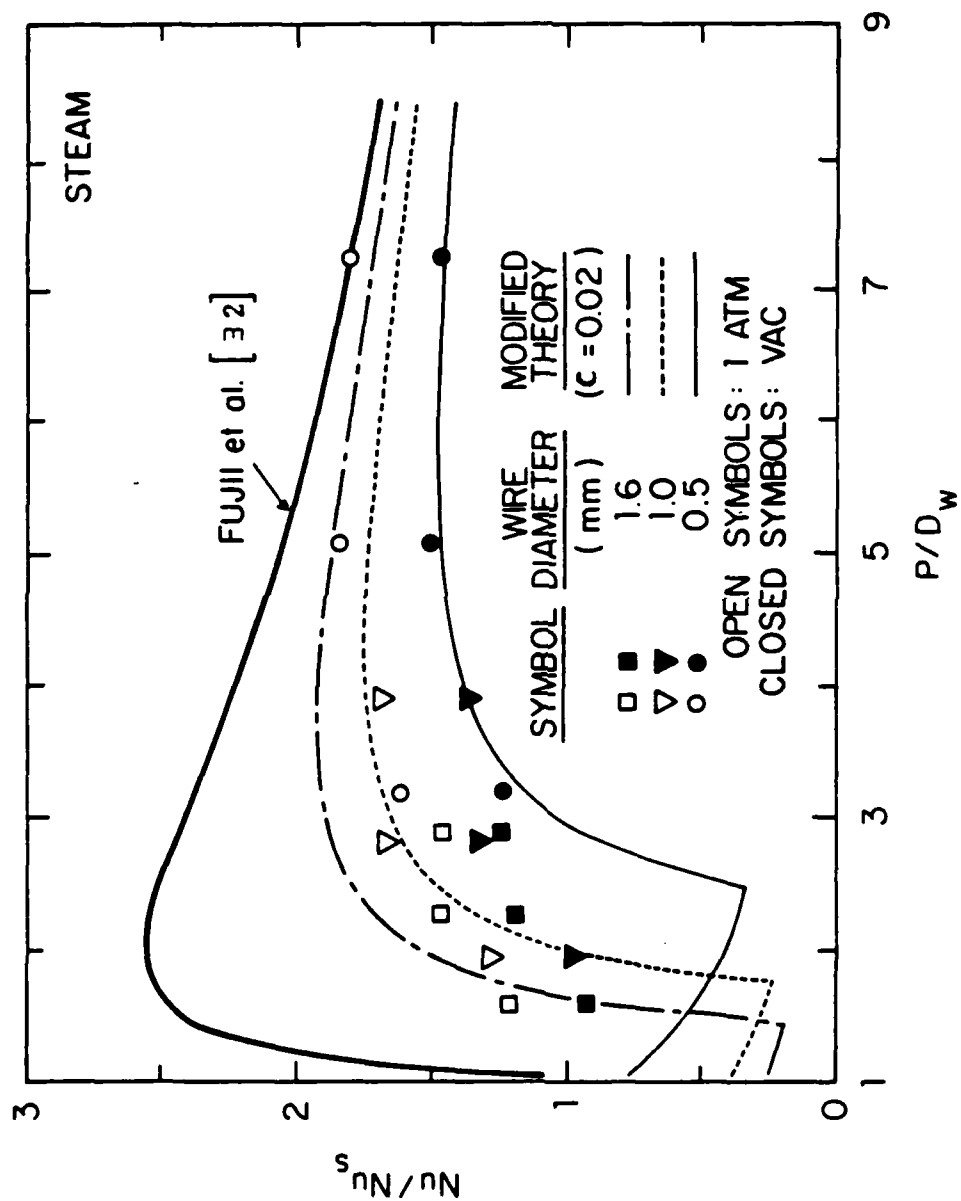


Figure 5.35 Effect of p/D_w Ratio on Enhancement Ratio for Wire-Wrapped tubes.

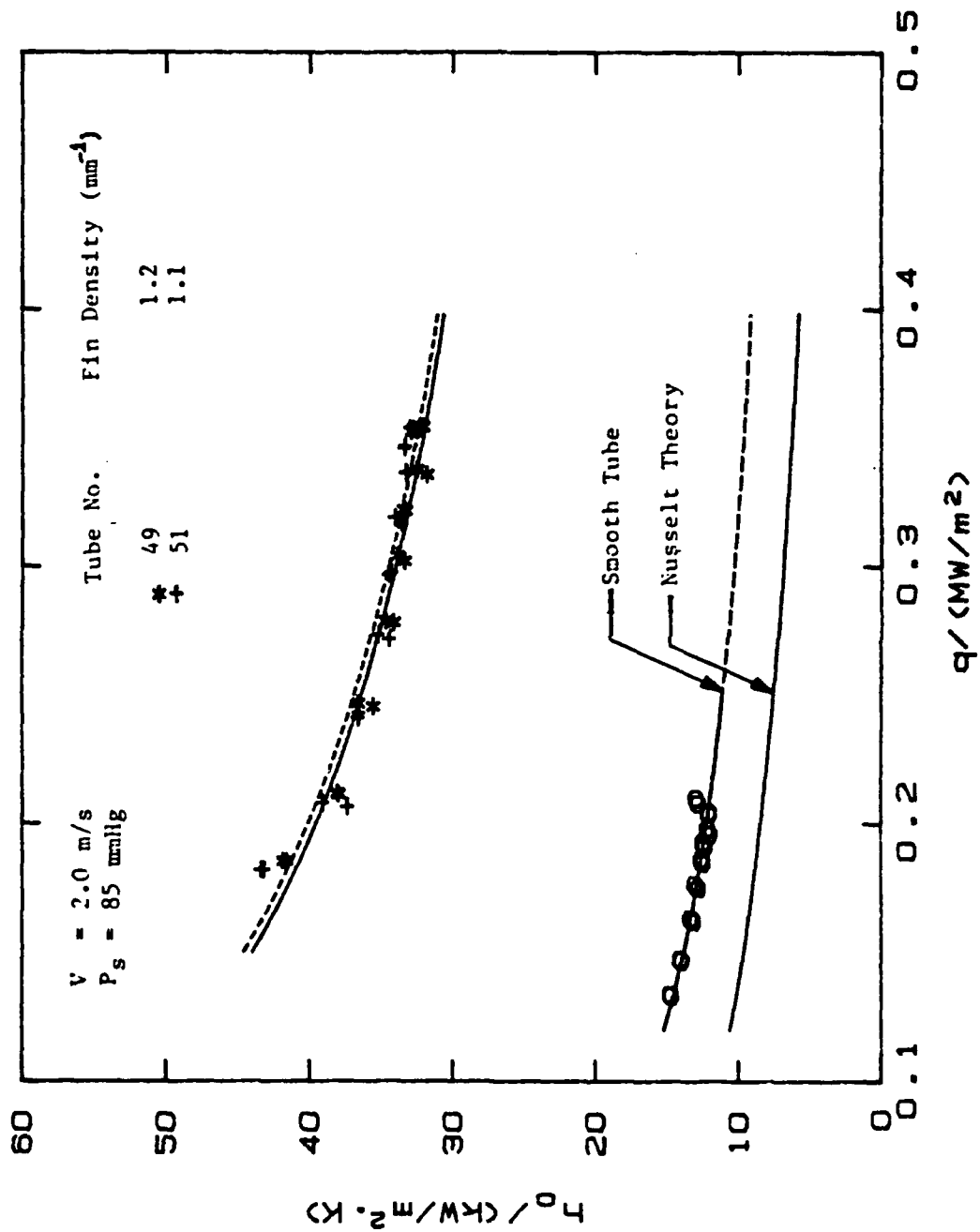


Figure 5.36 Variation of Heat-Transfer Coefficient with Heat Flux for High Performance Tubes (Vacuum Runs).

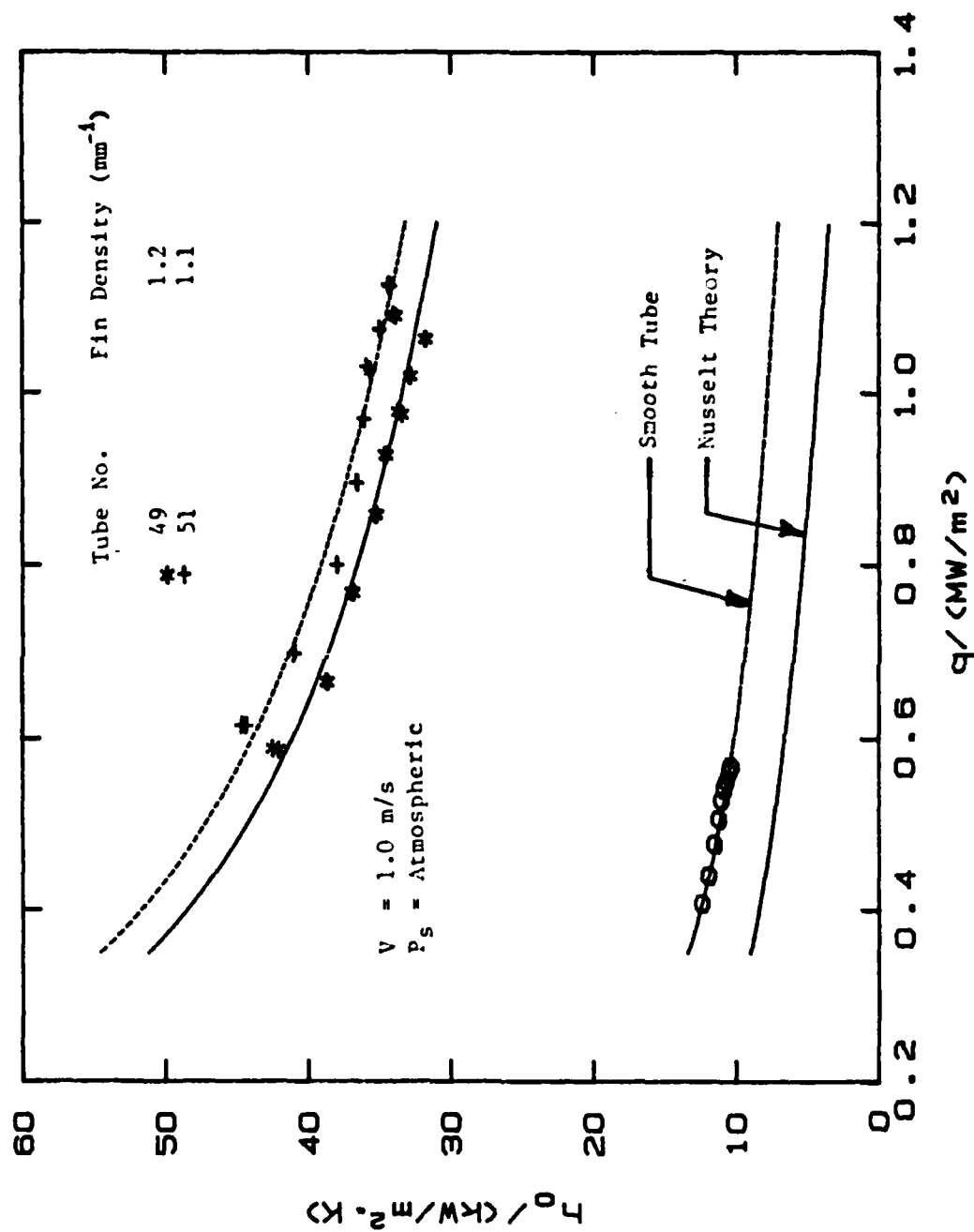


Figure 5.37 Variation of Heat-Transfer Coefficient with Heat Flux for High Performance Tubes (Atmospheric Runs).

VI. CONCLUSIONS AND RECOMMENDATIONS

A. CONCLUSIONS

1. The use of fins lead to significant enhancement of the steam-side heat-transfer coefficient, which is greater than the area ratio (finned tube area to smooth tube area) despite condensate retention between fins.
2. Enhancement ratios as high as 1.84 and 2.6 under vacuum and at atmospheric conditions, respectively, were realized for the wire-wrapped tube with a wire diameter of 0.5 mm and a pitch of 5.1 mm. This is due to the surface-tension effect resulting in thinning of the condensate between wires.
3. The Webb et al. [31] model was successfully modified to predict the condensate retention angle for the wire-wrapped tubes. Maximum error of 15 percent was found.
4. The Fujii et al. [32] model was modified to predict the vapor-side heat-transfer coefficient for high-surface-tension fluids (i.e., water). A favorable agreement between the modified Fujii et al. model and the experimental data was found.
5. The tube with a "parabolic" fin profile outperformed the tubes with triangular, trapezoidal and rectangular fin shapes. For the tube with "parabolic" fins, enhancement ratios of 4.1 and 6.2 under vacuum and at atmospheric pressure, respectively, were obtained.
6. For tubes with spiral triangular fins, the optimum pitch was found to be about of 1.6 mm. Enhancement ratios of 3.9 and 6.1 under vacuum and at atmospheric pressure, respectively, were obtained for this tube.
7. The High Performance tubes, although they have the highest area ratio among all the tubes tested, show poorer performance than most of the other tubes. This is mainly owing to the high condensate retention angle. Enhancement ratios as high as 3.5 and 5.2 under vacuum and at atmospheric pressure, respectively, were obtained.
8. The enhancement ratios for finned tubes are proportional to the tube thermal conductivity. For the tubes with different thermal conductivity, the highest enhancement was obtained for the copper tube, while the stainless steel tube had a performance even less than the smooth tube under vacuum conditions. This is due to the high wall thermal resistance of the stainless steel tube.

B. RECOMMENDATIONS

1. Attach drainage strips on some of the existing tubes to investigate the effect of the strips on the condensate retention angle and the vapor-side heat-transfer coefficient and compare with the already existing data.
2. Take data on a tube with a more nearly parabolic fin profile and compare them with the existing data of fins with triangular, trapezoidal and rectangular profiles.
3. Take data with different tube diameters to investigate its effect on the heat-transfer performance.
4. Take data with different vapor velocities to investigate the effect of vapor shear on the heat-transfer performance.
5. Take data using different fluids to study the dependence of the heat-transfer coefficient on the fluid properties.

APPENDIX A

DERIVATION OF THE HEAT-TRANSFER COEFFICIENT OF FLOODED REGION FOR WIRE-WRAPPED TUBES

Assuming one-dimensional heat conduction for a differential element dx , the differential heat transfer is given by equation (A.1):

$$dQ = \frac{\Delta T}{\Sigma R(x)} \pi D_o dx \quad (A.1)$$

where

$$\Sigma R(x) = \frac{2y(x)}{k_f} + \frac{D_w - 2y(x)}{k_w} \quad (A.2)$$

where $y(x)$ is the vertical distance between the wire surface and the horizontal tube surface (see Figure A.1), and is given by equation (A.3):

$$y(x) = R_w - (R_w^2 - x^2)^{1/2} \quad (A.3)$$

x is the axial coordinate along the tube. Substituting equation (A.2) for $\Sigma R(x)$ into equation (A.1) and integrating

$$Q = \pi D_o \Delta T \int_0^{D_w/2} \frac{dx}{\frac{2y(x)}{k_f} + \frac{D_w - 2y(x)}{k_w}} \quad (A.4)$$

Also heat transfer is given by equation (A.5):

$$Q = h \pi D_o \frac{D_w}{2} \Delta T \quad (A.5)$$

Combining equations (A.4) and (A.5), the heat-transfer coefficient can be expressed as:

$$h_f = \frac{1}{D_w} \int_0^{D_w} \frac{dx}{\frac{2y(x)}{k_f} + \frac{D_w - 2y(x)}{k_w}} \quad (A.6)$$

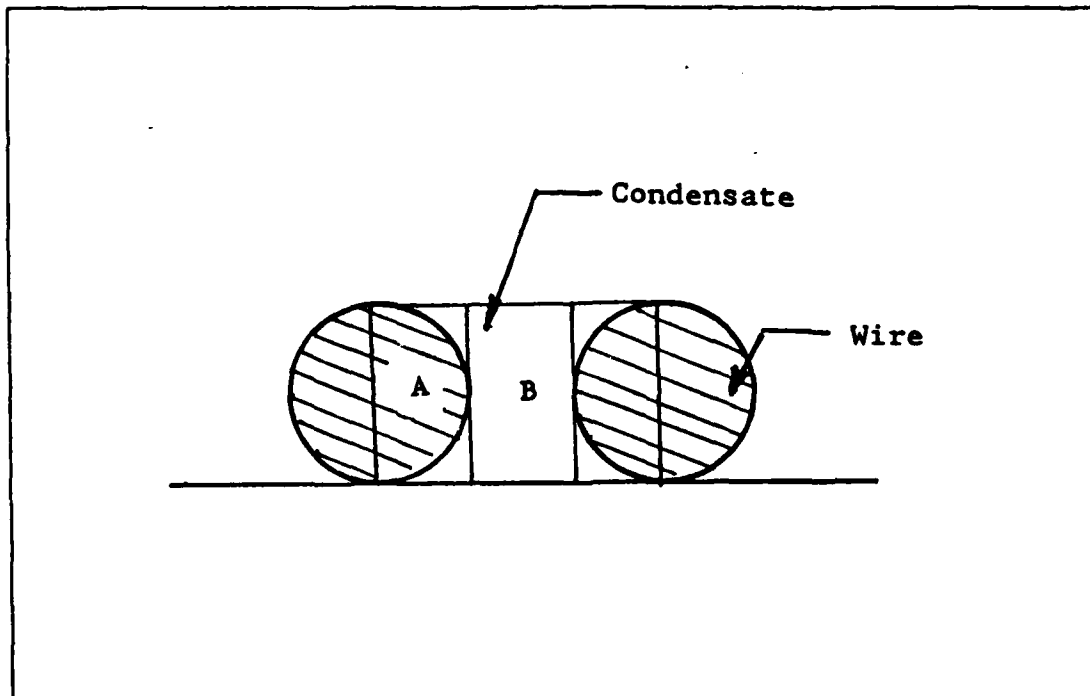


Figure A.1 Condensate Film Profile for Fully Flooded Wire-Wrapped Tube.

APPENDIX B
LISTING OF RAW DATA

The following pages contain raw data obtained for tubes number 6, 17, 36, 38 and 45 thru 71 under vacuum conditions and at atmospheric pressure.

TABLE VIII

RAW DATA FOR TUBE WITH RECTANGULAR FIN PROFILE
OF $S = 1.5$ MM, $T = 1.0$ MM AND $E = 1.0$ MM

Tube Number: 06					Tube Number: 06				
File Name: F06V145					File Name: F06A226				
Pressure Condition: Vacuum					Pressure Condition: Atmospheric				
Steam Velocity: 2.0 (m/s)					Steam Velocity: 1.0 (m/s)				
Data #	Vw (m/s)	Tin (C)	Tout (C)	Is (C)	Data #	Vw (m/s)	Tin (C)	Tout (C)	Is (C)
1	4.39	22.56	23.70	48.55	1	4.40	21.45	25.01	99.96
2	4.39	22.59	23.74	48.63	2	4.40	21.51	25.08	99.93
3	3.85	22.80	24.05	48.46	3	3.86	21.60	25.51	100.02
4	3.85	22.83	24.08	48.52	4	3.86	21.59	25.51	100.05
5	3.42	22.92	24.26	48.49	5	3.43	21.68	25.91	100.01
6	3.42	22.92	24.27	48.45	6	3.43	21.67	25.91	100.00
7	2.99	22.99	24.45	48.55	7	3.00	21.74	26.35	100.00
8	2.99	23.00	24.46	48.55	8	3.00	21.74	26.35	99.93
9	2.51	23.09	24.69	48.43	9	2.51	21.81	26.93	99.89
10	2.51	23.09	24.69	48.37	10	2.51	21.81	26.93	99.91
11	1.97	23.23	25.07	48.45	11	1.97	21.95	27.84	99.95
12	1.97	23.23	25.08	48.51	12	1.97	21.95	27.84	99.89
13	1.48	23.41	25.54	48.53	13	1.49	22.13	29.00	99.94
14	1.48	23.41	25.55	48.56	14	1.49	22.14	29.01	99.91
15	1.16	23.61	26.02	48.45	15	1.16	22.33	30.18	100.01
16	1.16	23.61	26.01	48.39	16	1.16	22.34	30.19	99.99
17	4.39	22.86	23.99	48.46	17	4.40	21.56	25.16	100.06
18	4.39	22.86	23.99	48.48	18	4.40	21.55	25.15	99.93

TABLE IX

RAW DATA FOR TUBE WITH RECTANGULAR FIN PROFILE
OF $S = 1.5$ MM, $T = 0.5$ MM AND $E = 1.0$ MM

Tube Number: 17					Tube Number: 17				
File Name: F17V190					File Name: F17A210				
Pressure Condition: Vacuum					Pressure Condition: Atmospheric				
Steam Velocity: 2.0 (m/s)					Steam Velocity: 1.0 (m/s)				
Data #	Vw (m/s)	Tin (C)	Tout (C)	Is (C)	Data #	Vw (m/s)	Tin (C)	Tout (C)	Is (C)
1	4.40	21.86	23.04	48.51	1	4.39	22.51	26.13	99.92
2	4.40	22.07	23.24	48.50	2	4.39	22.53	26.15	99.95
3	3.86	22.33	23.61	48.47	3	3.86	22.63	26.60	99.87
4	3.86	22.34	23.61	48.47	4	3.86	22.64	26.60	99.90
5	3.42	22.44	23.81	48.41	5	3.42	22.70	27.00	99.90
6	3.42	22.45	23.82	48.41	6	3.42	22.71	27.02	99.93
7	2.99	22.53	24.02	48.40	7	2.99	22.78	27.45	100.01
8	2.99	22.53	24.03	48.48	8	2.99	22.77	27.45	99.97
9	2.51	22.62	24.28	48.47	9	2.51	22.87	28.07	99.99
10	2.51	22.62	24.28	48.37	10	2.51	22.88	28.07	100.01
11	1.97	22.75	24.63	48.39	11	1.97	23.03	29.00	99.97
12	1.97	22.75	24.63	48.43	12	1.97	23.03	29.00	99.95
13	1.48	22.95	25.13	48.43	13	1.48	23.21	30.16	99.95
14	1.48	22.94	25.12	48.44	14	1.48	23.21	30.17	99.91
15	1.16	23.12	25.58	48.47	15	1.16	23.41	31.30	99.93
16	1.16	23.13	25.59	48.40	16	1.16	23.41	31.30	99.91
17	4.39	22.40	23.57	48.43	17	4.39	22.65	26.31	99.98
18	4.39	22.40	23.57	48.38	18	4.39	22.66	26.32	99.90

TABLE X

RAW DATA FOR TUBE WITH PARABOLIC FIN PROFILE
OF $S = 1.5$ MM, $T_B = 0.5$ MM AND $E = 1.0$ MM

Tube Number: 38					Tube Number: 38				
File Name: F38V196					File Name: F38A200				
Pressure Condition: Vacuum					Pressure Condition: Atmospheric				
Steam Velocity: 2.0 (m/s)					Steam Velocity: 1.0 (m/s)				
Data #	V_w (m/s)	T_{in} (C)	T_{out} (C)	T_s (C)	Data #	V_w (m/s)	T_{in} (C)	T_{out} (C)	T_s (C)
1	4.39	23.01	24.19	48.46	1	4.39	22.91	26.69	99.94
2	4.39	23.02	24.20	48.46	2	4.39	22.97	26.76	99.91
3	3.85	23.09	24.38	48.36	3	3.85	23.05	27.19	99.95
4	3.85	23.09	24.38	48.36	4	3.85	23.05	27.19	99.91
5	3.42	23.15	24.54	48.45	5	3.42	23.16	27.63	99.94
6	3.42	23.15	24.55	48.51	6	3.42	23.14	27.62	99.96
7	2.99	23.23	24.74	48.55	7	2.99	23.22	28.08	99.94
8	2.99	23.23	24.73	48.42	8	2.99	23.23	28.09	99.92
9	2.50	23.31	24.97	48.46	9	2.51	23.33	28.70	99.91
10	2.50	23.31	24.97	48.40	10	2.51	23.31	28.68	99.93
11	1.97	23.45	25.33	48.51	11	1.97	23.46	29.61	99.93
12	1.97	23.44	25.34	48.47	12	1.97	23.45	29.60	99.91
13	1.48	23.63	25.80	48.45	13	1.48	23.64	30.78	100.00
14	1.48	23.64	25.80	48.44	14	1.48	23.64	30.79	100.07
15	1.16	23.83	26.28	48.48	15	1.16	23.84	31.95	100.02
16	1.16	23.84	26.28	48.41	16	1.16	23.84	31.96	99.99
17	4.39	23.10	24.28	48.51	17	4.39	23.11	26.93	99.94
18	4.39	23.11	24.29	48.41	18	4.39	23.11	26.92	99.86

TABLE XI

RAW DATA FOR SPIRAL TUBES WITH FINS
OF $P = 2.1 \text{ MM}$ AND $E = 1.0 \text{ MM}$

Tube Number: 36					Tube Number: 36				
File Name: F36V141					File Name: F36A143				
Pressure Condition: Vacuum					Pressure Condition: Atmospheric				
Steam Velocity: 2.0 (m/s)					Steam Velocity: 1.0 (m/s)				
Data #	V_w (m/s)	I_{in} (C)	I_{out} (C)	I_s (C)	Data #	V_w (m/s)	I_{in} (C)	I_{out} (C)	I_s (C)
1	4.40	21.86	23.06	48.48	1	4.39	22.61	26.23	99.95
2	4.40	21.94	23.14	48.44	2	4.39	22.65	26.27	99.95
3	3.86	22.02	23.32	48.38	3	3.85	22.72	26.67	99.96
4	3.86	22.04	23.34	48.38	4	3.85	22.70	26.66	100.01
5	3.43	22.10	23.51	48.48	5	3.42	22.78	27.05	99.95
6	3.43	22.11	23.52	48.42	6	3.42	22.79	27.07	100.03
7	2.99	22.17	23.70	48.46	7	2.99	22.83	27.50	99.95
8	2.99	22.17	23.70	48.40	8	2.99	22.83	27.49	99.94
9	2.51	22.24	23.94	48.44	9	2.51	22.91	28.08	100.01
10	2.51	22.25	23.93	48.39	10	2.51	22.92	28.09	99.97
11	1.97	22.38	24.31	48.37	11	1.97	23.04	28.99	99.88
12	1.97	22.38	24.31	48.35	12	1.97	23.04	28.99	99.91
13	1.48	22.56	24.79	48.37	13	1.48	23.23	30.18	99.94
14	1.48	22.56	24.79	48.42	14	1.48	23.23	30.17	99.87
15	1.16	22.77	25.30	48.40	15	1.16	23.46	31.41	100.06
16	1.16	22.77	25.31	48.45	16	1.16	23.44	31.40	100.06
17	4.40	22.01	23.21	48.36	17	4.39	22.70	26.32	100.02
18	4.40	22.01	23.22	48.39	18	4.39	22.71	26.33	100.10

TABLE XII
RAW DATA FOR SPIRAL TUBES WITH FINS
OF $P = 2.5$ MM AND $E = 1.0$ MM

Tube Number: 45					Tube Number: 45				
File Name: F45V167					File Name: F45A159				
Pressure Condition: Vacuum					Pressure Condition: Atmospheric				
Steam Velocity: 2.0 (m/s)					Steam Velocity: 1.0 (m/s)				
Data #	Vw (m/s)	Tin (C)	Tout (C)	Is (C)	Data #	Vw (m/s)	Tin (C)	Tout (C)	Is (C)
1	4.40	22.20	23.39	48.42	1	4.39	23.33	27.07	99.98
2	4.39	22.37	23.56	48.42	2	4.39	23.34	27.07	99.95
3	3.86	22.48	23.76	48.44	3	3.85	23.41	27.50	100.00
4	3.85	22.51	23.80	48.41	4	3.85	23.40	27.50	100.07
5	3.42	22.57	23.96	48.48	5	3.42	23.47	27.90	99.96
6	3.42	22.58	23.97	48.51	6	3.42	23.48	27.90	99.84
7	2.99	22.77	24.27	48.49	7	2.99	23.51	28.35	99.95
8	2.99	22.78	24.28	48.37	8	2.99	23.51	28.35	99.95
9	2.51	22.92	24.57	48.40	9	2.50	23.64	29.00	100.04
10	2.51	22.93	24.58	48.41	10	2.50	23.63	29.00	100.08
11	1.97	23.12	25.02	48.52	11	1.97	23.75	29.92	99.94
12	1.97	23.13	25.01	48.50	12	1.97	23.75	29.91	99.90
13	1.48	23.39	25.58	48.49	13	1.48	23.94	31.15	100.10
14	1.48	23.39	25.57	48.53	14	1.48	23.92	31.07	99.98
15	1.16	23.62	26.08	48.42	15	1.16	24.13	32.26	99.96
16	1.16	23.61	26.07	48.43	16	1.16	24.12	32.25	99.98
17	4.39	22.85	24.01	48.42	17	4.39	23.42	27.04	99.87
18	4.39	22.84	24.01	48.50	18	4.39	23.42	27.05	99.96

TABLE XIII

RAW DATA FOR SPIRAL TUBES WITH FINS
OF P = 1.6 MM AND E = 1.0 MM

Tube Number: 46					Tube Number: 46				
File Name: F46V149					File Name: F46A158				
Pressure Condition: Vacuum					Pressure Condition: Atmospheric				
Steam Velocity: 2.0 (m/s)					Steam Velocity: 1.0 (m/s)				
Data #	Vw (m/s)	Tin (C)	Tout (C)	Is (C)	Data #	Vw (m/s)	Tin (C)	Tout (C)	Is (C)
1	4.40	21.84	23.06	48.47	1	4.39	22.61	26.37	100.02
2	4.40	21.89	23.11	48.50	2	4.39	22.63	26.39	99.91
3	3.86	22.06	23.37	48.49	3	3.85	22.73	26.84	99.94
4	3.86	22.06	23.37	48.53	4	3.85	22.73	26.84	99.88
5	3.43	22.14	23.56	48.48	5	3.42	22.79	27.24	99.98
6	3.43	22.15	23.56	48.47	6	3.42	22.79	27.24	100.02
7	2.99	22.23	23.76	48.43	7	2.99	22.85	27.67	99.84
8	2.99	22.25	23.78	48.46	8	2.99	22.86	27.68	99.90
9	2.51	22.34	24.03	48.44	9	2.51	22.94	28.29	100.09
10	2.51	22.34	24.03	48.44	10	2.51	22.94	28.29	100.11
11	1.97	22.48	24.40	48.39	11	1.97	23.05	29.17	99.95
12	1.97	22.48	24.40	48.34	12	1.97	23.06	29.18	99.87
13	1.48	22.67	24.90	48.51	13	1.48	23.23	30.33	99.88
14	1.48	22.68	24.92	48.56	14	1.48	23.24	30.35	99.92
15	1.16	22.88	25.38	48.39	15	1.16	23.43	31.49	99.81
16	1.16	22.88	25.38	48.42	16	1.16	23.44	31.50	99.83
17	4.40	22.14	23.33	48.50	17	4.39	22.68	26.48	99.91
18	4.40	22.14	23.35	48.54	18	4.39	22.69	26.48	99.73

TABLE XIV

RAW DATA FOR SPIRAL TUBES WITH FINS
OF P = 1.05 MM AND E = 1.0 MM

Tube Number: 47					Tube Number: 47				
File Name: F47V150					File Name: F47A157				
Pressure Condition: Vacuum					Pressure Condition: Atmospheric				
Steam Velocity: 2.0 (m/s)					Steam Velocity: 1.0 (m/s)				
Data #	V _w (m/s)	T _{in} (C)	T _{out} (C)	T _s (C)	Data #	V _w (m/s)	T _{in} (C)	T _{out} (C)	T _s (C)
1	4.39	22.81	23.96	48.48	1	4.40	22.25	25.89	99.91
2	4.39	22.83	23.98	48.45	2	4.40	22.29	25.96	99.95
3	3.85	22.89	24.14	48.50	3	3.86	22.43	26.44	99.92
4	3.85	22.89	24.14	48.44	4	3.86	22.44	26.46	99.89
5	3.42	22.95	24.29	48.42	5	3.42	22.53	26.91	99.93
6	3.42	22.95	24.29	48.36	6	3.42	22.53	26.91	99.95
7	2.99	23.00	24.46	48.41	7	2.99	22.59	27.35	99.88
8	2.99	22.99	24.46	48.43	8	2.99	22.59	27.34	99.84
9	2.51	23.06	24.67	48.46	9	2.51	22.67	27.94	99.93
10	2.51	23.06	24.68	48.39	10	2.51	22.67	27.94	99.89
11	1.97	23.14	24.96	48.37	11	1.97	22.81	28.85	100.05
12	1.97	23.13	24.96	48.38	12	1.97	22.80	28.84	100.03
13	1.48	23.29	25.41	48.33	13	1.48	23.00	30.02	99.94
14	1.48	23.29	25.41	48.37	14	1.48	23.00	30.01	99.92
15	1.16	23.49	25.88	48.38	15	1.16	23.20	31.19	100.01
16	1.16	23.48	25.89	48.48	16	1.16	23.20	31.20	100.04
17	4.39	22.73	23.88	48.51	17	4.40	22.45	26.18	99.87
18	4.39	22.72	23.88	48.54	18	4.40	22.45	26.17	99.81

TABLE XV

RAW DATA FOR COMMERCIALY AVAILABLE FINNED TUBES
WITH FINS OF $S = 0.5$ MM, $T_B = 0.3$ MM AND $E = 1.0$ MM

Tube Number: 49					Tube Number: 49				
File Name: F49V186					File Name: F49A248				
Pressure Condition: Vacuum					Pressure Condition: Atmospheric				
Steam Velocity: 2.0 (m/s)					Steam Velocity: 1.0 (m/s)				
Data #	Vw (m/s)	Tin (C)	Tout (C)	Is (C)	Data #	Vw (m/s)	Tin (C)	Tout (C)	Is (C)
1	4.29	21.71	22.81	48.46	1	4.40	21.50	24.81	100.05
2	4.29	21.75	22.85	48.44	2	4.40	21.50	24.80	99.98
3	3.86	21.93	23.10	48.51	3	3.86	21.59	25.22	100.01
4	3.86	21.97	23.15	48.47	4	3.86	21.60	25.23	99.93
5	3.43	22.06	23.34	48.44	5	3.43	21.66	25.58	99.96
6	3.43	22.06	23.34	48.41	6	3.43	21.66	25.59	99.94
7	2.99	22.16	23.54	48.54	7	3.00	21.75	26.03	99.89
8	2.99	22.17	23.55	48.51	8	3.00	21.75	26.02	99.92
9	2.51	22.27	23.79	48.44	9	2.51	21.86	26.59	99.99
10	2.51	22.28	23.80	48.52	10	2.51	21.86	26.58	100.03
11	1.97	22.45	24.18	48.35	11	1.97	22.00	27.40	99.95
12	1.97	22.46	24.18	48.42	12	1.97	22.00	27.40	99.94
13	1.48	22.65	24.62	48.39	13	1.49	22.22	28.43	99.93
14	1.48	22.65	24.62	48.44	14	1.49	22.22	28.43	99.94
15	1.16	22.85	25.06	48.44	15	1.16	22.44	29.44	99.93
16	1.16	22.85	25.06	48.46	16	1.16	22.44	29.46	99.99
17	4.29	22.14	23.24	48.61	17	4.40	21.68	25.08	99.91
18	4.29	22.14	23.24	48.46	18	4.40	21.68	25.08	99.95

TABLE XVI
RAW DATA FOR HPTI SMOOTH TUBE

Tube Number: 50				Tube Number: 50					
File Name: S50V184				File Name: S50A213					
Pressure Condition: Vacuum				Pressure Condition: Atmospheric					
Steam Velocity: 2.0 (m/s)				Steam Velocity: 1.0 (m/s)					
Data #	Vw (m/s)	Tin (C)	Tout (C)	Is (C)	Data #	Vw (m/s)	Tin (C)	Tout (C)	Is (C)
1	4.29	21.60	22.22	48.44	1	4.83	22.01	23.59	99.91
2	4.29	21.66	22.27	48.42	2	4.83	22.04	23.53	99.93
3	3.86	21.92	22.60	48.55	3	4.40	22.23	23.96	100.00
4	3.86	21.94	22.61	48.51	4	4.40	22.23	23.96	99.98
5	3.43	22.09	22.85	48.44	5	3.86	22.37	24.32	100.01
6	3.43	22.10	22.85	48.40	6	3.86	22.38	24.33	100.01
7	2.99	22.21	23.05	48.53	7	3.42	22.47	24.63	99.93
8	2.99	22.22	23.06	48.54	8	3.42	22.49	24.66	99.96
9	2.51	22.36	23.31	48.42	9	2.99	22.60	25.03	100.00
10	2.51	22.37	23.33	48.41	10	2.99	22.59	25.02	100.02
11	1.97	22.51	23.65	48.50	11	2.51	22.71	25.50	99.91
12	1.97	22.52	23.66	48.53	12	2.51	22.72	25.51	99.96
13	1.48	22.73	24.10	48.44	13	1.97	22.84	26.20	99.90
14	1.48	22.73	24.09	48.40	14	1.97	22.84	26.19	99.89
15	1.16	22.93	24.52	48.43	15	1.48	23.03	27.13	99.93
16	1.16	22.94	24.52	48.41	16	1.48	23.03	27.15	100.04
17	4.29	22.24	22.87	48.51	17	1.16	23.22	28.09	99.98
18	4.29	22.24	22.87	48.53	18	1.16	23.22	28.09	99.90

TABLE XVII

RAW DATA FOR COMMERCIALY AVAILABLE FINNED TUBES
WITH FINS OF $S = 0.6$ MM, $T_B = 0.3$ MM AND $E = 1.0$ MM

Tube Number: 51					Tube Number: 51				
File Name: F51V185					File Name: F51A245				
Pressure Condition: Vacuum					Pressure Condition: Atmospheric				
Steam Velocity: 2.0 (m/s)					Steam Velocity: 1.0 (m/s)				
Data #	Vw (m/s)	Tin (C)	Tout (C)	Is (C)	Data #	Vw (m/s)	Tin (C)	Tout (C)	Is (C)
1	4.29	21.71	22.75	48.56	1	4.40	21.13	24.46	99.96
2	4.29	21.81	22.85	48.48	2	4.40	21.13	24.46	99.98
3	3.86	22.04	23.15	48.51	3	3.86	21.19	24.83	99.96
4	3.86	22.05	23.17	48.48	4	3.86	21.19	24.84	100.00
5	3.43	22.26	23.46	48.42	5	3.43	21.24	25.18	99.98
6	3.42	22.28	23.48	48.49	6	3.43	21.24	25.17	99.94
7	2.99	22.44	23.73	48.33	7	3.00	21.30	25.55	100.00
8	2.99	22.46	23.76	48.44	8	3.00	21.30	25.55	99.92
9	2.51	22.58	24.00	48.46	9	2.51	21.39	26.08	100.00
10	2.51	22.59	24.01	48.43	10	2.51	21.39	26.08	100.00
11	1.97	22.76	24.37	48.36	11	1.97	21.51	26.86	100.01
12	1.97	22.78	24.40	48.56	12	1.97	21.51	26.86	99.96
13	1.48	22.98	24.81	48.50	13	1.49	21.70	27.90	99.95
14	1.48	22.98	24.83	48.43	14	1.49	21.70	27.90	99.91
15	1.16	23.18	25.25	48.48	15	1.16	21.92	28.91	99.97
16	1.16	23.19	25.26	48.46	16	1.16	21.92	28.91	99.95
17	4.29	22.50	23.52	48.51	17	4.40	21.14	24.48	99.95
18	4.29	22.51	23.53	48.47	18	4.40	21.14	24.47	99.88

TABLE XVIII

RAW DATA FOR TUBE WITH TRIANGULAR FIN PROFILE
OF $S = 1.5$ MM, $T_B = 0.5$ MM AND $E = 1.0$ MM

Tube Number: 52					Tube Number: 52				
File Name: F52V197					File Name: F52A208				
Pressure Condition: Vacuum					Pressure Condition: Atmospheric				
Steam Velocity: 2.0 (m/s)					Steam Velocity: 1.0 (m/s)				
Data #	Vw (m/s)	Tin (C)	Tout (C)	Is (C)	Data #	Vw (m/s)	Tin (C)	Tout (C)	Is (C)
1	4.39	23.10	24.23	48.45	1	4.39	22.97	26.59	99.98
2	4.39	23.11	24.24	48.44	2	4.39	23.02	26.64	99.91
3	3.85	23.20	24.44	48.47	3	3.85	23.11	27.07	99.97
4	3.85	23.21	24.46	48.45	4	3.85	23.13	27.09	99.95
5	3.42	23.29	24.63	48.40	5	3.42	23.19	27.48	99.98
6	3.42	23.29	24.62	48.48	6	3.42	23.20	27.49	99.91
7	2.99	23.35	24.80	48.45	7	2.99	23.27	27.94	99.98
8	2.99	23.34	24.79	48.34	8	2.99	23.27	27.94	100.02
9	2.50	23.43	25.03	48.43	9	2.51	23.38	28.55	99.98
10	2.50	23.44	25.04	48.48	10	2.51	23.38	28.56	100.00
11	1.97	23.56	25.39	48.44	11	1.97	23.52	29.47	100.01
12	1.97	23.56	25.39	48.49	12	1.97	23.53	29.48	100.02
13	1.48	23.76	25.86	48.51	13	1.48	23.74	30.66	99.93
14	1.48	23.75	25.86	48.49	14	1.48	23.73	30.64	99.97
15	1.16	23.96	26.34	48.50	15	1.16	23.93	31.82	100.02
16	1.16	23.96	26.34	48.51	16	1.16	23.93	31.83	99.99
17	4.39	23.21	24.35	48.48	17	4.39	23.20	26.83	100.02
18	4.39	23.21	24.35	48.52	18	4.39	23.18	26.81	100.01

TABLE XIX

RAW DATA FOR TUBE WITH TRAPEZOIDAL FIN PROFILE
OF $S = 1.5$ MM, $T_B = 0.5$ MM AND $E = 1.0$ MM

Tube Number: 53					Tube Number: 53				
File Name: F53V198					File Name: F53A202				
Pressure Condition: Vacuum					Pressure Condition: Atmospheric				
Steam Velocity: 2.0 (m/s)					Steam Velocity: 1.0 (m/s)				
Data #	Vw (m/s)	Tin (C)	Tout (C)	Is (C)	Data #	Vw (m/s)	Tin (C)	Tout (C)	Is (C)
1	4.39	23.11	24.25	48.43	1	4.39	22.82	26.41	99.94
2	4.39	23.12	24.25	48.43	2	4.39	22.83	26.42	99.99
3	3.85	23.17	24.41	48.53	3	3.85	23.06	27.02	99.95
4	3.85	23.17	24.41	48.44	4	3.85	23.06	27.02	99.98
5	3.42	23.22	24.56	48.44	5	3.42	23.17	27.45	100.00
6	3.42	23.22	24.55	48.42	6	3.42	23.17	27.45	100.00
7	2.99	23.28	24.73	48.46	7	2.99	23.31	27.98	99.95
8	2.99	23.27	24.72	48.53	8	2.99	23.32	27.99	100.00
9	2.50	23.35	24.95	48.45	9	2.51	23.43	28.60	99.95
10	2.50	23.35	24.96	48.47	10	2.51	23.44	28.62	100.00
11	1.97	23.47	25.31	48.47	11	1.97	23.59	29.54	99.99
12	1.97	23.47	25.31	48.48	12	1.97	23.60	29.55	100.00
13	1.48	23.65	25.77	48.53	13	1.48	23.77	30.70	99.97
14	1.48	23.65	25.77	48.48	14	1.48	23.77	30.70	99.96
15	1.16	23.84	26.23	48.54	15	1.16	23.95	31.85	100.00
16	1.16	23.84	26.23	48.48	16	1.16	23.95	31.85	99.96
17	4.39	23.09	24.23	48.52	17	4.39	23.23	26.88	99.98
18	4.39	23.10	24.23	48.42	18	4.39	23.24	26.87	99.95

TABLE XX

RAW DATA FOR TUBE WITH PARABOLIC FIN PROFILE
OF $S = 1.5$ MM, $T_B = 1.0$ MM AND $E = 1.0$ MM

Tube Number: 54					Tube Number: 54				
File Name: F54V228					File Name: F54A219				
Pressure Condition: Vacuum					Pressure Condition: Atmospheric				
Steam Velocity: 2.0 (m/s)					Steam Velocity: 1.0 (m/s)				
Data #	V _w (m/s)	T _{in} (C)	T _{out} (C)	T _s (C)	Data #	V _w (m/s)	T _{in} (C)	T _{out} (C)	T _s (C)
1	4.40	21.64	22.82	48.40	1	4.40	22.16	25.84	100.01
2	4.40	21.64	22.82	48.55	2	4.40	22.23	25.90	100.01
3	3.86	21.69	22.99	48.38	3	3.86	22.32	26.35	99.96
4	3.86	21.69	23.00	48.41	4	3.86	22.32	26.35	99.97
5	3.43	21.75	23.16	48.51	5	3.43	22.39	26.76	99.92
6	3.43	21.75	23.16	48.40	6	3.43	22.42	26.77	99.96
7	3.00	21.81	23.35	48.45	7	2.99	22.49	27.24	99.99
8	3.00	21.82	23.36	48.39	8	2.99	22.50	27.25	99.94
9	2.51	21.90	23.61	48.44	9	2.51	22.63	27.91	99.95
10	2.51	21.91	23.61	48.38	10	2.51	22.62	27.90	99.99
11	1.97	22.04	24.00	48.53	11	1.97	22.76	28.82	99.97
12	1.97	22.05	24.00	48.53	12	1.97	22.75	28.81	100.02
13	1.48	22.25	24.52	48.44	13	1.48	22.96	30.06	99.94
14	1.48	22.25	24.51	48.37	14	1.48	22.95	30.05	99.92
15	1.16	22.46	25.03	48.42	15	1.16	23.16	31.27	99.99
16	1.16	22.46	25.01	48.35	16	1.16	23.17	31.28	99.95
17	4.40	21.72	22.92	48.53	17	4.40	22.40	26.07	99.97
18	4.40	21.73	22.92	48.61	18	4.40	22.42	26.08	99.91

TABLE XXI

RAW DATA FOR TUBE WITH TRAPEZOIDAL FIN PROFILE
OF $S = 1.5$ MM, $T_B = 1.0$ MM AND $E = 1.0$ MM

Tube Number: 55 File Name: F55V238 Pressure Condition: Vacuum Steam Velocity: 2.0 (m/s)					Tube Number: 55 File Name: F55A234 Pressure Condition: Atmospheric Steam Velocity: 1.0 (m/s)				
Data #	V _w (m/s)	T _{in} (C)	T _{out} (C)	T _s (C)	Data #	V _w (m/s)	T _{in} (C)	T _{out} (C)	T _s (C)
1	4.40	20.95	22.20	48.41	1	4.40	21.57	25.17	99.93
2	4.40	20.99	22.26	48.58	2	4.40	21.58	25.18	99.98
3	3.86	21.15	22.53	48.54	3	3.86	21.65	25.61	100.01
4	3.86	21.17	22.54	48.50	4	3.86	21.66	25.62	100.00
5	3.43	21.26	22.74	48.37	5	3.43	21.74	26.05	99.95
6	3.43	21.27	22.75	48.43	6	3.43	21.74	26.05	99.93
7	3.00	21.33	22.93	48.46	7	3.00	21.80	26.50	99.94
8	3.00	21.33	22.94	48.44	8	3.00	21.80	26.50	99.93
9	2.51	21.39	23.17	48.55	9	2.51	21.89	27.15	100.00
10	2.51	21.39	23.17	48.45	10	2.51	21.89	27.14	100.00
11	1.97	21.51	23.53	48.41	11	1.97	22.01	28.07	99.97
12	1.97	21.51	23.53	48.36	12	1.97	22.02	28.08	99.90
13	1.49	21.68	24.01	48.44	13	1.49	22.19	29.30	99.94
14	1.49	21.65	23.99	48.55	14	1.49	22.20	29.31	100.03
15	1.16	21.85	24.50	48.54	15	1.16	22.40	30.50	99.96
16	1.16	21.83	24.48	48.49	16	1.16	22.40	30.51	99.96
17	4.40	21.05	22.31	48.40	17	4.40	21.64	25.27	99.97
18	4.40	21.04	22.31	48.45	18	4.40	21.65	25.26	99.91

TABLE XXII

RAW DATA FOR TUBE WITH TRIANGULAR FIN PROFILE
OF $S = 1.5$ MM, $T_B = 1.0$ MM AND $E = 1.0$ MM

Tube Number: 56				Tube Number: 56					
File Name: F56V241				File Name: F56A237					
Pressure Condition: Vacuum				Pressure Condition: Atmospheric					
Steam Velocity: 2.0 (m/s)				Steam Velocity: 1.0 (m/s)					
Data #	Vw (m/s)	Tin (C)	Tout (C)	Is (C)	Data #	Vw (m/s)	Tin (C)	Tout (C)	Is (C)
1	4.40	21.42	22.66	48.51	1	4.40	21.18	24.92	99.89
2	4.40	21.43	22.66	48.47	2	4.40	21.21	24.94	99.90
3	3.86	21.49	22.84	48.40	3	3.86	21.30	25.38	100.00
4	3.86	21.49	22.84	48.44	4	3.86	21.31	25.38	99.99
5	3.43	21.55	23.01	48.54	5	3.43	21.40	25.81	99.94
6	3.43	21.55	23.01	48.45	6	3.43	21.40	25.81	99.99
7	3.00	21.60	23.19	48.45	7	3.00	21.49	26.30	100.02
8	3.00	21.60	23.19	48.48	8	3.00	21.49	26.30	99.93
9	2.51	21.68	23.44	48.48	9	2.51	21.58	26.92	99.87
10	2.51	21.68	23.43	48.43	10	2.51	21.58	26.92	99.90
11	1.97	21.79	23.80	48.44	11	1.97	21.73	27.89	99.96
12	1.97	21.78	23.79	48.41	12	1.97	21.74	27.89	99.96
13	1.49	21.95	24.26	48.48	13	1.49	21.94	29.15	99.97
14	1.49	21.96	24.27	48.44	14	1.49	21.94	29.15	99.97
15	1.16	22.15	24.77	48.45	15	1.16	22.16	30.44	99.96
16	1.16	22.15	24.78	48.48	16	1.16	22.16	30.43	100.00
17	4.40	21.39	22.63	48.51	17	4.40	21.40	25.11	99.96
18	4.40	21.39	22.63	48.53	18	4.40	21.39	25.10	99.94

TABLE XXIII

RAW DATA FOR SPIRAL COPPER TUBE WITH TRIANGULAR FIN PROFILE
OF $P = 2.1$ MM, $E = 1.0$ MM AND $DO = 13.7$ MM

Tube Number: 57					Tube Number: 57				
File Name: F57V252					File Name: F57A275				
Pressure Condition: Vacuum					Pressure Condition: Atmospheric				
Steam Velocity: 2.0 (m/s)					Steam Velocity: 1.0 (m/s)				
Data #	Vw (m/s)	Tin (C)	Tout (C)	Ts (C)	Data #	Vw (m/s)	Tin (C)	Tout (C)	Ts (C)
1	4.40	20.90	22.03	48.55	1	4.41	20.44	23.57	99.95
2	4.40	20.90	22.04	48.49	2	4.41	20.46	23.60	100.01
3	3.86	20.99	22.22	48.45	3	3.87	20.55	24.02	100.01
4	3.86	21.00	22.22	48.44	4	3.87	20.55	24.03	100.09
5	3.43	21.08	22.42	48.43	5	3.43	20.65	24.45	100.02
6	3.43	21.08	22.43	48.48	6	3.43	20.67	24.48	99.97
7	3.00	21.16	22.61	48.45	7	3.00	20.74	24.92	99.95
8	3.00	21.16	22.62	48.45	8	3.00	20.73	24.92	99.98
9	2.51	21.25	22.88	48.44	9	2.51	20.89	25.59	99.94
10	2.51	21.26	22.88	48.41	10	2.51	20.89	25.60	99.90
11	1.97	21.39	23.26	48.53	11	1.97	21.04	26.53	100.02
12	1.97	21.40	23.28	48.54	12	1.97	21.04	26.53	100.03
13	1.49	21.59	23.76	48.39	13	1.49	21.21	27.71	100.05
14	1.49	21.59	23.76	48.42	14	1.49	21.23	27.73	100.07
15	1.16	21.80	24.28	48.42	15	1.16	21.46	28.92	99.99
16	1.16	21.80	24.29	48.44	16	1.16	21.46	28.93	99.99
17	4.40	21.04	22.17	48.34	17	4.41	20.72	23.93	99.96
18	4.40	21.04	22.18	48.42	18	4.41	20.71	23.93	99.97

TABLE XXIV

RAW DATA FOR SPIRAL COPPER-NICKEL TUBE WITH TRIANGULAR
FIN PROFILE OF $P = 2.1$ MM, $E = 1.0$ MM AND $DO = 13.7$ MM

Tube Number: 58					Tube Number: 58				
File Name: F58V273					File Name: F58A261				
Pressure Condition: Vacuum					Pressure Condition: Atmospheric				
Steam Velocity: 2.0 (m/s)					Steam Velocity: 1.0 (m/s)				
Data #	V_w (m/s)	T_{in} (C)	T_{out} (C)	T_s (C)	Data #	V_w (m/s)	T_{in} (C)	T_{out} (C)	T_s (C)
1	4.41	20.61	21.34	48.39	1	4.40	20.95	23.27	99.95
2	4.41	20.63	21.36	48.33	2	4.40	20.96	23.28	100.00
3	3.87	20.69	21.50	48.27	3	3.86	21.03	23.61	99.97
4	3.87	20.69	21.50	48.30	4	3.86	21.03	23.62	99.90
5	3.43	20.78	21.67	48.51	5	3.43	21.10	23.93	100.00
6	3.43	20.78	21.67	48.53	6	3.43	21.11	23.94	99.94
7	3.00	20.86	21.85	48.46	7	3.00	21.18	24.31	99.98
8	3.00	20.86	21.85	48.44	8	3.00	21.17	24.30	99.97
9	2.51	20.96	22.07	48.46	9	2.51	21.26	24.81	99.94
10	2.51	20.96	22.07	48.49	10	2.51	21.28	24.82	100.00
11	1.97	21.09	22.41	48.49	11	1.97	21.42	25.58	99.93
12	1.97	21.09	22.42	48.44	12	1.97	21.42	25.58	99.92
13	1.49	21.29	22.87	48.53	13	1.49	21.62	26.62	99.94
14	1.49	21.29	22.87	48.47	14	1.49	21.62	26.62	99.93
15	1.16	21.48	23.31	48.44	15	1.16	21.82	27.64	100.03
16	1.16	21.51	23.33	48.41	16	1.16	21.83	27.66	100.03
17	4.41	20.74	21.47	48.47	17	4.40	21.10	23.42	99.95
18	4.41	20.74	21.47	48.53	18	4.40	21.10	23.42	99.99

TABLE XXV

RAW DATA FOR SPIRAL STAINLESS STEEL TUBE WITH TRIANGULAR
FIN PROFILE OF $P = 2.1$ MM, $E = 1.0$ MM AND $DO = 14.5$ MM

Tube Number: 59					Tube Number: 59				
File Name: F59V271					File Name: F59A265				
Pressure Condition: Vacuum					Pressure Condition: Atmospheric				
Steam Velocity: 2.0 (m/s)					Steam Velocity: 1.0 (m/s)				
Data #	Vw (m/s)	Tin (C)	Tout (C)	Is (C)	Data #	Vw (m/s)	Tin (C)	Tout (C)	Is (C)
1	4.40	21.00	21.37	48.41	1	4.41	20.67	21.84	100.02
2	4.40	20.99	21.37	48.47	2	4.41	20.68	21.84	100.03
3	3.86	21.02	21.44	48.38	3	3.87	20.76	22.08	99.94
4	3.86	21.00	21.43	48.34	4	3.87	20.76	22.08	99.92
5	3.43	21.03	21.51	48.40	5	3.43	20.83	22.30	99.89
6	3.43	21.02	21.50	48.40	6	3.43	20.84	22.31	99.96
7	3.00	21.06	21.60	48.33	7	3.00	20.90	22.55	99.93
8	3.00	21.06	21.59	48.33	8	3.00	20.91	22.56	99.93
9	2.51	21.12	21.74	48.35	9	2.51	21.00	22.90	99.89
10	2.51	21.12	21.74	48.30	10	2.51	21.00	22.91	99.91
11	1.97	21.23	21.99	48.31	11	1.97	21.14	23.45	99.89
12	1.97	21.22	21.98	48.24	12	1.97	21.14	23.46	99.96
13	1.49	21.39	22.32	48.30	13	1.49	21.33	24.20	99.93
14	1.49	21.39	22.32	48.39	14	1.49	21.34	24.21	99.93
15	1.16	21.55	22.67	48.33	15	1.16	21.55	25.01	99.97
16	1.16	21.57	22.69	48.43	16	1.16	21.56	25.02	99.98
17	4.40	20.81	21.18	48.43	17	4.41	20.80	21.96	100.02
18	4.40	20.80	21.17	48.46	18	4.41	20.80	21.97	99.96

TABLE XXVI

RAW DATA FOR SPIRAL ALUMINUM TUBE WITH TRIANGULAR
FIN PROFILE OF $P = 2.1$ MM, $E = 1.0$ MM AND $DO = 13.7$ MM

Tube Number: 60					Tube Number: 60				
File Name: F60V254					File Name: F60A258				
Pressure Condition: Vacuum					Pressure Condition: Atmospheric				
Steam Velocity: 2.0 (m/s)					Steam Velocity: 1.0 (m/s)				
Data #	Vw (m/s)	Tin (C)	Tout (C)	Is (C)	Data #	Vw (m/s)	Tin (C)	Tout (C)	Is (C)
1	4.35	20.87	21.87	48.42	1	4.40	21.16	23.91	99.96
2	4.35	20.87	21.85	48.39	2	4.40	21.16	23.90	99.96
3	3.86	20.93	22.01	48.37	3	3.86	21.23	24.27	99.92
4	3.86	20.93	22.01	48.41	4	3.86	21.22	24.26	99.89
5	3.43	20.99	22.17	48.46	5	3.43	21.28	24.59	99.96
6	3.43	21.00	22.17	48.42	6	3.43	21.28	24.59	100.00
7	3.00	21.06	22.34	48.47	7	3.00	21.34	25.00	99.96
8	3.00	21.07	22.35	48.39	8	3.00	21.35	25.00	100.04
9	2.51	21.15	22.59	48.42	9	2.51	21.45	25.56	100.05
10	2.51	21.15	22.59	48.46	10	2.51	21.45	25.57	100.01
11	1.97	21.29	22.94	48.49	11	1.97	21.58	26.36	100.02
12	1.97	21.29	22.94	48.51	12	1.97	21.58	26.35	99.91
13	1.49	21.48	23.43	48.55	13	1.49	21.77	27.44	99.88
14	1.49	21.48	23.43	48.47	14	1.49	21.78	27.46	99.93
15	1.16	21.68	23.90	48.46	15	1.16	21.98	28.56	100.01
16	1.16	21.69	23.91	48.53	16	1.16	21.98	28.56	100.00
17	4.35	20.94	21.92	48.30	17	4.40	21.24	24.01	100.01
18	4.35	20.94	21.93	48.37	18	4.40	21.24	24.00	100.02

TABLE XXVII

RAW DATA FOR COPPER-NICKEL TUBE WITH RECTANGULAR FIN PROFILE
OF $S = 1.5$ MM, $T = 1.0$ MM, $E = 1.0$ MM

Tube Number: 61					Tube Number: 61				
File Name: F61V272					File Name: F61A263				
Pressure Condition: Vacuum					Pressure Condition: Atmospheric				
Steam Velocity: 2.0 (m/s)					Steam Velocity: 1.0 (m/s)				
Data #	Vw (m/s)	Tin (C)	Tout (C)	Is (C)	Data #	Vw (m/s)	Tin (C)	Tout (C)	Is (C)
1	4.41	20.62	21.30	48.33	1	4.41	20.75	23.02	99.98
2	4.41	20.63	21.30	48.46	2	4.41	20.77	23.04	99.93
3	3.87	20.69	21.45	48.47	3	3.87	20.87	23.38	99.95
4	3.87	20.69	21.46	48.39	4	3.87	20.86	23.38	99.89
5	3.43	20.75	21.60	48.33	5	3.43	20.95	23.71	99.99
6	3.43	20.76	21.59	48.37	6	3.43	20.94	23.71	99.94
7	3.00	20.83	21.75	48.37	7	3.00	21.02	24.08	99.97
8	3.00	20.83	21.76	48.31	8	3.00	21.02	24.08	99.96
9	2.51	20.93	21.98	48.42	9	2.51	21.12	24.58	99.97
10	2.51	20.93	21.98	48.48	10	2.51	21.12	24.58	100.04
11	1.97	21.07	22.31	48.55	11	1.97	21.29	25.35	99.94
12	1.97	21.07	22.31	48.50	12	1.97	21.29	25.35	99.93
13	1.49	21.26	22.73	48.40	13	1.49	21.49	26.35	99.96
14	1.49	21.26	22.74	48.40	14	1.49	21.50	26.36	99.92
15	1.16	21.48	23.18	48.39	15	1.16	21.71	27.36	99.98
16	1.16	21.48	23.19	48.38	16	1.16	21.72	27.35	99.98
17	4.41	20.72	21.40	48.46	17	4.40	20.97	23.25	99.96
18	4.41	20.71	21.40	48.38	18	4.40	20.96	23.25	99.98

TABLE XXVIII

RAW DATA FOR ALUMINUM TUBE WITH RECTANGULAR FIN PROFILE
OF $S = 1.5$ MM, $T = 1.0$ MM, $E = 1.0$ MM AND $DO = 13.7$ MM

Tube Number: 62					Tube Number: 62				
File Name: F62V276					File Name: F62A259				
Pressure Condition: Vacuum					Pressure Condition: Atmospheric				
Steam Velocity: 2.0 (m/s)					Steam Velocity: 1.0 (m/s)				
Data #	Vw (m/s)	Tin (C)	Tout (C)	Is (C)	Data #	Vw (m/s)	Tin (C)	Tout (C)	Is (C)
1	4.41	20.13	21.00	48.49	1	4.41	20.84	23.64	99.97
2	4.41	20.16	21.03	48.49	2	4.41	20.85	23.65	100.05
3	3.87	20.30	21.27	48.55	3	3.86	21.00	24.09	99.99
4	3.87	20.32	21.29	48.51	4	3.86	20.99	24.08	100.04
5	3.43	20.43	21.48	48.42	5	3.43	21.06	24.43	99.96
6	3.43	20.44	21.51	48.38	6	3.43	21.07	24.44	99.91
7	3.00	20.55	21.71	48.41	7	3.00	21.18	24.86	99.92
8	3.00	20.56	21.72	48.37	8	3.00	21.18	24.87	99.94
9	2.51	20.67	21.97	48.41	9	2.51	21.28	25.42	99.94
10	2.51	20.67	21.98	48.44	10	2.51	21.29	25.43	99.97
11	1.97	20.86	22.38	48.50	11	1.97	21.45	26.25	100.03
12	1.97	20.86	22.37	48.55	12	1.97	21.45	26.25	100.00
13	1.49	21.06	22.84	48.52	13	1.49	21.68	27.34	100.01
14	1.49	21.06	22.84	48.49	14	1.49	21.68	27.33	99.88
15	1.16	21.26	23.31	48.48	15	1.16	21.89	28.39	99.94
16	1.16	21.27	23.31	48.55	16	1.16	21.90	28.41	100.00
17	4.41	20.53	21.41	48.37	17	4.40	21.22	24.02	99.87
18	4.41	20.53	21.41	48.43	18	4.40	21.21	24.01	99.86

TABLE XXIX

RAW DATA FOR WIRE-WRAPPED TUBE WITH
 $D_W = 1.6 \text{ MM}$ AND $P = 2.5 \text{ MM}$

Tube Number: 63					Tube Number: 63				
File Name: S63V279					File Name: S63A317				
Pressure Condition: Vacuum					Pressure Condition: Atmospheric				
Steam Velocity: 2.0 (m/s)					Steam Velocity: 1.0 (m/s)				
Data #	Vw (m/s)	Tin (C)	Tout (C)	Is (C)	Data #	Vw (m/s)	Tin (C)	Tout (C)	Is (C)
1	4.41	20.03	20.69	48.52	1	4.42	18.91	20.98	100.02
2	4.41	19.91	20.57	48.47	2	4.42	18.91	20.98	99.98
3	3.87	19.82	20.58	48.52	3	3.88	18.99	21.30	99.96
4	3.87	19.81	20.56	48.53	4	3.88	19.02	21.33	99.92
5	3.44	19.75	20.59	48.43	5	3.44	19.08	21.64	99.93
6	3.44	19.75	20.58	48.38	6	3.44	19.10	21.66	99.97
7	3.01	19.78	20.72	48.41	7	3.01	19.18	22.02	99.93
8	3.01	19.77	20.70	48.45	8	3.01	19.20	22.04	99.95
9	2.52	19.84	20.91	48.51	9	2.52	19.29	22.53	99.95
10	2.52	19.83	20.91	48.43	10	2.52	19.31	22.55	99.94
11	1.98	19.95	21.24	48.45	11	1.98	19.43	23.30	99.99
12	1.98	19.95	21.23	48.43	12	1.98	19.45	23.31	99.97
13	1.49	20.12	21.68	48.45	13	1.49	19.61	24.32	99.98
14	1.49	20.12	21.68	48.47	14	1.49	19.65	24.37	99.95
15	1.16	20.31	22.15	48.47	15	1.17	19.79	25.35	99.98
16	1.16	20.32	22.15	48.56	16	1.17	19.86	25.42	99.90
17	4.41	19.53	20.20	48.48	17	4.42	19.15	21.23	99.92
18	4.41	19.53	20.20	48.40	18	4.42	19.15	21.22	99.90

TABLE XXX

RAW DATA FOR WIRE-WRAPPED TUBE WITH
 $D_w = 1.6 \text{ MM}$ AND $P = 3.6 \text{ MM}$

Tube Number: 64					Tube Number: 64				
File Name: S64V280					File Name: S64A307				
Pressure Condition: Vacuum					Pressure Condition: Atmospheric				
Steam Velocity: 2.0 (m/s)					Steam Velocity: 1.0 (m/s)				
Data #	Vw (m/s)	Tin (C)	Tout (C)	Is (C)	Data #	Vw (m/s)	Tin (C)	Tout (C)	Is (C)
1	4.41	19.37	20.17	48.53	1	4.42	19.40	21.77	99.94
2	4.41	19.37	20.17	48.48	2	4.42	19.43	21.78	99.98
3	3.87	19.43	20.33	48.52	3	3.87	19.52	22.13	99.98
4	3.87	19.43	20.33	48.44	4	3.87	19.53	22.14	99.95
5	3.44	19.49	20.48	48.41	5	3.44	19.60	22.47	99.94
6	3.44	19.50	20.49	48.41	6	3.44	19.60	22.48	99.96
7	3.01	19.56	20.66	48.44	7	3.01	19.68	22.87	99.92
8	3.01	19.56	20.66	48.53	8	3.01	19.69	22.87	99.96
9	2.52	19.66	20.89	48.48	9	2.52	19.78	23.38	99.98
10	2.52	19.65	20.90	48.46	10	2.52	19.78	23.39	99.97
11	1.98	19.79	21.27	48.51	11	1.98	19.91	24.21	99.98
12	1.98	19.79	21.26	48.46	12	1.98	19.93	24.23	100.01
13	1.49	19.98	21.75	48.49	13	1.49	20.13	25.32	100.05
14	1.49	19.99	21.75	48.42	14	1.49	20.14	25.33	100.02
15	1.16	20.20	22.26	48.44	15	1.17	20.38	26.45	99.97
16	1.16	20.21	22.26	48.48	16	1.17	20.39	26.45	99.93
17	4.41	19.43	20.24	48.49	17	4.41	19.64	21.97	100.02
18	4.41	19.43	20.24	48.47	18	4.41	19.63	21.96	100.02

TABLE XXXI

RAW DATA FOR WIRE-WRAPPED TUBE WITH
 $D_w = 1.6 \text{ MM}$ AND $P = 4.6 \text{ MM}$

Tube Number: 65					Tube Number: 65				
File Name: S65V281					File Name: S65A308				
Pressure Condition: Vacuum					Pressure Condition: Atmospheric				
Steam Velocity: 2.0 (m/s)					Steam Velocity: 1.0 (m/s)				
Data #	Vw (m/s)	Tin (C)	Tout (C)	Ts (C)	Data #	Vw (m/s)	Tin (C)	Tout (C)	Ts (C)
1	4.41	19.35	20.17	48.44	1	4.42	19.40	21.72	99.98
2	4.41	19.36	20.18	48.41	2	4.41	19.45	21.77	100.00
3	3.87	19.42	20.33	48.40	3	3.87	19.54	22.13	99.92
4	3.87	19.43	20.33	48.35	4	3.87	19.58	22.18	99.94
5	3.44	19.49	20.49	48.45	5	3.44	19.68	22.54	100.09
6	3.44	19.49	20.48	48.43	6	3.44	19.67	22.53	100.02
7	3.01	19.56	20.67	48.44	7	3.01	19.74	22.91	99.93
8	3.01	19.56	20.67	48.50	8	3.01	19.75	22.93	99.93
9	2.52	19.65	20.91	48.50	9	2.52	19.84	23.44	99.96
10	2.52	19.65	20.91	48.46	10	2.52	19.85	23.45	99.94
11	1.98	19.79	21.26	48.47	11	1.98	19.99	24.26	100.07
12	1.98	19.79	21.27	48.43	12	1.98	20.01	24.28	100.05
13	1.49	19.98	21.75	48.44	13	1.49	20.20	25.36	100.06
14	1.49	19.98	21.77	48.40	14	1.49	20.21	25.37	100.06
15	1.16	20.18	22.26	48.51	15	1.17	20.37	26.50	100.00
16	1.16	20.19	22.27	48.47	16	1.16	20.44	26.56	99.94
17	4.41	19.44	20.26	48.45	17	4.41	19.69	22.02	100.07
18	4.41	19.44	20.26	48.38	18	4.41	19.69	22.02	99.97

TABLE XXXII

RAW DATA FOR WIRE-WRAPPED TUBE WITH
 $D_W = 1.0 \text{ MM}$ AND $P = 2.0 \text{ MM}$

Tube Number: 66 File Name: S66V282 Pressure Condition: Vacuum Steam Velocity: 2.0 (m/s)					Tube Number: 66 File Name: S66A309 Pressure Condition: Atmospheric Steam Velocity: 1.0 (m/s)				
Data #	V _w (m/s)	T _{in} (C)	T _{out} (C)	I _s (C)	Data #	V _w (m/s)	T _{in} (C)	T _{out} (C)	I _s (C)
1	4.41	19.72	20.41	48.56	1	4.41	20.54	22.65	99.96
2	4.41	19.71	20.41	48.58	2	4.41	20.55	22.66	100.01
3	3.87	19.73	20.50	48.36	3	3.87	20.56	22.93	99.96
4	3.87	19.73	20.51	48.38	4	3.87	20.54	22.91	99.90
5	3.44	19.76	20.61	48.50	5	3.43	20.55	23.18	100.04
6	3.44	19.76	20.62	48.48	6	3.43	20.53	23.16	100.05
7	3.01	19.82	20.77	48.46	7	3.00	20.55	23.46	99.96
8	3.01	19.81	20.77	48.49	8	3.00	20.52	23.44	100.02
9	2.52	19.90	20.99	48.48	9	2.52	20.57	23.91	100.01
10	2.52	19.90	20.99	48.40	10	2.52	20.55	23.89	100.02
11	1.98	20.02	21.32	48.44	11	1.98	20.63	24.61	100.03
12	1.98	20.03	21.32	48.51	12	1.98	20.63	24.61	100.00
13	1.49	20.22	21.80	48.49	13	1.49	20.75	25.62	100.05
14	1.49	20.22	21.80	48.41	14	1.49	20.73	25.60	100.05
15	1.16	20.41	22.26	48.42	15	1.16	20.87	26.60	100.04
16	1.16	20.42	22.27	48.47	16	1.16	20.88	26.62	100.00
17	4.41	19.64	20.34	48.39	17	4.41	20.11	22.24	100.00
18	4.41	19.64	20.33	48.48	18	4.41	20.09	22.22	99.89

TABLE XXXIII

RAW DATA FOR WIRE-WRAPPED TUBE WITH
 $D_w = 1.0$ MM AND $P = 2.8$ MM

Tube Number: 67					Tube Number: 67				
File Name: S67V284					File Name: S67A319				
Pressure Condition: Vacuum					Pressure Condition: Atmospheric				
Steam Velocity: 2.0 (m/s)					Steam Velocity: 1.0 (m/s)				
Data #	Vw (m/s)	Tin (C)	Tout (C)	Is (C)	Data #	Vw (m/s)	Tin (C)	Tout (C)	Is (C)
1	4.41	20.23	21.07	48.40	1	4.42	19.11	21.67	99.98
2	4.41	20.22	21.06	48.35	2	4.42	19.12	21.68	99.97
3	3.87	20.23	21.16	48.47	3	3.88	19.17	22.02	99.98
4	3.87	20.21	21.16	48.46	4	3.88	19.18	22.03	99.95
5	3.44	20.23	21.27	48.48	5	3.44	19.23	22.37	99.95
6	3.44	20.21	21.24	48.46	6	3.44	19.25	22.39	99.96
7	3.00	20.23	21.38	48.53	7	3.01	19.31	22.77	99.90
8	3.00	20.21	21.36	48.41	8	3.01	19.31	22.78	99.97
9	2.52	20.28	21.57	48.35	9	2.52	19.39	23.31	100.01
10	2.52	20.26	21.56	48.39	10	2.52	19.40	23.33	99.98
11	1.98	20.37	21.89	48.43	11	1.98	19.52	24.16	99.99
12	1.98	20.36	21.89	48.40	12	1.98	19.53	24.17	100.02
13	1.49	20.52	22.35	48.54	13	1.49	19.69	25.28	100.05
14	1.49	20.53	22.35	48.50	14	1.49	19.71	25.30	100.10
15	1.16	20.71	22.82	48.34	15	1.17	19.88	26.41	100.10
16	1.16	20.70	22.82	48.31	16	1.17	19.92	26.44	100.01
17	4.41	19.88	20.75	48.55	17	4.42	19.18	21.74	99.89
18	4.41	19.88	20.74	48.50	18	4.42	19.17	21.74	99.93

TABLE XXXIV

RAW DATA FOR WIRE-WRAPPED TUBE WITH
 $D_w = 1.0 \text{ MM}$ AND $P = 3.9 \text{ MM}$

Tube Number: 68					Tube Number: 68				
File Name: S68V283					File Name: S68A311				
Pressure Condition: Vacuum					Pressure Condition: Atmospheric				
Steam Velocity: 2.0 (m/s)					Steam Velocity: 1.0 (m/s)				
Data #	Vw (m/s)	Tin (C)	Tout (C)	Ts (C)	Data #	Vw (m/s)	Tin (C)	Tout (C)	Ts (C)
1	4.41	19.57	20.44	48.40	1	4.41	19.51	22.08	100.03
2	4.41	19.57	20.45	48.33	2	4.41	19.52	22.09	99.96
3	3.87	19.65	20.63	48.34	3	3.87	19.57	22.44	99.95
4	3.87	19.65	20.63	48.38	4	3.87	19.58	22.45	99.98
5	3.44	19.72	20.79	48.43	5	3.44	19.63	22.79	99.96
6	3.44	19.73	20.80	48.37	6	3.44	19.64	22.81	99.97
7	3.01	19.80	20.98	48.44	7	3.01	19.70	23.20	100.00
8	3.01	19.81	20.99	48.46	8	3.01	19.71	23.21	99.95
9	2.52	19.90	21.23	48.45	9	2.52	19.80	23.77	99.98
10	2.52	19.90	21.24	48.46	10	2.52	19.80	23.79	100.03
11	1.98	20.05	21.61	48.49	11	1.98	19.93	24.64	100.06
12	1.98	20.06	21.62	48.48	12	1.98	19.95	24.67	100.03
13	1.49	20.26	22.14	48.44	13	1.49	20.13	25.82	100.06
14	1.49	20.27	22.14	48.41	14	1.49	20.14	25.82	99.98
15	1.16	20.48	22.65	48.47	15	1.17	20.27	26.93	100.00
16	1.16	20.49	22.66	48.47	16	1.17	20.34	27.00	99.99
17	4.41	19.72	20.60	48.42	17	4.41	19.59	22.18	99.87
18	4.41	19.72	20.60	48.36	18	4.41	19.58	22.17	99.94

TABLE XXXV

RAW DATA FOR WIRE-WRAPPED TUBE WITH
 $D_w = 0.5$ MM AND $P = 1.6$ MM

Tube Number: 69					Tube Number: 69				
File Name: S69V294					File Name: S69A303				
Pressure Condition: Vacuum					Pressure Condition: Atmospheric				
Steam Velocity: 2.0 (m/s)					Steam Velocity: 1.0 (m/s)				
Data #	Vw (m/s)	Tin (C)	Tout (C)	Ts (C)	Data #	Vw (m/s)	Tin (C)	Tout (C)	Is (C)
1	4.41	20.61	21.42	48.36	1	4.41	19.55	22.11	99.90
2	4.41	20.56	21.37	48.36	2	4.41	19.57	22.12	99.89
3	3.87	20.49	21.40	48.38	3	3.87	19.63	22.48	99.95
4	3.87	20.47	21.37	48.44	4	3.87	19.63	22.49	99.94
5	3.43	20.45	21.45	48.43	5	3.44	19.69	22.85	100.03
6	3.43	20.42	21.43	48.50	6	3.44	19.70	22.86	100.03
7	3.00	20.41	21.52	48.43	7	3.01	19.78	23.29	99.95
8	3.00	20.34	21.45	48.50	8	3.01	19.79	23.31	100.03
9	2.52	20.37	21.64	48.40	9	2.52	19.89	23.91	99.96
10	2.52	20.34	21.62	48.47	10	2.52	19.88	23.89	100.01
11	1.98	20.43	21.94	48.43	11	1.98	20.02	24.78	100.03
12	1.98	20.41	21.94	48.53	12	1.98	20.04	24.79	99.98
13	1.49	20.52	22.32	48.45	13	1.49	20.22	25.95	100.02
14	1.49	20.50	22.31	48.44	14	1.49	20.24	25.97	100.00
15	1.16	20.66	22.77	48.44	15	1.16	20.45	27.13	100.00
16	1.16	20.62	22.72	48.39	16	1.16	20.45	27.14	99.97
17	4.41	19.77	20.60	48.49	17	4.41	19.70	22.25	99.97
18	4.41	19.76	20.59	48.59	18	4.41	19.69	22.24	99.85

TABLE XXXVI
RAW DATA FOR WIRE-WRAPPED TUBE WITH
 $D_w = 0.5$ MM AND $P = 2.5$ MM

Tube Number: 70					Tube Number: 70				
File Name: S70V286					File Name: S70A313				
Pressure Condition: Vacuum					Pressure Condition: Atmospheric				
Steam Velocity: 2.0 (m/s)					Steam Velocity: 1.0 (m/s)				
Data #	Vw (m/s)	Tin (C)	Tout (C)	Is (C)	Data #	Vw (m/s)	Tin (C)	Tout (C)	Is (C)
1	4.41	19.53	20.47	48.34	1	4.41	19.58	22.35	99.89
2	4.41	19.56	20.50	48.35	2	4.41	19.58	22.35	99.88
3	3.87	19.62	20.67	48.45	3	3.87	19.63	22.72	99.97
4	3.87	19.62	20.67	48.49	4	3.87	19.64	22.72	100.03
5	3.44	19.71	20.86	48.51	5	3.44	19.75	23.13	99.98
6	3.44	19.70	20.86	48.49	6	3.44	19.76	23.14	99.94
7	3.01	19.77	21.03	48.42	7	3.01	19.83	23.56	99.92
8	3.01	19.77	21.03	48.36	8	3.01	19.84	23.56	99.99
9	2.52	19.86	21.28	48.37	9	2.52	19.95	24.16	100.06
10	2.52	19.87	21.29	48.35	10	2.52	19.97	24.18	99.99
11	1.98	20.01	21.67	48.41	11	1.98	20.14	25.10	100.02
12	1.98	20.01	21.67	48.50	12	1.98	20.15	25.10	100.03
13	1.49	20.20	22.18	48.52	13	1.49	20.34	26.27	100.03
14	1.49	20.21	22.18	48.51	14	1.49	20.36	26.29	99.98
15	1.16	20.42	22.69	48.36	15	1.16	20.57	27.49	100.05
16	1.16	20.42	22.69	48.35	16	1.16	20.59	27.50	100.12
17	4.41	19.65	20.59	48.51	17	4.41	19.89	22.62	99.89
18	4.41	19.65	20.59	48.43	18	4.41	19.90	22.63	99.87

TABLE XXXVII

RAW DATA FOR WIRE-WRAPPED TUBE WITH
 $D_w = 0.5$ MM AND $P = 3.6$ MM

Tube Number: 71					Tube Number: 71				
File Name: S71V296					File Name: S71A314				
Pressure Condition: Vacuum					Pressure Condition: Atmospheric				
Steam Velocity: 2.0 (m/s)					Steam Velocity: 1.0 (m/s)				
Data #	Vw (m/s)	Tin (C)	Tout (C)	Is (C)	Data #	Vw (m/s)	Tin (C)	Tout (C)	Is (C)
1	4.41	19.40	20.33	48.38	1	4.41	20.38	23.10	100.03
2	4.41	19.41	20.34	48.36	2	4.41	20.38	23.09	99.89
3	3.87	19.48	20.50	48.47	3	3.87	20.41	23.43	99.97
4	3.87	19.48	20.51	48.52	4	3.87	20.42	23.44	99.92
5	3.44	19.56	20.69	48.31	5	3.44	20.46	23.79	99.91
6	3.44	19.56	20.69	48.36	6	3.44	20.45	23.78	99.96
7	3.01	19.62	20.86	48.45	7	3.00	20.51	24.20	99.93
8	3.01	19.63	20.87	48.45	8	3.00	20.52	24.21	99.98
9	2.52	19.71	21.11	48.32	9	2.52	20.59	24.75	100.02
10	2.52	19.72	21.12	48.45	10	2.52	20.59	24.75	100.01
11	1.98	19.86	21.51	48.40	11	1.98	20.72	25.64	99.99
12	1.98	19.86	21.52	48.48	12	1.98	20.72	25.64	100.04
13	1.49	20.02	21.97	48.44	13	1.49	20.91	26.78	100.07
14	1.49	20.05	22.01	48.55	14	1.49	20.91	26.78	100.01
15	1.16	20.26	22.50	48.37	15	1.16	21.06	27.91	100.01
16	1.16	20.26	22.52	48.34	16	1.16	21.09	27.95	100.10
17	4.41	19.48	20.41	48.45	17	4.41	20.35	23.04	99.96
18	4.41	19.48	20.41	48.48	18	4.41	20.35	23.05	99.90

APPENDIX C
UNCERTAINTY ANALYSIS

Experimentally determined quantities are always associated with uncertainties owing to the measuring device accuracy, calibration of the device, and the operator's experience. During this thesis effort, numerical data were taken and, together with theoretical formulation, the steam-side heat-transfer coefficients were calculated. Since the devices used during this experiment to read steam temperature, inlet and outlet cooling water temperatures, flowrate of the cooling water in finally computing the steam-side heat-transfer coefficient, the final result may be distorted due to the uncertainty propagation during calculations. In cases where the final results show large uncertainties, it may be unwise to accept the experimental results. The uncertainty on a computation can be determined using the following equation proposed by Kline and McClintok [35] shown below:

$$W_R = \left[\left(\frac{\partial R}{\partial x_1} W_1 \right)^2 + \left(\frac{\partial R}{\partial x_2} W_2 \right)^2 + \dots + \left(\frac{\partial R}{\partial x_n} W_n \right)^2 \right]^{1/2} \quad (C.1)$$

where

W_R is the uncertainty of the desired dependent variable

x_1, x_2, \dots, x_n are the measured (independent) variables

w_1, w_2, \dots, w_n are the uncertainties in the measured variables

Using program "UNA7" which is listed at the end of this appendix the uncertainties associated with various quantities during this investigation were obtained. Also, listed in this appendix are some of the selected uncertainty evaluations. A complete discussion on the uncertainty analysis used for this experiment is given by Georgiadis [5].

```

1000! FILE NAME : UNA7
1005! REVISED : February 28, 1986
1010!
1015 COM /Cc/ C(7)
1020 DIM E(4)
1025 DATA 0.10086091,25727.94369,-767345.8295,78025595.81
1030 DATA -9247486589,6.97688E+11,-2.66192E+13,3.94078E+14
1035 READ C(*)
1040 PRINT
1045 PRINTER IS 701
1050 PRINT USING "10X,""DATA FOR THE UNCERTAINTY ANALYSIS:"""
1051 PRINT
1055 BEEP
1060 INPUT "ENTER FILE NAME".File$
1065 PRINT USING "10X,""File Name:           "",12A";File$
1070 BEEP
1075 INPUT "ENTER DATA SET NUMBER FOR UNCERTAINTY ANALYSIS".Ids
1080 BEEP
1085 INPUT "ENTER PRESSURE CONDITION (0=V,1=A) ".Prc
1090 Prc=Prc+1
1095 BEEP
1100 INPUT "ENTER C1".C1
1105 ASSIGN @File TO File$
1110 ENTER @File:Ifg,Inn
1115 IF Ifg=0 THEN ENTER @File:Dd
1120 IF Ifg=1 THEN ENTER @File:Dd,Dd,Dd
1125 FOR I=1 TO Ids
1130 ENTER @File:Bvol,Bamp,Vtran,Etp,E(*),Fm,Tci,Tco,Phg,Pwater
1135 NEXT I
1140 Emf=E(0)
1145 IF Prc=1 THEN
1150 BEEP
1155 PRINT USING "10X,""Pressure Condition: Vacuum (11 kPa)""
1160 ELSE
1165 PRINT USING "10X,""Pressure Condition: Atmospheric (101 kPa)""
1170 END IF
1205 BEEP
1210 PRINTER IS 1
1215 PRINT USING "4X,""Select Material Code:"""
1220 PRINT USING "6X,""0 Copper      1 Stainless steel""
1225 PRINT USING "6X,""2 Aluminum   3 90:10 Cu-Ni""
1230 PRINT USING "6X,""4 HPTI""
1235 INPUT Itt
1240 IF Itt=0 THEN
1245 BEEP
1250 INPUT "SELECT (0=THIN, 1=THICK)".Iwt
1255 END IF
1260 PRINTER IS 701
1265 IF Itt=0 THEN
1270 Di=.0127      ! Inside diameter of test tube
1275 Kc=385
1280 Dkc=10
1285 IF Iwt=0 THEN
1290 Do=.0137
1295 ELSE
1300 Do=.01905      ! Outside diameter of test tube
1305 END IF

```

```

1310 END IF
1315 IF Itt=1 THEN
1320 Kc=16
1325 Dkc=1
1330 Di=.01245
1335 Do=.0145
1340 END IF
1345 IF Itt=2 THEN
1350 Kc=167
1355 Dkc=5
1360 Do=.0137
1365 Di=.0127
1370 END IF
1375 IF Itt=3 THEN
1380 Kc=45
1385 Dkc=2
1390 Di=.0127
1395 Do=.0137
1400 END IF
1405 IF Itt=4 THEN
1410 Kc=385
1415 Dkc=10
1420 Di=.0156
1425 Do=.0175
1430 END IF
1435 D1=.01905
1440 D2=.01587
1445 IF Itt=4 THEN D2=.01905
1450 PRINTER IS 701
1455 Ts=FNTvsv(Emf)
1460 PRINT USING "10X." "Steam Temperature" = ".3D.2D," (Deg
C)"";Ts
1465 PRINT USING "10X." "Water Flow Rate (%)" = ".3D.2D";Fm
1470 Dtc1=.01
1475 Dtco=.01
1480 BEEP
1485 Demf=1.0E-6
1490 Dts=SQR(((C(1)+2*C(2)+Emf+3*C(3)+Emf*2+4*C(4)+Emf*3)*Demf)*2)
1495 T=(Tc1+Tco)/2 ! FILM TEMPERATURE
1500! UNCERTAINTY IN THE COOLING WATER
1505 Drho=.5 ! ERROR IN WATER DENSITY
1510 Dmf=.0044 ! ERROR IN MASS FLOW RATE
1515 Rho=FNRho(T) ! WATER DENSITY
1520 Mf=1.04805E-2+6.80932E-3*Fm ! MASS FLOW RATE OF COOLING WATER
1525! CORRECT MF FOR THE TEMPERATURE EFFECT
1530 Mf=Mf*(1.0365-1.96644E-3*Tc1+5.252E-6*Tc1*2)/.995434
1535 A1=(PI*D1*2)/4 ! TUBE INSIDE CROSS SECTION AREA
1540 Ddi=.000025
1545 Dai=PI*D1*Ddi/2 ! ERROR OF INSIDE TUBE CROSS AREA
1550! COMPUTE THE WATER VELOCITY
1555 Vw=Mf/(Rho*A1) ! WATER VELOCITY
1560 PRINT USING "10X." "Water Velocity" = ".Z.DD," (m/
s)"";Vw
1565! CORRECT OUTLET WATER TEMP. FOR THE MIXING CHAMBER EFFECT
1570 IF Inn=1 OR Inn=5 THEN Tco=Tco-.004*Vw*2
1575 IF Inn=0 THEN Tco=Tco-(-.00138+.001*Vw*2)
1580 T=(Tc1+Tco)*.5 ! FILM TEMPERATURE
1585! COMPUTE THE ERROR IN WATER VELOCITY
1590 Dvw=Vw*SQR((Dmf/Mf)*2+(Drho/Rho)*2+(Dai/A1)*2)
1595! UNCERTAINTY IN THE REYNOLDS NUMBER

```

```

1600 Mw=FNW(T) ! WATER VISCOSITY
1605 Dmw=6.E-6 ! ERROR OF WATER VISCOSITY
1610 Re=(Rho*Vw*D1)/Mw
1615 Dre=Re*SQR((Drho/Rho)^2+(Dvw/Vw)^2+(Dd1/D1)^2+(Dmw/Mw)^2)
1620 ! UNCERTAINTY IN THE HEAT TRANSFERRED
1625 Cpw=FNCpw(T)
1630 Q=Mf*(Tco-Tci)*Cpw
1635 Dcpw=8
1640 Dq=Q*SQR((Dmf/Mf)^2+((Dtco/(Tco-Tci)))^2+((Dtci/(Tco-Tci)))^2+(Dcpw/Cpw)^2)
1645 ! UNCERTAINTY IN THE HEAT FLUX
1650 D1=.0005 ! ERROR IN TUBE LENGHT
1655 Ddo=.000025
1660 L=.13335 ! CONDENSING TUBE LENGTH
1665 Qp=Q/(PI*Do*L) ! HEAT FLUX
1670 PRINT USING "10X,""Heat Flux" - "Z.3DE," (W/m^2)"
1675 PRINT USING "10X,""Tube-metal thermal conduc. - "Z.3D.D," (W/m.
K)" :Kc
1680 PRINT USING "10X,""Sieder-Tate constant - "Z.4D":Ci
1685 Dqp=Qp*SQR((Dq/Q)^2+(Ddo/Do)^2+(D1/L)^2)
1690 Lmtd=(Tco-Tci)/LOG((Ts-Tci)/(Ts-Tco))
1695 Uo=Qp/Lmtd ! OVERALL HEAT TRANSFER COEF.
1700 A1=Dts*(Tci-Tco)/((Ts-Tci)*(Ts-Tco)*LOG((Ts-Tci)/(Ts-Tco)))
1705 A2=Dtci/((Ts-Tci)*LOG((Ts-Tci)/(Ts-Tco)))
1710 A3=Dtco/((Ts-Tco)*LOG((Ts-Tci)/(Ts-Tco)))
1715 Dlmtd=Lmtd*SQR(A1^2+A2^2+A3^2)
1720 Duo=Uo*SQR((Dqp/Qp)^2+(Dlmtd/Lmtd)^2)
1725 M=Mw
1730 T1=(T+273.15)/273.15
1735 Kw=FNKw(T1)
1740 Ac=0. ! INTERSCEPT FROM SIEDER PROGRAM
1745 L1=.060325 ! LENGTH OF UNFINNED LEFT PART OF TUBE
1750 L2=.034925 ! LENGTH OF UNFINNED RIGHT PART OF TUBE
1755 Pr=Cpw*Mw/Kw
1760 Muw=FNMuw(T)
1765 ! UNCERTAINTY OF INSIDE HEAT-TRANSFER COEFF.
1770 Cf=1.
1775 H1=(Kw/D1)*(Ci*Re^.8*Pr^.333*Cf+Ac)
1780 Dt1=Q/(PI*D1*(L+L1*Fe1+L2*Fe2)*H1)
1785 Cfc=(Muw/FNMuw(T+Dt1))^.14
1790 IF ABS((Cfc-Cf)/Cfc)>.01 THEN
1795 Cf=(Cf+Cfc)*.5
1800 GOTO 1775
1805 END IF
1810 P1=PI*(D1+D1)
1815 B1=(D1-D1)*PI*(D1+D1)*.5
1820 M1=(H1*P1/(Kc*B1))^.5
1825 P2=PI*(D1+D2)
1830 B2=(D2-D1)*PI*(D1+D2)*.5
1835 M2=(H1*P2/(Kc*B2))^.5
1840 Fe1=FNTanh(M1*L1)/(M1*L1)
1845 Fe2=FNTanh(M2*L2)/(M2*L2)
1850 Dtc=Q/(PI*D1*(L+L1*Fe1+L2*Fe2)*H1)
1855 IF ABS((Dtc-Dt1)/Dtc)>.01 THEN 1775
1860 Dkw=.0010 ! ERROR IN WATER THERMAL CONDUCTIVITY
1865 Dci=.0005 ! ERROR IN SIEDER-TATE COEFFICIENT
1870 Dpr=.05 ! ERROR IN PRANDTL NUMBER
1875 Dcf=8.E-6
1880 A4=.14*Dcf/Cf

```



```

1885 Dh1=Hi*SQR((Dkw/Kw)^2+(Ddi/Di)^2+(.9*Dre/Re)^2+(.333*Dpr/Pr)^2+(Dci/Ci)^2+
A4)
1890! UNCERTAINTY OF OUTSIDE HEAT-TRANSFER COEFF.
1895 Rw=Do*LOG(Do/Di)/(2*Kc) ! WALL RESISTANCE
1900 Ho=1/((1/Uo)-(Do*L/(Di*(L+L1*Fe1+L2*Fe2)*Hi)))-Rw)
1905 Dtw=Rw*SQR((Ddo/Do)^2+(Dkc/Kc)^2+(Ddo/(Do*LOG(Do/Di)))^2+(Ddi/(Di*LOG(Do/D
1)))^2)
1910 A5=1/Uo-Rw-(Do*L/(Di*(L+L1*Fe1+L2*Fe2)*Hi))
1915 A6=Duo/(Uo^2*A5)
1920 A7=Dtw/A5
1925 A8=((Do/(Di*Hi))*(Dh1/Hi))/A5
1930 PRINT
1935 Dho=Ho*SQR(A6^2+A7^2+A8^2)
1940! CALCULATE THE % UNCERTAINTY IN Ho
1945 Prho=Dho*100/Ho
1950! CALCULATE THE % UNCERTAINTY IN REYNOLDS NUMBER
1955 Prre=Dre*100/Re
1960! CALCULATE THE % UNCERTAINTY IN MASS FLOW RATE
1965 Prmf=Dmf*100/Mf
1970! CALCULATE THE % UNCERTAINTY IN HEAT TRANSFER
1975 Prqp=Dqp*100/Qp
1980! CALCULATE THE % UNCERTAINTY IN LMTD
1985 Prlmtc=Dlmtc*100/Lmtc
1990! CALCULATE THE % UNCERTAINTY IN Rw
1995 Prrw=Dtw*100/Rw
2000! CALCULATE THE % UNCERTAINTY IN OVERALL HEAT TRANSFER COEF.
2005 Pruo=Duo*100/Uo
2010! CALCULATE THE % UNCERTAINTY IN INSIDE HEAT TRANSFER COEFF.
2015 Prhi=Dh1*100/Hi
2020 PRINT
2025 PRINT USING "10X, ""UNCERTAINTY ANALYSIS: ""
2030 PRINT
2035 PRINT USING "10X, "" VARIABLE PERCENT UNCERTAINTY ""
2040 PRINT
2045 PRINT USING "10X, ""Mass Flow Rate, Md ""Z.2D,":Prmf
2050 PRINT USING "10X, ""Reynolds Number, Re ""Z.2D,":Prre
2055 PRINT USING "10X, ""Heat Flux, q ""Z.2D,":Prqp
2060 PRINT USING "10X, ""Log-Mean-Tem Diff, LMTD ""Z.2D,":Prlmtc
2065 PRINT USING "10X, ""Wall Resistance, Rw ""DD.2D,":Prmw
2070 PRINT USING "10X, ""Overall H.T.C., Uo ""DD.2D,":Pruo
2075 PRINT USING "10X, ""Water-Side H.T.C., Hi ""3D.2D,":Prhi
2080 PRINT USING "10X, ""Steam-Side H.T.C., Ho ""3D.2D,":Prho
2085 END
2090 DEF FNMu(T)
2095 A=247.8/(T+133.15)
2100 Muw=2.4E-5*10^A
2105 RETURN Muw
2110 FNEND
2115 DEF FNTanh(X)
2120 P=EXP(X)
2125 Q=EXP(-X)
2130 Tanh=(P-Q)/(P+Q)
2135 RETURN Tanh
2140 FNEND
2145 DEF FNKw(T1)
2150 Kw=-.92247+T1*(2.8395-T1*(1.8007-T1*(.52577-.07344*T1)))
2155 RETURN Kw
2160 FNEND
2165 DEF FNMw(T)
2170 A=247.8/(T+133.15)

```

```

2175 Mw=2.4E-5*10^A
2180 RETURN Mw
2185 FNEND
2190 DEF FNRho(T)
2195 Rho=999.52946+T*(.01269-T*(5.482513E-3-T*1.234147E-5))
2200 RETURN Rho
2205 FNEND
2210 DEF FNCpw(T)
2215 Cpw=(4.21120858-T*(2.26826E-3-T*(4.42361E-5+2.71428E-7*T)))*1000
2220 RETURN Cpw
2225 FNEND
2230 DEF FNTvsv(Emf)
2235 COM /Cc/ C(7)
2240 T=C(0)
2245 FOR I=1 TO 7
2250 T=T+C(I)*Emf*I
2255 NEXT I
2260 RETURN T
2265 FNEND

```

DATA FOR THE UNCERTAINTY ANALYSIS:

File Name: F06V145
 Pressure Condition: Vacuum (11 kPa)
 Steam Temperature = 48.55 (Deg C)
 Water Flow Rate (%) = 80.00
 Water Velocity = 4.39 (m/s)
 Heat Flux = 3.329E+05 (W/m²)
 Tube-metal thermal conduc. = 385.0 (W/m.K)
 Sieder-Tate constant = 0.0658

UNCERTAINTY ANALYSIS:

VARIABLE	PERCENT UNCERTAINTY
Mass Flow Rate, Md	0.79
Reynolds Number, Re	1.12
Heat Flux, q	1.53
Log-Mean-Tem Diff, LMTD	1.24
Wall Resistance, R _w	2.67
Overall H.T.C., U _o	1.97
Water-Side H.T.C., H _i	1.23
Steam-Side H.T.C., H _o	5.10

DATA FOR THE UNCERTAINTY ANALYSIS:

File Name: F06V145
 Pressure Condition: Vacuum (11 kPa)
 Steam Temperature = 48.39 (Deg C)
 Water Flow Rate (%) = 20.00
 Water Velocity = 1.16 (m/s)
 Heat Flux = 1.842E+05 (W/m²)
 Tube-metal thermal conduc. = 385.0 (W/m.K)
 Sieder-Tate constant = 0.0658

UNCERTAINTY ANALYSIS:

VARIABLE	PERCENT UNCERTAINTY
Mass Flow Rate, Md	3.01
Reynolds Number, Re	3.11
Heat Flux, q	3.10
Log-Mean-Tem Diff, LMTD	0.60
Wall Resistance, R _w	2.67
Overall H.T.C., U _o	3.15
Water-Side H.T.C., H _i	2.63
Steam-Side H.T.C., H _o	20.05

DATA FOR THE UNCERTAINTY ANALYSIS:

File Name: F06A226
 Pressure Condition: Atmospheric (101 kPa)
 Steam Temperature = 99.96 (Deg C)
 Water Flow Rate (%) = 80.00
 Water Velocity = 4.40 (m/s)
 Heat Flux = 1.038E+06 (W/m^2)
 Tube-metal thermal conduc. = 385.0 (W/m.K)
 Sieder-Tate constant = 0.0630

UNCERTAINTY ANALYSIS:

VARIABLE	PERCENT UNCERTAINTY
Mass Flow Rate, Md	0.79
Reynolds Number, Re	1.12
Heat Flux, q	0.99
Log-Mean-Tem Diff, LMTD	0.40
Wall Resistance, Rw	2.67
Overall H.T.C., Uo	1.07
Water-Side H.T.C., Hi	1.25
Steam-Side H.T.C., Ho	3.22

DATA FOR THE UNCERTAINTY ANALYSIS:

File Name: F06A226
 Pressure Condition: Atmospheric (101 kPa)
 Steam Temperature = 99.99 (Deg C)
 Water Flow Rate (%) = 20.00
 Water Velocity = 1.16 (m/s)
 Heat Flux = 6.036E+05 (W/m^2)
 Tube-metal thermal conduc. = 385.0 (W/m.K)
 Sieder-Tate constant = 0.0630

UNCERTAINTY ANALYSIS:

VARIABLE	PERCENT UNCERTAINTY
Mass Flow Rate, Md	3.00
Reynolds Number, Re	3.11
Heat Flux, q	3.04
Log-Mean-Tem Diff, LMTD	0.18
Wall Resistance, Rw	2.67
Overall H.T.C., Uo	3.04
Water-Side H.T.C., Hi	2.64
Steam-Side H.T.C., Ho	19.36

LIST OF REFERENCES

1. Thomas, D. G., and Hayes, P. H., "High Performance Heat Transfer Surfaces," *Industrial and Engineering Chemistry*, Vol. 62, No. 2, February 1970, pp. 4-9
2. Krohn, R. L., *An Experimental Apparatus to Study Enhanced Condensation Heat-Transfer of Steam on Horizontal Tubes*, M. S. Thesis, Naval Postgraduate School, Monterey, California, June, 1982.
3. Graber, K. A., *Condensation Heat Transfer of Steam on a Single Horizontal Tube*, M. S. Thesis, Naval Postgraduate School, Monterey, California, June, 1983.
4. Poole, W. M., *Filmwise Condensation of Steam on Externally-Finned Horizontal Tubes*, M.S. Thesis, Naval Postgraduate School, Monterey, California, December, 1983.
5. Georgiadis, I. V., *Filmwise Condensation of Steam on Low Integral-finned Tubes*, M.S. Thesis, Naval Postgraduate School, Monterey, California, September, 1984.
6. Flook, F. V., *Filmwise Condensation of Steam on Low Integral-finned Tubes*, M.S. Thesis, Naval Postgraduate School, Monterey, California, March, 1985.
7. Gregorig, R., "Hautkondensation an Feingewellten Oberflächen," bei Berücksichtigung der Oberflächenspannungen," *Zeitschrift für Angewandte Mathematik und Physik*, Vol. V, 1954, pp. 36-49. Translation by D. K. Edwards.
8. Mori, Y., Hijikata, k., Hirasawa, S., Nakayama, W., "Optimized Performance of Condensers with Outside Condensing Surface," *Condensation Heat-Transfer*, Presented at 20th National Heat-Transfer Conference, San Diego, California, August, 1979, pp. 59 - 62
9. Yau, K. K., Cooper, J. R., and Rose, J. W., "Effects of Fin Spacing and Drainage Strips on the Condensation Heat-Transfer Performance of Horizontal Low Integral-Fin Tubes," *Fundamentals of Phase Change: Boiling and Condensation*, HTD-Vol 38, pp. 151-156. C. T. Avedisian and T. M. Rudy (Eds.), ASME, 1984.
10. Wanniarachchi, A. S., Marto, P. J., and Rose, J. W., *Filmwise Condensation of Steam on Externally-Finned Horizontal Tubes*, *Fundamentals of Phase Change: Boiling and Condensation*, HTD-Vol. 38, C. T. Avedisian and T. M. Rudy (Eds.), ASME, 1984, pp. 133-141.

11. Katz, D. L., Hope, R. E., and Dasko, S. C., "Liquid Retention on Finned Tubes," Dept. of Eng. Research, University of Michigan, Ann Arbor, Michigan, Project M 592, 1946.
12. Rudy, T. M., and Webb, R. L., "Condensate Retention of Horizontal Integral-Fin Tubes," *Advances in Enhanced Heat-Transfer*, 1981, HTD-Vol. 18, Presented 20th National Heat-Transfer Conference, Milwaukee, Wisconsin, August, 1981, pp. 35-41.
13. Rifert, Y. G., "Steam Condensation on Profiled Surfaces," *Heat and Mass-Transfer Processes in Porous Media With Phase Transformation*, Academy of Science, BSSR, A. B. Lykov (Ed), Minsk, 1982, pp. 149-170.
14. Rudy, T. M., and Webb, R. L., "An Analytical Model to Predict Condensate Retention on Horizontal Integral-Fin Tubes," *ASME/JSME Thermal Engng. Joint Conf.*, Vol. 1, March 20-24, 1983, pp. 373-378.
15. Owen, R. G., Sardesai, R. G., Smith, R. A., and Lee, W. C., "Gravity Controlled Condensation on a Low-Fin Tube," I.Chem.E. Symposium Series No. 75, pp. 415-425.
16. Honda, H., Nozu, S., Mitsumori, K., "Augmentation of Condensation on Horizontal Finned Tubes By Attaching Porous Drainage Plates," *Proc. ASME-JSME Thermal Engineering Conference*, Hawaii, 1983, pp. 289-296.
17. Rudy, T. M., and Webb, R. L., "An Analytical Model to Predict the Condensate Retention on Horizontal Integral-Fin Tubes," *ASME Journal of Heat Transfer*, Vol. 107, 1985, pp. 361-368.
18. Beatty, B. O., and Katz, D. L., "Condensation of Vapors on Outside of Finned Tubes," *Chemical Engineering Progress*, Vol. 44, No. 1, January, 1948, pp. 55-69.
19. Karkhu, V. A., and Borovkov, V. P., "Film Condensation of Vapor at Finely-Finned Horizontal Tubes," *Heat Transfer-Soviet Research*, Vol. 3, No. 2, March-April 1971, pp. 183-191.
20. Edwards, D. K., Gier, K. d., Ayyaswamy, P. S., and Catton, i., "Evaporation and Condensation in Circumferential Grooves on Horizontal Tubes," *ASME-AIChE Heat Tranfer Conference*, Atlanta, August 1973.
21. Zozulya, N. V., Karkhu, V. A., and Borovkov, V. P., "An Analytic and Experimental Study of Heat Transfer in Condensation of Vapor on Finned Surfaces," *Heat Transfer-Soviet Research*, Vol. 9, No. 2, March-April 1977, pp. 18-22.
22. Webb, R. L., "A Generalized Procedure for the Design and Optimization of Fluted Gregorig Condensing Surfaces," *Journal of Heat Transfer*, Vol. 101, May 1979, pp. 335-339.

23. Rifert, V. G., "A New Method for Calculating Rates of Condensation on Finned Tubes," *Heat Transfer-Soviet Research*, Vol. 12, No. 3, May-June, 1980, pp. 142-147.
24. Adamek, T., "Bestimmung der Kondensationsgrößen auf feingewellten Oberflächen zur Auslegung optimaler Wandprofile," *Wärme-und-Stoffübertragung*, Vol. 15, 1981, pp. 255-270.
25. Shklover, G. G., Mil'man, O. O., Baskov, V. S., and Ankudinov, G. A., "Heat Transfer in Condensation of Steam on Finely-Finned Horizontal Tubes," *HEAT TRANSFER-Soviet research*, Vol. 13, No. 2, March-April 1981, pp. 108-114.
26. Webb, R. L., Keswani, S. T., Rudy, T. M., "Investigation of Surface-Tension and Gravity Effects in Film Condensation," *Proceedings of 7th International Heat-Transfer Conference*, Munich, Fed. Rep. of Germany, Sept. 6-10, 1982, Hemisphere Publishing Co., Washington D.C., Vol. 5, pp. 175-180.
27. Nusselt, W., "Surface Condensation of Water Vapor," *Z. Ver. dt. Ing.*, Vol. 60, pp. 541-546 and 569-575, 1916. (in German).
28. Rudy, T. M., *A Theoretical and Experimental Study of Condensation on Single, Integral-Fin Tubes*, Ph.D. Thesis, Department of Mechanical Engineering, The Pennsylvania State University, University Park, Pa., May, 1982.
29. Rudy, T. M., and Webb, R. L., "Theoretical Model for Condensation on Horizontal, Integral-Fin Tubes," *Heat Transfer*, Seattle, AIChE Symp. Ser., Vol. 79, No. 225, 1983, pp. 11-18.
30. Honda, H., Nozu, S., "A Prediction Method for Heat Transfer During Film Condensation on Horizontal Low Integral-Finned Tubes," *Fundamentals of Phase Change: Boiling and Condensation*, HTD-Vol 38, C. T. Avedisian and T. M. Rudy (Eds.) ASME, 1984, pp. 107-114.
31. Webb, R. L., Rudy, T. M., and Kedzierski, M. A., "Prediction of the Condensation Coefficient on Horizontal Integral-Fin Tubes," *Journal of Heat Transfer*, Vol. 107, 1985, pp. 369-376.
32. Fujii, T., Wang, W., Koyama, S., and Shimizu, Y., "Heat-Transfer Enhancement for Gravity Controlled Condensation on a Horizontal Tube by Coiled Wires," *Beijing Conference*, 1985.
33. Briggs, D. E., and Young, E. H., "Modified Wilson Plot Techniques for Obtaining Heat Transfer Correlations for Shell and Tube Heat exchangers," *Heat Transfer - Philadelphia*, Vol. 65, No. 92, 1969, pp. 35-45.

34. Fujii, T., Honda, H., "Condensation of Steam on a Horizontal Tube," *Condensation Heat Transfer*, ASME, New York, 1979.
35. Kline, S. J., and McClintock, F. A., "Describing Uncertainties in Single-Sample Experiments," *Mech. Eng.*, Vol. 74, January 1953, pp. 3-8.

INITIAL DISTRIBUTION LIST

	No.	Copies
1. Defense Technical Information Center Cameron Station Alexandria, Virginia 22304-6145	2	
2. Library, Code 0142 Naval Postgraduate School Monterey, California 93943	2	
3. Department Chairman, Code 69 Department of Mechanical Engineering Naval Postgraduate School Monterey, California 93943	1	
4. Professor P.J. Marto, Code 69Mx Department of Mechanical Engineering Naval Postgraduate School Monterey, California 93943	5	
5. Dr. John W. Rose Department of Mechanical Engineering Queen Mary College London E1 4NS England	1	
6. Dr. A.S. Wanniarachchi, Code 69Wa Department of Mechanical Engineering Naval Postgraduate School Monterey, California 93943	3	
7. Dr. Win Aung Program Director for Heat Transfer Division of Engineering National Science Foundation Washington , D. C. 20008	1	
8. Professor D. Salinas, Code 69Sa Department of Mechanical Engineering Naval Postgraduate School Monterey, California 93943	1	
9. Dr. M. Katsuta, Code 69Ka Department of Mechanical Engineering Naval Postgraduate School Monterey, California 93943	1	
10. Hellenic Navy General Staff Department of Education c/o Embassy of Greece Office of Naval Attache 2228 Massachusetts Avenue, N.W Washington, D.C. 20008	3	
11. Lt. Mitrou Evangelos, H.N. 19, Filikis Eterias St, Koridalos Athens, Attiki Greece	5	

- | | | |
|-----|---|---|
| 12. | Lt. Georgiadis Ioannis, H.N.
67, Peloponissou St, Agia Paraskevi
Athens, Attiki
Greece | 1 |
| 13. | Lt. Frederick A. Flook, USN
Long Beach Naval Shipyard
Long Beach, California 90822 | 1 |
| 14. | Mr. Krohn, R.
Supervisor of Configuration Management
Clinton Power Station
Decatur, Illinois 62526 | 1 |

END
DTIC

7-86